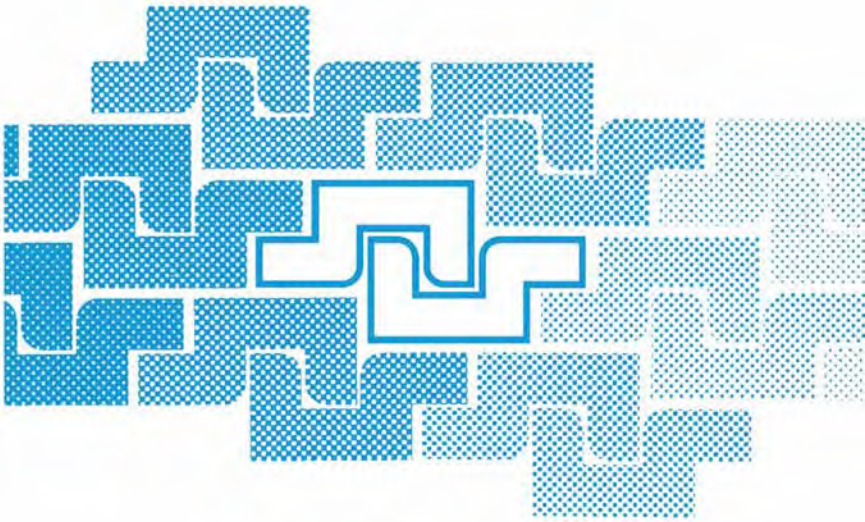

New Challenges in Superconductivity: Experimental Advances and Emerging Theories

Edited by

J. Ashkenazi, Mikhail V. Eremin, Joshua L. Cohn, Ilya Eremin, Dirk Manske, Davor Pavuna and Fulin Zuo

NATO Science Series

II. Mathematics, Physics and Chemistry – Vol. 183

CD-ROM INCLUDED

New Challenges in Superconductivity: Experimental Advances and Emerging Theories

NATO Science Series

A Series presenting the results of scientific meetings supported under the NATO Science Programme.

The Series is published by IOS Press, Amsterdam, and Springer (formerly Kluwer Academic Publishers) in conjunction with the NATO Public Diplomacy Division.

Sub-Series

I. Life and Behavioural Sciences	IOS Press
II. Mathematics, Physics and Chemistry	Springer (formerly Kluwer Academic Publishers)
III. Computer and Systems Science	IOS Press
IV. Earth and Environmental Sciences	Springer (formerly Kluwer Academic Publishers)

The NATO Science Series continues the series of books published formerly as the NATO ASI Series.

The NATO Science Programme offers support for collaboration in civil science between scientists of countries of the Euro-Atlantic Partnership Council. The types of scientific meeting generally supported are "Advanced Study Institutes" and "Advanced Research Workshops", and the NATO Science Series collects together the results of these meetings. The meetings are co-organized by scientists from NATO countries and scientists from NATO's Partner countries — countries of the CIS and Central and Eastern Europe.

Advanced Study Institutes are high-level tutorial courses offering in-depth study of latest advances in a field.
Advanced Research Workshops are expert meetings aimed at critical assessment of a field, and identification of directions for future action.

As a consequence of the restructuring of the NATO Science Programme in 1999, the NATO Science Series was re-organized to the four sub-series noted above. Please consult the following web sites for information on previous volumes published in the Series.

http://www.nato.int/science
http://www.springeronline.com
http://www.iospress.nl

Series II: Mathematics, Physics and Chemistry – Vol. 183

New Challenges in Superconductivity: Experimental Advances and Emerging Theories

edited by

J. Ashkenazi
University of Miami, FL, U.S.A.

Mikhail V. Eremin
Kazan State University, Kazan, Russian Federation

Joshua L. Cohn
University of Miami, FL, U.S.A.

Ilya Eremin
Freie Universität Berlin, Germany

Dirk Manske
Max-Planck-Institute for Solid State Research, Stuttgart, Germany

Davor Pavuna
EPFL, Institute of Physics of Complex Matter, Lausanne, Switzerland

and

Fulin Zuo
University of Miami, FL, U.S.A.

Springer

Proceedings of the NATO Advanced Research Workshop on
New Challenges in Superconductivity: Experimental Advances and Emerging Theories
Miami, Florida, U.S.A.
11–14 January 2004

A C.I.P. Catalogue record for this book is available from the Library of Congress.

ISBN-10 1-4020-3084-3 (PB)
ISBN-13 978-1-4020-3084-0 (PB)
ISBN-10 1-4020-3083-5 (HB)
ISBN-13 978-1-4020-3083-3 (HB)
ISBN-10 1-4020-3085-1 (e-book)
ISBN-13 978-1-4020-3085-7 (e-book)

Published by Springer,
P.O. Box 17, 3300 AA Dordrecht, The Netherlands.

www.springeronline.com

Printed on acid-free paper

Printed in the Netherlands.

NATO OTAN

ARW

UNIVERSITY OF Miami

DEPARTMENT OF PHYSICS

Contents

Contributing Authors

J. Ashkenazi
Department of Physics, University of Miami, P.O. Box 248046, Coral Gables, FL 33124, USA

N. Bontemps
Laboratoire de Physique du Solide, 10 rue Vauquelin 75005 Paris, France

G. Deutscher
School of Physics and Astronomy, Tel Aviv University, 69978 Tel Aviv, Israel

J. D. Dow
Department of Physics, Arizona State University, 6031 East Cholla Lane, Scottsdale, AZ 85253, USA

T. Egami
Department of Physics and Astronomy, University of Tennessee, Knoxville, TN 37996, USA

M. V. Eremin
Physics Department, Kazan State University, 420008 Kazan, Russian Federation

B. V. Fine
Max Planck Institute for the Physics of Complex Systems, Noethnitzer Str. 38, D-01187, Dresden, Germany

L. P. Gor'kov
Florida State University, NHMFL 1800 East Paul Dirac Drive Tallahassee, FL 32306-4005, USA

D. R. Harshman
Condensed Matter Research, Physikon Research Corporation, P.O. Box 1014, Lynden, WA 98264, USA

N. E. Hussey
H. H. Wills Physics Laboratory, University of Bristol, Tyndall Avenue, Bristol, BS8 1TL, United Kingdom

J. Jung
Department of Physics, University of Alberta, Edmonton AB, T6G 2J1, Canada

R. A. Klemm
Department of Physics, University of North Dakota, Box 7129, Grand Forks, ND 58202-7129, USA

V. Z. Kresin
Lawrence Berkeley Laboratory, 1 Cyclotron Road, Berkeley, CA 94720, USA

S. Kruchinin
Bogolyubov Institute for Theoretical Physics, 14-b Metrologichna, Kiev 03144, Ukraine

K. Kumagai
Div. of Physics, Graduate School of Science, Hokkaido Univ., Sapporo 060-0810, Japan

A. Lanzara
Department of Physics, University of California, Berkeley, Berkeley, CA 94720-7300, USA

R. Lobo
Laboratoire de Physique du Solide, 10 rue Vauquelin 75005 Paris, France

T. Mamedov
Faculty of Engineering, Baskent University, Baglica 20.Km, 06530 Ankara, Turkey

D. Manske
Max-Planck-Institute for Solid State Research, Heisenbergstr.1, D-70569 Stuttgart, Germany

M. M. Maska
Department of Theoretical Physics, University of Silesia, Uniwersytecka 4, 40-007 Katowice, Poland

D. K. Morr
Department of Physics, University of Illinois at Chicago, Chicago, IL 60607, USA

I. Mrkonjic
Department of Physics, University of Zagreb, Bijenicka 32, P.O. Box 331, 10002 Zagreb, Croatia

Y. Nechaev
Clean Energy Research Institute, Mechanical Engineering Department, University of Miami, P.O. Box 248294, Coral Gables, FL 33124, USA

M. Oda
Department of Physics, Hokkaido University, Kita 10, Nishi 8, Sapporo, Hokkaido 060-0810, Japan

C. Ogretir
Osmangazi University, Faculty of Arts and Sciences, Chemistry Department 26470 Eskisehir, Turkey

M. S. Osofsky
Naval Research Laboratories, Code 6360, 4555 Overlook Ave SW, Washington, DC 20375-5320, USA

Y. W. Park
School of Physics and Condensed Matter Research Institute, Seoul National University, Seoul 151-747, Korea

D. Pavuna
Institute of Physics of Complex Matter, EPFL, CH-1015 Lausanne, Switzerland

W. E. Pickett
Department of Physics, University of California Davis, Davis CA 95616, USA

D. Pines
Los Alamos National Laboratory, Los Alamos, NM 87545, USA

K. Scharnberg
I. Institut für Theoretische Physik, Fachbereich Physik der Universität Hamburg, Jungiusstr. 9, 20355 Hamburg, Germany

R. Stern
Department of Chemical Physics, NICPB, Akadeemia tee 23, Tallinn 12618, Estonia

K. Takada
National Institute for Materials Science (NIMS), Tsukuba, Ibaraki 305-0044, Japan

C. M. Varma
Bell laboratories, Murray Hill, NJ 07974, USA

F. Vidal
Department of Condensed Matter Physics, University Santiago de Compostela E-15782, Spain

I. K. Yanson
B.I. Verkin Institute for Low Temperature Physics and Engineering, 310164 Kharkiv, Ukraine

A. Zimmers
Laboratoire de Physique du Solide, 10 rue Vauquelin 75005 Paris, France

Preface

This volume contains the proceedings of the 2004 University of Miami Workshop on Unconventional Superconductivity. The workshop was the fourth in a series of successful meetings on High-T_C Superconductivity and related topics, which took place at the James L. Knight Physics Building on the University of Miami campus in Coral Gables, Florida, in January 1991, 1995, 1999, and 2004.

The workshop consisted of two consecutive events: 1. NATO Advanced Research Workshop (ARW) on New Challenges in Superconductivity: Experimental Advances and Emerging Theories, held on January 11-14, 2004; 2. Symposium on Emerging Mechanisms for High Temperature Superconductivity (SEMHTS), held on January 15-16, 2004.

It is hard to write a balanced preface to a volume like this one, yet at least we try to offer the reader a taste of what was happening in this workshop. There were close to a hundred scientists from around the world, albeit fewer Russians than we had originally hoped for. Nevertheless, the workshop was very lively and we trust that this is demonstrated in this volume.

The workshop included high-quality presentations on state of the art works, yet a key issue, discussed by many, was how homogeneous the cuprates are. STM data, as well as other reports, showed that the cuprate superconductors (SC's) studied were inhomogeneous, especially in the underdoped regime; while experiments, like ARPES and magnetoresistance have established the existence of a Fermi Surface (FS), at least above some doping level, in the cuprates.

This leaves us with the question of how would one understand the existence of an FS in a sample consisting of a 2 nm wide island of an SC embedded in (and eventually connected by) a bad exotic metal. Thus it is necessary to understand the meaning of the FS within the scale in which it exists. It seems to be established that a quasiparticle peak is the signature of the SC islands; yet there are different views on the meaning of this peak.

As usual, there have been almost as many interpretations and definitions of the pseudogap temperature T* as there were participants. Thus, there was hardly any convergence on this topic, especially that different thoughts exist concerning the normal state. Consequently there were at least five generic phase diagrams presented that imply different frameworks. Convincing data has been shown that a glassy state persists up to about x=0.19 in LSCO; yet that still did not clarify controversies concerning the existence of quantum critical points.

Most scientists consider d-wave symmetry to be confirmed in the cuprates; yet there were several reports that the situation may be more complicated. In general, experiments have shown more convergence than high-T_C theories. There is definitely no consensus on the high-T_C mechanism, although two broad groups exist: those around the extended "Big Tent" homogenous scheme, and those who assume an intrinsic inhomogeneous state. Another division could be viewed between those who consider the high-T_C mechanism to be essentially of an electronic-magnetic origin (with no role played by the lattice), and those who assign an important role to the lattice.

There seems to be a consensus that MgB_2 and the fullerenes are simpler SC's than the cuprates, while work on ruthenocuprates and the coexistence of SC and ferromagnetism still provides new stimuli to research and understanding. Interest was drawn also by the new $Na_xCoO_2 \cdot yH_2O$ SC. Although this is a low-T_C material, its physical properties have a similarity to those of the cuprates; thus research on this system seems to be important for the understanding of high T_C SC.

In conclusion, the workshop showed that more outstanding experimental and theoretical work is necessary to elucidate high T_C SC and related phenomena. Thus further challenges await all of us!

The Editors

Acknowledgments

The editors acknowledge NATO for Grant PST.ARW.9800700 which enabled this Advanced Research Workshop to take place.

The University of Miami is acknowledged for providing its facilities.

The workshop participants and Advisory Committee are thanked for their contributions which made this event possible.

Acknowledged for their assistance are the University of Miami Physics Department staff members: Nancy Brady, Judy Mallery, Riquie Mathews, Marco Monti, and Leonardo Rodriquez; the graduate students: Corneliu Chiorescu, Simona Khizroev, and Hengsog Zhang; and the faculty members: George Alexandrakis, Thomas Curtright, and others.

The assistance of Nina Travel is also acknowledged.

LATTICE DYNAMICS AND ELECTRON PAIRING IN HIGH TEMPERATURE SUPERCONDUCTORS

A. Lanzara[1,2], G.-H. Gweon[2], S. Y. Zhou[1]

[1]*Department of Physics, University of California, Berkeley, CA 94720, U.S.A.*
[2]*Materials Sciences Division, Lawrence Berkeley National Laboratory, Berkeley, CA 94720, U.S.A.*

Abstract: Angle resolved photoemission spectroscopy combined with isotope substitution (^{16}O ^{18}O) sample preparation method is used to probe the effect of the lattice degrees of freedom on the electron dynamics of optimally doped $Bi_2Sr_2CaC_2O_{8+\delta}$ high temperature superconductors, as a function of momentum and temperature. Our data show that the lattice dynamics strongly renormalizes the electron dispersion and the photoemission line shapes. The renormalization is enhanced near the anti-nodal region and in the superconducting state, i.e. as the superconducting gap opens up. This unusual behavior is direct evidence that the electron-phonon interaction is correlated with the electron pairing in the high temperature superconductivity.

Key words: Electron-lattice interaction, phonons, Spin Peierls, Angle Resolved Photoemission spectroscopy, Isotope Substitution

1. INTRODUCTION

One of the ongoing debates in the field of high temperature superconductors is whether the lattice degrees of freedom are responsible for some of the unusual electronic properties of the cuprates. While many experiments have pointed out that the lattice is heavily involved in several properties of the cuprate superconductors [1], the lack of experiments probing directly the electronic response to the lattice has kept the debate open. In addition, the absence of a pronounced conventional isotope effect

J. Ashkenazi et al. (eds.), New Challenges in Superconductivity: Experimental Advances and Emerging Theories, 1-8.

[2] on the critical temperature (T_c) [3, 4] has reinforced the belief that the magnetic interaction is the main player instead. However, the meaning of this small isotope coefficient of T_c is unclear since even for conventional superconductors screening can induce small and/or negative value of the isotope coefficient [5]. Indeed, there are several experiments suggesting the presence of a strong electron-phonon interaction in the cuprates, for example the observation of a phonon "kink" in the quasiparticle dispersion measured by photoemission spectroscopy [6], the presence of a very large isotope effect on the pseudogap formation temperature [7,8] and the magnetic susceptibility [9], and the observation of an anomalous isotope effect on the in-plane far-infrared optical conductivity [10].

2. ISOTOPE EFFECT ON THE ELECTRON DYNAMICS

To probe directly the response of the electronic degrees of freedom to the lattice degrees of freedom we propose a novel experiment where Angle Resolved Photoemission Spectroscopy (ARPES) is combined with oxygen isotope substitution on high temperature superconductors. This allows monitoring how changes in the lattice induce changes in the electronic structure. While ARPES in fact is the only technique that probes the electronic structure in a momentum resolved manner, isotope substitution control the lattice degrees of freedom.

ARPES data were collected at beamline 10.0.1 of the Advance Light Source using a SCIENTA 2000 analyzer on optimally doped oxygen isotope substituted $Bi_2Sr_2CaC_2O_{8+\delta}$ (Bi2212) (T_c=92K) superconductors. Upon isotope substitution ($^{16}O \rightarrow ^{18}O$), T_c changes to 91K. The details of isotope substitution are described elsewhere [11]. The energy resolution was of 15 meV FWHM and the angular resolution of 0.15 degree, corresponding to momentum resolution better than 0.01 π/a. The vacuum during the measurement was better than 5 x 10^{-11} Torr. The photon energy was 33 eV. Data were collected for scans parallel to the nodal cut ΓY, (0, 0) to (π, π), of the Brillouin zone, at two different temperatures, below (25K) and above (100K) T_c. Each cut is assigned a cut number, which is the angle offset from the nodal direction. For example, cut 0 will mean a nodal cut, and cut 6 will mean a cut 6 degrees displaced from the nodal cut.

In Figure 1 we show the raw ARPES data as image plots, for several cuts in the momentum space, from the nodal ΓY (panel a0 and b0) to half way towards the M point (π, 0) (panels a6 and b6), for the two isotope substituted samples. The color scale represents the photoelectron intensity versus the momentum and binding energy, with maximum in black and minimum in

white. The reversibility of the isotope effect upon the isotope re-substitution ($^{18}O \rightarrow ^{16}O$) has been shown elsewhere [11].

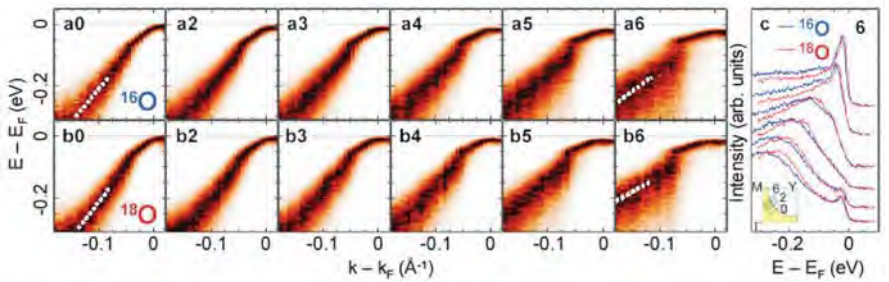

Figure 1. Low temperature (25 K) ARPES data of optimally doped $Bi_2Sr_2CaC_2O_{8+\delta}$ high temperature superconductors with oxygen isotope ^{16}O (panels a) and ^{18}O (panels b). These maps are normalized so that the intensity of each EDC goes from 0 to 1 (see text for details). The panels are labeled with a cut number, i.e. angle offset from the nodal cut. Inset of panel c shows the cut numbers. In panel c, isotope dependence of a few selected EDC's are shown for cut 6. The top pair corresponds to $k=k_F$, i.e. momentum value on the normal state Fermi surface, shown as a curve in the inset.

The intensity maps shown in Figure 1 were normalized (i.e. shifted and scaled in intensity) in such a way that each energy distribution curve (EDC) at each momentum value has intensity range from 0 to 1. This new way of presenting the data allows an easy overview of main differences between the two isotopes, because the information regarding the energy-momentum dispersion relation and the line widths can be already "read off" from the images, without actually applying EDC fit procedures, which are not so straightforward in general. Because of this reason, we will refer to these maps as "pro-EDC maps."

In particular, the maps in Figure 1 make it very easy to see the dichotomy of two dispersing branches, sharp low energy branch (sharp peaks) and broad high-energy branch (broad humps). Note that throughout this paper we use the terms energy and binding energy interchangeably. Following the Fermi liquid terminology, we refer to the low energy branch as coherent branch, while we refer to the high-energy branch as incoherent branch. Also, we will loosely refer to the sharp peak near Fermi level (E_F; defined as zero throughout the paper) as "coherent quasi-particle" peak.

In these pro-EDC maps, the kink phenomenon [6] is visualized as the crossover from the low energy quasi-particle branch to the high-energy incoherent branch. This crossover region is the region of low intensity (indicated by white dashed line, and blue and red arrows), where the two dispersions mix and give rise to a double peak structure, commonly referred to as a "peak-dip-hump" structure, of EDC's [6,12-14]. In this terminology,

the dip energy corresponds to the kink energy, and coincides with the position of the dispersion kink, i.e. change of velocity, in momentum distribution curve (MDC) analysis [15].

Another feature to note in Figure 1 is the superconducting gap, which increases as we approach the antinodal point (from cut 0 to cut 6). The isotope dependence of the gap was discussed in details in Ref.'s [11,16]. Note that in pro-EDC maps, the apparent gap, i.e. the closest approach of the low energy branch to the Fermi level, is often given by the instrumental energy resolution, which is the case for near-nodal cuts in Figure 1. This is of course not the true gap. However, when the true gap value becomes bigger than the energy resolution, the peak position is a good representation of the gap, as for cuts 5-6. For smaller gaps, MDC analysis, presented before [11], is essential.

We will now focus on the differences between the two isotope samples. As is well known in band theory [17], the total energy range of the dispersion decreases as we move towards the antinodal point (cut 6). Upon a close inspection of the images (see also white dotted lines extracted from EDC peak position), we find that the most striking change induced by the isotope substitution occurs at high energy and is manifested by a reduction of the binding energy of the incoherent branch, all the way up to the highest energy shown (see black arrows in panels a and b). On the contrary, the low energy dispersion is weakly isotope dependent, similar to its weak doping dependence [18].

This isotope dependence is strongly momentum dependent. As we move from the nodal (panels a0, b0) to the antinodal region (panels a6,b6), comparison between the upper (^{16}O data) and the lower (^{18}O data) panels clearly shows that the isotope-induced changes are enhanced closer to the antinodal region (cuts 5,6). More specifically we see that the isotope substitution induces a narrowing of the band width up to 20%, near the antinodal region (compare panel a6 to b6), by a factor of two bigger, in absolute energy, than along the nodal direction [11]. We note that the shift of the incoherent peak in the EDC's cannot be accounted for by a rigid shift due to the isotope-induced change of the superconducting gap, which decreases only by few meV upon isotope substitution, as can be seen from the change in the leading edge position.

Another important observation is that, in addition to the isotope-induced change in the band width, there is a clear isotope-induced narrowing of the EDC's [16], as can be noticed by the broader black shadowed area for ^{16}O sample (upper panels), with respect to the ^{18}O sample (lower panels). The width changes become appreciable only in the incoherent part of the dispersion. Again the changes are maximum near the antinodal region. Panel c shows an explicit comparison of the EDC's where the EDC narrowing of the ^{18}O sample can be clearly noted.

Figure 1 summarizes our main findings: a) the isotope substitution strongly affect the high energy incoherent quasiparticle spectra, inducing a reduction of the bandwidth and a narrowing of the line shape width upon ^{18}O substitution, b) The isotope effect is energy dependent: i.e. it is negligible at low energy scale and is strongly enhanced at high energy; c) the kink energy separates the low energy region where the isotope effect is negligible from the high energy region where the effect is strong, thus putting a strong constraint on the phonon involvement in the kink dynamics.

In Figure 2 we report raw normal state (100K) ARPES data for similar cuts as in figure 1. The most striking observation from the data is the similarity between the ^{16}O and ^{18}O data, (compare upper and lower panels). The reduction of the isotope effect can be also seen from the EDC peaks (panel c). No appreciable change of the peak position or peak width is observed at this high temperature. The reduction of the isotope effect in the normal state suggests that the low temperature behavior is associated with the onset of additional scattering mechanism. This unusual temperature dependence is also consistent with other experimental results where an enhancement of the isotope effect is observed below T^*.

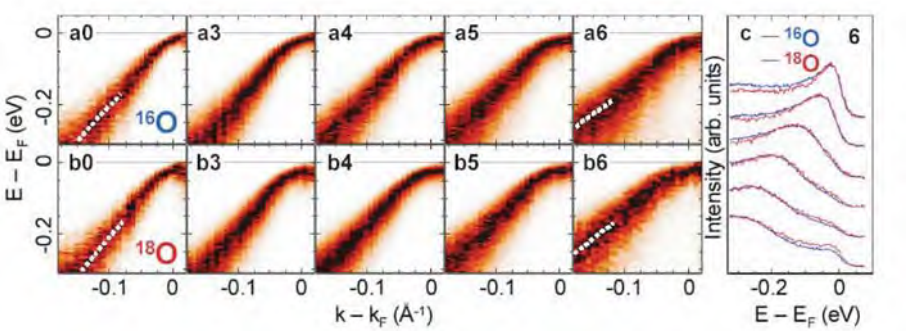

Figure 2. Same as Fig. 1, except for the high measurement temperature (100 K).

The onset of electron-phonon interaction in the superconducting state is unusual in term of conventional electron-phonon interaction where one would expect that the phonon contribution is weakly dependent on the temperature [19], and *increase* at high T. Indeed, based on this naive expectation, this type of unconventional T dependence has been often used to *rule out* phonons. Here, however, we see clearly that this reasoning is not justified. Moreover, this type of unconventional enhancement of the electron phonon interaction below a characteristic temperature scale is actually expected for other systems such as spin-Peierls systems or charge density wave (CDW) systems. Thus, our results put an important constraint on the nature of the electron phonon interaction in these systems.

In Figure 3 we report a quantitative comparison of the isotopes-induced changes in peak positions and line shapes. Panel a shows the momentum dependence of the high-energy isotope-induced changes of the EDC peak positions, plotted as a function of the superconducting energy gap (Δ). Clearly the isotope induced changes increase as the antinodal direction is approached, consistent with the observations made above with Figures 1 and 2. Additionally there is a strong correlation of the isotope-induced change of the dispersion with the momentum dependence of the superconducting gap [11]. This observation strongly suggests that the high-energy states are correlated with the superconducting transition.

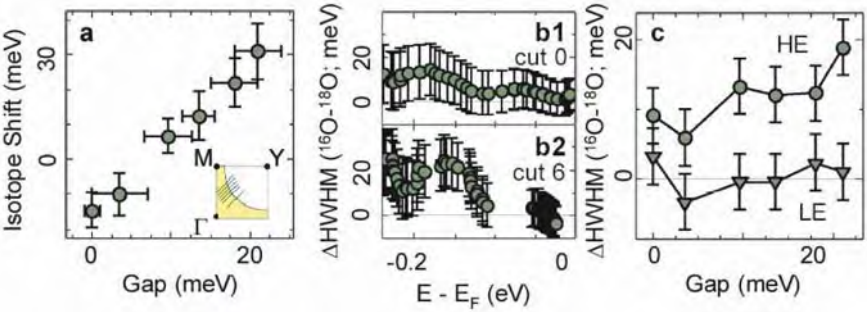

Figure 3. (a) The isotope shift of the high energy EDC vs. the superconducting gap (Δ), for the 6 cuts shown in Fig. 1. The isotope shift is measured at the same energy (220 meV, isotope average) for all cuts. The superconducting gap is the average value between the two isotope samples. (b) The isotope difference of the EDC widths for cuts 0 and 6. The width is measured in HWHM, on the low energy side of each EDC, i.e. between the peak position and the Fermi energy. The horizontal axis corresponds to the peak position at which the isotope difference of the width was extracted. (c) Isotope difference for each cut, averaged and plotted as a function of the isotope-averaged superconducting gap. HE (circles) refers to average over high energy (-220 meV to -70 meV) and LE (triangles) refers to average over low energy (-70 meV to 0).

In panels b1 and b2 we show the difference of the EDC widths between the two isotopes, as a function of energy (peak position), for the nodal and antinodal cuts respectively (cuts 0 and 6). The difference is taken in the superconducting state. For the measure of the width, the FWHM on the low energy side is used since the FWHM on the high-energy side is difficult to extract due to the strong high-energy intensity tail. We observe that the isotope-induced changes in both cases turn on gradually above ≈60meV, which corresponds to the kink position. This effect may already be observed qualitatively in Figure 1, and coincides with the other two phenomena discussed with that figure, namely sudden broadening of EDC peak and sudden increase of the isotope effect of EDC dispersion as energy increases

beyond the kink energy. Clearly the effect is stronger in the antinodal direction (panel b2) where the total isotope-induced narrowing of the peak width is by a factor of two bigger than for the nodal direction. To study the details of the momentum dependence of the incoherent peak width upon isotope substitution, in panel c we report FWHM of the high-energy isotope-induced changes versus superconducting gap. The overall trend is an increase of the effect as the antinodal is approached (large gap). On the other hand, in the low energy part, the isotope dependence of the width is negligible and slightly dependent of the momentum (i.e. superconducting gap). There are two major important observations from these analyses. The first is that there is overall a narrowing of the peak width upon isotope substitution. Such narrowing could be due to multi-phonon contribution [11]. In addition the narrowing of the peak becomes stronger as we approach the antinode. This result clearly suggests that low energy quasi-particles are more heavily dressed in the superconducting state and near the anti-nodal region. The strong isotope dependence means that phonons are an important part of this dressing.

3. IMPLICATIONS OF THE ANOMALOUS ISOTOPE EFFECT TO SUPERCONDUCTIVITY

In conclusion our data clearly point to a picture where the electron dynamics is strongly renormalized by interaction with the lattice. Further, this renormalization has a strong correlation with the superconducting gap, since it is large in the anti-nodal region and at low temperature. In terms of energy dependence, the renormalization of the quasiparticle dynamics is strongest in the energy window of J to 2J, where J is the anti-ferromagnetic exchange interaction, and is reduced for larger energies [11]. Thus, the energy region where phonons are active coincides with the energy region dominated by the strong electron correlation. This is strongly suggestive that there is a cooperative interplay between the two degrees of freedom, lattice and spin. Specifically, we have proposed [11] that the dynamic spin-Peierls physics [20] summarizes the essence of our results, and is responsible for the enhanced electron-phonon interaction at low temperature.

In view of this scenario, it is expected that the exchange interaction J is affected by the isotope substitution.

ACKNOWLEDGMENTS

We would like to thank Dung-Hai Lee for useful discussions. H. Takagi and T. Sasagawa for providing us with high quality oxygen isotope substituted single crystals and J. Graf for experimental help. This work was supported by the Department of Energy's Office of Basic Energy Science, Division of Materials Sciences and Engineering Contract No. DEAC 03-76SF00098; the National Sciences Foundations, Grant No. DMR-0349361 and the Alfred P. Sloan Foundation.

REFERENCES

1. *International Conference on Stripes, Lattice Instabilities and High Tc Superconductivity*, edited by A. Bianconi and N. L. Saini, J. Supercond. 10, no.4 (1997); *Lattice effect in High Tc superconductors* edited by Y. Bar-Yam, T. Egami, J. Mustre de Leon and A. R. Bishop (World Scientific, Singapore 1992)
2. E. Maxwell. *Phys. Rev*. **78**, 477 (1950).
3. M. K. Crawford, *et al*. *Science* **250**, 1390 (1990)
4. For a review see J. P. Franck in *Physical Properties of High Temperature Superconductivity IV*, edited by D. S. Ginsberg (World Scientific Singapore, 1994).
5. T. H. Geballe *et al*. *Phys. Rev*. **78**, 275 (1961); J. W. Garland *Phys. Rev. Lett*. **11**, 114 (1963).
6. A. Lanzara, P. V. Bogdanov, X. J. Zhou, S. A. Kellar, D. L. Feng, E. D. Lu, T. Yoshida, H. Eisaki, A. Fujimori, K. Kishio, J. I. Shimoyama, T. Noda, S. Uchida, Z. Hussain, Z. X. Shen, *Nature* **412**, 510-514 (2001).
7. A. Lanzara, *et al*. *J. Phys. Condens. Mat.* **11**, L541-L544 (1999).
8. D. R. Temprano *et al. Phys. Rev. Lett*. **84**, 1990 (2000)
9. G. M. Zhao, H. Keller and K. Conder, *J. Phys. Condens. Matt.* **13**, R569 (2001) and references therein
10. C. Bernhard, T. Holden, A. V. Boris, N. N. Kovaleva, A. V. Pimenov, J. Humlicek, C. Ulrich, C. T. Lin and J. L. Tallon, *Phys. Rev. Lett*. 69, 052502 (2004)
11. G. H. Gweon, T. Sasagawa, S. Y. Zhou, J. Graf, H. Takagi, D. H. Lee and A. Lanzara. *To be published* Nature (2004)
12. D. S. Dessau, *et al*. *Phys. Rev. Lett.* **66**, 2160-2163 (1991)
13. Z. –X. Shen and J. R. Schrieffer, *Phys. Rev. Lett.* **78**, 1771-1774 (1997)
14. M. R. Norman, *et al*. *Phys. Rev. Lett.* **79**, 3506-3509 (1997)
15. P. V. Bogdanov, A. Lanzara, S. A. Kellar, X. J. Zhou, E. D. Lu, W. J. Zheng, G. Gu, J. I. Shimoyama, K. Kishio, H. Ikeda, R. Yoshizaki, Z. Hussain and Z. X. Shen, *Phys. Rev. Lett*. **85**, 2581-2584 (2000)
16. G.-H. Gweon, S. Y. Zhou, J. Graf, T. Sasagawa, H. Takagi, A. Lanzara in preparation)
17. M. R. Norman, M. Randeria, H. Ding, and J. C. Campuzano, *Phys. Rev. B* **52**, 615-622 (1995)
18. X. J. Zhou, *et al*. *Nature* **423**, 398 (2003)
19. D. J. Scalapino, in *Superconductivity* (ed. Parks, R. D.) 449 (Marcel Dekker, New York, 1969)
20. E. Pytte *Phys. Rev. B* **10**, 4637–4642 (1974)

DIRECT ARPES AND T_C ENHANCEMENT IN COMPRESSIVELY STRAINED LSCO-214 FILMS

Davor Pavuna*, Mike Abrecht, Daniel Ariosa, Dominique Cloetta
Institute of Physics of Complex Matter, FSB, Ecole Polytechnique Fédérale de Lausanne (EPFL), CH-1015 Lausanne, Switzerland (* davor.pavuna@epfl.ch)

Abstract: Direct ARPES studies on *in-situ* grown strained LSCO-214 films show striking strain effects on the electronic structure. The Fermi surface (FS) of LSCO-214 evolves with doping, yet changes even more significantly with strain. The compressive strain changes the Fermi surface topology from hole-like to electron-like and causes band dispersion along k_x and the Fermi level crossing before the Brillouin zone boundary, in sharp contrast to the 'usual' flat band remaining ≈30meV below E_F measured on unstrained samples. The associated reduction of the density of states does not diminish the superconductivity; rather, T_c is strongly enhanced (up to factor of two) in compressively strained thin films.

Key words: Cuprates, superconductivity, photoemission, films, strain, T_c, laser ablation

1. INTRODUCTION

In order to truly understand the mechanism of high-T_c superconductivity it is important to combine complementary studies like ARPES (surface) and transport (bulk) on in-house made (systematically monitored and characterized) single crystals and thin films. This was indeed our strategy in this complex field. In general, films of high-T_c oxides are *different* from single crystals even when they are of the highest quality [1-3]. Namely, it is often difficult to fully oxygenate single crystals, and there is always certain amount of growth induced strain (and also disorder) induced in films (at least up to ~25nm). Moreover, most of the crucial ARPES studies were performed on *cleaved* BSCCO-2212 single crystals or films [2] and there is still not sufficient systematic data of equal quality on numerous other

J. Ashkenazi et al. (eds.), New Challenges in Superconductivity: Experimental Advances and Emerging Theories, 9-14.

relevant phases. There are no reports on ARPES on thin oxide films (<30nm), or the role of strain and consequent changes of the electronic structure. The effect of strain in high-T_c cuprates was initially demonstrated by Sato and Naito et. al. (NTT-Tokyo) [4] and Locquet et al (IBM- Rüschlikon) [5] who have shown that in LSCO-214 films can enhance the T_c roughly by about 50%. Bozovic et al. have recently shown that it is important to 'fill' the films with oxygen: this, combined with the growth induced strain, can enhance T_c in LSCO-214 films up to 51K [6]. We were able to confirm the T_c enhancement due to compressive strain in thin LSCO-214 films, and in the first direct ARPES studies (without cleaving the samples) observed some striking effects on the electronic structure.

2. DIRECT PHOTOEMISSION ON HTSC FILMS

Since 1996 we have performed systematic photoemission studies (PES) on *in-situ* grown thin films of high-T_c and related oxides at the Synchrotron Radiation Center (SRC) in Wisconsin. We have successfully solved several non-trivial technical problems inherent in combining the epitaxial film growth by pulsed laser ablation (PLD), usually with 300mbar of oxygen pressure at substrate temperature of ~1030K, with photoemission measurements performed in an adjacent UHV chamber (10^{-10}-10^{-11} Torr) at low temperatures (300-6K). We have optimized an off-axis growth procedure (with deposition rate of only ~1Ås^{-1}) mostly on (100) $SrTiO_3$ substrates and on $SrLaAlO_3$ (SLAO) for strained LSCO films. The result is high epitaxial quality of c-axis oriented films with an in-plane crystal coherence of up to ~1μm [7-11]. We have studied thin cuprate films (down to ~1UC) and fabricated films of manganites and ruthenocuprates. We have mastered the transfer of *in-situ* grown films under vacuum to the adjacent PES chamber and systematically performed core level spectroscopy[11]. A summary of some of the most relevant results was given in a recent article [14,15].

In Figure 1 we schematically illustrate the changes of the Fermi surface (FS) topology with compressive strain: There is an evolution of the FS shape with strain, from the hole-like to the electron-like. This has been convincingly confirmed in our measurements on overdoped LSCO-214 films: while the measurements on the unstrained film give effectively the same ('flat band') spectra as reported by Ino et. al. on scraped single crystals [12], those on strained films unambigously show the band crossing. Therefore, we can confidently consider the data measured on unstrained films as equivalent to those on scraped single crystals. However, the fact that the saddle point near (π, 0) is no longer detected in the strained samples [13-15] is rather surprising since the associated sharp reduction of the DOS

near E_F ("hot spot") according to several models does not favor the T_c enhancement from 38 to 44K, as measured in our optimally doped strained film. This is also consistent with our studies of underdoped and overdoped strained LSCO films discussed at length elsewhere [14,15].

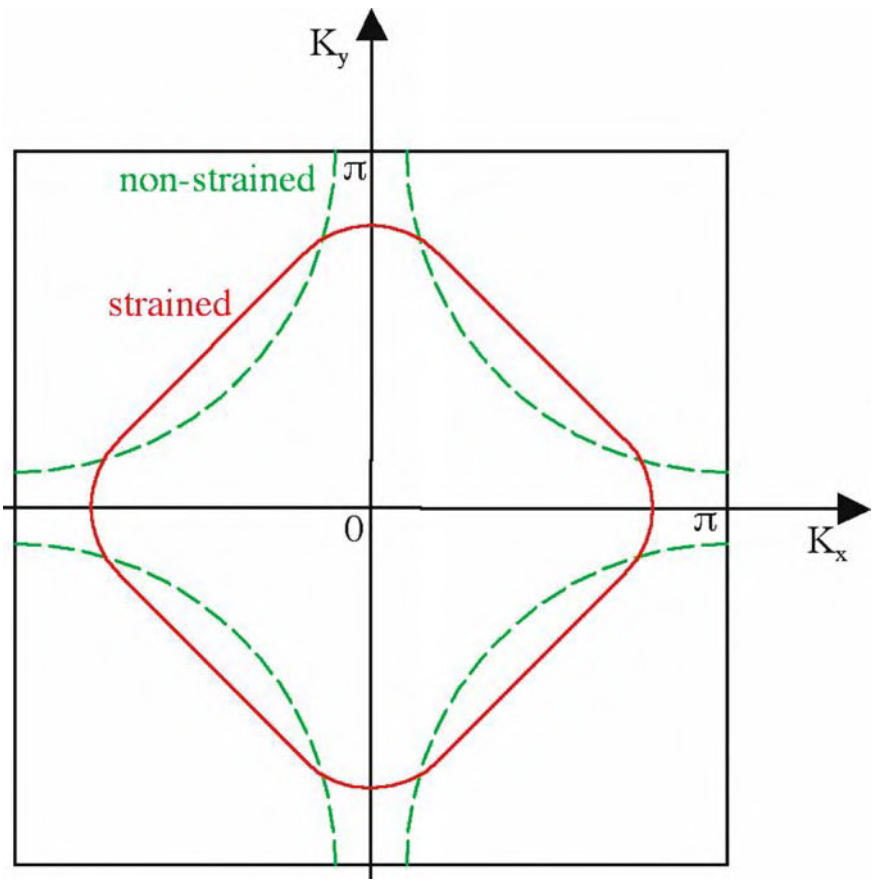

Figure 1: Schematic illustration of the Fermi surface topology change from the 'hole-like' of an unstrained film or single crystal (dashed line) to an 'electron–like' in a thin film grown under compressive strain (straight line) [13-15].

Our results on strained cuprate films seem imply that the changes in density of states may not be the sole explanation of the measured high T_c. However, we note that the nesting may play an important role and recent detailed calculations of the effective band structure of cuprates, taking into account strong correlation effects, seem to accurately reproduce measured energy bands of LSCO-214, Bi2212 and Y-123 [16]. Our experimental results seem to be in accordance with the two-component scenario developed for the inhomogenous cuprate superconductors [17], and our results are evidently closely related to previous measurements of local displacements and doping variations in LSCO-214, critical lattice fluctuations as well as the Hall effect studies of strained LSCO films [18]. Still, more detailed studies are required before we can clearly favor or rule out some of the existing theoretical models.

3. T_C-ENHANCEMENT AND DISCUSSION

As shown in Table 1, T_c is enhanced in all our compressively strained films. What is truly striking is that by using essentially the same growth and oxydation procedure in underdoped (x=0.1) and overdoped (x=0.2) films we essentially double T_c in both cases simply by changing the substrate of the film (thereby altering the compressive strain) [14, 15].

Table 1: Measured critical temperature T_c of the unstrained and compressively strained LSCO-214 films:

Doping, x	**No strain/**T_c(K)	Strain / T_c(K)
0.10	20	40
0.15	38	44
0.20	24	40

It is highly unlikely that the aforementioned changes in the in-plane electronic structure alone (see the discussion in the previous section) can account for the measured T_c-enhancement effects. Especially striking is the case of overdoped films (x=0.2); in that regime, where samples should behave almost as in the Fermi liquid / BCS picture, an enhancement of density of states would be a natural explanation, yet that doesn't seem to be

the case according to our ARPES results [13]. As the compressive strain clearly alters the lattice and increases the c-axis length, one has to take seriously models that take into account the role of the lattice and of the strain (see contributions by authors cited in ref. [17]); it seems difficult to argue that some sort of 'magnetic' mechanism that completely neglects the lattice effects would give such a T_c-enhacement, especially in the overdoped samples, yet this possibility still cannot be ruled out without further work.

4. CONCLUDING REMARKS

In summary, the main success of our new method, direct ARPES on in-situ grown thin films, was demonstrated by the first ever ARPES studies on the low energy electronic structure of any high T_c superconductor under strain. In particular, we have confirmed that the Fermi surface (FS) topology of LSCO-214 evolves with doping toward electron like, yet changes even more significantly with in-plane compressive strain. For a given doping, the FS becomes electron-like for in-plane compressed samples (for all doping values x studied, $0.1<x<0.2$) whereas the FS of non-strained samples are hole-like (except for doping values exceeding $x\approx0.22$) [13-15]. This result is rather surprising since the associated reduction of the density of states near the Fermi level, according to many existing models, does not favor the increase of T_c observed in our films. The carriers from all over the Fermi surface seem to contribute to superconductivity, since T_c-enhancing compressive strain transfers carriers from 'hot spots' to the 'cold spots'.

Further experimental work is evidently needed to clarify some more subtle aspects. Namely, several theorists claim that our ARPES and T_c results [13-15] can be interpreted differently within their proposed models [19]; yet very detailed data sets are needed to prove or disprove such statements. Furthermore, clear evidence of the superconducting gap, a sharp quasiparticle feature, and the variation of the pseudogap of LSCO films with doping and strain will require even better sample control and improved ARPES energy resolution. Moreover, the role of tensile stress in LSCO will is currently studied and the experiments on Bi-2201 compounds are being performed. The latter, in addition to unusually high T^*/T_c ratio, enable us also a direct comparison with numerous published results on cleaved single crystals of the 2212 'reference' phase. We also note that we can in many cases even control the termination of uppermost block of our films. We will ultimately also perform 'usual' substitutions (like Zn or Ni instead of Cu in the cuprate ab-plane) and perform systematic experiments on strained CMR manganite films. In brief, with our *direct*, *in-situ* ARPES on cuprate films a milestone has been set for a different, *complementary* type of photoemission spectroscopy studies which will certainly receive in the coming years, more

attention from the photoemission, thin films and nanotechnology communities, as well as the beam scientists at newly built synchrotrons.

ACKNOWLEDGEMENTS

We gratefully acknowledge financial support by the EPFL and the Swiss National Fond for Scientific Research. This work is based upon research conducted at the Synchrotron Radiation Center, University of Wisconsin-Madison, which is supported by the NSF under Award No. DMR-0084402. DP gratefully acknowledges many stimulating discussions with numerous friends and colleagues within condensed matter community worldwide.

REFERENCES

1. J. Bok, G. Deutscher, D. Pavuna, S.A. Wolf (eds.): *The Gap Symmetry and Fluctuations in High-T_c Superconductors*, NATO-ASI B371, Kluwer (1998)
2. D.W.Lynch, C.G.Olsen *Photoemission Studies of High-T_c Superconductors* Cambridge (1999)
3. I. Bozovic and D. Pavuna (eds): "*Oxide Superconductor Physics and Nano-engineering III, IV, V''* SPIE - vols. 3481 and 4058 - Bellingham (1998, 2000, 2002)
4. H. Sato and M. Naito, Physica C **274** 221 (1997)
5. J.P. Locquet et.al., Nature **394**, 453 (1998)
6. I. Bozovic et. al. Phys. Rev. Lett. **89** (10) 107001-1 (2002)
7. We gratefully acknowledge the input of M. Onellion, T. Schmauder and X.X. Xi who have actively participated in the first 4 years of this work
8. M. Abrecht, D. Ariosa, M. Onellion, G. Margaritondo and D. Pavuna, J. of Appl Phys vol. 91, no.3; 1187 (2002)
9. D. Ariosa et al., *Proc. SPIE* **4058**, 129 (2000)
10. M. Abrecht et al., *Surface Rev. Lett.* **7,** 495 (2000)
11. M. Abrecht, D. Ariosa, D. Cloetta, G. Margaritondo, D. Pavuna: vol. 4811, SPIE, Bellingham (2002)
12. A. Ino *et al.*, Phys. Rev. B **65**, 094504/1-11 (2002)
13. M. Abrecht et al, Phys. Rev. Lett. 91, 057002 (2003)
14. M. Abrecht's D.Sci.Thesis (EPFL 2003) and updates can be downloaded from the web page: http://ipmc.epfl.ch/page31440.html
15. M. Abrecht et al, JPCS **65**, (8-9) 1391 (2004)
16. I. Mrkonjic and S. Barisic, EuroPhysics Journal B **34**, 69 (2003)
17. K.A. Müller, A. Bianconi, A. Boussman-Holder, A.Bishop, T. Egami, D. Mihailovic, J. Ashkenazi, J.C. Phillips personal communications (2004)
18. N.L. Saini, H. Oyanagi, V. Scagnoli, T. Ito, K. Oka, A. Bianconi, EPL 63, 128 (2003)
19. Independently Ole Andersen, Stewart Barnes, Julien Bok (among others) argue that their respective models offer somewhat different yet correct explanation of our measurements.

FULL FERMI SURFACE OF A HIGH TEMPERATURE SUPERCONDUCTOR REVEALED BY ANGULAR MAGNETORESISTANCE OSCILLATIONS

Full Fermi surface of a high-T_c superconductor

N. E. HUSSEY[1], M. ABDEL-JAWAD[1], A. CARRINGTON[1], A. P. MACKENZIE[2] AND L. BALICAS[3]

[1]*H. H. Wills Physics Laboratory, University of Bristol, Tyndall Avenue, Bristol, BS8 1TL, UK*
[2]*School of Physics and Astronomy, University of St. Andrews, St. Andrews, Fife, UK*
[3]*NHMFL, Florida State University, Tallahassee, Florida 32306, USA*

We report the first observation of polar angular magnetoresistance oscillations in the high-T_c cuprate $Tl_2Ba_2CuO_6$. These measurements establish the existence of a coherent three-dimensional Fermi surface on the overdoped, superconducting side of the cuprate phase diagram, even in materials with extreme electrical anisotropy. Detailed analysis of the oscillations reveals that *c*-axis dispersion vanishes at specific symmetry points. This observation has implications for our understanding of a wide range of unusual metallic and superconducting properties of cuprates.

Key words: High-T_c cuprate, Fermi surface,

1. INTRODUCTION

To many, the high-T_c superconductors represent perhaps the most striking example to date of the breakdown of Landau's Fermi-liquid description of metals. One of the fundamental signatures of a Fermi-liquid is a Fermi surface, the locus in reciprocal space of long-lived quasi-particle excitations that govern the electronic properties at low temperatures. In conventional metals, these excitations have well-defined momenta with components in all three dimensions. The failure to unambiguously observe such an entity in the

J. Ashkenazi et al. (eds.), New Challenges in Superconductivity: Experimental Advances and Emerging Theories, 15-20.

cuprates, coupled with their unusual, highly 2D electronic properties above T_c, have led to an intensive theoretical search for novel (strongly correlated) electronic ground states in two dimensions.

Polar angular magnetoresistance oscillations or AMRO [1] have been used extensively to probe the topology of the Fermi surface in other layered metals, particularly the organics. The applicability of AMRO to the cuprates however has been hampered principally by their large scattering rates and the correspondingly small probability of cyclotron motion. With this in mind, we set out to observe AMRO in crystals of the cleanest cuprate (overdoped $Tl_2Ba_2CuO_{6+\delta}$ (Tl2201)) using the world's highest persistent magnetic field (45 Tesla) [2]. The simple band structure of Tl2201 [3], coupled with an absence of additional conducting elements, e.g. CuO chains, makes interpretation of any AMRO data in principle straightforward.

Tl2201 crystals (typical dimensions 0.2 x 0.1 x 0.02 mm^3) were mounted in a quasi-Montgomery configuration and the resultant zero-field c-axis resistivity curves ρ_c were found to exhibit good metallicity despite a large resistive anisotropy $\rho_c/\rho_{ab} > 1000$. The high-field magnetoresistance measurements were carried out inside a ^{3}He cryostat inserted into the 45T Hybrid magnet at the NHMFL in Florida, USA.

2. RESULTS AND DISCUSSION

Fig. 1A shows AMRO data $\Delta\rho_c(\phi, \theta)$ for one crystal ($T_c \sim 20$K) taken at 4.2K and 45T. Similar features were observed in 6 other crystals. The different traces represent polar AMRO sweeps at given azimuthal angles ϕ relative to the Cu-O-Cu bond direction ($\{k_x, k_y\} = (\pi, 0)$). Each sweep contains significant θ-dependent structure that is summarised as follows. (i) a sharp dip in ρ_c at $\theta = 90^o$ for low ϕ, which we attribute to the onset of superconductivity at angles where $H_{c2}(\phi, \theta)$ is maximal, (ii) a broad peak around $\boldsymbol{H}//ab$ ($\theta = 90^o$) that is maximal for $\phi \sim 45^o$, consistent with previous *azimuthal* AMRO studies in overdoped Tl2201 [4], (iii) a small peak at $\boldsymbol{H}//c$ ($\theta = 0^o$) and (iv) a second peak in the range $25^o < \theta < 45^o$ whose position and intensity vary strongly with ϕ.

Such strong θ- and ϕ-dependence can only arise from a coherent open Fermi surface with significant in-plane anisotropy. The Fermi surface of such a quasi-two dimensional metal is most elegantly expressed in the form of an expansion in cylindrical coordinates [5]:

$$k_F(\phi,\kappa) = \sum_{\substack{m,n=0 \\ n\,\text{even}}} k_{mn} \cos n\kappa \begin{cases} \cos m\phi & (m \bmod 4 = 0) \\ \sin m\phi & (m \bmod 4 = 2) \end{cases} \quad (1)$$

where $\kappa = k_z d$ and d is the interlayer spacing (= 1.16 nm for Tl2201). The crystal structure of monolayer Tl2201 has the tetragonal I4/mmm representation with consecutive CuO_2 layers being displaced by half a unit cell. This body-centred-tetragonal symmetry of the crystal lattice imposes certain symmetry constraints on the resultant Fermi surface, namely that coefficients k_{mn} are non-zero only for n even and m divisible by 4, or for n odd and $m$mod4 = 2 [5]. Following the standard procedure for a series expansion, we proceed by expanding to the lowest order necessary to satisfy these constraints and fit to the data.

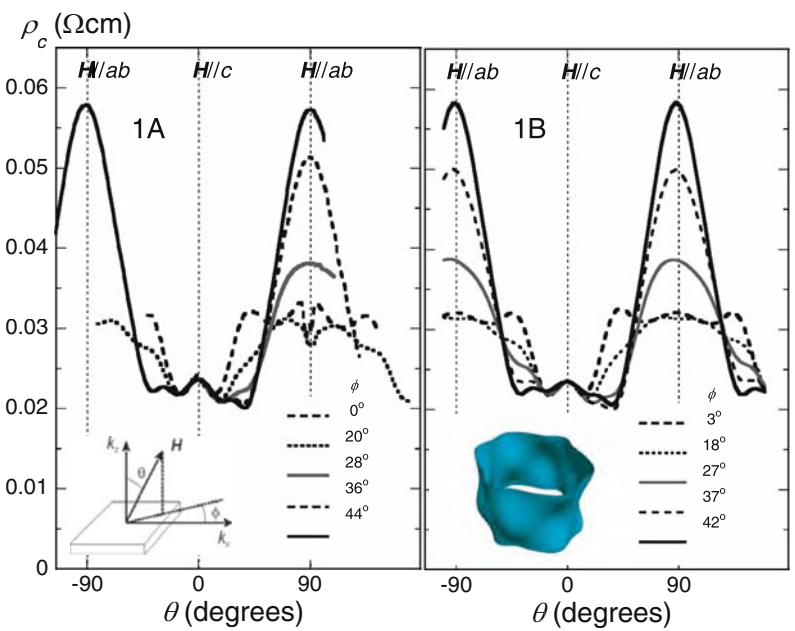

FIGURE 1. Experimental (A) and simulated (B) polar AMRO data for overdoped Tl2201 (T_c = 20K). A schematic of the experimental geometry (A) and resultant Fermi surface (B) are shown as insets.

In order to simulate the experimental data, we calculated $\Delta\rho_c(\phi, \theta)$ using the Shockley-Chambers tube-integral form of the Boltzmann transport

equation modified for a Q2D metal. $\omega_c\tau$ is another free parameter that sets the magnitude, but not the angular dependence, of the oscillations and is set to $\omega_c\tau = 0.45$, the value which best matched the overall scale of the AMRO. As shown in Figure 1B, excellent overall agreement with the experimental data was found with the following combinations of harmonic terms $k_F(\phi,\kappa) = k_{00} + k_{40}\cos4\phi + \cos\kappa(k_{21}\sin2\phi + k_{61}\sin6\phi + k_{101}\sin10\phi)$ with $k_{00} = 7.45$, $k_{40} = -0.19$, $k_{21} = 0.031$, $k_{61} = 0.022$ and $k_{101} = -0.0085$. All k_{mn} coefficients are expressed in units of nm^{-1}. Note that the aymmetry in the AMRO signal, due to slight misalignment of the crystal in the rotating plane, has also been accounted for in the fitting procedure. The absolute values of k_{21}, k_{61} and k_{101} were estimated from the resistive anisotropy ($\rho_c/\rho_{ab} \sim 1000$) and have an associated error in their relative values of order $\pm$10%. Some contributions to AMRO were neglected in our calculation of $\Delta\rho_c(\phi, \theta)$, such as in-plane anisotropy in τ and v_F, but since these are likely to be small in such an overdoped cuprate, we believe that the above expression represents a robust empirical determination of the Fermi surface dispersion of Tl2201. As a consistency check on our fitting procedure, $\omega_c\tau$ was estimated independently from in-plane measurements of the Hall coefficient R_H and resistivity ρ_{ab} on similarly doped crystals [6]. Given $R_H \sim 8$ (1) x 10^{-8} m^3C^{-1} and $\rho_{ab} \sim 8$ (2) $\mu\Omega$cm, we find $\omega_c\tau = B\sigma_{xy}/\sigma_{xx} = BR_H/\rho_{ab} \sim 0.45$ (0.1) in 45 Tesla, in agreement with our AMRO analysis.

The overall shape of the Fermi surface, shown schematically in Fig. 1B, is consistent with features of band structure calculations for optimally doped Tl2201 [3] and other cuprates [7] using the local density approximation. The Fermi surface occupies around 62% of the first Brillouin zone, equivalent to a hole doping per Cu atom of $p = 0.24$. Moreover, the particular form of $k_F(\phi)$ is consistent with the tetragonal symmetry of Tl2201 and gives the FS the appearance of a slightly rounded square within the *ab*-plane. The peak observed at $\boldsymbol{H}//c$ coupled with the remarkable sensitivity of our analysis to fine details in the *c*-axis warping provides compelling evidence that coherent motion takes place between adjacent planes in overdoped Tl2201.

Fig. 2 shows our empirically determined Tl2201 Fermi surface projected onto the *ab*-plane in order to highlight the in-plane variation of the *c*-axis hopping integral $t_\perp(\phi)$. Significantly, *c*-axis dispersion is found to vanish along eight specific symmetry lines of the Brillouin zone, in the so-called nodal directions along (π, π), where the in-plane quasiparticles are longest-lived, *and* in the anti-nodal regions (π, 0), where in-plane scattering is most intense and quasiparticles (at optimal doping and below) are incoherent above T_c [8]. In the superconducting state, the nodes in $t_\perp(\phi)$ also coincide with the gap nodes of the *d*-wave superconducting order parameter [9].

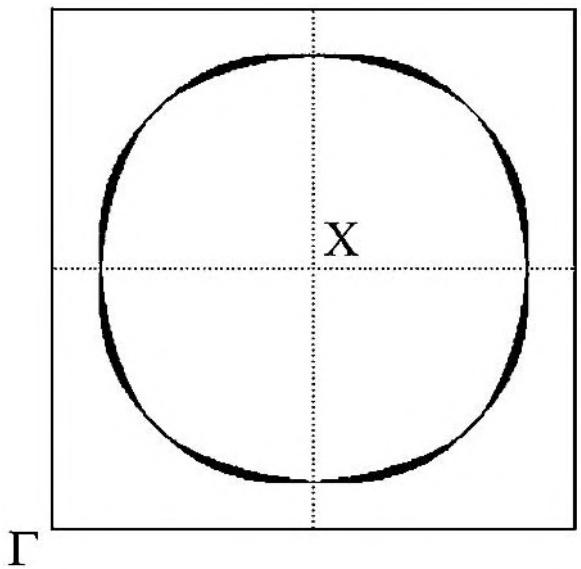

FIGURE 2. Projection of the deduced Fermi surface of Tl2201 onto the *ab*-plane. The magnitude of the *c*-axis warping has been increased three-fold to emphasise the 8 loci where k_z dispersion vanishes. The Brillouin zone has also been simplified as to accommodate the full *ab*-plane projection.

Recognition of the role of oxygen bonding and virtual Cu 4s orbitals in *c*-axis conduction led to a well-known prediction [7] of the existence of dispersive nodes in tetragonal cuprates. These dispersive nodes have formed an integral part of numerous theoretical treatments of the physics of high-T_c cuprates, in both the normal and superconducting states, but until now their presence had never been directly confirmed experimentally. This locally non-dispersive structure has been invoked, for example, to explain the striking differences observed between the in- and out-of-plane normal state conductivities $\sigma_{ab}(\omega,T)$ and $\sigma_{\perp}(\omega,T)$ [10,11] and the in- and out-of-plane penetration depths $\lambda_{ab}(T)$ and $\lambda_{\perp}(T)$ [12]. This information about the warping structure should also prove invaluable to the interpretation of several other important experimental techniques, including scanning tunnelling microscopy and *c*-axis tunnelling, which rely heavily on knowledge of *c*-axis tunnelling matrix elements.

3. CONCLUSIONS

The observation of AMRO in the overdoped cuprate $Tl_2Ba_2CuO_{6+\delta}$ establishes the existence of a coherent three-dimensional Fermi surface in high-T_c cuprates and represents a significant challenge to models of high-T_c superconductivity based on purely 2D electron motion within the CuO_2 planes. Whilst Tl2201 at this level of doping clearly comes from the side of the phase diagram in which more conventional behaviour is observed [13], it is still a high-T_c superconductor (T_c ~ 20K). Moreover, its normal state resistive anisotropy (ρ_c/ρ_{ab} ~1000) is actually *larger* than that seen in some optimally doped materials, suggesting that the findings reported here will apply to a wide range of the superconducting phase diagram.

The Fermi surface shows many features consistent with band structure calculations, including the vanishing of *c*-axis dispersion along certain symmetry points in the Brillouin zone. This anisotropic warping structure offers a natural explanation of several features of the high-T_c physics that were previously considered as anomalous. Finally, these measurements reveal that the superconducting cuprates at high doping levels can be understood within a model of the normal state based around fermionic quasiparticles, in common with other studies of Tl2201 [14]. How and where this model breaks down as the Mott insulator is approached at half-filling remains an important outstanding issue. However, in providing crucial information on the dimensionality of the conducting planes, AMRO may prove to become the ideal complementary probe to ARPES in exploring this evolution of the electronic ground state in cuprates across the phase diagram.

REFERENCES

[1] K. Yamaji, J. Phys. Soc. Japan **58**, (1989) 1520.
[2] N. E. Hussey *et al*., Nature (London) **425**, (2003) 814.
[3] D. J. Singh and W. E. Pickett, Physica **203C**, (1992) 193.
[4] N. E. Hussey *et al*., Phys. Rev. Lett. **76**, (1996) 122.
[5] C. Bergemann *et al*., Phys. Rev. Lett. **84**, (2000) 2662.
[6] A. P. Mackenzie *et al*., Phys. Rev. B. **53**, (1996) 5848.
[7] O. K. Andersen *et al*., J. Phys. Chem. Solids **56**, (1995) 1573.
[8] N. E. Hussey, Euro. Phys. J. B **31**, (2003) 495.
[9] For a review, see N. E. Hussey, Adv. Phys. **51**, (2002) 1685.
[10] L. B. Ioffe and A. J. Millis, Phys. Rev. B **58**, (1998) 11631.
[11] D. van der Marel, Phys. Rev. B **60**, (1999) R765.
[12] T. Xiang and J. M. Wheatley, Phys. Rev. Lett. **76**, (1996) 4632.
[13] S. Nakamae *et al*., Phys. Rev. B **68**, (2003) 100502(R).
[14] C. Proust *et al*., Phys. Rev. Lett. **89**, (2002) 147003.

SUM RULES and ENERGY SCALES in BiSrCaCuO

A.F. Santander-Syro, R.P.S.M. Lobo, N. Bontemps
Laboratoire de Physique du Solide (UPR5 CNRS) ESPCI
10 rue Vauquelin, 75231 Paris cedex 05, France
nicole.bontemps@espci.fr

Abstract From very high accuracy reflectivity spectra, we have derived the optical conductivity and estimated the spectral weight up to various cut-off frequencies in underdoped $Bi_2Sr_2CaCu_2O_{8+\delta}$ (Bi-2212). We show that, when evaluating the optical spectral weight over the full conduction band (1 eV), the kinetic energy decreases in the superconducting state, unlike in conventional BCS superconductors. As a consequence, the Ferrell-Glover-Tinkham sum rule is not satisfied up to this energy scale. This stands as a very unconventional behavior, contrasted with the overdoped Bi-2212 sample.

Keywords: High Tc superconductors, infrared conductivity, spectral weight

Introduction

A long lasting debate about the cuprate superconductors, stems from the differences and similarities with BCS behavior. The actual pairing mechanism, which eventually results in lowering the free energy of the system, is not yet known. In BCS superconductors, the free energy gain results from a competition of electronic kinetic energy increase and an eventually larger potential energy decrease. If the free energy in cuprates can be (somewhat arbitrarily) separated between potential and kinetic energy [1, 2], then the latter is measured by optics [3, 4]. The kinetic energy can be inferred from the partial sum rule or spectral weight W, defined as:

$$W(\Omega) = \int_0^{\Omega} \sigma_1(\omega, T) d\omega \tag{1}$$

where $\sigma_1(\omega, T)$ is the frequency (ω) and temperature (T) dependent conductivity, and Ω is a cut-off frequency. Setting $\Omega = \Omega_B$, where Ω_B is the conduction band widht, one can get the kinetic energy E_k per copper site [4], through:

$$W(\Omega_B) = \frac{\pi}{2} \frac{e^2}{\hbar^2} \frac{a^2}{V_u} [-E_k] \tag{2}$$

J. Ashkenazi et al. (eds.), New Challenges in Superconductivity: Experimental Advances and Emerging Theories, 21-26.

where a is the lattice parameter, and V_u the volume per Cu site.

In the superconducting state, the integral in eq.1 or 2 includes the contribution of the superfluid, i.e. the weight of the $\delta(\omega)$ function centered at zero frequency. The Ferrell-Glover-Tinkham (FGT) sum rule [5, 6] requires that the spectral weight lost at finite frequency in the superconducting state must be retrieved in the spectral weight W_s of the δ function. In conventional superconductors, it was found to be fulfilled if integrating up to $\hbar\Omega_0 \sim 4\Delta$ (Δ is the superconducting gap). $\hbar\Omega_0$ is a characteristic energy of the boson spectrum responsible for the pairing mechanism. The FGT sum rule would then be exhausted for cuprates, if conventional, for $\hbar\Omega_0 \sim 0.1$ eV (assuming $\Delta \sim$ 25 meV) [7, 8].

The studies of the FGT sum rule, first performed from c-axis (interlayer) optical conductivity data, showed a strong violation, interpreted as a change of interlayer kinetic energy [3, 9]. However, the amount of kinetic energy saving which was found is too small to account for the condensation energy. Although *in-plane* data appeared firstly to yield a conventional behavior [9], these early results were subsequently contradicted by ellipsometric and infrared data [10]. Our own infrared-visible reflectivity experiments, in Bi-2212, showed that in-plane spectral weight lost from the visible range is transferred into the δ function [11]. These two independent sets of data yielded a *decrease* of kinetic energy below T_c of the order of 1 meV.

The present paper implements our previous report [11] by using the *partial sum rule* in Eq.2. Although this is in principle equivalent to the FGT sum rule, we found this method to be more robust, because we can trace the entire temperature evolution of the spectral weight. We focus here on the underdoped thin film from the Bi-2212 family. We pin down the raw reflectivity data which allows to establish small changes at high energy (up to 10000 cm^{-1}) in the conductivity, hence in the spectral weight, thus illustrating why our unprecedented resolution is a necessary condition to trace this phenomenon. Our present, more elaborate analysis confirms that within error bars, the in-plane kinetic energy, calculated from Eq.2, decreases in the superconducting state. Using the partial sum rule in Eq.2 (and not only the FGT sum rule, as in [11]) shows qualitatively the opposite, conventional behavior in the case of the overdoped sample [12].

1. Experimental results

Reflectivity spectra, recorded in the range 30-25000 cm^{-1} for 15 temperatures between 300 K and 10 K, are reported elsewhere [13]. An example is recalled in Fig.1, for selected temperatures, up to 3000 cm^{-1}, for the underdoped sample (T_c=70 K). Most of the change with temperature occurs below 1000 cm^{-1}. However, the difference between the spectra at 10 K and 100 K

extends up to 5000 cm^{-1}, displaying a reflectivity increase in the superconducting state of 0.3%, in this range, to be compared to the 4% increase below 1000 cm^{-1} (see inset of fig.1).

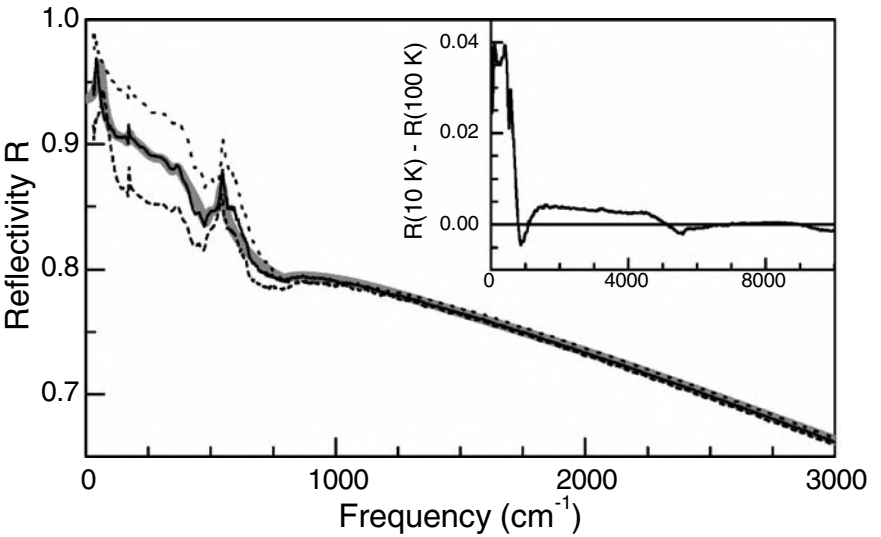

Figure 1. Reflectivity spectra in the 0,3000 cm^{-1} range at three temperatures: 200 K: dashed, 100 K: solid, 10 K: dotted line. The thick gray line is the fitted spectrum at 100 K. Inset: difference R(10 K)- R(100 K) between the reflectivity at 10 K and 100 K.

A standard thin film fitting procedure was applied in order to derive the optical conductivity [13, 14]. The fit is accurate enough so as to reproduce within less than 0.1 %, the small reflectivity difference between 100 and 10 K. This illustrates the accuracy of our data *and* analysis. A Kramers-Kronig based argument shows that such a small difference in reflectivity over a given frequency range $\Delta\omega$ results into changes in conductivity extending over a frequency range 2-3 $\Delta\omega$ [14]. The changes of spectral weights over an unusually large frequency range (possibly up to 16000 cm^{-1} as discussed further), arises from this general argument. Without the ability of resolving 0.1 % in the reflectivity, the results to be described further could not possibly be firmly established. The optical conductivity is shown in Fig.2, in the same frequency range and the same temperatures as in Fig.1.

2. Kinetic energy

From the optical conductivity, we compute the spectral weight or partial sum rule defined in Eq.1. We show in Fig3-a and -b the temperature variation

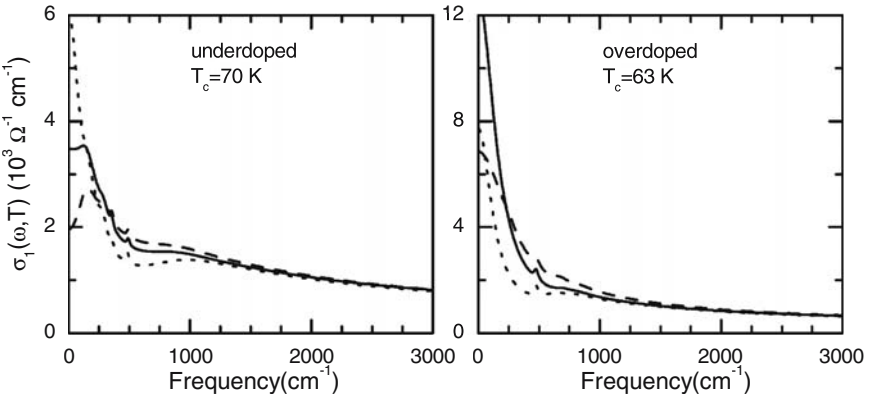

Figure 2. Real part $\sigma_1(\omega, T)$ of the optical conductivity, for the underdoped and overdoped (for comparison) samples. Temperatures are the same as in fig.1. Note that, in the former, [a] very large Drude-like contribution persists in the superconducting state.

of the spectral weight for selected cut-off frequencies Ω ranging from 500 to 8000 cm^{-1}, both for the underdoped sample (500, 1000, 8000 cm^{-1}), and for the overdoped sample (8000 cm^{-1}). For sake of clarity, we have normalized each spectral weight to its value at 300K. The integration starting from 0^+ , in the superconducting state, does not include the spectral weight W_s of the δ function. We have added below T_c the weight of the superfluid, using the input parameter determined by the best fit [15]. We thus obtain, below T_c, the data represented by the open symbols in Fig.3, hereafter referred to as the *total* spectral weight. We have carefully worked out the accuracy of the data by using various sets of fitting parameters (mainly the superfluid weight and the Drude contribution) and by estimating the uncertainty on each experimental point accordingly. The size of symbols in Fig.3-b has been adjusted so as to represent the uncertainty.

We see in Fig.3-a that, when integrating up to 1000 cm^{-1}, the normal state spectral weight above T_c follows a T^2 increase, as indicated by a dotted line. The total spectral weight exceeds significantly this normal state spectral weight. Considering 1000 cm^{-1} as a conventional energy scale as discussed in the introduction, we are led to conclude that the energy scale over which one must extend the integration, in order to retrieve the spectral weight of the δ function, exceeds significantly any conventional scale. The excess in total spectral weight in the superconducting state, with respect to the normal state, is present throughout the conduction band, i.e. up to typically 1 eV=8000 cm^{-1} (fig.3-b). In this range, the spectral weight follows a T^2 behavior down to 130 K, then levels off. Between the normal (horizontal dotted line) and su-

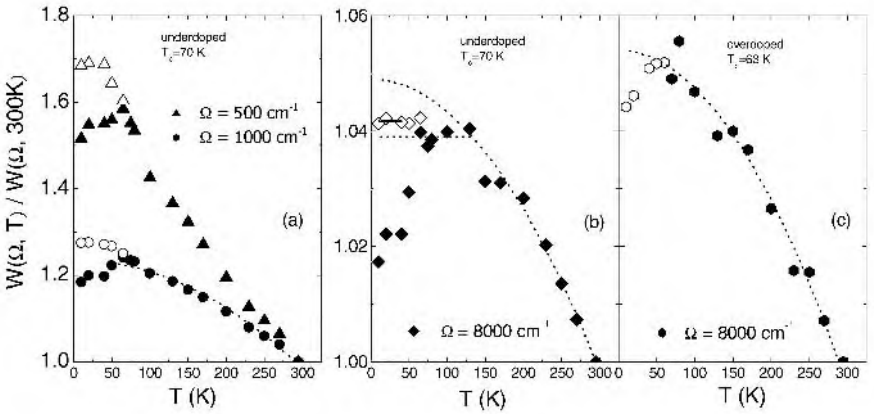

Figure 3. Partial sum rule shown for underdoped (a) and (b), and overdoped (c) samples, for selected cutoff frequencies. Full symbols represent the spectral weight, integrated from 0^+, hence without the superfluid contribution. Open symbols include (below T_c) the superfluid weight. Fig3-b and -c represent the intraband spectral weight, hence $-E_k$, as a function of temperature. The dotted lines are T^2 best fits to the normal state data.

perconducting state (horizontal solid line), we observe a small but definite increase. Equation 2 yields then the change of kinetic energy associated with this change of spectral weight. We find $\Delta E_k = -(0.5 \pm 0.3)$ meV per copper site, thus consistent with our early data [11] and confirming that the onset of superconductivity in the underdoped Bi-2212 sample is associated with a decrease of kinetic energy. In contrast, the overdoped sample displays a very clear decrease of spectral weight when performing the integration up to 8000 cm^{-1} (fig.3-c), i.e. an *increase* of kinetic energy. This is the conventional BCS behavior [17]. In order to make the connection with our earlier work, we now translate briefly these results in terms of the FGT sum rule. The FGT sum rule is fulfilled for the overdoped sample over a conventional range (1000 cm^{-1}) [11]. Conversely, it is *not satisfied* up to 8000 cm^{-1} in the underdoped sample. With our refined analysis, we can set a lower limit of 10000 cm^{-1} and an upper limit of 16000 cm^{-1} for the energy scale required to satisfy the FGT sum rule. Recent work also shows a much larger energy scale for the exhaustion of the FGT sum rule in underdoped YBCO, as compared to the optimal doping [18]. Such large energy scale is difficult to reconcile with a simple phonon mechanism, and seems therefore to call for a different excitation spectrum or more elaborate mechanisms.

Condensation by kinetic energy saving [19, 20] has been considered by several groups, sometimes with reasonable quantitative agreement [19]. Other models have been discussed in order to account for these data [21].

3. Summary

In conclusion, we have shown that according to the doping level in Bi-2212, the onset of superconductivity is associated with a decrease of kinetic energy in the underdoped material, whereas the overdoped material exhibits an increase of kinetic energy. Such a drastic difference confirms that the superconducting state in the underdoped regime of cuprates is unconventional.

Acknowledgments

The authors wish to thank M. Norman for numerous discussions and illuminating remarks, and Z. Konstantinovic, Z.Z. Li and H. Raffy for kindly providing high quality films.

References

[1] S. Chakravarty, H.Y. Kee and E. Abrahams, Phys. Rev. B **82**, 2366 (1999).

[2] R. Haslinger and A. Chubukov, Phys. Rev. B **67**, 140504 (2003).

[3] D.N. Basov *et al.*, Phys. Rev. B **63**, 134514 (2003) and references therein.

[4] M.R. Norman and C.Pépin, Rep. Prog. Phys. **66**, 1547 (2003).

[5] R.A. Ferrell and R.E. Glover, Phys. Rev. **109**, 1398 (1958).

[6] M. Tinkham and R.A. Ferrell, Phys. Rev. Lett. **2**, 331 (1959).

[7] C. Renner *et al.*, Phys. Rev. Lett **80**, 149 (1998).

[8] H. Ding et al, Phys. Rev. **54**, R9678 (1996).

[9] D.N. Basov *et al.*, Science **283**, 49 (1999).

[10] H.J.A. Molegraaf *et al.*, Science **295**, 2239

[11] A.F. Santander-Syro *et al.*, Europhys. Lett **62**, 568 (2003).

[12] A.F. Santander-Syro *et al.*, to be published.

[13] A. Santander-Syro at al. , Phys. Rev. Lett. **88**, 097005 (2002).

[14] http://www.espci.fr/recherche/labos/lps/thesis.htm and A. Santander-Syro at al., to be published.

[15] When a large Drude-like contribution is present, the standard derivation of the superfluid weight from either $\epsilon_1(\omega)$ versus ω^{-2} as in ref. [11] or $\omega\sigma_2(\omega)$ versus ω is biased. The best estimate comes out to be the input value of our fit [16].

[16] M. Norman, private communication

[17] D. van der Marel et al Chapter in "Concepts in electron correlation", Editors A. Hewson and V. Zlatic (KLUWER, 2003) and Condmat/0302169

[18] C.C. Homes et al, Phys. Rev. B **69**, 0024514 (2004)

[19] M.R. Norman and C.Pépin, Phys. Rev. B **66**, 100506(R) (2002). **66**, 100506(R) (2002).

[20] T. Eckl et al, Phys. Rev. B **68**, 014505 (2003); T.A. Maier et al Phys. Rev. Lett. **92**, 027005) (2004).

[21] J. Hirsch and F. Marsiglio, Phys. Rev. B **62**, 15131 (2000) and references therein; L. Benfatto et al, Condmat/0305276; T. Stanescu and P. Phillips, Condmat/0301254;J. Ashkenazi, Coondmat/0308153; J.P. Carbotte and E. Schachinger, Condmat/0404192.

OPTICAL PROPERTIES OF $(Pr,Ce)_2CuO_4$

A. Zimmers,[1] N. Bontemps,[1] R.P.S.M. Lobo,[1] C.P. Hill,[2] M.C. Barr,[2]
R.L. Greene,[2] C.C. Homes,[3] and A.J. Millis[4]
[1] *Laboratoire de Physique du Solide (UPR5 CNRS) ESPCI, 75231 Paris cedex 05, France*
[2] *Center for Superconductivity Research, Department of Physics, University of Maryland, College Park, Maryland 20742, USA.*
[3] *Department of Physics, Brookhaven National Laboratory, Upton, New York 11973, USA.*
[4] *Physics Department, Columbia University, New York, New York 10027, USA.*

Abstract We studied the optical conductivity of electron doped $Pr_{1-x}Ce_xCuO_4$ from the underdoped to the overdoped regime. The observation of low to high frequency spectral weight transfer reveals the presence of a gap, except in the overdoped regime. A Drude peak at all temperatures shows the partial nature of this gap. The close proximity of the doping at which the gap vanishes to the antiferromagnetic phase boundary leads us to assign this partial gap to a spin density wave.

Keywords: Electron doped cuprates, optical conductivity, normal state gap

1. Introduction

The electron and hole doped cuprates phase diagram shows a global symmetry. However, many aspects of the electron doped compounds, including the nature of the superconducting gap, the behavior of the normal state charge carriers, and the presence of a normal state (pseudo)gap are still unclear. A pseudogap phase is now well established on the hole doped side [1]. In $Bi_2Sr_2CaCu_2O_{8+\delta}$, angle resolved photoemission spectroscopy measurements (ARPES) indicate a pseudogap opening along the $(0,\pi)$ direction in k space [2]. However, the in-plane optical conductivity does not show any direct evidence of this pseudogap [3]. The optical conductivity of non superconducting $Nd_{2-x}Ce_xCuO_4$ (NCCO) single crystals ($x = 0$ to 0.125) suggests the opening of a high energy partial gap well above T_{Neel} [4]. Low temperature ARPES reveals a Fermi surface characterized by the presence of pockets [5].

We determined the temperature evolution of the optical conductivity in a set of $Pr_{2-x}Ce_xCuO_4$ thin films. Our data reveals the onset of a "high energy" partial gap below a characteristic temperature T_W which evolves with doping.

J. Ashkenazi et al. (eds.), New Challenges in Superconductivity: Experimental Advances and Emerging Theories, 27-30.

It is clearly detected for 0.13, it is absent down to 20 K for $x = 0.17$ and it has a subtle signature for $x = 0.15$ (optimal doping). The proximity of our samples to the antiferromagnetic phase makes a spin density wave (SDW) gap the natural interpretation for our observations, consistent with ARPES [5].

2. Experimental

The thin films studied in this work were epitaxially grown by pulsed-laser deposition on a $SrTiO_3$ substrate [6]. The samples studied are (i) $x = 0.13$ (underdoped) $T_c = 15$ K (thickness 3070 A), (ii) $x = 0.15$ (optimally doped), $T_c = 21$ K (thickness 3780 A) and (iii) $x = 0.17$ (overdoped) $T_c = 15$ K (thickness 3750 A). All T_c's were characterized by electrical resistance measurements. We checked the $x = 0.15$ sample homogeneity by electron microscopy analysis (using the micron scale X-ray analysis of an EDAX system) and found no dispersion at the micron scale in the Pr, Ce or Cu concentrations. Thin films are easy to anneal but, most important, they can be made superconducting in the underdoped regime, whereas this seems difficult for crystals [4]. Infrared-visible reflectivity spectra (at an incidence angle of 8°), were measured for all the films in the 25–21000 cm^{-1} spectral range with a Bruker IFS-66v Fourier Transform spectrometer within an accuracy of 0.2%. Typically 12 temperatures (controlled better than 0.2 K) were measured between 25 K and 300 K. The far-infrared frequency range (10–100 cm^{-1}) was measured for samples (ii) and (iii) utilizing a Bruker IFS-113v at Brookhaven National Laboratory.

3. Results and Discussion

Figure 1(a) shows the raw reflectivity (R) from 25 to 6000 cm^{-1} for a set of selected temperatures. As the temperature decreases, an unconventional depletion of R appears for $x = 0.13$. This feature, denoted by an arrow, is still visible for $x = 0.15$ as a subtle change in R. Conversely, the reflectivity of the $x = 0.17$ sample increases monotonously with decreasing temperature over the whole spectral range shown. We applied a standard thin film fitting procedure to extract the optical conductivity from this data set [3]. The real part $\sigma_1(\omega)$ of the optical conductivity is plotted in Fig. 1 (b). At low energies, for all concentrations, the Drude-like contribution narrows as the temperature is lowered in the normal state from 300 K to 25 K (Fig. 1 inset). This corresponds to a quasiparticle lifetime increasing in agreement to the metallic behavior of the resistivity. Figure 1(b) shows that the feature in the reflectivity of the $x = 0.13$ sample produces a dip/hump structure in σ_1 with a peak at ~ 1500 cm^{-1}. For $x = 0.15$ the reflectivity behavior is not clearly seen in σ_1. A similar feature was observed in NCCO single crystals only for doping levels where

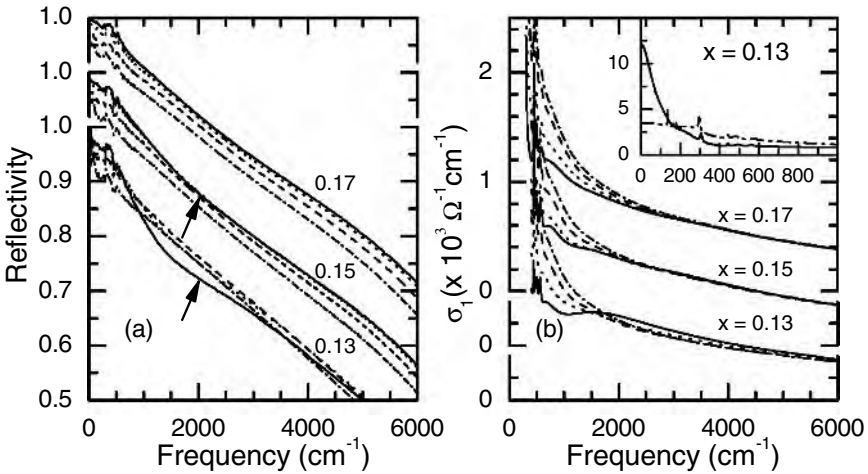

Figure 1. (a) Infrared reflectivity of $x = 0.13$, 0.15 and 0.17 samples. Curves are shifted from one another by 0.1 for clarity. (b) Real part of the optical conductivity from 400 to 6000 cm^{-1}. Curves are shifted by 400 Ω^{-1} cm^{-1}. The inset shows the low energy (0-1000 cm^{-1} free carrier contribution to $\sigma_1(\omega)$ of the x=0.13 sample at 300 K and 25 K. In both panels the temperatures shown are 300 K (dash-dotted); 200 K (dashed), 100 K (dotted) and 25 K(solid).

such crystals are *not superconducting* [4], whereas we observe it in the x=0.13 sample.

4. Partial gap

To understand the dip/hump structure, we define the partial sum rule $W(\omega) = \int_0^\omega \sigma_1(\omega')d\omega'$. Making $\omega \to \infty$ yields the standard f-sum rule $W = \pi ne^2/2m$. When integrated over our full measured spectral range, we find a temperature independent W in all samples. Figure 2(a) shows the normalized temperature dependence $W(2000\text{ cm}^{-1}, T)/W(2000\text{ cm}^{-1}, 300\text{ K})$ for all films. The continuous increase of W with decreasing T observed in the $x = 0.17$ sample is a signature of decreasing scattering rate. In the $x = 0.13$ sample $W(2000\text{ cm}^{-1})$ decreases for $T < 150$ K, corresponding to the opening of a gap. As a Drude peak is present at all T's, we conclude that the gap covers only part of the Fermi surface. The behavior of the $x = 0.15$ sample is intermediate, suggesting a small or broadened gap.

A possible interpretation for the origin of the gap is a commensurate (π, π) spin density wave. It induces a symmetry breaking, folding the Fermi surface upon itself, and a partial gap Δ_{SDW} opens at the intersection of the antiferromagnetic Brillouin zone, creating pockets in the Fermi surface [5].

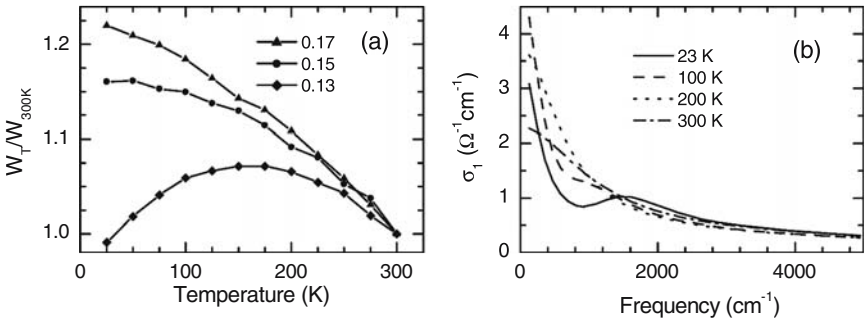

Figure 2. (a) Temperature dependence of partial sum rule for samples with $x = 0.13$, 0.15 and 0.17 integrating σ_1 up to 2000 cm^{-1}. (b) Optical conductivity calculated by a spin density wave model for $x = 0.125$.

Figure 2(b) shows calculations [7] using a Marginal Fermi liquid with parameters chosen to reproduce $\rho(T)$ for $T > 200$ K, combined with a commensurate (π, π) SDW gap opening for $T < 200$ K. The $T = 0$ gap magnitude was adjusted to correctly locate the maximum in σ at $T = 0$. The calculation is seen to reproduce the data fairly well [compare to Fig. 2(b)].

5. Summary

We have measured with great accuracy the reflectivity of electron doped $Pr_{2-x}Ce_xCuO_4$ at various Ce doping levels. An optical conductivity spectral weight analysis shows that a partial gap opens at low temperatures for Ce concentrations up to $x = 0.15$. A spin density wave model reproduces satisfactorily the data.

Research supported in part by NSF-DMR-0102350 (Maryland) and NSF-DMR-0338376 (Columbia).

References

[1] T. Timusk, and B. Statt, Rep. Prog. Phys **62**, 61 (1999).

[2] J.C. Campuzano, M.R. Norman and M. Randeria, condmat/0209476 [to appear in "Physics of Conventional and Unconventional Superconductors", ed. K. H. Bennemann and J. B. Ketterson (Springer-Verlag)].

[3] A. Santander-Syro at al. , Phys. Rev. Lett. **88**, 097005 (2002).

[4] Y. Onose *et al.*, Phys. Rev. B **69**, 024504 (2004).

[5] N. P. Armitage *et al.*, Phys. Rev. Lett. **88**, 257001 (2002).

[6] P. Fournier et al., Physica C **297**, 12 (1998).

[7] A.J. Millis, to be published.

TUNNELING SPECTRA NEAR T_c IN OVERDOPED $Bi_2Sr_2CaCu_2O_{8+\delta}$

M. Oda, Y. Tanaka, A. Hashimoto, N. Momono and M. Ido
Department of Physics, Hokkaido University, Sapporo 060-0810, Japan

Abstract In this article, we focus on the dip structure of tunneling spectra in overdoped $Bi_2Sr_2CaCu_2O_{8+\delta}$ (Bi2212), measured in Bi2212/vaccum/Bi2212 junctions, which are of the superconductor/insulator/superconductor (SIS) type below T_c. It is confirmed that the dip structure appears at voltages $|V| \sim (2\Delta_0+E_{res})/e$ in the SIS type tunneling spectra, where $2\Delta_0$ is twice the d-wave superconducting (SC) gap amplitude and E_{res} the energy of an antiferromagnetic (AF) resonance mode. Furthermore, it is demonstrated that the temperature evolution of the dip structure is in good agreement with that of the AF resonance mode, which also develops below T_c. These results suggest that the tunneling dip structure will be associated with the development of AF resonance mode in accordance with the SC transition.

Keywords: high-T_c superconductor, electronic energy spectrum, tunneling spectroscopy

1. Introduction

One of the striking features for the SC state of $Bi_2Sr_2CaCu_2O_{8+\delta}$ (Bi2212) is a strong suppression of spectral weights for the electronic excitations, the so-called "dip structure" in the electronic energy spectrum, in the energy regions just outside the d-wave SC gap edges ($E = \pm\Delta_0$). It has recently been demonstrated in angle-resolved photoemission spectroscopy (ARPES) and tunneling spectroscopy experiments [1, 2, 3, 4] that the energy difference Ω of the dip from the SC gap edge is almost the same with the characteristic energy E_{res} ($\sim$40 meV) of an antiferromagnetic (AF) resonance mode, which is directly observed in neutron scattering experiments [5, 6] and also seen as the excitation responsible for the sharp onset of scattering in infrared absorption spectra [7]. The AF resonance mode seems to develop markedly in accordance with the SC transition. On the basis of these results, the origin of the dip structure in the electronic energy spectrum has been argued in terms of strong couplings of electrons with the magnetic resonance mode. Interestingly, the Ω and E_{res}values exhibit a hole doping level (p) dependence similar to that of T_c;

J. Ashkenazi et al. (eds.), New Challenges in Superconductivity: Experimental Advances and Emerging Theories, 31-36.

namely, they roughly scale with T_c [1, 4], which will be an important clue for the understanding of the SC transition mechanism.

In this article, we discuss the origin of the dip structure on the basis of tunneling spectra, which were measured in overdoped Bi2212/vaccum/Bi2212 (BVB) junctions fabricated using a scanning tunneling microscope (STM). We have confirmed that Ω is comparable to $E_{\rm res}$ and roughly scales with T_c, and shown that the temperature evolution of the dip structure strongly correlates with that of the AF resonance mode. These facts suggest that the dip structure of tunneling spectra in the SC state will be brought through couplings of electrons with the AF spin excitations.

2. Experiments

Single crystals of Bi2212 were grown by the TSFZ method. The SC critical temperature T_c of the as-grown crystals was ~ 90 K, indicating that their hole-doping level p was nearly optimal ($p \sim 0.18$). The as-grown crystals were annealed at 700°C in a high-pressure (20 atm) oxygen gas; thus, the p value was increased to a slight overdoping one, $p \sim 0.22$, and the T_c value was reduced to 81 K. In the present tunneling experiments, BVB junctions, which are of the superconductor/insulator/superconductor (SIS) type below T_c, were fabricated in an STM system using the fabrication technique that was first achieved in a point-contact tunneling spectroscopy system by Miyakawa *et al.* [8]. The fabrication process was reported in Ref. [9].

3. Results and discussion

3.1 Tunneling characteristics of BVB junction at $T \ll T_c$

A typical example of BVB junction characteristics at $T = 10$ K ($\ll T_c$) is shown in Fig. 1; the upper and lower panels, (a) and (b), are a current-voltage (I-V) curve and the corresponding dI/dV-V curve (tunneling spectrum), respectively. In the inset in Fig. 1 (a), the I-V curve is magnified in the V range around the zero-bias voltage. One can see in the inset that the I-V curve exhibits a steep increase of current at $V \sim 0$, corresponding to the sharp zero-bias dI/dV peak in Fig. 1 (b). As mentioned above, the BVB junction is of the SIS type below T_c. This fact suggests that the steep increase of current at $V \sim 0$ will be due to the Josephson coupling. However, it should be noticed that the junction is not superconductive but resistive at $V = 0$. More interestingly, a negative resistance is observed, following the steep increase of current at $V \sim 0$, in the I-V curve. Such I-V characteristics around $V = 0$ could be explained in terms of thermal phase-fluctuation effects on the Josephson coupling in a small SIS type junction, which will be discussed elsewhere in detail.

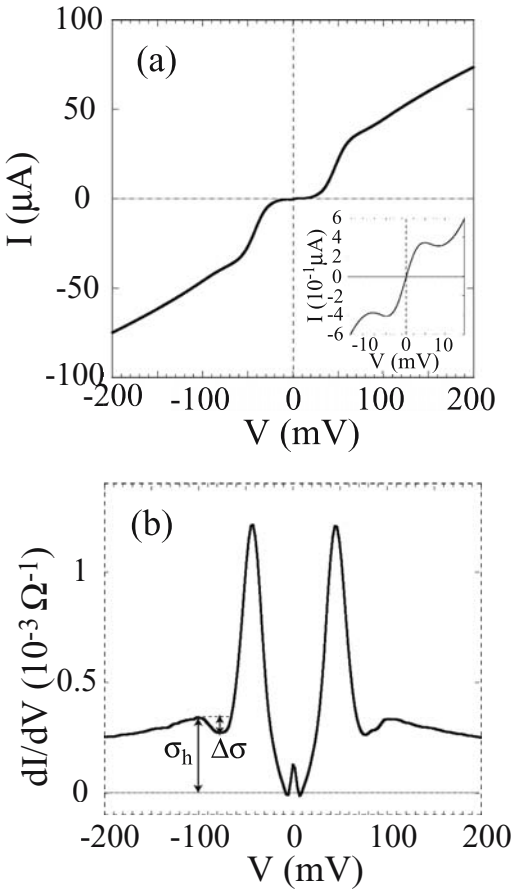

Figure 1. (a) I-V and (b) dI/dV-V curves for an overdoped BVB junction with $p \sim 0.22$

The tunneling conductance dI/dV exhibits sharp, large peaks, the so-called "coherence peaks", at voltages $|V| = V_p$ (45 mV), corresponding to twice the d-wave gap amplitude $2\Delta_0$ because the junction is of the SIS type. Furthermore, it also exhibits a clear dip and hump structure in the voltage regions just outside the coherence peaks. Such a peak-dip-hump structure is a characteristic feature of the tunneling spectrum in the SC state of Bi2212, as reported in Ref. [4], [8] and [9]. The energy difference of the dip from the peak, Ω, is estimated to be $\sim$ 36 meV, and follows the relation between Ω and T_c, $\Omega \sim 5k_BT_c$, which holds for a wide doping range including under- and overdoped regions in Bi2212 [4]. Interestingly, a similar relation holds for an effective SC gap magnitude $2\Delta_{\rm eff}$ and T_c, which was introduced in explaining the unusual re-

duction of SC condensation energy in underdoped La214 samples [10]. The value of Ω obtained for $p \sim 0.22$ is comparable to the energy $E_{\rm res}$ of an AF resonance mode, which was demonstrated to develop below $\sim T_{\rm c}$ in neutron scattering experiments for almost the same doping level on Bi2212 [11], suggesting that the dip structure of the electronic energy spectrum in the SC state will be due to couplings of electrons with the magnetic resonance mode. In the following subsection, we discuss their relation for the temperature evolution.

3.2 Temperature evolution of tunneling dip below $T_{\rm c}$

Figure 2 is a three dimensional illustration of BVB tunneling spectra around $T_{\rm c}$ for a slight overdoping level $p \sim 0.22$. One can see in the figure that the spectrum changes markedly in accordance with the SC transition at $T_{\rm c} = 81$ K. In the normal state, the spectrum exhibits a weak suppression in an energy region comparable to the SC gap. This gap like behavior is called "small energy-scale pseudogap" or "small pseudogap (SPG)", to distinguish it from the other pseudogap with a several times larger energy scale, the so-called "large pseudogap (LPG)" [9]. The LPG, which has been considered to be due to the gradual development of AF spin correlations, is associated with the downward shift of flat bands from the Fermi level $E_{\rm F}$, and becomes less evident in the overdoped region. In the SC state, the SC gap structure develops in the SPG energy region, together with the rapid growth of coherence peaks in the vicinity of $T_{\rm c}$. Furthermore, one can see that the dip structure develops gradually just outside the SC gap or the coherence peaks below $\sim T_{\rm c}$.

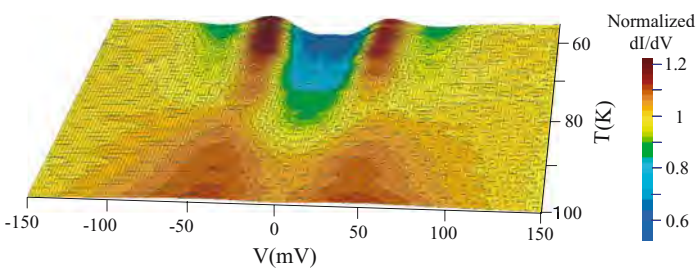

Figure 2. 3D illustration of the tunneling spectrum for a slightly overdoped Bi2212 crystal with $p \sim 0.22$ and $T_{\rm c}$ = 81 K. This was generated by using a 3D imaging software from the spectra measured at a temperature interval of every one or two K. The spectrum at each temperature is normalized with the value at V = -150 mV.

As shown in Fig. 1 (b), the dip depth is defined as the difference of tunneling conductance $\mathrm{d}I/\mathrm{d}V(\equiv \sigma)$ between the dip and hump, $\Delta\sigma$, normalized with the hump value $\sigma_{\rm h}$, and plotted as a function of temperature in Fig. 3. The $\Delta\sigma/\sigma_{\rm h}$ value becomes larger with the lowering of temperature and is saturated

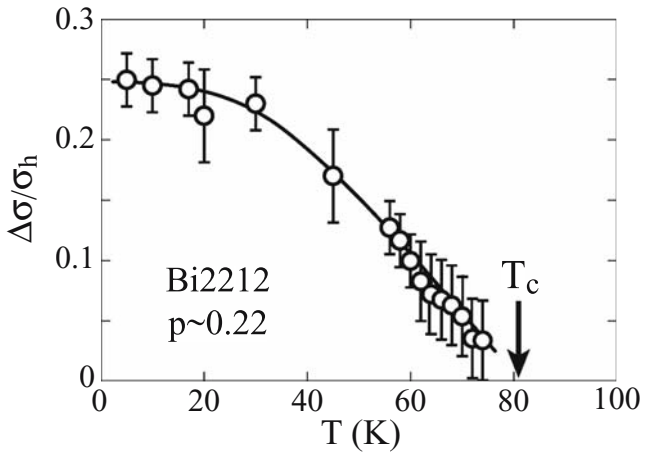

Figure 3. Temperature dependence of normalized dip depth in the tunneling spectra (Fig. 2).

at low temperatures. This temperature dependence of $\Delta\sigma/\sigma_{\rm h}$ is very similar to the development of a kink structure of the electronic dispersion curves near $E_{\rm F}$ in the antinodal region around $(\pi, 0)$ and $(0, \pi)$, which has recently been reported in ARPES experiments on Bi2212 [12, 13, 14]; these features appear to be related. As is well known, a similar kink structure also exists in the dispersion curves near $E_{\rm F}$ along the nodal directions. However, it is almost independent of temperature and seen in both the normal and SC states [2, 15]. The temperature-independent kink structure along the nodal directions has been reproduced very well in terms of strong electron-phonon couplings [15]. On the other hand, the temperature evolution of the kink in the antinodal region, corresponding to the dip structure of tunneling spectra, is different from that of the kink in the nodal region. It has been found in the present study that the temperature dependence of the dip structure, which appears at $|V| = (2\Delta_0 + E_{\rm res})/e$ in the SIS-type tunneling spectra, is in good agreement with that of the intensity of neutron scattering due to the AF resonance mode with a characteristic energy $E_{\rm res}$ ($\sim$40 meV) [5]. Evidently, the tunneling dip structure or the kink in the antinodal dispersion curves are related to the coupling of antinodal electrons with the AF spin excitations.

4. Summary

In the present study, we examined the SIS-type tunneling spectrum of slightly overdoped Bi2212 over a wide temperature range including both the normal and SC states, and demonstrated that the temperature evolution of the dip structure, observed at $|V| = (2\Delta_0 + E_{\rm res})/e$, correlates with that of the

AF resonance mode with a characteristic energy $E_{\rm res}$. Very recently, it has been shown in neutron inelastic scattering experiments on the phonon structure of $YBa_2Cu_3O_7$ that the spectral weights of Cu-O stretching modes change slightly in a manner similar to that of the AF resonance mode below $T_{\rm c}$ [16]. This fact suggests that the AF spin excitations will also couple with such phonon modes, as proposed in some theoretical studies [17, 18], and raises an interesting question as to whether antinodal electrons couple with the AF spin excitations directly or through their interactions with phonons. The present study seems to support the contention that the tunneling dip structure will be associated with the development of AF resonance mode below $T_{\rm c}$. However, further studies are needed to achieve a better understanding of the mechanism of coupling between electrons and AF spin excitations.

Acknowledgments

This work was supported in part by Grant-in-Aids for Scientific Research on Priority Area (No. 407) and on Projects (Nos. 13440104, 15340104 and 15740193) from the Ministry of Education, Culture, Sports, Science and Technology of Japan, and by Kurata Foundation.

References

[1] J. Mesot *et al.*, Physica C **341-348**, 2105 (2000).
[2] A. Kaminski *et al.*, Phys. Rev. Lett. **86**, 1070 (2001).
[3] P. D. Johnson *et al.*, Phys. Rev. Lett. **87**, 177007 (2001).
[4] J. F. Zasadzinski *et al.*, Phys. Rev. Lett. **87**, 067005 (2001).
[5] H. F. Fong *et al.*, Nature **398**, 588 (1999).
[6] P. C. Die *et al.*, Science **284**, 1344 (1999).
[7] J. Hwang *et al.*, Cond-mat/0402612v1 .
[8] N. Miyakawa *et al.*, Phys. Rev. Lett. **80**, 157 (1998).
[9] R. M. Dipasupil *et al.*, J. Phys. Soc. Jpn. **71**, 1535 (2002).
[10] N. Momono *et al.*, J. Phys. Soc. Jpn. **71**, 2832 (2002).
[11] H. He *et al.*, Phys. Rev. Lett. **86**, 1610 (2001).
[12] A. D. Gromko *et al.*, Cond-mat/0202329 .
[13] T. Sato *et al.*, Phys. Rev. Lett. **91**, 1570031 (2003).
[14] T. K. Kim *et al.*, Phys. Rev. Lett **91**, 1670021 (2003).
[15] A. Lanzara *et al.*, Nature **412**, 510 (2001).
[16] J.-H. Chung *et al.*, Phys. Rev. B **67**, 014517 (2003).
[17] M. Tachiki *et al.*, Phys. Rev. B **67**, 174506 (2003).
[18] A. Bussmann-Holder *et al.*, J. Condens. Matter **13**, l169 (2001).

ANDREEV – SAINT JAMES REFLECTIONS AS A TOOL FOR THE STUDY OF UNCONVENTIONAL SUPERCONDUCTORS

GUY DEUTSCHER
School of Physics and Astronomy,Ramat Aviv,Tel Aviv University 69978,Israel

Abstract: Andreev – Saint James reflections have been observed at normal metal contacts and tunnel junctions with YBCO, LSCO, BSCCO and other High Temperature Superconductors. The characteristic feature of these reflections is an enhanced conductance at low bias. Its observation implies the existence of extended quasi-particle arcs around the nodal directions. The enhancement persists up to Tc and so far has not been observed above it. Return to the normal state conductance occurs at an energy that scales with Tc, including in the pseudogap regime. In YBCO, the detailed shape of the conductance at low bias is consistent with a pure d-wave symmetry of the order parameter in the optimally doped and underdoped regimes, and with a mixed symmetry in the overdoped one.

Key words: superconductivity; quasi-particles; pseudo-gap; bound states

1. INTRODUCTION

One of the clearest manifestations of the existence of electron pairs in the superconducting state is the enhancement by a factor of 2 of the conductance of a normal metal to superconductor contact at small bias. Although specifically described only in 1982 by Blonder, Tinkham and Klapwijk (1) (BTK), this enhancement follows directly from the reflection mechanism at the interface, described originally in chronological order by de Gennes and Saint James (2), Andreev (3) and Saint James (4). An incoming electron from the normal side N is reflected as a hole along the trajectory of the incoming electron, while a Cooper pair flows in the superconducting side S:

J. Ashkenazi et al. (eds.), New Challenges in Superconductivity: Experimental Advances and Emerging Theories, 37-42.

a charge of 2e flows on both sides of the contact, compared with a charge of e in the normal state (above Tc, or at a bias larger than the gap). The conversion from quasi-particles to pairs takes place over a coherence length. Two fundamental conditions are essential for this mechanism to take place. First of all, there must exist quasi-particle excitations on the S side that can match those on the N side. Second of all, the velocity of these quasi-particles must be nearly equal to each other, otherwise normal reflections at the interface will dominate. The mere observation of an enhanced low bias conductance at normal metal – HTS contacts introduces therefore important constraints on HTS theories.

When the N side of the contact has a finite thickness d_N, an interesting cycle, first described explicitly by Saint James (4), takes place. After being reflected at the interface as a hole, the particle undergoes a normal reflection at the free surface of N, comes back to the interface, is reflected as a hole, which itself is normal reflected at the free surface, thus completing the cycle. During this Saint James cycle, composed of four legs instead of two for a usual particle in a potential well, the particle is an electron half of the time, and a hole the other half, a hall mark of an excitation in a superconductor at the gap edge. Solutions are bound states of finite energy in N, decaying over a coherence length in S. As first shown by Hu (5), the situation is different when S is a d-wave superconductor, and the normal to the interface corresponds to a node direction. Then, the Saint James cycle has for solution zero energy states. This is because of the difference of phase of π of the order parameter, between the two successive reflections at the interface. Note that these zero energy states persist down to $d_N = 0$. Thus, in addition to being sensitive to the nature and the velocity of the electronic excitations in S, the experiment is also a powerful tool for the study of the symmetry of the order parameter. Because of the chronological order of the publications, and the importance of the Saint James cycle, we propose to use the name "Andreev – Saint James reflections", or in short ASJ reflections.

2. ASJ REFLECTIONS ALONG ANTI NODAL DIRECTIONS

Experiments performed along the anti-nodal direction using point contacts on a variety of cuprates at or near optimum doping such as YBCO (6,7) have shown an enhanced zero bias conductance up to a rather well defined gap edge. These early results established the existence of quasi particles in the cuprates for that range of doping. They may not be compatible with theories of the normal state such as RVB in which the charge and spin degrees of freedom are separated. However, RVB has not

considered in detail ASJ reflections. The results also imply that the Fermi velocities of the quasi-particles on the S and N sides are not very different, which is a priori surprising in view of the small Fermi velocity in the cuprates as determined either by ARPES or from values of the superconducting coherence length (8). These values are typically of the order of about 2.10^7 cm/s, almost one order of magnitude less than the Fermi velocity in Gold. Actually, it has been shown (8) that the Fermi velocity that determines the mismatch is not the fully dressed velocity. It is possible from the ratio of the fully dressed velocity, as obtained for instance from the coherence length, to that which fits the low conductance bias, to calculate renormalization effects. They are qualitatively similar to those in heavy fermions, where ASJ reflections have also been observed.

3. ASJ SURFACE BOUND STATES

Experiments showing the existence of ASJ surface bound states have been performed using tunnel junctions (9,10) or Scanning Tunneling Microscopy (STM) (11) on surfaces perpendicular to the CuO planes. Here the low energy states show up as a Zero Bias Conductance Peak (ZBCP). It is interesting to note that the zero energy states are quite easily detected, even though reflections at the surface are certainly not in majority specular as assumed in theoretical models. In fact, a ZBCP is observed even if the normal to the surface is the [100] direction, an orientation for which for reasons of symmetry ASJ states are not expected. The reason for this deviation from theoretical predictions may precisely be the non specular character of the normal reflections. For part of the trajectories, a difference of phase of π between two successive reflections may occur also for a [100] orientation. Likewise, this difference of phase will not exist for some of the trajectories when the orientation is [110]. The net result of this non specularity is that for ordinary surfaces there is not much difference between the two orientations.

ASJ states are a good tool for the study of the underdoped regime. This is because in this regime it is in general difficult to obtain good contacts with a normal metal tip. This difficulty may be due to the presence of a "dead layer", or to the occurrence of the pseudogap (see below). By contrast, ASJ states have been observed at all doping levels, including in strongly underdoped samples of YBCO (12) and BSCCO (13). This is an important result, because it implies that there are nodal quasi-particle excitations, over a substantial arc, even in underdoped samples. Otherwise, the reflections that give rise to the ASJ surface states could not take place, since in a Saint

James cycle electron and hole excitation play symmetric roles. It is not clear how the Saint James cycle could take place if the *only* excitations in the HTS were holons and spinons (14). At a minimum, additional excitations are necessary (15).

4. ASJ BOUND STATES AND THE PSEUDOGAP ISSUE

The conclusion that there are extended quasi-particle excitations along nodal arcs is in good agreement with the STM observations by the group of S.Davis, as reported in these proceedings (16). When measuring the STM tunneling spectrum over the sample's surface they observe that the low bias part, up to about 20 meV, is quite homogeneous, including in underdoped samples. The high bias part, on the other hand, is inhomogeneous on the nanometer scale with conductance peaks ranging up to more than 50 meV. They show that the low bias part corresponds to regions of the Fermi surface around the nodes, while the high bias part (the large gaps, or pseudo-gaps seen prominently in underdoped samples) correspond to anti-nodal regions. The bias range of up to about 20 meV where the spectra are homogeneous corresponds precisely to the energy scale observed by ASJ scattering, which never reaches energies characteristic of the pseudo-gap (17). The two sets of experiments are therefore in excellent agreement. The nodal regions or Fermi arcs are unaffected by the pseudo-gap phenomenon. The gap is homogeneous and the quasi-particles are of a conventional nature in these regions, giving rise to ASJ reflections and ASJ bound states. The extension of these arcs around the nodes is not known exactly, but is always substantial even in deeply underdoped samples (otherwise ZBCPs would not be observed), and they possibly extend up to the anti-nodal points in overdoped samples.

A related property of ASJ bound states is that they disappear at Tc, contrary to the pseudo-gap. This is the case even in deeply underdoped samples where pseudo-gap values are several times larger than Tc (12,13). This behavior is in line with the above conclusions, and with the observation that the energy scale that characterizes ASJ bound states varies as Tc, decreasing in the underdoped regime, while the pseudo-gap keeps increasing (17). It may also be noted that a strong pseudo-gap, whether it reflects the formation of incoherent Cooper pairs or a different order appearing at high temperatures, is incompatible with ASJ reflections, as shown by Pistolesi and Nozieres (18). The observation of ASJ bound states in strongly underdoped samples having a large pseudo-gap, is by itself sufficient to prove that there is no pseudo-gap along extended nodal arcs.

5. ORDER PARAMETER MINORITY COMPONENT

The existence of a minority component in the cuprates remains a point of controversy. It is related to the High Tc mechanism itself, because some of them (the magnetic ones) require a pure d-wave symmetry, while others (phonon mechanisms) don't. The most recent data is not converging on this issue. Tsuei et al. conclude from their tricrystal experiments that there is no detectable minority component even away from optimum doping in YBCO, LSCO and BSCO, and imply that this is a general property of all cuprates, a conclusion that would support a magnetic model (19). But a recent measurement of the field dependence of the heat capacity in the electron doped cuprate PCCO has shown a linear dependence characteristic of an s-wave symmetry (20). Cuk et al. have uncovered a coupling of the electronic bands to a 40 meV phonon mode which they propose is important for the pairing mechanism, which would not imply a d-wave symmetry (21).

The possible existence of a minority component has been examined by ASJ spectroscopy as a function of doping, magnetic field (22) and in a proximity effect situation (23). In the bound state geometry, an imaginary minority component lifts the degeneracy between states carrying opposite surface currents, and results in a net surface current that produces a split of the ZBCP. Such a split, increasing with doping, was observed in overdoped YBCO (22). It may be of course that the minority imaginary component occurs only at the surface of the sample. But even if this were the case, this occurrence would show that there is substantial coupling of the electronic states with a phonon mode, getting stronger in the overdoped regime (24). A detailed analysis of the conductance of point contacts in the anti-nodal direction has shown that there must exist an imaginary component, possibly having the is symmetry, that develops in the HTS near the interface with the normal metal (23). No theory is available at the moment for this situation, but again the appearance of such a component requires that the corresponding coupling channel be present.

A splitting of the ZBCP is also observed in the presence of a magnetic field applied parallel to the sample's surface and perpendicular to the CuO planes. Meissner screening currents in increasing fields will produce such a split. But since initially these currents increase in proportion to the applied field, splitting should be linear in field (24). It has been shown that this is not the case at or near optimum doping (22). Again, this may only be a surface phenomenon, but even in that case a substantial phonon coupling is necessary to explain the result (25). The observation of a splitting varying as the square root of the applied field in decreasing fields and under field cooled conditions has also been reported fir YBCO films having the (110)

orientation, and discussed as possibly resulting from a field induced id_{xy} component (26).

6. CONCLUSIONS

Andreev – Saint James spectroscopy gives important indications on some of the remarkable properties of the cuprates. Amongst them are the existence of quasi-particle excitations along extended arcs around the nodal directions, including in the underdoped regime, and the absence of a pseudo-gap in same. In the pure d-wave symmetry, the Saint James cycle leads to the formation of zero energy surface bound states. The energy of these states is modified by time reversal symmetry breaking, due for instance to Meissner currents or to an imaginary component of the order parameter.

Illuminating conversations with P.Nozieres and F.Pistolesi are gratefully acknowledged. This work was supported by the Israel Science Foundation, the Heinrich Hertz Minerva Center for High temperature Superconductivity and by the Oren Family Chair for Experimental Solid State Physics.

References

1. Blonder G.E., M.Tinkham and T.M.Klapwijk, Phys.Rev.B**25,** 4515 (1982).
2. De Gennes P.G. and D.Saint James, Phys.Lett. **4**, 151 (1963).
3. Andreev A.F., Soviet Physics JETP **19**, 1228 (1964).
4. Saint James D., J. de Physique **25**, 899 (1964).
5. Hu Chia-Ren, Phys.Rev.Lett.**72**, 1526 (1994).
6. Hass N. et al., J. of Superconductivity **5**, 191 (1992).
7. Wei J.Y.T et al., Phys.Rev.Lett. **81**, 2542 (1998).
8. Deutscher G. and P.Nozieres, Phys.Rev.B **50**, 13557 (1994).
9. Aprili M., E.Badica and L.H.Greene, **83**, 4630 (1999).
10. Krupke R. and G.Deutscher, Phys.Rev.Lett.**83**, 4634 (1999).
11. Sharoni A. et al., Phys.Rev.B **65**, 134526 (2002).
12. Dagan et al., Phys.Rev.B **61**, 7012 (2000).
13. Sinha S. and K.-W. Ng, Phys.Rev.Lett. **80**, 1296 (1998).
14. Anderson P.W., in these Proceedings
15. Altman E. and A.Auerbach, Phys.Rev.B **65**, 104508 (2002).
16. McElroy et al., cond-mat/0404005.
17. Deutscher G., Nature **397,** 411 (1999).
18. Pistolesi F.and P.Nozieres, unpublished.
19. Tsuei et al., cond-mat/0402655.
20. Balci H. and R.L.Greene, cond-mat/0402263
21. Cuk T. et al., cond-mat/0403521.
22. Dagan Y.and G.Deutscher, Phys.Rev.Lett.**87,** 177004 (2001).
23. Kohen A., G.Leibovitch and G.Deutscher, Phys.Rev.Lett.**90** (207005 (2003).
24. Fogelstrom M., D.Rainer and G.Deutscher, Phys.Rev.Lett., **79, 281 (1997).**
25. Fogelstrom M., D.Rainer and J.A.Sauls, con-mat1/0302197 (2003).
26. R.Beck, Y.Dagan, A.Milner, A.Gerber and G.Deutscher, to appear in Phys.Rev.B.

$BI_2SR_2CACU_2O_{8+\delta}$ C-AXIS BICRYSTAL TWIST AND CROSS-WHISKER EXPERIMENTS

Richard A. Klemm
Department of Physics, University of North Dakota, Grand Forks, ND 58202-7129 USA
richard.klemm@und.nodak.edu

Abstract The combined bicrystal, artificial cross-whisker, and natural cross-whisker c-axis twist experiments on $Bi_2Sr_2CaCu_2O_{8+\delta}$ (Bi2212) provide strong evidence that the superconducting order parameter is predominantly s-wave for $T \leq T_c$, and that the c-axis tunneling is strongly incoherent.

Keywords: Order parameter; incoherent tunneling; Josephson junctions

Introduction

There has long been a raging debate over the orbital symmetry of the superconducting order parameter (OP) in the high transition temperature (T_c) superconductors.[1] Many experiments were interpreted as providing evidence for a predominantly $d_{x^2-y^2}$-wave OP, but others were interpreted as providing evidence for a predominantly s-wave OP. Müller argued that the OP is d-wave on the surface and s-wave in the bulk.[1]

$Bi_2Sr_2CaCu_2O_{8+\delta}$ (Bi2212) forms a disordered array of superconducting and non-superconducting pseudogap nanodomains, as revealed by scanning tunneling microscopy studies.[2] Hence, only phase-sensitive experiments can distinguish s-wave from d-wave OP's in Bi2212.

1. Bicrystal Twist Josephson Junctions

Li *et al.* made extraordinarily perfect artificial c-axis twist bicrystal junctions.[3] These junctions were extensively characterized using high resolution transmission electron microscopy (HRTEM), electron energy loss spectroscopy, and low energy electron diffraction, etc., and the results were compared with computer simulations.[4] More recently, off-axis electron holography provided compelling evidence of the remarkable atomic perfection and reproducibility of the twist junctions.[5]

J. Ashkenazi et al. (eds.), New Challenges in Superconductivity: Experimental Advances and Emerging Theories, 43-48.

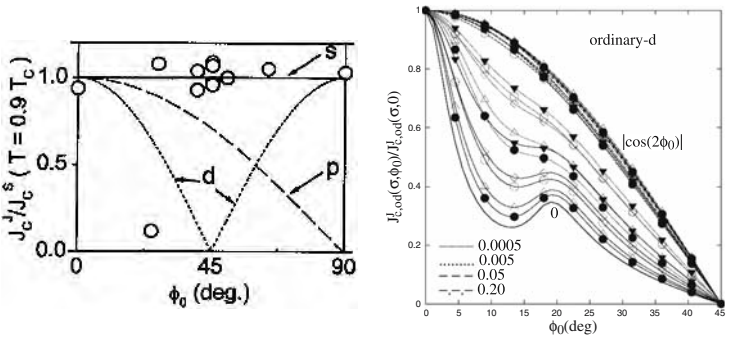

Figure 1. Left: Plot of the bicrystal $J_c^J(\phi_0)/J_c^S$ at $0.9T_c$.[3] The curves refer to the incoherent limits for single OP components. Right: Weak tunneling $J_c(\phi_0)^J/J_c^J(0)$ at 0.9 T_c assuming the tight-binding Fermi surface appropriate for Bi2212 and a $d_{x^2-y^2}$-wave OP.[6] The σ^2 values are given in the legend. Curves marked 0 and $|\cos(2\phi_0)|$ are the coherent and incoherent limits, respectively. The Gaussian (•), exponential (○), rotationally invariant Lorentzian (△), stretched Lorentzian (solid inverted triangles), and Lorentzian (◇) tunneling model results are shown. [6]

Li *et al.* measured the critical current densities J_c^J and J_c^S across the twist junction and constituent single crystals for 12 samples with different ϕ_0 values. They found $J_c^J(\phi_0)/J_c^S = 1$ near to T_c, as shown in the left panel of Fig. 1.[3]

Since $d_{x^2-y^2}$-wave and d_{xy} OP's are orthogonal, $J_c(45°) = 0$ for a single d-wave OP component in a tetragonal crystal with weak interlayer tunneling.[6] Although Bi2212 is slightly orthorhombic, $J_c(\phi_0^*) = 0$ for a d-wave OP, where $\phi_0^* \approx 45°$, inconsistent with the Li *et al.* data. [3, 7] The mixing of OP components to compensate for the physical twist junction might allow a predominant $d_{x^2-y^2}$-wave OP to result in a substantially ϕ_0-independent J_c^J for $T \ll T_c$, but not for $T \approx T_c$, where the measurement was performed.[3, 7] An additional d-wave scenario leading to a non-vanishing (albeit very small) $J_c(45°)$ could arise if the c-axis tunneling were strong and coherent.[8] Those authors also showed that the overlap of two tight-binding Fermi surfaces rotated ϕ_0 with respect to each other decreases greatly with increasing ϕ_0, leading to a substantial reduction in the coherent tunneling matrix element.[8]

Bille *et al.* studied the weak tunneling case of a tetragonal crystal with a variety of single-component OP and tunneling matrix element forms. In each tunneling model, the single parameter σ^2 characterizes the change $\Delta \boldsymbol{k}$ in the intralayer wave vector relative to π/a, where a is the lattice constant, with $\sigma^2 \to 0, \infty$ in the coherent and incoher-

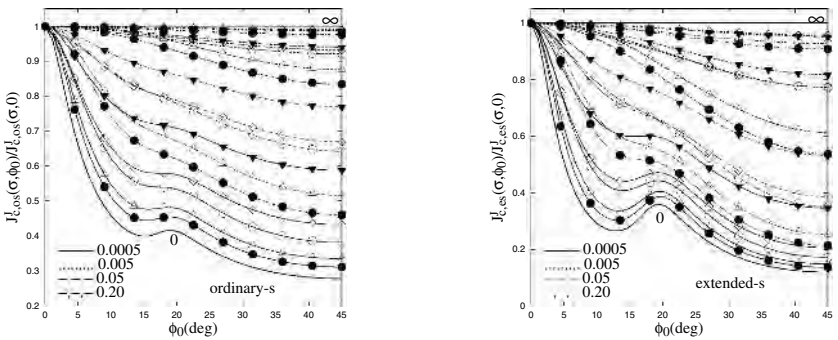

Figure 2. Plots at $0.9T_c$ of $J_c^J(\phi_0/J_c^J(0)$ for the isotropic s-wave (left)and extended-s-wave (right) OP's, respectively. The lines marked ∞ indicate the incoherent limit; the other labels are as in the right panel of Fig. 1.[6]

ent limits, respectively. Their results for the $d_{x^2-y^2}$-, ordinary-s-, and extended-s-wave ($\propto |\cos(k_x a) - \cos(k_y a)|$) OP's are shown in Figs. 1 and 2.[6]

2. Artificial Cross-Whisker Junctions

Bi2212 whiskers naturally have insulating surfaces. Takano *et al.* weakly sintered two different whiskers together, obtaining artificial cross-whisker junctions (ACWJ).[9] The measured $J_c(\phi_0)$ varied substantially with ϕ_0, being rather flat for $30° \leq \phi_0 \leq 60°$, as shown in the right panel of Fig. 3 and in Fig. 4. However, the resistivity for $T > T_c$ increased monotonically with decreasing ϕ_0,[10] suggesting that some of the $J_c(\phi_0)$ ACWJ data might be extrinsic.[10, 11]

In 4-5 45° ACWJ's, $J_c(45°)$ was nearly sample independent and non-vanishing.[12] For these ACWJ's, they obtained Fraunhofer-like patterns and performed Shapiro step analyses, indicating that their junctions were *weak and first order*. They also found $J_c^J(\phi_0)$ to be independent of T for 4.2 K$\leq T \leq$ 60K.[9, 12] Hence, the non-vanishing $J_c(45°)$ precludes a pure d-wave OP, even near to T_c.

Although coherent tunneling in Bi2212 is highly unlikely,[2] Figs. 1 and 2 show that incoherent tunneling cannot possibly fit the ACWJ data for any OP form. In the right panel of Fig. 3, we show our best weak, first-order coherent tunneling fits to the data, with the tight-binding Fermi surface and a dominant d-wave OP. Although the curves fit the data nicely for $\phi_0 \approx 90°$, they fail to do so for $\phi_0 \approx 45°$, rendering a dominant d-wave OP highly unlikely. In the left panel of Fig. 4, we fit

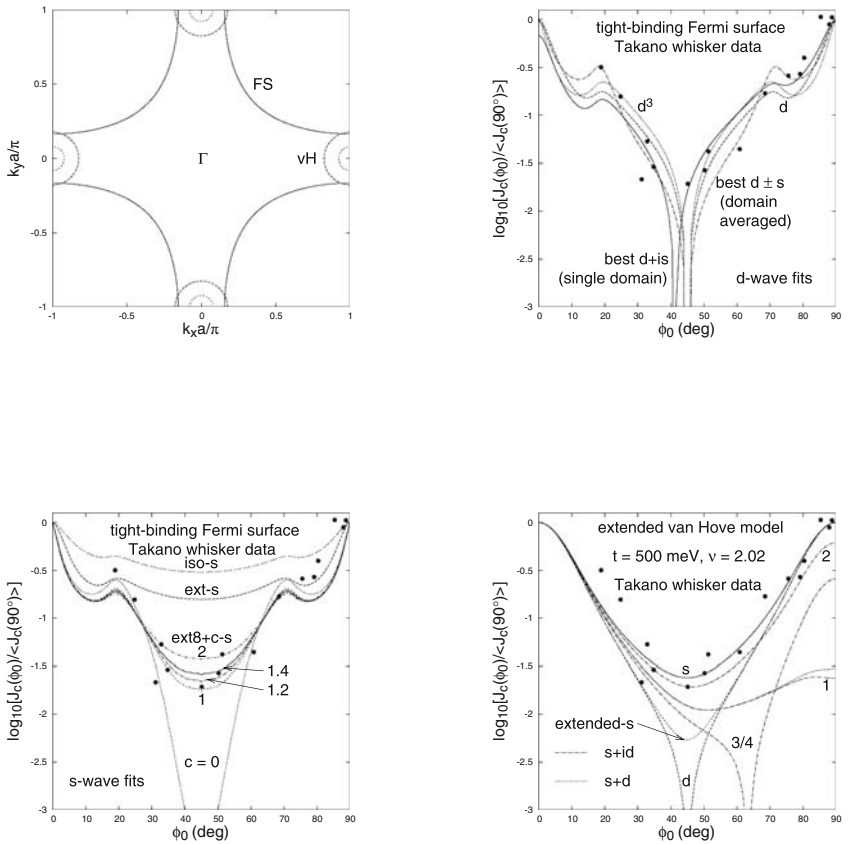

Figure 4. Best coherent tunneling fits to the ACWJ data.[9, 11] Left: tight-binding FS, anisotropic-s-wave OP. Right: van Hove (vH) states, variosu OP's.

the data quantitatively using the same tight-binding Fermi surface and a highly anisotropy s-wave OP of the form $\Delta_c + \Delta_0[\cos(k_x a) - \cos(k_y a)]^8$, where $\Delta_c \approx 1.0 - 2.0$ meV. In the right panel of Fig. 4, we assumed the van Hove normal state scenario with coherent tunneling, and found that an isotropic s-wave OP could fit the data quantitatively.[11]

3. Natural Cross-Whisker Junctions

Very recently, Latyshev *et al.* annealed naturally-occurring cross whiskers, forming natural cross-whisker junctions (NCWJ's), and studied their properties.[13] The normal state resistance per square $R_\square^J$ across the NCWJ was independent of ϕ_0, and roughly a factor 60 higher than

$R_\square^S$ for the intrinsic junctions in bulk Bi2212. At low T, they measured $J_c^J(\phi_0)$ three ways: (a) from the zero-field I_c^J, (b) from the oscillatory part of the Fraunhofer-like $I_c^J(B)$, and (c) from the sharp rise in the I/V characteristics at $V = 2\Delta$. These three different measurements were consistent, and the overall conclusion is that $J_c^J(\phi_0)$ is independent of ϕ_0. Although $J_c^J(\phi_0) \approx J_c^S/40$, where J_c^S is the critical current density across intrinsic bulk junctions, since $J_c^J R_\square^J \approx J_c^S R_\square^S$, this is consistent with the twist junctions being uniformly weaker than the bulk junctions. Latyshev *et al.* also showed that the ϕ_0-independence of J_c^J holds for 4.2K$\leq T \leq T_c$.[13]

In Fig. 5, we have plotted $\log_{10}[J_c^J(\mathrm{A/cm^2})]$ versus ϕ_0 at 4.2 K for the NCWJ's,[13] along with the ACWJ data (open circles) of Takano *et al.*,[9, 10] and the $J_c^J(\phi_0)$ bicrystal data (solid diamonds) at $0.9T_c$ from Table 1 of Li *et al.*,[3] multiplied by a factor of $4.00 = J_c(0)/J_c(0.9T_c)$ expected from the Ambegaokar-Baratoff formula. The data from measurements (a), (b), and (c) are represented by the stars, solid circles, and solid squares, respectively. The solid and dot-dashed lines represent the averages of the bicrystal and NCWJ data from measurements (b) and (c), respectively. The NCWJ data are consistent with the ACWJ data for $30° \leq \phi_0 \leq 60°$, but differ substantially from the ACWJ data outside that region. The bicrystal data of Li *et al.* are nearly consistent with much of the ACWJ data outside that region. Combining all three experiments, the main (constant) difference between the bicrystal data and the NCWJ data arises from the uniformly different junction matrix elements, and the strong ACWJ $J_c^J(\phi_0)$ dependence most likely arises from an extrinsic ϕ_0 dependence of the tunneling matrix elements.

4. Summary

The bicrystal c-axis twist junctions are by far the best characterized Josephson junctions studied to date, and $J_c(\phi_0)$ was independent of ϕ_0.[3] Although the ACWJ data of Takano *et al.* exhibited an extrinsic $J_c^J(\phi_0)$ dependence,[9] the NCWJ data also showed $J_c(\phi_0)$ independent of ϕ_0. These experiments are only consistent with a predominantly s-wave OP for $T \leq T_c$, and with strongly incoherent c-axis tunneling.

Acknowledgments

The author would like to thank Y. Takano and Yu. I. Latyshev for their unpublished results, and M. Tachiki for helpful discussions.

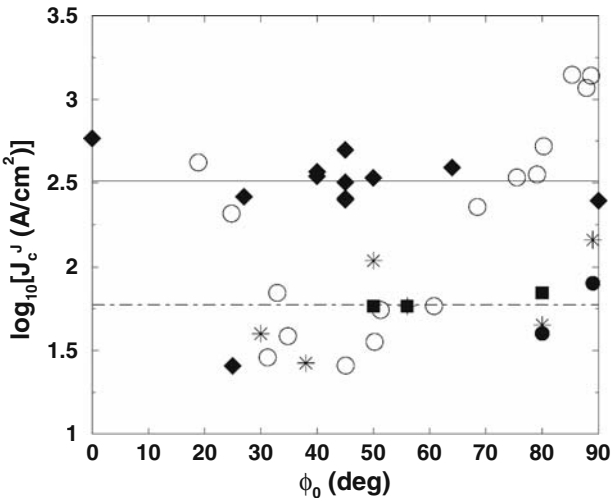

Figure 5. A comparison of $\log_{10}[J_c^J(\mathrm{A/cm^2})]$ versus ϕ_0 data at 4.2 K of the bicrystal data multiplied by 4.00 as described in the text (solid diamonds),[3] with the ACWJ data,[9] (open circles), and the NCWJ data, measured with methods (a) (stars), (b) (solid circles), and (c) (solid squares).[13]

References

[1] K. A. Müller, Phil. Mag. Lett. **82**, 279 (2002).

[2] K. M. Lang, V. Madhavan, J. E. Hoffman, E. W. Hudson, H. Eisaki, S. Uchida, and J. C. Davis, Nature (London) **415**, 412 (2002).

[3] Q. Li, Y. N. Tsay, M. Suenaga, R. A. Klemm, G. D. Gu, and N. Koshizuka, Phys. Rev. Lett. **83**, 4160 (1999).

[4] Y. Zhu, Q. Li, Y. N. Tsay, M. Suenaga, G. D. Gu, and N. Koshizuka, Phys. Rev. B **57**, 8601 (1998).

[5] M. A. Schofield, L. Wu, and Y. Zhu, Phys. Rev. B **67**, 224512 (2003).

[6] A. Bille, R. A. Klemm, and K. Scharnberg, Phys. Rev. B **64**, 174507 (2001).

[7] R. A. Klemm, C. T. Rieck, and K. Scharnberg, Phys. Rev. B **58** 1051 (1998); **61**, 5913 (2000).

[8] G. B. Arnold, and R. A. Klemm, Phys. Rev. B **62**, 661 (2000).

[9] Y. Takano, T. Hatano, M. Ohmori, S. Kawakami, A. Ishii, S. Arisawa, S.-J. Kim, T. Yamashita, K. Togano, and M. Tachiki, J. Low. Temp. Phys. **131**, 533 (2003).

[10] Y. Takano, T. Hatano, A. Fukuyo, M. Ohmori, P. Ahmet, T. Naruke, K. Nakajima, T. Chikyow, K. Ishii, S. Arisawa, K. Togano, and M. Tachiki, Sing. J. Phys. **18**, 67 (2002).

[11] R. A. Klemm, Phys. Rev. B **67**, 174509 (2003).

[12] M. Tachiki, (private communications).

[13] Yu. Latyshev, A. P. Orlov, A. M. Nikitina, P. Monceau, and R. A. Klemm (unpublished) (cond-mat/0401488).

NODELESS PAIRING STATE IN $YBa_2Cu_3O_7$

Dale R. Harshman[1,2,3], John D. Dow[2], W. J. Kossler[4], A. T. Fiory[5], A. J. Greer[6], D. R. Noakes[7], C. E. Stronach[7], and E. Koster[8]

[1]*Physikon Research Corporation, Lynden, WA 98264 USA**

[2]*Arizona State University, Tempe, AZ 85287 USA*

[3]*University of Notre Dame, Notre Dame, IN 46556 USA*

[4]*College of William and Mary, Williamsburg, VA 23187 USA*

[5]*New Jersey Institute of Technology, Newark, NJ 07102 USA*

[6]*Gonzaga University, Spokane WA 99258 USA*

[7]*Virginia State University, Petersburg, VA 23806 USA*

[8]*University of British Columbia, Vancouver, B.C., V6T 1Z1 Canada*

Abstract Muon spin rotation (μ^+SR) results are reported on single-crystal $YBa_2Cu_3O_7$, having a transition temperature of T_c = 91.3 K with $\Delta T_c < 0.5$ K (in zero applied field). Flux motion and de-pinning can mask intrinsic properties such as the true underlying pairing state, and has led to misinterpretations of data. The present data exhibit a non-monotonic behavior for the second moment of the internal field distribution as a function of field as T→0, which rules out any single pairing state explanation of the data, without including other *extrinsic* effects. The data are, however, consistent with *s*-wave (or extended *s*-wave) pairing, provided that field-dependent and temperature-activated vortex de-pinning are first taken into account. Applying a self-consistent vortex de-pinning model, the data are found to be best described by an underlying two-fluid model, yielding a London penetration depth value of λ_{ab}(T=0,H=0) = 127.6 nm. Attempts to fit the data using BCS theory with varying coupling strengths and a *d*-wave model produced much poorer fits. In fact, the probability that the *d*-wave model gives a better fit than the two-fluid model is less that 4×10^{-6}. This work reveals that the *d*-wave interpretations are incorrect, confirms earlier work (Refs. 1-3) which first established *s*-wave pairing in $YBa_2Cu_3O_7$ powders and (heavily twinned) crystals, and re-establishes *s*-wave pairing for superconductivity in this material.

Keywords: High-T_c superconductivity, pairing state, muon spin rotation

J. Ashkenazi et al. (eds.), New Challenges in Superconductivity: Experimental Advances and Emerging Theories, 49-54.

1. Introduction

Already by 1990, the high-temperature superconductivity of $YBa_2Cu_3O_7$ had been observed (and confirmed) to reflect *s*-wave (or extended *s*-wave) pairing of holes, both in powders[1,2] and in single crystals,[3] using muon spin rotation (μ^+SR). Not only is μ^+SR a bulk probe, but it is one of the few measurements that probes *only the superconducting bands*, and is thus superior to many other techniques probing the high-T_c pairing state. The single-crystal measurements confirmed the earlier conclusion from powders that the pairing state was either *s*-wave or extended *s*-wave for both the 90 K ($\delta \sim 0.05$) and the 60 K ($0.3 \leq \delta \leq 0.4$) bulk phases (with oxygen content $7-\delta$). In all of the above-cited experiments, the vortex lattice was strongly pinned, suppressing fluxon motion and temperature-dependent de-pinning effects below T_c.

A comparable demonstration of agreement with *s*-wave pairing was also provided in 1991 for unannealed $Bi_2Sr_2CaCu_2O_8$ crystals.[4] In this case, the effects of vortex motion and temperature-activated de-pinning were clearly evident at 0.3 and 0.4 Tesla. However, the effects of vortex motion and de-pinning were suppressed in higher fields (1.5 Tesla), revealing the true underlying *s*-wave character, a result that has been recently corroborated.[5] Since these effects were much less evident in powder samples,[6] it was concluded that they were suppressed by the stronger pinning forces present in the powder samples.

Following this $Bi_2Sr_2CaCu_2O_8$ work, others,[7] citing primarily surface sensitive probes, have argued that the hole-pairing in high-T_c materials is primarily *d*-wave pairing. Indeed, other μ^+SR data on single-crystal $YBa_2Cu_3O_7$ were produced, from which the authors claimed evidence for *d*-wave pairing.[8]

In this paper, we concentrate on the μ^+SR measurements and determine if $YBa_2Cu_3O_7$ is a bulk *s*-wave (nodeless) superconductor, as determined in Refs. 1-3, or a *d*-wave superconductor, whose order parameter $\Delta(\mathbf{k})$, changes sign as a function of $\mathbf{k}$, as claimed in Ref. 8. In making this determination, we show that the features observed in the single-crystal data of Ref. 8 are actually due to temperature-activated fluxon de-pinning, an effect which is not readily observable in strongly pinned systems such as the early powder samples or the early heavily-twinned crystals.

To prove the *s*-wave character of the superconductivity, we first present μ^+SR data acquired in a high-quality $YBa_2Cu_3O_{6.95}$ crystal at applied magnetic fields of 0.05, 1.0, 3.0, and 6.0 Tesla. The measured temperature- and field-dependences of the second moment of the local field distribution, σ(T,H), are carefully compared using a self-consistent analysis in which deviations from *s*-wave symmetry are attributed to weak fluxon de-pinning phenomena, rather than to *d*-wave effects. We show that the purported intrinsic *d*-wave behavior previously claimed for muon experiments is actually not due to *d*-waves but is an extrinsic phenomenon caused by flux de-pinning.[9]

2. Experiment and Analysis

The $YBa_2Cu_3O_{6.95}$ crystal measured for the present work was grown in a Y-stabilized ZrO_2 crucible according to methods described elsewhere.[9] The sample exhibits a transition temperature of T_c=91.3 K, has a transition width of $\Delta T_c < 0.5$ K (in zero applied field), and has dimensions $5 \times 4 \times 0.75$ mm^3. The μ^+SR experiments were conducted at the TRIUMF cyclotron facility in Vancouver, B.C., Canada, using the LAMPF (low-field) and Belle (high-field) spectrometers. Transverse-field measurements were employed in time differential mode, yielding a relaxation function $G_{xx}(t)$, consisting of a relaxation envelope modulating a precessing muon spin amplitude. Data were taken at magnetic fields applied along the *c*-direction of 0.05, 1.0, 3.0, and 6.0 Tesla.

The analysis of the μ^+SR data is given in detail elsewhere,[9] so only a brief description will be presented here. Our present analysis retains λ and ξ as constants, and employs a cut-off London model with the cut-off parameter ξ_0 fixed at 0.1 nm for all four fields analyzed (*i.e.,* all vortices were treated as virtually point vortices). The relaxation function $G_{xx}(t)$ is obtained (the dipolar broadening contribution is determined by fitting above T_c) by first deriving the field probability distribution function, dn(b)/db, numerically from the cut-off London model. A Gaussian convolution is also performed, of width σ_M (the smearing parameter), to better account for variations in the local or internal field arising from distortions in the vortex lattice. Finally, a Gaussian decaying signal is added to describe the small signal from the muons that stop outside the superconducting sample, but are not vetoed by the electronics. From this, the fitted parameters σ_M(T,H) and λ(T,H) are obtained, which model the magnetic field distribution in the vortex lattice distorted by pinning. Results for the second moment of the field distribution are calculated using the expression, $\sigma^2(T,H) = \sigma_L^2 + \sigma_M^2$, where $\sigma_L = 0.0609\ \Phi_0/\lambda^2$ (triangular lattice) and Φ_0 is the flux quantum (the model field distribution is used to obtain the moments).

3. Results and Interpretation

By plotting σ against temperature for the four fields studied,[9] H = 0.05, 1.0, 3.0 and 6.0 Tesla, one finds qualitatively similar features to previous data (see *e.g.,* Ref. 10), but also certain features that rule out *d*-wave pairing, and which provide clues regarding the *extrinsic* effects (*i.e.,* effects not directly associated with the gap function symmetry) that play a role in shaping them. Specifically, these data show (i) a distinctive inflection point in σ(T,H) versus temperature near $T \approx 20$ K, which is most evident at intermediate fields (*i.e.,* H=1.0 and 3.0 Tesla), and is reminiscent of earlier data on $Bi_2Sr_2CaCu_2O_8$,[4] and (ii) a non-monotonic dependence of the quantity $\sigma(T \rightarrow 0,H)$ on applied magnetic field H. These two effects cannot be adequately explained with either an *s*-wave or a *d*-wave model alone.

Instead of forcing the data to conform to the *d*-wave picture, we take the approach that the deviations from *s*-wave behavior are due to quantifiable phenomena, most notably temperature-dependent fluxon de-pinning. Since the maximum temperature for the data acquired at each field is below the melting curve (see Fig. 4 of Ref. 11), the vortex lattice is subject to pinning, as occurs in very clean crystals where the flux lattice becomes locked-in by weak pinning at oxygen vacancies and/or other defects.

4. Collective pinning model

The experimental results for σ(T,H) incorporate pinning and vortex motion, coupled with an underlying pairing symmetry.[9] Using a self-consistent approach, we determine the true nature of the underlying pairing state [*i.e.,* λ_{ab}(T,H)], and extract the London penetration depth, λ_{ab}(T=0,H=0). From our analysis, the resulting effective underlying magnetic penetration depth, λ_{ab}(T,H), was found to be a monotonically increasing function of temperature and magnetic field,[9] as expected. Specifically, we find λ_{ab}(T=0,H=0) of 127.6 $\pm$ 1.5 nm, a T_c of 90.8 $\pm$ 0.5 K, and a de-pinning temperature of about 19.6 (+18.2/-12.2) K, with a χ^2 per degree of freedom of 2.38, assuming a two-fluid pairing state symmetry. Extrapolating to zero field, the result for λ_{ab}(T,H=0) is shown in Fig. 1. The collapse of all of the data onto a single curve clearly illustrates that the self-consistent agreement between the pinning theory detailed here and elsewhere,[9] assuming an *s*-wave ground state, far exceeds the comparatively poor agreement found using the non-local *d*-wave theory of Ref. 10. For example, the best *d*-wave model fit yielded λ_{ab}(T=0,H=0) = 120.5 $\pm$ 1.8 nm and T_c = 90.6 $\pm$ 0.7 K with $\chi^2 \approx 13$. This poor χ^2 value is attributed primarily to the inability of the underlying *d*-wave function to deal with the non-linear temperature dependence in our 0.05 Tesla data. The probability that the *d*-wave model gives a better fit than the two-fluid model is less than 4×10^{-6}.

Experiments utilizing microwave cavity resonance, *ac* susceptibility, or *rf* resonance[12] have been executed on $YBa_2Cu_3O_7$ to test theoretical predictions of *d*-wave pairing theory for the non-linear Meissner effect.[13] The predicted effects turned out to be either absent or unobservably small. Moreover, the predicted four-fold symmetry in the *ab* plane for the d($x^2 - y^2$) order parameter is also absent.[14]

5. Conclusion

From the data and analyses presented, and the comparison with the non-local *d*-wave theory of Ref. 10, it is clear that there is no evidence in any of the μ^+SR data for *d*-wave pairing. All of the data are, however, completely consistent with temperature-activated vortex de-pinning that masks an under-

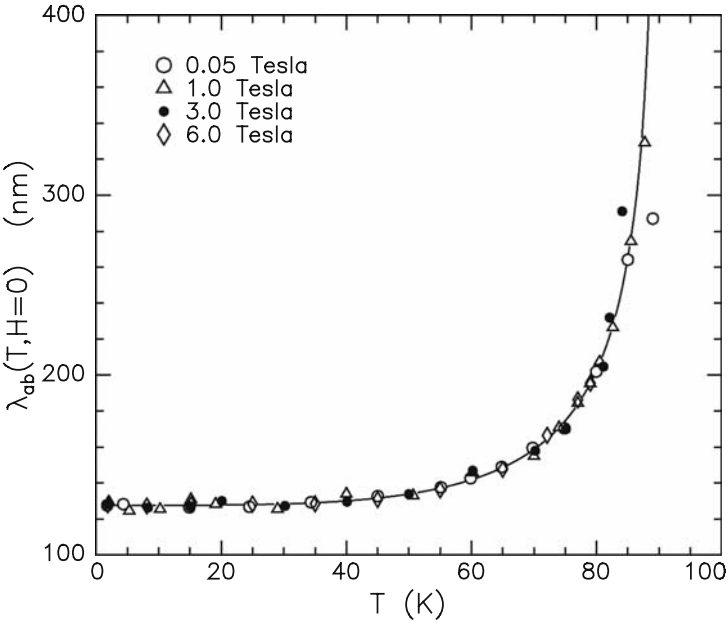

Figure 1. The temperature dependence of the zero-field penetration depth, λ_{ab}(T,H=0), with the fitted effects of pinning removed. The data are fitted with a London penetration depth of λ_{ab}(T=0,H=0) = 127.6 $\pm$ 1.5 nm. The curve shown represents the two-fluid model.

lying strong-coupled *s*-wave (or extended *s*-wave) pairing state. Clearly, *d*-wave pairing, even with pinning effects included, cannot adequately explain the μ^+SR data. As in the case of unannealed $Bi_2Sr_2CaCu_2O_8$ single crystals,[4] temperature-activated de-pinning produces a strong departure from *s*-wave behavior, which is suppressed in higher magnetic fields, revealing the *s*-wave character of the underlying pairing function. Thus, the bulk superconductivity of $YBa_2Cu_3O_7$ (and of $Bi_2Sr_2CaCu_2O_8$) is unquestionably strong-coupled *s*-wave (or extended *s*-wave) in character.

Since the CuO_2 plane bands are a linear combination of the *d* (Cu) and other (mostly oxygen) bands, one would expect that superconducting carriers in these bands would exhibit some strong *d*-wave composition. Our observation that the superconducting bands detected by μ^+SR have *s*-wave character, strongly indicates that the superconducting band is not a Cu band, and hence likely not a CuO_2 band. On the other hand, the BaO bands have virtually no *d*-wave character, and so are strong candidates for the superconducting layer. This same conclusion has been reached before, by different methods.[15]

Acknowledgments

We thank the TRIUMF Cyclotron Facility staff, U.S. Office of Naval Research (Contract No. N00014-03-1-0375), and the U.S. Air Force Office of Scientific Research (Contract No. F49620-97-1-0297).

* Permanent address.

References

1. D. R. Harshman, G. Aeppli, E. J. Ansaldo, B. Batlogg, J. H. Brewer, J. F. Carolan, R. J. Cava, M. Celio, A. C. D. Chaklader, W. N. Hardy, S. R. Kreitzman, G. M. Luke, D. R. Noakes, and M. Senba, Phys. Rev. **B 36**, 2386 (1987).
2. B. Pümpin, H. Keller, W. Kündig, W. Odermatt, I. M. Savic, J. W. Schneider, H. Simmler, P. Zimmermann, E. Kaldis, S. Rusiecki, Y. Maeno, and C. Rossel, Phys. Rev. **B 42**, 8019 (1990).
3. D. R. Harshman, L. F. Schneemeyer, J. V. Waszczak, G. Aeppli, R. J. Cava, B. Batlogg, L. W. Rupp, Jr., E. J. Ansaldo, and D. Ll. Williams, Phys. Rev. **B 39**, 851 (1989).
4. D. R. Harshman, R. N. Kleiman, M. Inui, G. P. Espinosa, D. B. Mitzi, A. Kapitulnik, T. Pfiz, and D. L. Williams, Phys. Rev. Lett. **67**, 3152 (1991).
5. R. A. Klemm, Intl. J. Mod. Phys. **B12,** 2920 (1998), and references therein.
6. E. J. Ansaldo, B. Batlogg, R. J. Cava, D. R. Harshman, L. W. Rupp, Jr., T. M. Riseman, and D. Ll. Williams, Physica **C 162-164,** 259 (1989).
7. D. A. Wollman, D. J. Van Harlingen, J. Giapintzakis, and D. M. Ginsberg, Phys. Rev. Lett. **74**, 797 (1995); C. C. Tsuei, J. R. Kirtley, Z. F. Ren, J. H. Wang, H. Raffy, and Z. Z. Li, Nature **387**, 481 (1997).
8. J. E. Sonier, J. H. Brewer, and R. F. Kiefl, Rev. Mod. Phys. **72**, 769 (2000).
9. D. R. Harshman, W. J. Kossler, X. Wan, A. T. Fiory, A. J. Greer, D. R. Noakes, C. E. Stronach, E. Koster, and J. D. Dow, "Nodeless pairing state in single-crystal $YBa_2Cu_3O_7$," Phys. Rev. **B,** in press; D. R. Harshman, W. J. Kossler, X. Wan, A. T. Fiory, A. J. Greer, D. R. Noakes, C. E. Stronach, E. Koster, A. Erb, and J. D. Dow, Intl. J. Mod. Phys. **B 17,** 3582 (2003).
10. M. H. S. Amin, M. Franz, and I. Affleck, Phys. Rev. Lett. **84**, 5864 (2000).
11. B. Billon, M. Charalambous, J. Chaussy, R. Kock, and R. Liang, Phys. Rev. **B 55,** 14753 (1997).
12. K. Zhang, D. A. Bonn, S. Kamal, R. Liang, D. J. Baer, W. N. Hardy, D. Basov, and T. Timusk, Phys. Rev. Lett. **73,** 2482 (1994); C. P. Bidinosto, W. N. Hardy, D. A. Bonn, and R. Liang, Phys. Rev. Lett. **83,** 3277 (1999); A. Carrington, R. W. Giannetta, J. T. Kim, and J. Giapintsakis, Phys. Rev. **B 59,** 14173 (1999).
13. D. Xu, S. K. Yip, and J. A. Sauls, Phys. Rev. **B 51,** 16233 (1995).
14. A. Bhattacharya, I. Zutic, O. T. Valls, A. M. Goldman, U. Welp, and B. Veal, Phys. Rev. Lett. **82,** 3232 (1999).
15. J. D. Dow and D. R. Harshman, J. Phys. Chem. Solids **63,** 2309 (2002).

NUCLEAR SPIN RELAXATION AND INCOMMENSURATE MAGNETISM IN DOPED CUPRATES

L. P. Gor'kov,*
NHMFL, Florida State University, Tallahassee, FL 32310, USA
and L.D.Landau Institute for Theoretical Physics, 142432 Chernogolovka, Russia

G. B. Teitel'baum,†
E.K.Zavoiskii Institute for Technical Physics of the RAS, 420029 Kazan, Russia

Abstract Existing data on ^{63}Cu-nuclear spin relaxation reveal two independent relaxation processes: the one that is temperature independent we link to incommensurate peaks seen by neutrons, while the "universal" temperature dependent contribution coincides with $1/^{63}T_1(T)$ for two-chain YBCO 124. We argue that this new result substitutes for a "pseudogap" regime in a broad class of high-T_c cuprates and stems from the 1st order phase transition that starts well above the superconductivity T_c but becomes frustrated because of broken electroneutrality in the CuO_2 plane.

Keywords: superconductivity, pseudogap, magnetic properties, NMR

One of the most intriguing normal properties of the high-T_c (HT_c) cuprates is the so called "pseudogap" (PG) phenomenon. It is commonly presented in the (T, x) plane as a line that starts from rather high temperatures (at small x) and reaches the superconductivity (SC) T_c "dome" below at or above optimal $x \sim 0.16$. In a broad sense x means the hole concentration in the CuO_2- plane, but more often than not one refers to properties of the Sr-doped $La_{2-x}Sr_xCuO_4$ The PG feature was seen in numerous experiments (NMR, tunneling spectra, resistivity etc.; see for example reviews [1, 2]). It has been stressed [3] that the PG temperature is not defined unambiguously.

*E-mail: gorkov@magnet.fsu.edu
†E-mail: grteit@dionis.kfti.knc.ru

J. Ashkenazi et al. (eds.), New Challenges in Superconductivity: Experimental Advances and Emerging Theories, 55-62.

A widespread view is that the feature comes from some crossover in the electronic density of states (DOS). The main result of the present paper is that after a proper re-arrangement of the experimental data no PG feature exists in the ^{63}Cu nuclear spin relaxation time behaviour. Instead, the data show two independent parallel relaxation mechanisms: a temperature independent one that we attribute to stripes caused by the presence of external dopants and an "universal" temperature dependent term which turns out to be exactly the same as in the stoichiometric compound YBCO 124.

We attempt below to put the results in the context of a phase separation [4]. The decomposition of $1/^{63}T_1(T,x)$ into two terms, as it will be discussed below in more details, manifests itself in a broad temperature interval above T_c. It is limited from above by a T^* that depends on the concentration, x. We consider T^* defined in this way as a temperature of a 1st order phase transition, which, however, cannot complete itself in spatial coexistence of two phases because of the electroneutrality condition [5]. It was already argued in [4] that such a frustrated 1st order phase transition may actually bear a dynamical character. The fact that a single resonant frequency for the ^{63}Cu nuclear spin is observed in the NMR experiments, confirms this suggestion. Although in what follows, we use the notions of the lattice model [4, 5], even purely electronic models [6–9] for cuprates may reveal a tendency to phase separation.

The basic assumption in [4, 5] are the following. At large enough doping holes move between coppers and oxygens. Spins in the system are d^9-holes trapped to the Cu-sites at the expense of local lattice distorsions. Elastic attractive interactions between these distorsions give rise to a lattice driven frustrated transition below some T^*. Exchange interactions, as in the parent La_2CuO_4, tend to organize the Cu-spins in the antiferromagnetic (AF) sub-phases. Excess charge of the dopants' ions in AF regions must be compensated by accumulation of holes in "metallic" regions.

We now turn to experimental data. In what follows we address only $1/^{63}T_1$ behaviour because for cuprates AF fluctuations prevail over the Korringa mechanisms.

In Fig. 1a we collected data on $1/^{63}T_1$ in LSCO from [10]. Note the following: 1) according to [11] $1/^{63}T_1(T)$ at higher temperatures tends to 2.7 msec^{-1} *for all* Sr concentrations, in spite of considerable spread seen in Fig. 1a. Beginning of deviation from that value could serve us as a definition of $T^*(x)$; 2) note that dissipation $1/^{63}T_1$ monotonically decreases from small x to 0.24; 3) after an appropriate *vertical* offset all curves in Fig. 1a collapse onto the T dependence of $1/^{63}T_1$ for the "optimal" $x = 0.15$ above 50 K (Fig. 1b). We have checked that last

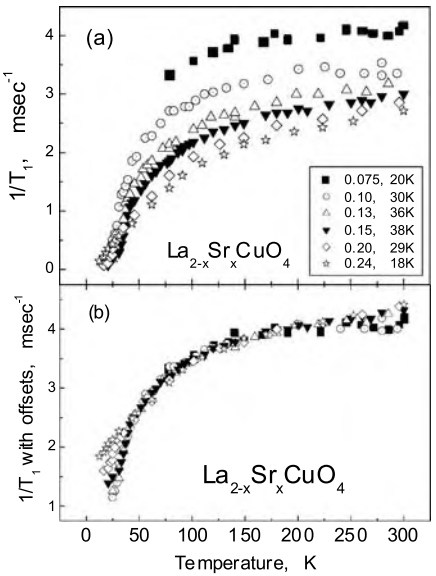

Figure 1. The temperature dependence of $1/^{63}T_1(x)$ for LSCO: a) the plots for different x and T_c (see inset) are taken from [10], at higher temperatures all of them converge to the same value of 2.7 msec^{-1} [11] ; b) the same dependencies collapsing to the single curve after the corresponding vertical offsets.

tendency works well for YBCO (6.5) doped with Ca i.e., the data for different z in $Y_{1-z}Ca_zBa_2\ Cu_3\ O_{6.5}$ [12] may be put on the top of each other after proper offsets.

This prompts us to verify whether same "off-settings" of the $1/^{63}T_1$ data apply to a broader group of materials. The stoichiometric $YBa_2Cu_4O_8$ possesses no structural or defect disorder and we adjust all data to the $1/^{63}T_1$ behaviour for this material [3]. Fig. 2 shows that after a vertical shift in $1/^{63}T_1$ all the materials indeed follow the same "universal" temperature dependence above their T_c and below 300 K. In other words, in this temperature range the nuclear spin relaxation in these cuprates is a sum of contributions from two parallel processes:

$$1/^{63}T_1 = 1/^{63}\overline{T}_1(x) + 1/^{63}\widetilde{T}_1(T) \qquad (1)$$

In eq. (1) $1/^{63}\overline{T}_1(x)$ depends on a material and a degree of disorder (x), but does not depend on temperature, while $1/^{63}\widetilde{T}_1(T)$, depends only on temperature, is the same for all these compounds and coincides with the $1/^{63}T_1$ for the two chains YBCO 124 above its T_c=62 K.

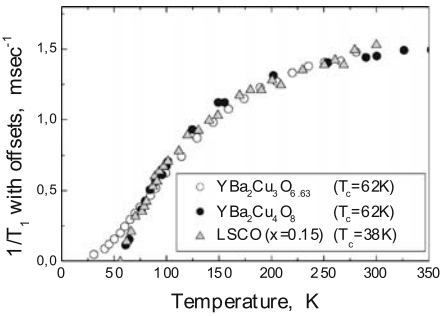

Figure 2. The temperature dependence of $1/^{63}T_1$ for different compounds: the $1/^{63}T_1$ for YBCO (123) [13] overlayed with that for LSCO [10] and YBCO (124) [3].

Thus, to some surprise the only "pseudogap" feature in the NMR data that may be discerned in Fig.2 is the one for YBCO 124: a change in the temperature regime between 130 and 180 K. It would be tempting to take again this feature as a mark of the PS regime taking place now in the stoichiometric material where doping most definitely comes about as a spill-over of carriers from the CuO-chains into CuO_2 planes. It is also natural to think that the number of the transferred carriers is not small: actually the low temperature Hall effect measurements [15–17] show a rapid increase in the number of carriers (i.e. Fermi surface size) up to one hole per unit cell even in the single layer material like LSCO, at the optimal doping $x \sim 0.15$. Recall, however, that little is known for the "homogeneous" phase (i.e. above $T^*(x)$). Properties of both YBCO 124 and the optimally doped LSCO (see [1] for review) are unusual and best described in a very broad temperature interval in terms of the "marginal" Fermi liquid [18]. We have not found a reliable experiment to define T^* for these compounds and therefore leave the origin of the $1/^{63}\widetilde{T}_1(T)$-term for further discussions.

The decomposition (1) into two parallel dissipation processes show that usual definitions of T^* [19] have no grounds. In Fig.1a the LSCO data with $x < 0.15$ are spread even above 250 K. As a rough estimate for T^*, it is much higher than the SC onset temperature.

Fig. 3 presents the dependence on x for $1/^{63}\overline{T}_1$ in $La_{2-x}Sr_xCuO_4$. The inset provides the "offsets" (i.e. $1/^{63}\overline{T}_1$ terms) for other materials. We return to discussion of Fig.3 later.

The observation that is central for the following is that in all the materials with non-zero $1/^{63}\overline{T}_1$ (see the inset in Fig.3) incommensurate (IC) peaks have been observed in neutron scattering [20]. Peaks are

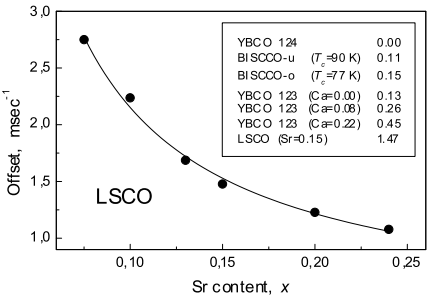

Figure 3. The offset $1/^{63}\overline{T}_1(x)$ vs Sr content x for LSCO (relative to that for YBCO 124), line is a guide for eyes. Inset: the offsets for some other compounds (data for underdoped (u) and overdoped (o) BISCCO 2212 deduced from [14]; to compare BISCCO with LSCO and YBCO materials the hyperfine constants have to be properly adjusted).

close to the $[\pi,\pi]$ – point: at $[\pi(1\pm\delta),\pi]$ and $[\pi,\pi(1\pm\delta)]$ [21]. We will now look for the connection between these two phenomena.

We first make an attempt to agree on a semi-quantitative level the observed IC magnetic peaks in $La_{2-x}Sr_xCuO_4$ with the values of the first term in eq. (1). We concentrate on $La_{1.86}Sr_{0.14}CuO_4$ for which the most detailed data are available [22].

With the notation from [23]

$$1/T_1 = \frac{k_BT}{2\mu_B^2\hbar^2\omega}\sum_i F(Q_i)\int\frac{d^2q}{(2\pi)^2}\chi''(q,\omega\to 0) \tag{2}$$

where Q_i stands for one peak, hyperfine "tensor" $F(Q) = \{A_\perp + 2B[\cos(Q_x)+\cos(Q_y)]\}^2$ and for $\chi''(q,\omega\to 0)$ we take near single peak, say $[\pi(1-\delta),\pi]$

$$\chi''(q,\omega) = \frac{\chi''_{peak}(T)\omega}{[1+(x\xi_x)^2+(y\xi_y)^2]^2} \tag{3}$$

where $(x,y) = (q_x-\pi(1-\delta); q_y-\pi)$ and ξ_x and ξ_y are the correlation lengths in the two proper directions. After integration the contribution from stripes with q along the x-direction is

$$1/^{63}T_1 = \frac{k_BT}{\pi\mu_B^2\hbar\xi_x\xi_y}\{A_\perp - 2B[\cos(\pi\delta)+1]\}^2\chi''_{peak} \tag{4}$$

Experimentally [22] $\chi''_{peak}(T)\propto T^{-2}$ and for $x=0.14$ $\quad\delta=0.245\sim 1/4$. Assuming the T^{-1} dependence [22] only for the one of ξ's, ξ_x and us-

ing for $A_\perp$ and B the known values [23] one obtains: $1/^{63}T_1 = (4/\xi_y)$ msec^{-1}. With the AF correlation length $\xi_y \sim 4$ this is the correct order of magnitude.

The descending dependence of the offset (Fig.3) agrees qualitatively with the behavior of $\delta(x)$ [24] in eq.(4). For a quantitative description one need to know the x-dependence for $\chi''_{peak}(T)$. Such data in the absolute units are absent yet except [22]. Another fact that may underlie this behaviour is that with the x-increase buckling in the CuO_2-planes is known to decrease diminishing pinning effects and making the local symmetry of the CuO_2-unit same as in other materials from the class with small offset in Fig.3. Also, the system grows more metallic with a high holes' content [15–17].

Next comes the question concerning the origin and the role played by IC peaks and the physics of fluctuations related to them.

Discovery of IC spin fluctuations presented a challenge for explaining the NMR results for the oxygen spin relaxation times: hyperfine field "leaks" originated by the AF incommensurate fluctuations, would considerably increase the oxygen's relaxation rates, but this was not seen experimentally. Slichter (see in Ref.[25]) interpreted these contradictions in terms of "discommensurations": a periodic array of soliton-like walls separating regions with a short-range AF order. Unlike neutrons, the NMR as a local probe, does not feel the overall periodicity.

Existence of stripes looks just natural in terms of a static phase separation. At doping the system (LSCO) must screen the excess charge (Sr^{2+}-ions) in AF regions. Therefore stripes of the AF ordered phase must alternate with "metallic" domain walls. The stripe arrangement by itself is nothing but an optimization of the competing Coulomb and lattice forces [7]. (The phenomena is well known in physics of surface.)

Stripes in a dynamical regime need better understanding. For instance, often the IC peaks are seen by neutrons only at low enough temperatures or for large energy transfer at an inelastic scattering [20]. At low temperatures stripes may form a long-range order even in LSCO (at smaller x, [26]), breaking the symmetry of the ground state. A better example of the "pinned" stripe order is given by Nd (or Eu)-doped LSCO [27–30]. ($La_{1.6-x}Nd_{0.4}Sr_xCuO_4$ reproduces all features of $La_{1-x}Sr_xCuO_4$, including SC and same positions for IC peaks at given x.) The transition into the ordered stripe phase is driven by appearance first of the lattice/charge peaks [29]. At finite temperatures stripes could be viewed as a new type of excitations above the ordered state.

On the other hand in LSCO itself "stripes" are seen through the inelastic scattering processes for arbitrary low energy transfer even at high temperatures 100-300 K [22]. while the ordered IC ground state

sets in only well below, at about $T \sim 30$K [26]. This example provides the argument against treating "stripes" as "excitations": at so high a temperature the underlying "long-range" IC ground state would be already melted. Therefore the two-phase description seems to be closer to reality meaning that in the dynamical regime the AF regions get coupled via Coulomb forces with the "metallic" layer. Note that with the further x-increase $\delta(x)$ increases as well and saturates making it meaningless to speak in terms of a strictly "monolayer" wall already above $x \sim 0.14$, where $\delta \approx 1/4$ [22]. (Note the difference in notations for IC peaks: (δ from [22] equals 2ϵ from [29] equals 2δ from [24]). Fig.3 demonstrates same tendency to increase the share of the "metallic" fraction with increase of Sr-concentration: $1/^{63}\overline{T}_1(x)$ continues to drop with x above 1/8.

Coexistence of a SC and the IC AF phases at low temperatures was confirmed recently by the neutron diffraction experiments [31] for $La_{2-x}Sr_xCuO_4$ ($x = 0.10$) in the vortex state. (The coexistence of SC and AF formations was found also from the μSR spectra [32]). The way of the "coexistence" of SC and the stripe order in the same sample remains unresolved: one view treats the new stripe symmetry as a superstructure superimposed on the Fermi surface that changes the energy spectrum like any SDW/CDW can do it (e.g. [33]). Another plausible alternative would be a spatially inhomogeneous coexistence of the nonsuperconducting IC AF phase and a "metallic" phase with strong fluctuations.

We have found that in a temperature interval above T_c and below some $T^* \sim$300 K the nuclear spin relaxation for a broad class of cuprates comes from two independent mechanisms: relaxation on the"stripe"-like excitations that leads to a temperature independent contribution to $1/^{63}T_1$ and an "universal" temperature dependent term. For $La_{1.86}Sr_{0.14}CuO_4$ we obtained a correct quantitative estimate for the value of the first term. We concluded from eq.(1) and Fig.3 that "stripes" always come about with external doping and may be pinned by structural defects. We argue that the whole pattern fits well the notion of the dynamical PS into coexisting metallic and IC magnetic phases. Experimentally, it seems that with the temperature decrease dynamical PS acquires the static character with the IC symmetry breaking for AF phase dictated by the competition between the lattice and the Coulomb forces. The form of coexistence of the IC magnetism with SC below T_c remains not understood as well as behaviour of stoichiometric cuprates.

The work of L.P.G. was supported by the NHMFL through NSF cooperative agreement DMR-9527035 and the State of Florida, that of G.B.T. through the RFFR Grant N 04-02-17137.

References

[1] T. Timusk and B. Statt, Rep. Prog. Phys. **62**, 61 (1999).

[2] J.L. Tallon and J.M. Loram, Physica C **349**, 53 (2001).

[3] G.V.M. Williams *et al.*, Phys. Rev. B **58**, 15053 (1998).

[4] L.P. Gor'kov and A.V. Sokol, JETP Lett. **46**, 420 (1987).

[5] L.P. Gor'kov, Journ. Supercond. **14**, 365 (2001).

[6] J.E. Hirsh, E. Loch *et al.*, Phys. Rev. B **39**, 243 (1989).

[7] J. Zaanen *et al.*, Phys. Rev. B **40**, 7391 (1989).

[8] V.J. Emery *et al.*, Phys. Rev. Lett. **64**, 475 (1990).

[9] M. Grilli *et al.*, Phys. Rev. Lett. **67**, 259 (1991).

[10] S.Oshugi *et al.*, J. Phys. Soc. Jpn. **63**, 700 (1994).

[11] T. Imai *et al.*, Phys. Rev. Lett. **70**, 1002 (1993).

[12] P. M. Singer *et al.*, Phys. Rev. Lett. **88**, 187601 (2002).

[13] M. Takigawa *et al.*, Phys. Rev. B **43**, 247 (1991).

[14] R.E. Walstedt *et al.*, Phys.Rev. B **44**, 7760 (1991).

[15] S. Uchida *et al.*, Physica C **162-164,** 1677 (1989).

[16] T. Nishikawa *et al.*, J. Phys. Soc. Jpn. **62**, 2568 (1993).

[17] F. Balakirev *et al.*, Nature **424**, 912 (2003).

[18] C. M. Varma *et al.*, Phys. Rev. Lett. **63**, 1996 (1989).

[19] J. Schmallian *et al.*, Phys.Rev. B **60**, 667 (1999). H.A.

[20] S.W. Cheong *et al.*, Phys. Rev. Lett. **67**, 1791 (1991); ys. Mook *et al.*, Nature **395**, 580 (1998); M. Arai *et al.*, Ph B Rev. Lett. **83**, 608 (1999); A. Bianconi, Int. J.Mod.Phys. **14**, 3289 (2000); P. Dai *et al.*, Phys. Rev. B **63**, 054525 (2001).

[21] J.M. Tranquada *et al.*, Nature **375**, 561 (1995).

[22] H. Aeppli *et al.*, Science **278**, 1432 (1997).

[23] Y. Zha *et al.*, Phys. Rev. B **54**, 7561(1996).

[24] K.Yamada *et al.*, Phys. Rev. B **57**, 6165 (1998).

[25] V. Barzykin *et al.*, Phys. Rev. B **50**, 16052 (1994).

[26] M. Fujita *et al.*, Phys.Rev. B **65**, 0654505 (1991).

[27] M.K. Crawford *et al.*, Phys. Rev. B **44**, 7749 (1991).

[28] J.M. Tranquada *et al.*, Phys. Rev.Lett. **78**, 338 (1997).

[29] J.M. Tranquada *et al.*, Phys. Rev. B **54**, 7489 (1996).

[30] J.M. Tranquada *et al.*, Phys. Rev. B **59**, 14712 (1999).

[31] B. Lake *et al.*, Nature **415**, 299 (2002).

[32] Ch. Niedermeier *et al.*, Phys. Rev.Lett. **80**, 3483 (1998).

[33] M.I.Salcola *et al.*, Phys. Rev. Lett. **77**, 155 (1996);
R.S.Markiewicz *et al.*, Phys. Rev. B **65**, 064520 (2002).

ANTIFERROMAGNETIC VORTEX CORE IN HTSC STUDIED BY SPATIALLY-RESOLVED NMR

K. Kumagai[1], K. Kakuyanagi[1], Y. Matsuda[2], and M. Hasegawa[3]

[1] *Division of Physics, Graduate School of Science, Hokkaido Univrsity, Sapporo 060-0810, Japan,*

[2]*Institute for Solid State Physics, University of Tokyo, Kashiwa, Chiba 277-8581, Japan,*

[3]*Institute of Materials Research, Tohoku University, Sendai, 980-8577, Japan*

corresponding to kumagai@phys.sci.hokudai.ac.jp

Abstract Spatially-resolved NMR is used to probe antiferromagnetism in the vortex state of nearly optimally doped high-T_c cuprate $Tl_2Ba_2CuO_{6+\delta}$ ($T_c = 85$ K). The broadened ^{205}Tl-spectra below 20 K and the temperature dependence of the enhanced nuclear spin-lattice relaxation rate $^{205}T_1^{-1}$ at the vortex core region indicate clear evidences of the antiferromagnetic order inside the vortex core of $Tl_2Ba_2CuO_{6+\delta}$.

Keywords: NMR, Antiferromagnetism, High-T_c superconductor, $Tl_2Ba_2CuO_{6+\delta}$

1. Introduction

Strong antiferromagnetic (AF) fluctuations play a crucial role in determining many physical properties of cuprate superconductors, and the electronic structure of vortex core in high-T_c superconductors (HTSC) with d-wave symmetry is very different from that of ordinary superconductors. As vortex cores are region of the suppressed superconductivity, how the antiferromagnetism emerges when the d-wave superconducting order parameter is suppressed comes out to be a fundamental problem in HTSC. [1] A new class of theories have emphasized the importance of the magnetism arising from the strong electron correlation for accounting for the microscopic vortex core structure. Possible competing orders, such as AF [2–6], staggered flux [7], and stripe orderings [8, 9] in and around cores have been discussed.

Neutron scattering experiment on $La_{2-x}Sr_xCuO_4$ has reported that an applied magnetic field enhances the AF correlation in the superconducting state [10]. A checkerboard halo of the local density of states (LDOS) around the core has been reported in $Bi_2Sr_2CaCu_2O_{8+\delta}$. [11] However, the relation between the observed phenomena and antiferromagnetism within vortex cores is not clear, because of lack of a spatial resolution of the magnetism.

Recent experimental [12, 13] and theoretical [14] NMR studies have established that the frequency dependence of spin-lattice relaxation rate T_1^{-1} in the

J. Ashkenazi et al. (eds.), New Challenges in Superconductivity: Experimental Advances and Emerging Theories, 63-68.

vortex state serves as a probe for the low energy excitation spectrum at different spatial regions of the vortex lattice. In this paper, we provide local information on the AF correlations in the different regions of the vortex lattice by performing a spatially-resolved NMR imaging on ^{205}TI-nuclei in nearly optimal doped $Tl_2Ba_2CuO_{6+\delta}$.[15]

2. Experimental

NMR measurements were carried out on the c-axis oriented polycrystalline powder of high quality $Tl_2Ba_2CuO_{6+\delta}$ ($T_c = 85$ K) in the external field along the c-axis. The ^{205}TI spin echo signals were obtained by a pulse NMR spectrometer under the field cooling condition (FCC) in a constant field. The spectra was obtained by convolution of the respective fourier transform spectra of the spin echo signals measured with an increment of 50 kHz.

3. Results and Discussion

A very sharp spectrum ($\sim$50 kHz) of ^{205}Tl in $Tl_2Ba_2CuO_{6+\delta}$ above T_c becomes broad and asymmetric below T_c, which originates from the local field distribution associated with the vortex lattice (the Redfield pattern). The local field profile in the vortex state is given by approximating $H_{loc}(\boldsymbol{r})$ with the London result, as described in Ref. [13, 15] The solid line in Fig. 1 shows a histogram at a particular local field which is given by the local field distribution $f(H_{loc}) = \int_\Omega \delta[H_{loc}(\boldsymbol{r}) - H_{loc}]d^2\boldsymbol{r}$, where Ω is the magnetic unit cell. In the calculation we used $\xi_{ab} = 18$ Å and $\lambda_{ab} = 1700$ Å, and assumed the square vortex lattice. The inset of Fig. 1 shows the image of the magnetic field distribution in the vortex lattice. The magnetic field is lowest at the center of the vortex square lattice (point C), and it is highest at the center of the vortex core (point A). The intensity of the histogram shows a peak at the field corresponding to the saddle point (point B).

The real spectrum broadens due to imperfect orientation of the powder and distortion of the vortex lattice. The dotted line in Fig. 1 represents the simulation spectra in which the Lorentzian broadening function, $f(H_{loc}) = \sigma/(4H_{loc}^2 + \sigma^2)$, is convoluted to the Redfield pattern using $\sigma = 42$ kHz. The theoretical curve reproduces the data well in the whole frequency range at $T = 20$ K. On the other hand, the spectrum at 5 K shows significant broadening at high frequency region (core region), while it can be well fitted below 52.1 MHz as shown in Fig 1.

The filled circles in Fig. 2 display the line width at the high frequency tail, Δf, which is defined as a difference of frequency between the peak intensity and the frequency at which the intensity becomes 1% of the peak. For comparison, the line width calculated from the Readfield spectra (between A and C point)

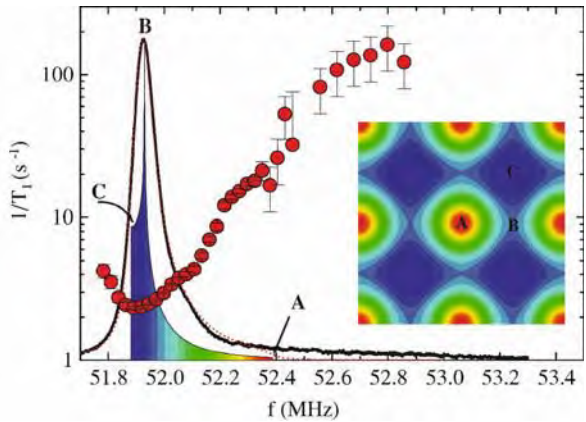

Figure 1. ^{205}Tl-NMR spectrum (solid line) at 5 K. The intensity is plotted in a linear scale. The thin solid line depict the histogram at particular local fields of the Readfield pattern. The dotted line represents the simulation spectrum convoluted with Lorentzian broadening function. The filled circles show the frequency dependence of $^{205}T_1^{-1}$ at the Tl site. The inset shows the image of the field distribution in the vortex square lattice; center of vortex core (A), saddle point (B) and center of vortex lattice (C).

is plotted by a dashed line. At high temperatures Δf agrees well with the calculation, while below 20 K it becomes much larger. We also plot δf which represents the line width at the half intensity (open circles). The fact that δf changes little even below 20 K confirms that the line broadening occurs only

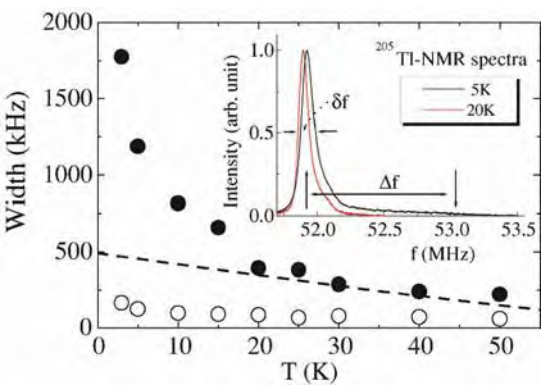

Figure 2. The line widths of the ^{205}Tl-NMR spectrum plotted as a function of T. Δf (filled circles) indicates the line width determined by the frequency at which the intensity becomes 1% of the peak. The dashed line represents the line width calculated from the simulation spectrum without taking into account the core magnetism. Open circles represent δf which is defined as the line width at the half intensity. Inset shows the spectrum at 5 K and 20 K and the definitions of Δf and δf.

in the high frequency core region. It should be noted that because of large transfer hyperfine coupling between Tl nuclei and Cu moment, the broadening of the Tl-NMR spectrum associated with the static magnetism is pronounced. Therefore, the observed broadening below ∼20 K is naturally explained by the appearance of static magnetism within cores below ∼20 K.

We can obtain the spatially-resolved information of T_1 by analyzing the frequency distribution of T_1 in the corresponding NMR spectrum. [13] The filled circles in Fig. 1 show the frequency dependence of $^{205}T_1^{-1}$ of the vortex state in $Tl_2Ba_2CuO_{6+\delta}$. [15] On scanning from the outside into the core (C → B → A), $^{205}T_1^{-1}$ increases rapidly after showing a minimum near the saddle point (B). The magnitude of $^{205}T_1^{-1}$ near the core region (A) is almost two orders of magnitude larger than that near the saddle point (B). This large enhancement of $^{205}T_1^{-1}$ is in striking contrast to $^{17}T_1^{-1}$ at ^{17}O sites in the under doped YBa_2CuO_8 [13]. $^{205}T_1^{-1}$ can monitor AF fluctuations sensitively, because the Tl atoms are located just above the Cu atoms and there exist large transferred hyperfine interactions between Tl and Cu nuclei through the apical oxygen. Thus, as $^{205}T_1^{-1}$ thus is dominated by Cu spin fluctuations, the remarkable enhancement (more than 100 times) of $^{205}T_1^{-1}$ around the core provides microscopically a direct evidence that the AF correlations are strongly enhanced near the vortex core region.

Figure 3 shows the T-dependences of $(T_1T)^{-1}$ and T_1^{-1} of ^{205}Tl nuclei within the core (filled circles) and at the frequency corresponding to the saddle point (open circles) in $Tl_2Ba_2CuO_{6+\delta}$. From high temperatures down to about 120 K, $(T_1T)^{-1}$ obeys the Curie-Weiss law, $(T_1T)^{-1} \propto 1/(T+\theta)$. The lowest

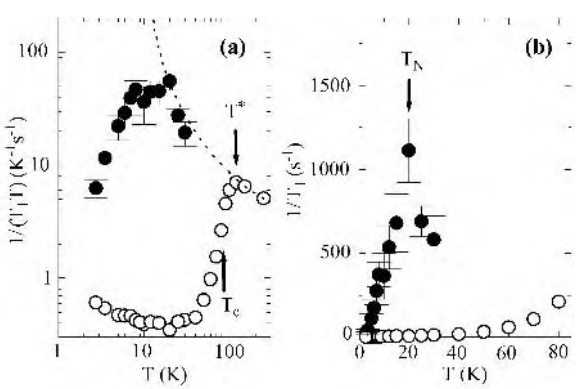

Figure 3. T-dependence of $(^{205}T_1T)^{-1}$ (a) and of $^{205}T_1^{-1}$ (b) at low temperatures. The filled and open circles represent the data at vortex cores and at the saddle point, respectively. $T^* \simeq 120$ K is the pseudogap temperature. The dotted line represents the Curie-Weiss law which is determined above T^*. In (b), T_N is the temperature at which $^{205}T_1^{-1}$ at the core exhibits a sharp peak.

T at which this law holds is conveniently called the pseudogap temperature T^*. Below T^*, $(T_1T)^{-1}$ decreases rapidly without showing any distinct anomaly associated with the superconducting transition at T_c, similar to other HTSC with pseudogap behavior.[16] Below 40K, $(T_1T)^{-1}$ is nearly T-independent down to 4 K due to the induced local DOS in d-wave superconductor.[17] An important signature is that $1/^{205}T_1$ at the core region exhibits a sharp peak at $T = 20$ K, which we label as T_N for future reference (Fig. 3(b)). Below T_N, $(^{205}T_1)^{-1}$ at the core region decreases rapidly with decreasing T. The sharp peak of $^{205}T_1^{-1}$ at T_N seems to support AF ordering. The broadening of the Redfield pattern at the high frequency region gives also additional evidence on AF ordering. On basis of these results, we are lead to conclude that the vortex core shows local AF ordering at $T_N = 20$ K; namely T_N corresponds to the Néel temperature within the core.

We finally discuss the spin structure within the core. The broadening occurs only at high frequencies, while it is absent at low frequencies. This fact indicates that the AF spins are oriented parallel to the CuO_2 layers. This follows by observing that the broadening should occur at both high and low frequency sides if the AF ordering occurs perpendicular to the layers, because in this case the direction of the alternating transferred hyperfine fields are parallel and antiparallel to the applied field. Using the hyperfine coupling constant, $A_{hf} = 56\text{kOe}/\mu_B$, the magnetic moments induced within the core is estimated to be $\sim 0.1\mu_B$.

In summary, we have obtained novel features for the vortex core antiferromagnetism by the spatially-resolved ^{205}Tl-NMR in $Tl_2Ba_2CuO_{6+\delta}$; (1) the strong enhancement of $(^{205}T_1)^{-1}$ (Fig. 1), (2) the peak of $(^{205}T_1)^{-1}$ at $T = 20$ K (Fig. 3), (3) the broadening of the NMR spectrum below $T \sim 20$ K (Fig. 2). All of these results provide direct evidence that in the vortex core region the AF spin correlation is extremely enhanced, and that the paramagnetic-AF order transition (freezing of spin fluctuations) of the Cu moments takes place at $T_N \sim 20$ K. The present results offer a new perspective on how the AF vortex core competes with the d-wave superconductivity.

Acknowledgments

We acknowledge helpful discussions with K. Machida and M. Ogata. The present work was supported by a grand-in-aid for Scientific Research from Ministry of Education, Culture, Sports, Science and Technology of Japan.

References

[1] S.A. Kivelson *et al.*, Rev. Mod. Phys. **75** 1201 (2003).
[2] S.C. Zhang, Science **275** (1997) 1089.
[3] D.P. Arovas *et al.*, Phys. Rev. Lett. **79** (1997) 2871.

[4] M. Franz and Z. Tesanović, Phys. Rev. Lett. **80** (1998) 4763.
[5] A. Himeda *et al.*, J. Phys. Soc. Jpn. **66** (1997) 3367, M. Ogata, Int. J. Mod. Phys. **B 13** (1999) 3560.
[6] J.H. Han and D.H. Lee, Phys. Rev. Lett. **85** (2000) 1100.
[7] J. Kishine, P.A. Lee PA, X.G. Wen, Phys. Rev. Lett. **86** (2001) 5365, and Q.H. Wang, J.H. Han, and D.H. Lee, Phys. Rev. Lett. **87** (2001) 167004.
[8] E. Demler, S. Sachdev, Y. Zhang, Phys. Rev. Lett. **87** (2001) 067202.
[9] M. Takigawa *et al.*, Phys. Rev. Lett **90** (2003) 047001.
[10] B. Lake *et al.*, Science 291 (2001) 1759, and Nature **415** (2002) 299.
[11] J.E. Hoffmann *et al.*, Science **295** (2002) 466.
[12] N.J. Curro, C. Milling, J. Hassee, C.P. Slichter, Phys. Rev. **B 62** (2000) 3473, and V. F. Mitrovic *et al.*, Nature 413 (2001) 501.
[13] K. Kakuyanagi, *et al.*, Phys. Rev. **B 65** (2002) 060503.
[14] M. Takigawa *et al.*, Phys. Rev. Lett. **83** (1999) 3057. R. Wortis, *et al.*, Phys. Rev. **B 61** (2000) 12342, D.K. Morr and R. Wortis, Phys. Rev. **B 61** (2000) R882, and D.K. Morr, Phys. Rev. **B 63** (2001) 214509.
[15] K. Kakuyanagi, K. Kumagai, Y. Matsuda, M. Hasegawa, Phys. Rev. Lett. **90** (2002) 197003.
[16] M. Takigawa *et al.*, Phys. Rev. **B 43** (1991) 247.
[17] G.E. Volovik, JETP Lett. **58** (1993) 469.

EXPLORING THE OXYGEN ORDER IN Hg -1223 AND Hg -1201 BY ^{199}Hg MAS NMR

Raivo Stern[1], Ivo Heinmaa[1], Dmitriy A. Pavlov[2], and Ingrid Bryntse[2]
[1]*National Institute of Chemical Physics and Biophysics (NICPB), 12618 Tallinn, ESTONIA,*
[2]*Department of Inorganic Chemistry, Arrhenius Laboratory, SE-10691 Stockholm, SWEDEN*

Abstract: We demonstrate the use of a high-resolution solid-state fast (45 kHz) magic angle spinning (MAS) NMR for mapping the oxygen distribution in Hg-based cuprate superconductors. We identify observed three peaks in ^{199}Hg spectrum as belonging to the different chemical environments in the HgO_δ layer with no oxygen neighbors, single oxygen neighbor, and two oxygen neighbors. We discuss observed differences between Hg-1201 and Hg-1223 materials.

Key words: ^{199}Hg NMR; MAS; High-T_c superconductors; oxygen order

1. INTRODUCTION

In many of high-temperature superconductors (HTSC) the charge balance is tuned by changing the oxygen content of the system. The final result depends sensitively not just on total number of added or removed oxygen atoms but also on their distribution patterns, the details of which are impossible to study by common X-ray or microscopy methods. Nuclear magnetic resonance (NMR) spectroscopy has served as an important tool to explore HTSC allowing one to obtain valuable information about the local environment of selected atoms. We propose a high-resolution NMR technique to study the oxygen distribution in mercury containing HTSC. These materials show record high transition temperatures of 133 K[1]. Due to its ½-spin the mercury isotope ^{199}Hg is a convenient nuclear spin label for the study of Hg based HTSC. As pointed out earlier by Hoffmann *et al.*[2], Gippius *et al.*[3], Suh *et al.*[4] and Horvatic´*et al.*,[5] the resolution of traditional NMR measurements on randomly oriented powder samples is not high enough to record any reliable ^{199}Hg Knight shift. Here we report first results

J. Ashkenazi et al. (eds.), New Challenges in Superconductivity: Experimental Advances and Emerging Theories, 69-72.

of ^{199}Hg NMR studies of the $HgBa_2CuO_{4+\delta}$ (Hg-1201) and $HgBa_2Ca_2Cu_3O_{8+\delta}$ (Hg-1223) phases using magic angle spinning (MAS) technique to obtain high resolution spectra.

2. EXPERIMENTAL DETAILS

We investigated five powder samples of Hg-1201 and Hg-1223 listed in Table 1. The Hg-1223 samples were synthesized in sealed silica tubes using an one-temperature furnace. Mixtures of oxides, with the starting nominal composition were annealed at 880 °C during 10 hours. All operations with air-sensitive reagents and products were performed in an Ar-filled glove box (MBraun Labmaster 100). The samples of Hg-1201 are as-prepared (almost optimally doped sample #4) and oxidized (overdoped sample #5).

Table 1. Superconducting properties of the samples: label, nominal composition, lattice constants a and c, onset of superconducting transition as measured by susceptibility (1-3) or deduced from lattice parameters[6] (4-5), isotropic shift σ_{iso} and full width at half maximum Δ of center bands or their components as on Fig. 1.

Nr	Nominal Composition	a [Å]	c [Å]	T_{co} [K]	σ_{iso} [ppm]	Δ [ppm]
1.	$HgBa_2Ca_2Cu_3O_{8+\delta}$	3.8541(1)	15.8043(7)	126	A -969(8)	100
					B -860(5)	61
					C -772(41)	90
2.	$Hg_{0.8}Tl_{0.2}Ba_2Ca_2Cu_3O_{8+\delta}$	3.8533(1)	15.854(1)	129	-840(3)	156
3.	$Hg_{0.8}Sc_{0.2}Ba_2Ca_2Cu_3O_{8+\delta}$	3.8593(3)	15.806(1)	110	A -982(3)	81
					B -868(2)	75
					C -756(4)	73
4.	$HgBa_2CuO_{4+\delta}$	3.8802(1)	9.5005(9)	77	-684(9)	237
5.	$HgBa_2CuO_{4+\delta}$	3.8751(2)	9.4984(8)	96	- 653(3)	152

We have made use of rather unique high-resolution solid-state NMR technique - so called fast-MAS NMR[7]. The lines of the ^{199}Hg nuclei are typically very broad due to large chemical or Knight shift anisotropy and therefore they are hard to observe. Fast-MAS of a powder sample results in narrow resonance line at isotropic shift value σ_{iso} (center band, marked by * on Fig. 1) and in number of spinning sidebands at multiples of spinning speed frequency. The sideband amplitudes approximately map the original broad powder pattern. In our experiments 44-46 kHz spinning speed was used. The volume of the spinning rotor (1.8 mm outer diameter) is very small, therefore, for a good quality Hg spectrum we need to average about for 24 hours. All the spectra were taken at room temperature, high spinning additionally heats the sample up by about 15 degrees. The chemical (Knight) shifts are given in Me_2Hg scale.

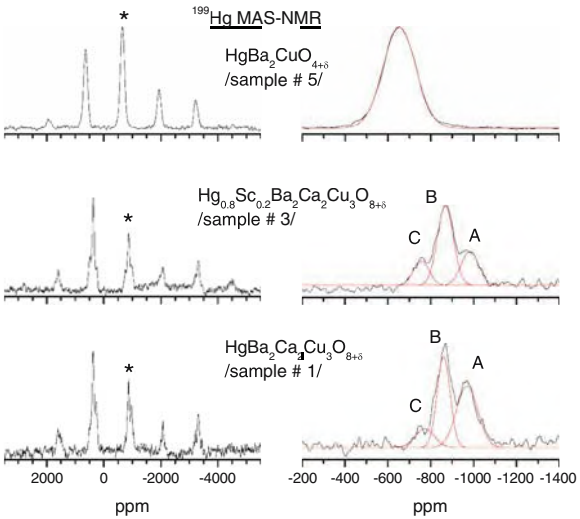

Figure 1. ^{199}Hg MAS NMR spectra recorded in 4.7T field (35.79MHz). The center bands (denoted by *****) of the full spectra are given in the right panels together with the Gaussian fits.

3. RESULTS AND DISCUSSION

The high resolution ^{199}Hg spectra of three samples are given in Fig 1, the data for all samples are given in Table 1. In case of Hg-1201 we observe a single gaussian ^{199}Hg line. The as-prepared sample (#4) has remarkably broader linewidth than the oxygen annealed one (#5), reflecting the higher homogeneity in the last one. In ^{199}Hg spectra of our Hg-1223 samples (except sample #2) we observe three narrow components (labeled A, B, and C in Fig. 1). Our interpretation of the three lines is following.

According to neutron scattering results[8] there is maximally about 30% of oxygen in HgO_δ layer. Therefore the following different environments of Hg nuclei are possible

- Hg with no oxygen nearest neighbors in HgO_δ plane (assigned to line A),
- Hg with 1 oxygen nearest neighbor (line B)
- Hg with 2 oxygen neighbors (line C).

In fact the sites with 3 and 4 nearest neighboring oxygen are thinkable, but the probability to find these sites is quite low and we do not see these lines in the spectrum.

Assuming random distribution of the oxygen atoms in the layer, one can easily calculate the probabilities for all five configurations.

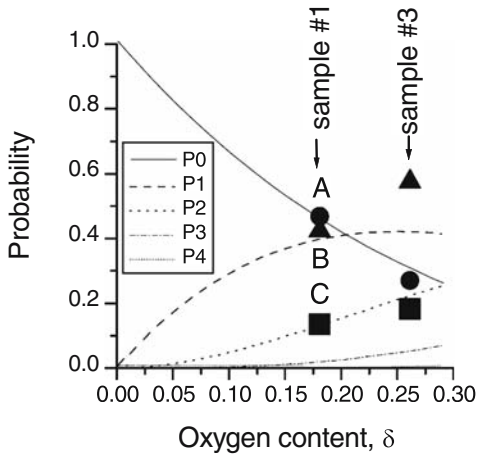

Figure 2. Probabilities P0, P1,..., P4 to find Hg sites with 0, 1 ...,4 oxygen neighbors in the HgO_δ layer, assuming random distribution, with the relative intensities of lines A, B, and C. The oxygen content δ for #1 and #3 is estimated from the lattice parameter a.[6]

Fig. 2 shows that relative intensities of the center band lines of the sample 1 fit well to the random scenario, whereas those of the sample 3 indicate deviation from the random distribution. Here the large intensity of the line B suggests that the oxygen atoms tend to be separated by at least one lattice period.

ACKNOWLEDGMENTS

The financial support by the Royal Swedish Academy of Sciences, the Estonian Science Foundation, and NHMFL is gratefully acknowledged.

REFERENCES

1. A. Schilling, M. Cantoni, J.D. Guo and H.R. Ott, Nature **363** (1993), 56.
2. W. Hoffmann, *et al*., Physica C **227** (1994) , 225.
3. A. A. Gippius, *et al*, Phys. Rev. **B59** (1999) , 654.
4. B. J. Suh, *et al*, Phys. Rev. **B50** (1994) , 651.
5. M. Horvatiç, *et al*, Physica C **235-240** (1994) , 1669.
6. E. V. Antipov, A. M. Abakumov, and S. N. Putilin, Supercond. Sci. Technol. **15** (2002), R31-R49
7. Samoson A., Tuherm T., and Past J., Chemical Physics Letters **365** (2002), 292.
8. Wagner J.L., Hunter B.A., Hinks D.G., Jorgensen J.D., Phys. Rev. **B51** (1995) , 15407.

TWO FLUIDS FORMATION IN THE NORMAL STATE OF HIGH-T_C SUPERCONDUCTOR

High Temperature Thermopower of $La_{2-x}Sr_xCuO_4$

J. S. Kim and Y. W. Park

School of Physics and Condensed Matter Research Institute, Seoul National University, Seou 151-747, Korea

Abstract: Thermoelectric power (TEP) of high-T_C superconductors has been investigated in a wide range of temperature ($T_C < T < 700$ K) for $La_{2-x}Sr_xCuO_4$. For wide doping level from underdoping to heavily overdoping, TEP follows the linear-T dependence above the broad peak temperature, T_p. At high temperatures, however, TEP shows deviation from the linear-T dependence at a certain temperature T_h, which is consistent with the pseudogap temperature. The systematic change of the TEP behavior is discussed in terms of the two fluids model of bound pairs and independent normal carriers.

Key words: High-T_C cuprates, Two fluids, Normal state, and High temperature thermoelectric power.

1. INTRODUCTION

The normal state properties in high-T_C cuprates are generally considered to be related to the origin of high-T_C superconductivity. From intensive studies in last two decades, it was found that the normal state properties show strong deviation from Fermi-liquid behavior, and such anomalous behavior is related to the pseudogap formation at the Fermi level (E_F)[1]. Below a characteristic temperature (T^*), both spin and charge gaps are gradually developed with decrease of temperature and connect smoothly to the superconducting gap across T_C. Also the *d*-wave symmetry observed in the pseudogap is the same as that of the superconducting gap.

J. Ashkenazi et al. (eds.), New Challenges in Superconductivity: Experimental Advances and Emerging Theories, 73-78.

The origin of pseudogap is at present a controversial subject. Based on such similarities between the pseudogap and superconducting gap, a promising explanation is the presence of bound pairs above T_C [2-5]. The appearance of pseudogap is originated from the formation of incoherent bound pairs, and as a result, the system undergoes the transition from the normal metallic state with independent normal electrons to an intriguing two-fluid state due to coexistence of normal electrons and bound pairs[2-3].

Since TEP is a sensitive probe of the entropy per carrier in the system, it can provide information about the anomalous properties of the two-fluid state in the normal state of high-T_C cuprates. Here we carefully investigated the TEP of $La_{2-x}Sr_xCuO_4$ (LSCO) for x = 0.05 ~ 0.35 using the newly developed TEP measurement technique at high temperatures up to 700 K. Based on our TEP results, the possibility of bound pair formation in the normal state is discussed as the origin of the intrinsic inhomogeneity in the normal state ($T_C < T < T_h$) of high-T_C superconductors.

2. EXPERIMENTS

The polycrystalline LSCO samples were synthesized using solid-state reaction method. X-ray diffraction and energy dispersive spectroscopy show all samples are homogenous and stoichiometric except the heavily doped ones, x = 0.325 and 0.35. In these two samples, small amount (less than 5 %) of impurity phase was found. TEP is measured using an ac steady-state method with low frequency (~ 0.033 Hz) [6]. Samples were kept in flowing oxygen to avoid the oxygen deficiency at high temperature. The TEP data are reproducible without any hysteresis upon thermal recycling from room temperature to 700K.

3. RESULTS AND DISCUSSION

Figure 1 shows the temperature dependence of TEP of LSCO for $T_C \leq T \leq$ 700 K. Below 300 K our results are in good agreement with other published data on polycrystalline and single-crystal samples [7]. For lightly doped sample (x = 0.05), the TEP rises towards a maximum near T_p and decreases linearly with temperature up to 700 K. As the doping concentration increases, the magnitude of TEP and T_p are decreased, and TEP begins to deviate from the linear-T dependence near T_h for $x > 0$. Such deviation from linear-T dependence is enhanced with doping up to x = 0.2 and eventually reduced on the heavily doped samples for $x > 0.25$ (See Fig. 1(b)). In heavily over-doped regime, the linear-T dependence is much

pronounced as shown in Fig. 1(b). However, up to $x = 0.35$, slight deviation from linear-T dependence at high temperature is observed and moreover, the broad peak of TEP at low temperature is still maintained.

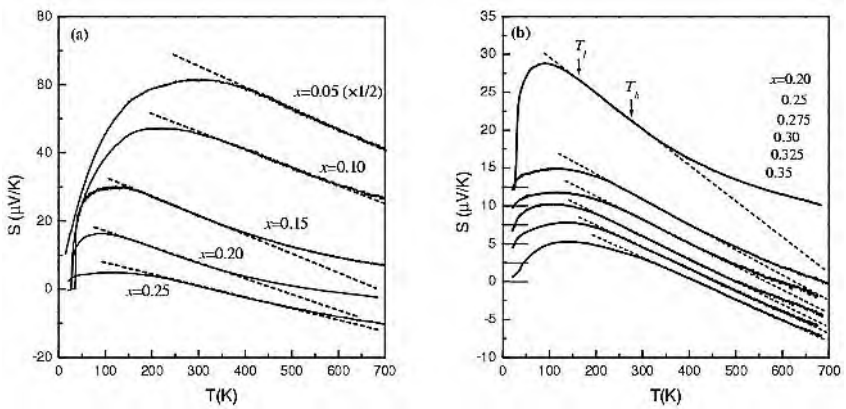

Figure 1. Temperature dependence of TEP for LSCO in wide temperature range ($T_C \le T \le$ 700 K) for (a) $0.05 \le x \le 0.20$ (b) $0.25 \le x \le 0.35$. For clarity, the TEP curves of (b) are offset by a constant. The dashed line is the fitting curve with linear-T dependence in the intermediate temperature regime. The arrows indicate T_l and T_h (See the text.)

Figure 2(a) presents the subtracted TEP ($\Delta S = S(T) - S_L(T)$) data with the linear fitting function $S_L(T) = \alpha T + \beta$ for typical LSCO samples. From this plot, we can clearly define the temperature range ($T_l \le T \le T_h$) for linear-T dependent TEP. If we plot T_h as a scaling temperature, all TEP data merge to a universal curve with the exponent ~ 0.34. T_h is changed systematically showing a minimum at $x \sim 0.2$. The inset shows the doping dependence of the slope (α) and offset (β) for $S_L(T)$. In Fig. 2(b), we compared the characteristic temperatures (T_h, T_l and T_p) with the previously reported pseudogap temperature [1]. For the underdoped and optimally doped LSCO, the pseudogap temperature coincides with T_h and the DOS near E_F begins to be suppressed as the pseudogap opens resulting the slope change of TEP. For the overdoped and heavily overdoped LSCO, T_h turns to increase with the hole doping in contrast to the pseudogap temperature that is saturated around 100 K. It indicates that T_h in the overdoped regime reflects another crossover behavior. If the crossover behavior is explained with the crossover from the strange metal to the normal metal as discussed in the photoemission data [8,9], the slope of TEP changes at the crossover. Therefore, T_h vs. hole doping concentration curve can be interpreted as the two crossover behaviors; one is from the strange metal to the large pseudogap regime for underdoped LSCO ($x < 0.2$) and the other is from the strange metal to the

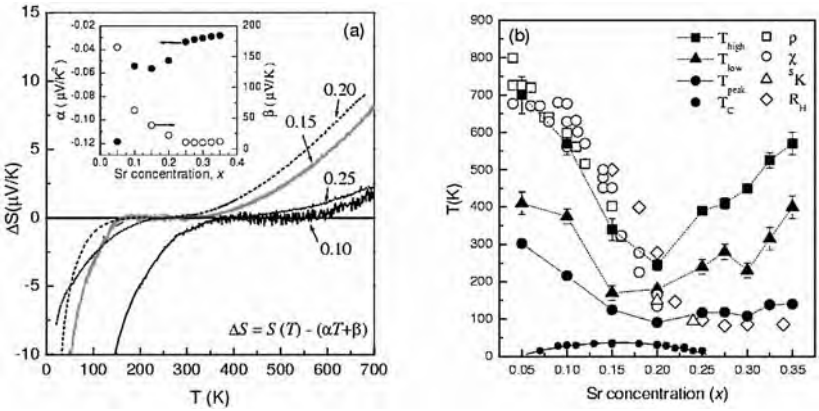

Figure 2. (a)The subtracted TEP ($\Delta S = S(T) - S_L(T)$) data with linear fitting function $S_L(T) = \alpha T+\beta$ for typical LSCO samples. The inset shows the doping dependence of the slope (α) and the offset (β) for $S_L(T)$. (b) Characteristic temperatures, T_C, T_h, T_l and T_p (See the text.) with the pseudogap temperatures reported from various experiments for LSCO (Ref. [1]).

conventional metallic regime for overdoped LSCO ($x > 0.2$).

One way of understanding the observed TEP behavior is the formation of bound pairs at T_h, which opens up the pseudogap resulting the enhancement of TEP upon cooling [2]. The number of bound pairs increases upon cooling until $T = T_l$. At T_l the pair-pair correlation between the bound pairs is turned on leading to the superconducting condensate at $T = T_C$. Therefore, for $T_C < T < T_h$, the bound pairs coexist with independent normal carriers forming a two-fluid state.

Since TEP is a measure of entropy per carrier, the TEP in the two-fluid state can be given by a combination of two contributions from the independent normal carriers (S_n) and the bound pairs (S_p) [2] as

$$S = [(n_n)\, S_n+(n_p/2)\, S_p]/N = \gamma[(1-x)\, S_n+(x/2)\, S_p], \text{ where}$$

$$S_n = (k_B/e)\, \partial \ln[n_a C n_n]/\partial n_t = (k_B/e) \ln [2\{1-(1-x)\rho\}/(1-x)\rho\}], \text{ and}$$

$$S_p = (k_B/e)\, \partial \ln[(n_a-n_n) C (n_p/2)]/\partial n_t = (k_B/e) \ln[\{1-(1-x/2)\rho\}/(x\rho/2))]$$

with $n_n + n_p = n_t$. Here $x = n_p/n_t$, $\rho = n_t/n_a$, $\gamma = \partial n_t/\partial N$ is a constant, n_p is the number of charge carrier forming the independent bound pairs, so that the

number of bound pairs is $n_p/2$, n_t is the total number of charge carriers contributing to the configuration entropy, n_n is the number of normal carriers, and n_a is the number of available sites and N is the total number of conducting charge carriers. The factor γ can be interpreted as only the γ fraction of the total number of conduction carriers contributes to the configuration entropy and the rest of them are locked inside the Fermi surface with no entropy contribution. As a result, the statistical factor is already encountered in our phenomenological two-fluid state model. The temperature dependence of x is assumed as,

$$1- x = n_n / n_t = 1 - \mathrm{Exp}[(T_c-T)/(T^*-T_c)].$$

In this assumption, $1- x$, *i. e.* the effective number of remnant normal carriers become 1 at high temperature where bound pairs does not exist, and become 0 at T_C when all electrons condensate into superconducting state. At $T \sim T^*$ the fraction of carriers (n_p/n_t) involved in the bound pair formation is around $1/e$ and increases with decreasing temperature becoming 1 at T_C. Figure 3(a) shows that the fitting results for underdoped, optimally doped, and overdoped LSCOs are surprisingly good. Fitting parameters ρ, γ, and T^* are shown in Fig. 3(b). It is interesting that the doping dependence of T^* coincides with T_l.

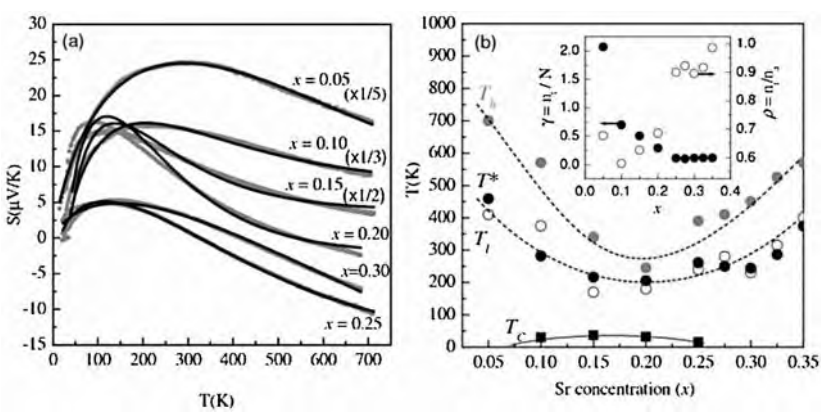

Figure 3. (a)The temperature dependence of TEP is reproduced with our mixed state model. (b) Hole doping dependence of one of fitting parameters T^* with the characteristic temperatures, T_h, T_l and T_c (See the text.). Fitting parameters, γ, and ρ are also shown with variation of doping concentration in the inset.

4. CONCLUSIONS

We have carried out the TEP measurement up to 700 K for the series of LSCO samples ($0.05 \leq x \leq 0.35$). For the whole doping range, we observed the linear-T dependence of TEP ($T_l < T < T_h$) even in the lightly doped nonsuperconducting sample ($x = 0.05$). At high temperature, the deviation from the T-linear dependence is observed, which becomes pronounced upon doping up to $x = 0.2$, but turns to be suppressed with further doping. The characteristic temperatures, T_p, T_l, and T_h change systematically with the hole doping. In comparison with the pseudogap temperatures from other experiments, we found that the pseudogap temperature coincides with T_h for underdoped regime. In overdoped regime, the slope change of TEP is also observed, which is attributed to the crossover from the strange metal to conventional metal. The possibility of bound pair formation in the normal state is discussed as the origin of the pseudogap in the normal state of high-T_C superconductors.

ACKNOWLEDGEMENTS

This work was supported by KISTEP under the contract No. M6-0301-00-0005, Ministry of Science and Technology (MOST), Korea.

REFERENCES

[1] T. Timusk and B. Statt, Rep. Rrog. Phys. 62, 61 (1999) and the references therein.
[2] Y. S. Song, H. Park, Y. S. Choi, Y. W. Park, M. S. Jang, H. C. Lee, and S. I. Lee, J. Korean Phys. Soc. 23, 492 (1990) ; Y. S. Song, Y. S. Choi, Y. W. Park, M. S. Jang, and S. K. Han, Physica C 185-189, 1341 (1991); Y. S. Song, Y. S. Choi, Y. W. Park, M. S. Jang, S. K. Han, J. Moscow Phys. Soc. 1, 293 (1991).
[3] P. Devillard and J. Ranninger, Phys. Rev. Lett. 84, 5200 (2000); J. Ranninger, and L. Ttripodi, Phys. Rev. B 67, 174521 (2003).
[4] Alain Sewer and Hans Beck, Phys. Rev. B 64, 224524 (2001); Philippe Curty, and Hans Beck, Phys. Rev. Lett. 91, 247002 (2003).
[5] V. J. Emery and S. A. Kivelson, Nature 374, 434 (1995).
[6] J. S. Kim, B. H. Kim, D. C. Kim and Y. W. Park, J. of Supercond. 17, 149 (2004).
[7] J. -S. Zhou and J. B. Goodenough, Phys. Rev. B 51, 3104 (1995); Y. Nakamura and S. Uchida, *ibid.* 47, 8369 (1993).
[8] A. Ino, T. Mizokawa, K. Kobayashi, A. Fujimori, T. Sasagawa, T. Kimura, K. Kishio, K. Tamasaku, H. Eisaki, and S. Uchida, Phys. Rev. Lett. 81, 2124 (1998).
[9] A. Kaminski, S. Rosenkranz, H. M. Fretwell, Z. Z. Li, H. Raffy, M. Randeria, M. R. Norman, and J. C. Campuzano, Phys. Rev. Lett. 90, 207003 (2003).

TEMPERATURE DEPENDENCE OF IN-PLANE RESISTIVITY OF YBCO

J.Jung
Department of Physics, University of Alberta
Edmonton, Alberta, Canada T6G 2J1
jung@phys.ualberta.ca

M.Abdelhadi
Department of Physics, University of Alberta
Edmonton, Alberta, Canada T6G 2J1 *
mabdel@phys.ualberta.ca

Abstract Variation of the magnitude and the temperature dependence of the normal state resistivity $\rho(T)$ has been very frequently observed in different $YBa_2Cu_3O_{7-\delta}$ (YBCO) single crystals (or YBCO thin films) of the same T_c. We investigated the origin of these changes by analyzing optimally doped and underdoped YBCO thin films (with $7-\delta = 6.80-6.95$) whose resistivity $\rho(T)$ was characterized by a "superlinear" temperature dependence [with a flattening of $\rho(T)$ below 230K]. We induced oxygen redistribution in these films without any change in the total oxygen content, by either careful annealing over a temperature range of $120-140^oC$ in argon, or by aging at room temperature in air. This procedure leads to a transition from a superlinear $\rho(T)$ towards the linear one, and an increase of both the magnitude of resistivity and T_c. Long-term aging yields a perfectly linear $\rho(T)$. We proposed a filamentary model of the changes in $\rho(T)$, which is based on a thermally activated redistribution of the interchain bridging oxygen O(5) in the chain-layer of YBCO. The results show that a perfectly linear $\rho(T)$ can be observed in YBCO of oxygen content $7-\delta$ as low as 6.8, which is essential for the development of theories of the normal state resistivity and the pseudo-gap state.

Keywords: Resistivity, $YBa_2Cu_3O_{7-\delta}$ superconductors, chain-layer, oxygen-redistribution.

*Present address: Physics Department, King Fahd University of Petroleum and Minerals, Dhahran, 31261 Saudi Arabia.

J. Ashkenazi et al. (eds.), New Challenges in Superconductivity: Experimental Advances and Emerging Theories, 79-84.

Several measurements of the temperature dependence of resistivity $\rho(T)$ in untwinned YBCO crystals [1, 2, 3] revealed a linear $\rho_a(T)$ in the a-b planes but a non-linear (a T^2-like, sometimes called a "superlinear") $\rho_b(T)$ along the chain (the b-) direction, with the magnitudes of $\rho_a(T)$ being larger than those of $\rho_b(T)$. On the other hand, $\rho_{ab}(T)$ measured in twinned optimally doped YBCO crystals (or YBCO thin films) of the same T_c was found to exhibit both linear and non-linear temperature dependencies [4, 5, 6] with the magnitudes of a linear $\rho_{ab}(T)$ being in general higher than those of a non-linear $\rho_{ab}(T)$.

Questions related to this problem are:

(a) What are the conditions that lead to these two different (linear and non-linear) forms of $\rho(T)$?

(b) What is the effect of oxygen distribution on $\rho(T)$?

(c) Is the linear temperature dependence of ρ characteristic of optimally doped YBCO only?

This paper presents the results of our investigation of the origin of a non-linear $\rho_{ab}(T)$ in YBCO films, i.e. the origin of a superlinear temperature dependence (with a flattening below approximately 230 K). We also investigated why the magnitudes of a non-linear $\rho_{ab}(T)$ are very often much smaller than those of a linear $\rho_{ab}(T)$ in samples of the same T_c. The studies were focused on the relationship between the temperature dependence of $\rho_{ab}(T)$ in YBCO thin films and oxygen distribution in these materials. It is known that annealings of YBCO at temperatures $120 - 140^oC$ (400-420 K) do not cause any change in the overall content of oxygen in the sample, but they could lead to a redistribution of oxygen in the chain layer [7]. In order to study the effect of oxygen redistribution on the temperature dependence of $\rho_{ab}(T)$, we performed series of annealings at $120 - 140^oC$ in argon, or at room temperature in air, of c-axis oriented optimally doped (T_c = 90-91 K) and underdoped (T_c = 81-85 K) YBCO thin films, whose $\rho_{ab}(T)$ has a non-linear dependence on temperature.

The measurements of $\rho_{ab}(T)$ were done using the four-probe method on $60\mu m$ wide thin film bridges over a temperature range between 80K and 300 K. The resistivity was measured on unannealed samples as well as on annealed ones after each 2-4 hour annealing interval. The results reveal an increase in resistivity and a reduction of non-linearity in $\rho_{ab}(T)$ with an increasing annealing time for all films studied (see Figures 1 and 2). For underdoped films with T_c = 84-85 K, annealing in argon at $120 - 140^oC$ leads also to an increase of T_c. Our interpretation of the data is based on the assumption that redistribution of oxygen during low temperature annealings takes place in the chain layer of YBCO. It is known that even optimally doped YBCO (or RBCO in general) contains

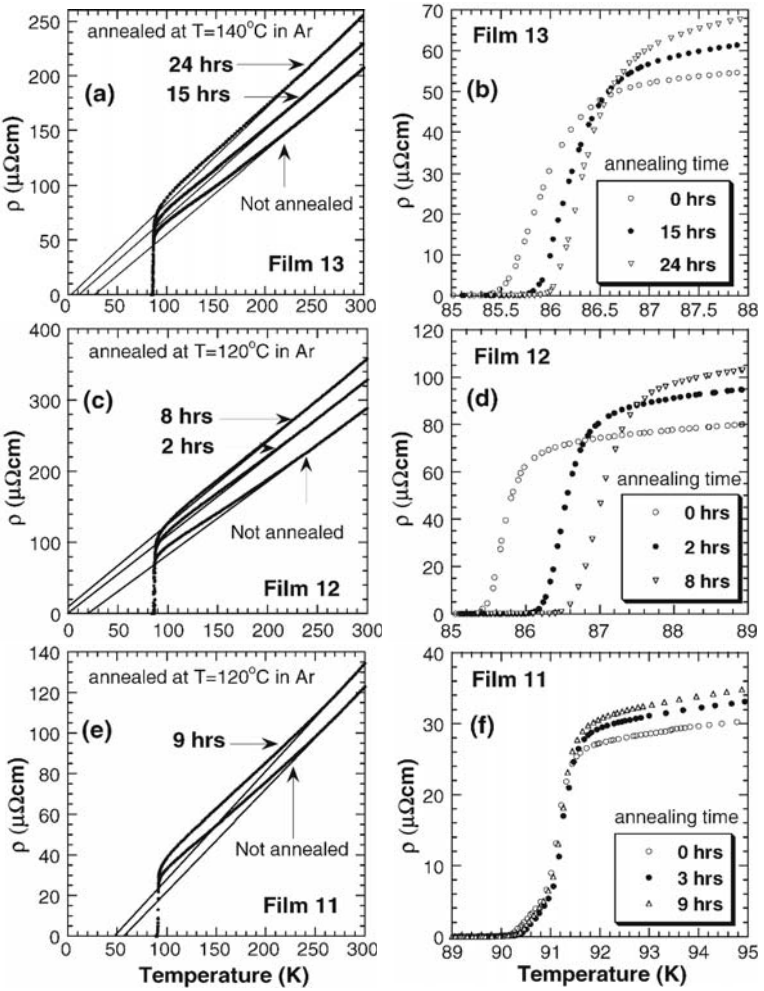

Figure 1. (a), (c) and (e) Temperature dependence of the in-plane resistivity ρ_{ab} measured in c-axis oriented YBCO thin films 13, 12 and 11 with $T_c = 85.5K$ and $90K$ before and after annealing in argon at $120 - 140^oC$. Note a systematic increase of resistivity and a reduction of a deviation from a linear temperature dependence with an increasing annealing time. (b), (d) and (f) Dependence of resistivity on temperature close to T_c before and after annealings. Note a systematic increase of T_c with an increasing annealing time for underdoped films.

a few percent of an interchain oxygen O(5) in the chain layers [8, 9]. O(5) oxygens form links between partially occupied chains of oxygen O(1) and allow the transport current in the chain layer to zigzag between the chains via O(5) sites. The overall resistivity of a sample $\rho_{ab}(T)$ is due to

a parallel combination of resistivity of the planes and the chain layers, and can be expressed by the formula: $1/\rho_{ab} = (1/\rho_{plane}) + (1/\rho_{chain})$, or $\rho_{ab} = \rho_{plane}\rho_{chain}/(\rho_{plane} + \rho_{chain})$.

According to the experimental results obtained on untwinned YBCO single crystals [1, 2, 3], temperature dependence of resistivity in the planes is linear, i.e. $\rho_{plane} = a_1 + a_2 T$, where a_1 and a_2 are constants. On the other hand, temperature dependence of the chain resistivity in YBCO was found to follow approximately a quadratic dependence, i.e. $\rho_{chain} = b_1 + b_2 T^2$, where b_1 and b_2 are constants [3]. T^2 dependence of resistivity is expected to occur in 1D wires due to electron-phonon scattering. In the presence of interchain O(5), the transport current can zigzag between the chains in the chain layer via O(5) bridges along the paths of the lowest resistance. In this case, electrical transport is still 1D and the resistivity should be proportional to T^2. The activation energy for the motion of O(5) oxygen between chains in the b-direction is small [10] and during annealing at temperatures of $120 - 140^o C$, O(5) is highly mobile in this direction. There are two important consequences of high mobility of O(5) during annealing. O(5) can fill some O(1) vacancies in the chains, which leads to a higher T_c. On the other hand, during this process, missing O(5) oxygens between the chains break the paths of the lowest resistance, which leads to an increase of the resistivity in the chain layer. One could consider the following explanation of an increase of resistivity with the annealing time in twinned optimally doped and underdoped YBCO. In the presence of oxygen O(5) the electrical transport in the chain layer is determined by the resistance of the chains and the interchain bridges through O(5) sites. The resistance of interchain parallel bridges is $R = R_o/N$, were R_o is the resistance of a single bridge and N is the number of effective O(5) bridges through which the current flows. During annealing due to high mobility of oxygen O(5) the number of effective bridges is reduced. We assume that this process is completely random and the number of bridge disintegrations that occurs is proportional to the number N of effective bridges present, i.e. $dN/dt = -\alpha N$, where α is a decay constant. The result for the dependence of N on time is then $N = N_o \exp(-\alpha t)$, where N_o is the number of effective bridges at $t = 0$. The resistance $R = R_o/N$ will then increase with time t according to the expression: $R = (R_o/N_o)\exp(\alpha t)$. Because of the exponential factor, R dominates the resistance in the chain layer.

Therefore, we could write the resistivity in the chain layer as a function of time and temperature in the simple form: $\rho_{chain}(t,T) = \rho_o(T)\exp(\alpha t) = (b_1 + b_2 T^2)\exp(\alpha t)$. We assume that ρ_{plane} is independent of time and depends only on temperature, i.e. $\rho_{plane} = a_1 + a_2 T$. Then the total resistivity $\rho_{ab}(t,T) = \rho_{plane}(T)/[1+\rho_{plane}(T)/\rho_{chain}(t,T)] = (a_1 + a_2 T)/\{1+$

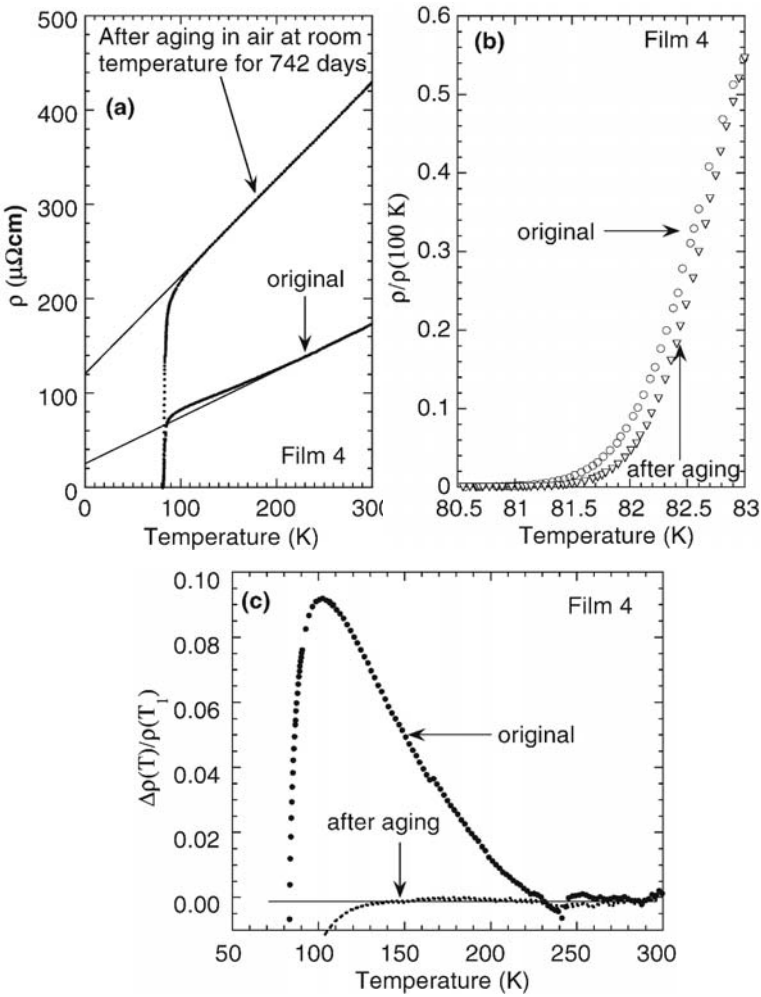

Figure 2. (a) Temperature dependence of the in-plane resistivity ρ_{ab} measured in a c-axis oriented underdoped YBCO thin film 4 with $T_c = 81K$ before and after aging for 742 days in air. Note the transformation of $\rho_{ab}(T)$ from a superlinear to a perfect linear temperature dependence after aging. (b) Dependence of resistivity on temperature close to T_c before and after aging. (c) Upward deviation of $\rho_{ab}(T)$ (measured for film 4) from a linear temperature dependence of resistivity $\rho(T)$, defined as $\Delta\rho(T)/\rho(T_1) = [\rho_{ab}(T) - \rho(T)]/\rho_{ab}(T_1)$, where T_1 is the temperature at which the maximum upward deviation of $\rho_{ab}(T)$ from a linear $\rho(T)$ occurs. Note the independence of $\Delta\rho(T)/\rho(T_1)$ on temperature after aging, which indicates a perfect linear temperature dependence.

$(a_1 + a_2T)/[(b_1 + b_2T^2)\exp(\alpha t)]\}$. We performed computer calculations of $\rho_{ab}(t, T)$ and compared them with the data for $\rho_{ab}(t, T)$ obtained for

c-axis oriented YBCO films. The fitting parameters are a_1, a_2 and α. In fact a_1 and a_2 are close to those found for $\rho_{plane}(T)$ in untwinned YBCO single crystals. Constants b_1 and b_2 in $\rho_{chain}(T) = b_1 + b_2 T^2$ were calculated using equation $\rho_{ab} = \rho_{plane}\rho_{chain}/(\rho_{plane} + \rho_{chain})$ and the experimental data for $\rho_{ab}(T, t = 0)$ of unannealed YBCO films. Good agreement between the experimental data for $\rho_{ab}(T, t)$ and this model was obtained. The most important results could be summarized as follows: (a) The temperature dependence of ρ can be linear in $YBa_2Cu_3O_{7-\delta}$ for an oxygen content $7 - \delta$ as low as 6.8; (b) A non-linear $\rho(T)$ approaches a linear dependence as a result of oxygen redistribution (most likely a redistribution of an interchain oxygen O(5) in the chain layer); (c) This is associated with an increase of the magnitude of ρ, and either no change or a small increase in T_c.

These results suggest that a non-linear (i.e. superlinear) $\rho(T)$ is caused by a filamentary flow of the current in the chain layer through interchain bridges formed by a residual amount of O(5). Breaking the interchain links (by low temperature annealing, for example) leads to an increase of the magnitude of $\rho(T) \propto T^2$ in the chain layer, and consequently to a higher (but linear) total resistivity which is dominated by the planes.

This work was supported by the Natural Sciences and Engineering Council of Canada. We thank M.Denhoff, J.Preston and R.Hughes for supplying us with YBCO thin films.

References

[1] J.P. Rice, J. Giapintzakis, D.M. Ginsberg and J.M. Mochel, Phys. Rev., B**44**, 10158 (1991).

[2] T. Ito, K. Takenaka and S. Uchida, Phys. Rev. Lett., **70**, 3995 (1993).

[3] R. Gagnon, C. Lupien and L. Taillefer, Phys. Rev., B**50**, 3458 (1994).

[4] V.M. Browning, E.F. Skelton, M.S. Osofsky, S.B. Quadri, J.Z. Hu, L.W. Finger and P. Caubet, Phys. Rev., B**56**, 2860 (1997).

[5] S.S. Laderman, R.C. Taber, R.D. Jacowitz, J.L. Moll, C.B. Eom, T.L. Hylton, A.F. Marshall, T.H. Geballe and M.R. Beasley, Phys. Rev., B**43**, 2922 (1991).

[6] U. Poppe, N. Klein, U. Dahne, H. Soltner, C.L. Jia, B. Kabius, K. Urban, A. Lubig, K. Schmidt, S. Hensen, S. Orbach, G. Muller and H. Piel, J. Appl. Phys., **71**, 5572 (1992).

[7] J.D. Jorgensen ANL, private communication.

[8] J.D.Jorgensen, B.W.Veal, A.P.Paulikas, N. J. Nowicki, G. W. Crabtree, H. Claus, and W. K. Kwok, Phys. Rev. B**41**, 1863 (1990).

[9] P.G. Radaelli, C.U. Segre, D.G. Hinks, and J.D. Jorgensen, Phys. Rev., B**45**, 4923 (1992).

[10] S.J. Rothman, J.L. Routbort, U. Welp and J.E. Baker, Phys. Rev., B**44**, 2326 (1991).

MEASUREMENTS OF THE DOPING EFFECTS ON THE IN-PLANE PARACONDUCTIVITY IN CUPRATE SUPERCONDUCTORS

Felix Vidal, Manuel V. Ramallo, Gonzalo Ferro, Jose Antonio Veira
Laboratorio de Baixas Temperaturas e Superconductividade,[*]
Departamento de Fisica da Materia Condensada,
Universidade de Santiago de Compostela, Santiago de Compostela E15782 Spain

Abstract We will summarize here some of our measurements of the superconducting fluctuations effects on the in-plane electrical resistivity (the so-called in-plane paraconductivity) in $La_{2-x}Sr_xCuO_4$ thin films with different Sr content. Our results suggest that these superconducting fluctuations effects are not related to the opening of a pseudogap in the normal-state of underdoped compounds.

1. Introduction: the questions that are and aren't addressed here

In Fig. 1, we represent an example of the temperature behaviour of the electrical resistivity of underdoped $La_{1.9}Sr_{0.1}CuO_4$. These data were taken from Refs. [1] and [2], and correspond to a bulk polycrystalline sample (Fig. 1a) and to a thin film (Fig. 1b). In these figures, T_C is the temperature where $\mathrm{d}\rho/\mathrm{d}T$ has its maximum (T_C is close to T_{C0}, the temperature where the measured resistivity vanishes), T^* is the temperature at which the pseudogap in the normal state opens, and T^C is the temperature at which the measured resistivity, $\rho(T)$, becomes indistinguishable from the background resistivity, $\rho_B(T)$. This background resistivity (solid line in Fig. 1b) is obtained by extrapolating through the transition the normal-state resistivity measured well above the superconducting transition. The details of this extrapolation procedure may be seen in Ref. [2].

The difference between $\rho(T)$ and $\rho_B(T)$ (dark region in Fig. 1b) is supposed to be due to the presence of coherent Cooper pairs created in the normal state by thermal fluctuations. As usual, these superconducting fluctuations (SCF) effects m ay be quantifi ed through the so-called in- plane paraconductivity,

[*]Unidad Asociada al ICMM, CSIC, Madrid, Spain

J. Ashkenazi et al. (eds.), New Challenges in Superconductivity: Experimental Advances and Emerging Theories, 85-90.

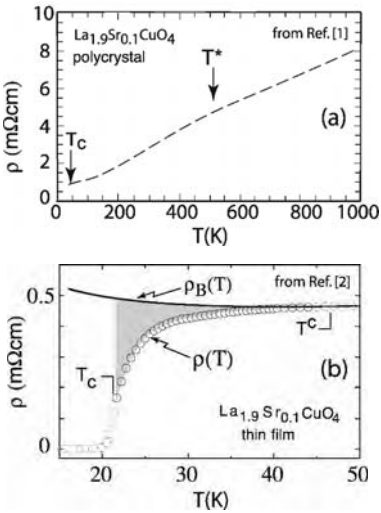

Figure 1. Temperature dependence of the resistivity of (a) a polycrystalline sample of the underdoped cuprate $La_{1.9}Sr_{0.1}CuO_4$, taken from [1], and (b) a film of the same composition and thickness ~ 150 nm, taken from [2]. In (b), the measurements correspond to the in-plane direction (parallel to the CuO_2 layers). The temperatures T^*, T^C and T_C correspond, respectively, to the pseudogap opening temperature, to the temperature where the SCF effects become indistinguishable, and to the (inflexion-point) observed normal-superconducting transition temperature.

defined by

$$\Delta\sigma(T) \equiv \frac{1}{\rho(T)} - \frac{1}{\rho_B(T)}. \tag{1}$$

The two questions that we will address here are: *i)* How $\Delta\sigma(T)$ is affected oping? This question may be directly answered by the experiments, independently of any theoretical approach. *ii)* Is the observed T_C a "good" mean-field critical temperature for the SCF, even up to T^C? This second question is related to the theoretical description of the SCF. We will answer it on the grounds of the Gaussian-Ginzburg-Landau (GGL) approach, extended up to T^C by introducing a "total-energy" cutoff that takes into account the limits imposed by the uncertainty principle to the shrinkage of the superconducting wave function when the temperature increases well above T_C.[2, 3] We are not going to directly address here another important (mainly to discriminate between the existing theoretical proposals for the pseudogap[4]) open question: Is T^* the "true" mean-field superconducting transition temperature?

To answer the above questions we will present measurements of the in-plane paraconductivity in $La_{2-x}Sr_xCuO_4$ thin films with different Sr concentrations.

Our experiments were detailed elsewhere.[2]. They extend to high reduced-temperatures the earlier measurements of Hikita and Suzuki.[5] Other original aspect of our present work is the analysis in terms of the "extended" GGL approach (other analyses by other groups of the paraconductivity at high reduced-temperatures in different HTSC[6, 7] did not take into account the quantum effects on the SCF, see also later).

2. How are affected by doping the superconducting fluctuations above T_C?

Some examples of the influence of the Sr content on the in-plane paraconductivity curves, $\Delta\sigma(\epsilon)_x$, measured as a function of the reduced temperature, $\epsilon \equiv \ln(T/T_C)$, are shown in Fig. 2. These data correspond to $La_{2-x}Sr_xCuO_4$ thin films, of about 150 nm thickness and grown on (100)$SrTiO_3$ substrates. Other experimental details may be seen in Ref.[2]

The "as-measured" data of Fig. 2 provide a direct answer to the question stated in the title of this section: The only appreciable effects of doping on the SCF is to change somewhat the slope of the $\log \Delta\sigma(\epsilon)_x$ versus $\log \epsilon$ curves in the low reduced-temperature region. We will see in the next section that these changes are associated with changes in the SCF dimensionality. However, these changes manifest themselves only in the overdoped regime: As directly illustrated by the data in Fig. 2a, in all the temperature range of our measurements (approximately $10^{-2} \leq \epsilon \leq 1$), the data for $x = 0.1$ and $x = 0.12$, which are well in the underdoped regime, agree well within the experimental uncertainties with those of the optimally-doped film ($x = 0.15$). Moreover, the results of Figs. 2a to 2c show that in all the cases the SCF vanish above a reduced temperature of around 0.7, which corresponds to $T^C \sim 2T_C$. Note already here that in the underdoped compounds $T^C \ll T^*$ (see also section 4, and Figs. 1 and 3). These different results already suggest, therefore, that the opening of the normal-state pseudogap is not related to the coherent Cooper pairs created above the superconducting transition by thermal fluctuations.

3. Is the observed $T_C(x)$ a "good" mean-field superconducting-normal transition temperature?

This question is also answered in Fig. 2, where we compare the experimental paraconductivity with the GGL approach extended to high reduced-temperatures by introducing a "total-energy" cutoff. This cutoff takes into account the limits imposed by the uncertainty principle to the shrinkage of the superconducting wave function, associated to the coherent Cooper pairs created by thermal fluctuations, when the temperature increases well above T_C.[3] The paraconductivity was calculated on the grounds of this "extended" GGL approach by Carballeira et al.[8] The corresponding expressions for a single-

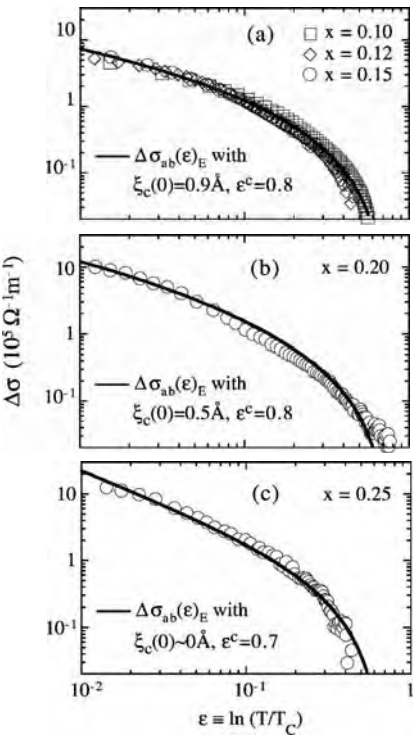

Figure 2. In-plane paraconductivity versus reduced temperature measured in Ref.[2], in $La_{2-x}Sr_xCuO_4$ films with thickness $\sim$ 150 nm and Sr contents covering the underdoped ($x < 0.15$), optimally-doped ($x = 0.15$) and overdoped ($x > 0.15$) compositions. The solid lines correspond to the best fit to those data using the GGL approach with a total-energy cutoff (Eq. (2)). See main text for details.

layered superconductor, which is the case well adapted to $La_{2-x}Sr_xCuO_4$, is [2, 8]

$$\Delta\sigma(\epsilon)_{\rm E} = \frac{{\rm e}^2}{16\hbar s}\left[\frac{1}{\epsilon}\left(1+\frac{B_{\rm LD}}{\epsilon}\right)^{-1/2} - \frac{1}{\epsilon^C}\left(2-\frac{\epsilon+B_{\rm LD}/2}{\epsilon^C}\right)\right], \qquad (2)$$

where $\hbar$ is the reduced Planck constant, e is the electron charge, s is the superconducting CuO_2 layers periodicity ($s = 0.66$ nm for $La_{2-x}Sr_xCuO_4$), $B_{\rm LD} \equiv [2\xi_c(0)/s]^2$ is the Lawrence-Doniach (LD) parameter and $\xi_c(0)$ is the superconducting coherence length amplitude in the c-direction (perpendicular to the CuO_2 layers). Note that in calculating this expression for $\Delta\sigma(\epsilon)_{\rm E}$ we have assumed the BCS-like value for the SCF relaxation time, $\tau_0 = (\pi\hbar/8k_BT_C)\epsilon^{-1}$ (for more details see Refs.[2, 8, 10]). The solid lines in Fig. 2 are the best fits

of Eq. (2) to the data points, with $\xi_c(0)$ and ϵ^C, the reduced-temperature where $\Delta\sigma(\epsilon)_x$ vanishes, as the only free parameters.

As may be observed in these figures, for all the samples the agreement between Eq. (2) and the experimental data is excellent, in the entire studied ϵ-region. The central result here is that this comparison strongly suggests then that the observed $T_C(x)$ is a "good" mean-field transition temperature for the measured SCF. This comparison also confirms the existence of a well-defined reduced-temperature, ϵ^C, of around 0.7, above which the in-plane paraconductivity vanishes. Taking into account the experimental uncertainties,[2] this value matches fairly well the value ~ 0.6 which may be roughly estimated on the grounds of the uncertainty principle, the mean-field ϵ-dependence of the in-plane coherence length, and the BCS relationship between the Pippard and the Ginzburg-Landau coherence lengths.[2, 3] Moreover, by comparing the obtained values of $\xi_c(0)$, which are given in the corresponding figures, with s, it is easy to conclude that in the underdoped and optimally doped samples the SCF have a 2D-3D crossover around $\epsilon \simeq 7 \times 10^{-2}$. In contrast, the SCF in the overdoped compounds are 2D in almost all the accessible ϵ-region.

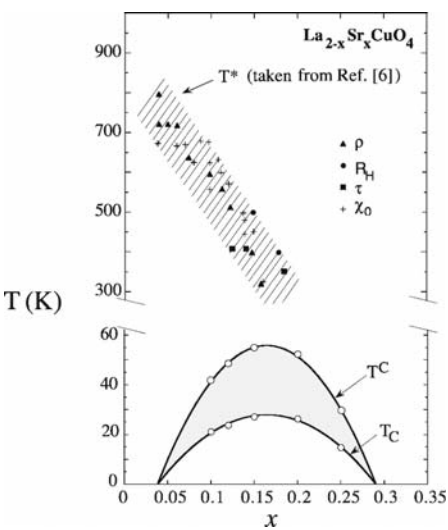

Figure 3. Comparison for $La_{2-x}Sr_xCuO_4$ between the temperatures of the pseudogap opening (T^*), of the vanishing of the in-plane paraconductivity (T^C), and of the normal-superconducting transition as observed in the resistivity measurements (T_C). The T^* values are taken from the compilation in Ref. [9], and correspond to resistivity measurements (ρ), Hall coefficient measurements (R_H), infrared measurements (τ), and static susceptibility measurements (χ_0)

4. Conclusions

The main conclusions of the experimental results and analyses presented here may be summarized as follows:

A model-independent conclusion: The general behaviour of the in-plane paraconductivity is *not* affected, even up to T^C, by doping. The SCF effects in $La_{2-x}Sr_xCuO_4$ thin films seem to be not related to the pseudogap.

t From the comparison of the measured paraconductivity with the "ex-ended" GGL approach: *i)* The measured T_C is a good mean-field critical temperature for the GGL approach. *ii)* Both the relaxation time of the SCF and the reduced temperature, ϵ^C, where the SCF vanish, are doping-independent and they take values close to those of BCS superconductors. This last result demands further studies.

The independence of the SCF and the pseudogap seems to be confirmed when three characteristic temperatures, T_C, T^C and T^*, are compared. This is done in Fig. 3, where the doping dependence of T_C, T^C and T^* is represented. The data for T^* where taken from Ref. [9]. This figure illustrates that in the underdoped $La_{2-x}Sr_xCuO_4$ superconductors not only T_C but also T^C is much lower than T^* and that the doping behaviour of both T_C and T^C is very different from the one of T^*.

References

[1] B. Batlogg, H.Y. Hwang, H. Takagi, R.J. Cava, H.L. Kao, and J. Kwo, Physica C **235-240**, 130 (1994).

[2] S.R. Curras, G. Ferro, M.T. Gonzalez, M.V. Ramallo, M. Ruibal, J.A. Veira, P. Wagner, and F. Vidal, Phys. Rev. B **68**, 094501 (2003).

[3] F. Vidal, C. Carballeira, S.R. Curras, J. Mosqueira, M.V. Ramallo, J.A. Veira, and J. Vina, Europhys. Lett. **59**, 754 (2002)

[4] See, e.g., J. Orenstein and A.J. Millis, Science **288**, 468 (2000). See also, B. Batlogg and C.M. Varma, Physics World, February 2000, p. 33.

[5] M. Suzuki and M. Hikita, Phys. Rev. B **44**, 249 (1991); **47**, 2913 (1993).

[6] E. Silva, S. Sarti, R. Fastampa, and M. Giura, Phys. Rev. B **64**, 144508 (2001).

[7] B. Leridon, A. Defossez, J. Dumont, J. Lesueur, and J.P. Contour, Phys. Rev. Lett. **87**, 197007 (2001); **90**, 179704 (2003). See also C.W. Luo, J.Y. Juang, J.-Y. Lin, K.H. Wu, T.M. Uen, and Y.S. Gou, Phys. Rev. Lett. **90**, 179703 (2003).

[8] C. Carballeira, S.R. Curras, J. Vina, J.A. Veira, M.V. Ramallo, and F. Vidal, Phys. Rev. B **63**, 144515 (2001).

[9] T. Timusk and B. Statt, Rep. Prog. Phys. **62**, 61 (1999).

[10] M.V. Ramallo, C. Carballeira, J. Vina, J.A. Veira, T. Mishonov, D. Pavuna, and F. Vidal, Europhys. Lett. **48**, 79 (1999).

A POSSIBILITY OF A PHASE FLUCTUATION-LIKE EFFECT IN HTSC CUPRATES

Yu. S. Nechaev
University of Miami, Clean Energy Research Institute, Coral Gables, FL 33124, USA
Permanent address:Bardin Institute of Ferrous Metallurgy, Moscow107005, RUSSIA

Abstract: On the basis of the thermodynamic analysis of the related experimental data, a possibility is shown of a manifestation of a phase fluctuation-like effect in the high-temperature superconducting (HTSC) cuprates, especially with respect to physical properties of melt-textured composites, thin films, coatings, nanomaterials and heterostructures.

Key words: Superconducting Y123, the diffusion controlled topo-chemical decomposition of Y123, the standard oxygenation treatment, a phase fluctuation-like effect

1. INTRODUCTION

As has been shown in numerous studies[1-5], the formation and growth of large (up to a few microns) stacking faults (SFs) occurs in $YBa_2Cu_3O_{6+X}$ / Y_2BaCuO_5 (123/211) melt-textured composites, from low-angle boundaries and especially around 211 precipitates, as well as degradation layers within gaps of microcracks around 211 precipitates, which themselves are filled with Cu-rich phases, upon increasing the oxygenation time (at $Po_2 = 1$ bar, $T = 723$ K, as used in study[1]). Both SFs and 123 matrix degradation layers are observed[1,5] along the (001) planes, giving rise to a pronounced two-dimensionality (2D) of the aged microstructure. SFs in 123 orthorhombic phase have been assumed[1,5] to consist of an additional CuO chain layer adjacent to the BaO plane, giving rise to a double chain layer, that is a local $YBa_2Cu_4O_8$ (124) structure or a $Y_2Ba_4Cu_7O_{14+Z}$ (247) structure. Large splitting widths observed in TEM studies have been assumed[1,5] to be

J. Ashkenazi et al. (eds.), New Challenges in Superconductivity: Experimental Advances and Emerging Theories, 91-96.

relevant to a negative SF energy which is associated with a local phase transformation to a 124 structure or to a 247 structure.

The dissolving of large SFs in the melt textured composites has been studied[2,3] (at Po_2=10^{-9}-10^{-10} bar, 613-629 K, and at 0.2-1 bar, 1073-1203 K, correspondently). The chemical character of the decomposition processes has been experimentally shown in studies[3,4].

In the present study, the thermodynamic analysis[6,7] of such processes in the cuprates has been carried out with the aim of finding the rate-controlling steps, the nature of the SFs-like precipitates, the role of the lattice defects' regions in the internal topo-chemical reactions, and finally – to show a possibility of a manifestation of a phase fluctuation-like effect.

2. RESULTS AND DISCUSSION

According to studies[8-12], the 123 orthorhombic structure is thermodynamically unstable at all temperatures and compositions, and particularly, in the experiment[1] conditions corresponding to a standard oxygenation treatment of the ceramics (Fig. 1, point [1]). The decomposition processes can occur as follows, within extrapolation of the corresponding lines in Fig. 1 to 723 K:

$$6YBa_2Cu_3O_{6+X}=Y_2BaCuO_5+2Y_2Ba_4Cu_7O_{14+Z}+3BaCuO_2 +0.5(6x-3-2z)O_2, \quad (1)$$

$$6YBa_2Cu_3O_{6+X}=2Y_2BaCuO_5+Y_2Ba_4Cu_7O_{14+Z}+3Ba_2Cu_3O_{5+Y} +0.5(6x-3-z-3y)O_2, \quad (2)$$

$$4YBa_2Cu_3O_{6+X}=2Y_2BaCuO_5+3Ba_2Cu_3O_{5+Y}+CuO+0.5(4x-2-3y)O_2; \quad (3)$$

reactions (1) and (2) correspond to the solid lines 1 and 2 in Fig. 1, and the metastable reaction (3) - to the chained-dotted line 3 in Fig. 1.

Some other reactions can be also taken into account, as follows[8-12]:

$$2\ YBa_2Cu_3O_{6+X} + CuO + 0.5\ (1 + z - 2x)\ O_2 = Y_2Ba_4Cu_7O_{14+Z}, \quad (4)$$

$$YBa_2Cu_3O_{6+X} + CuO + 0.5\ (1 - x)\ O_2 = YBa_2Cu_4O_8. \quad (5)$$

Then, the decomposition reaction can be considered as (1) or (2), where (2) can be combined as the sum of (3) and (4). Another decomposition reaction (6) can be combined as the sum of (3) and (5), and it results in:

$5YBa_2Cu_3O_{6+X}=YBa_2Cu_4O_8+2Y_2BaCuO_5+3Ba_2Cu_3O_{5+Y}+0.5(5x-3-3y)O_2$. (6)

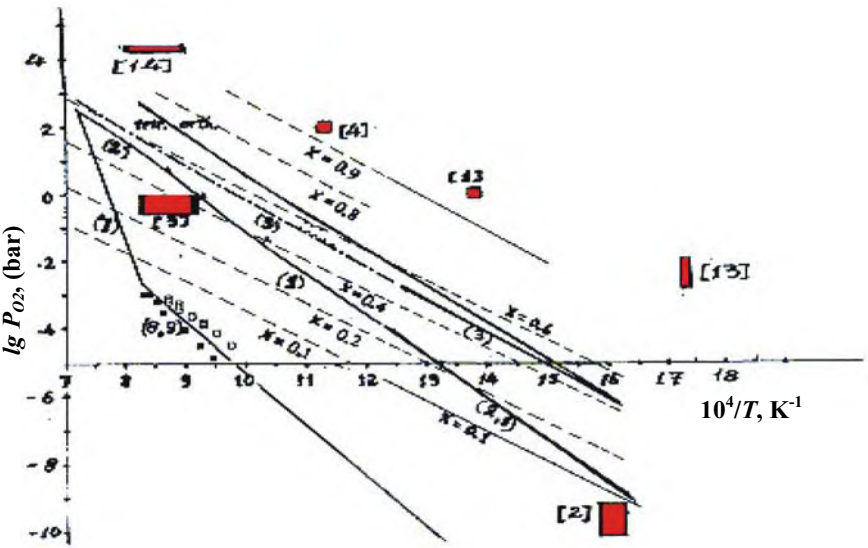

Figure 1. Evaluated and experimental stability range of Y123 phase, in the light of studies[8-12]. The dashed lines represent the intercalated oxygen content (x). The "tet/ort" line corresponds to the tetragonal-orthorhombic phase transition. Solid lines 7 - 9 represent: $YBa_2Cu_3O_{6+X}\rightarrow Y_2BaCuO_5+$*(Liquid phase)*$+O_2$; $9YBa_2Cu_3O_{6+X}=4Y_2BaCuO_5+ YBa_4Cu_3O_{8.5+Q}+10BaCu_2O_2+0.5(5.5+9x -q)O_2$; $2YBa_2Cu_3O_{6+X}=Y_2BaCuO_5+BaCuO_2+2BaCu_2O_2+0.5(2x+1)O_2$. The points ▲, □, ■, [1], [2], [3], [4], [13], [14] are the known experimental data.

All these reactions can be used for the interpretation of processes[1-5,13,14], if SFs are equivalent to two-dimensional 247 or 124 phases, as it has been mentioned above. The thickness of SFs is assumed[1,2,5] to be $h_{SF} \approx 2$ Å, that is the same as the double layer. The thickness of the SFs' phase of 247 may be assumed [6,7] to be $h_{SFP} \approx 10$ Å , comparable with the c-axis size of the cell of the 247 structure, that is the phase layer of a nanometer thickness.

There are reasons[1-12] to assume that the first (obviously, fast) step (3) of the decomposition reaction ((2) or (6)) is mainly localized in the vicinity of pre-existing 211 precipitates, which can grow due to the formation of new layers of 211 phase. Then it can provide the flowing of the second (obviously, sluggish) step [(4) or (5)] of the decomposition reaction [(2) or (6)]. It can be controlled[6,7] by the diffusion supply of oxygen and/or copper atoms (from the 211 vicinity) through the 123 matrix to the tops of the growing (from there) SFs of 124 or 247.

The apparent chemical diffusion coefficient can be evaluated as[6,7]:

$$D_{(app)} \approx L^2 / t, \qquad (7)$$

where L is the characteristic diffusion length (about the SFs´ linear size), and t is the oxygenation time. According to TEM data[1], the SFs elongated in one of two mutually perpendicular ‹100› directions about of 2 μm away from the 211/123 interface, from which they were originated (t = 156 h, T=723 K); hence, $D_{(app)} \approx 1 \cdot 10^{-13}$ cm^2/s.

The obtained value is smaller by about four orders of magnitude from experimental values[15,16] of the chemical diffusion coefficient for oxygen in the ab-plane of the 123 matrix ($D_{O(123)ab}$), and higher by five orders from the experimental value[15] of the tracer diffusion coefficient for copper in the ab-plane of the 123 matrix ($D^*_{Cu(123)ab}$), Table 1; the latter can be of the same order or by one order lower than the chemical diffusion coefficient[15,16].

Table 1. Experimental values[15,16] of the tracer diffusion coefficients (D^*, cm^2/s) and the chemical diffusion coefficients (D, cm^2/s) of the relevant elements in the Y(123) and Y(124) ceramics (for P_{O2}-T conditions[1]).

$D^*_{O(123)c}$	$D^*_{O(124)ab}$	$D_{O(123)ab}$	$D^*_{O(124)c}$	$D^*_{Cu(123)ab}$	$D^*_{Cu(123)c}$	$D^*_{Ba(123)ab}$
$1 \cdot 10^{-16}$	$3 \cdot 10^{-16}$	$7 \cdot 10^{-10}$	$3 \cdot 10^{-20}$	$1 \cdot 10^{-18}$	$3 \cdot 10^{-20}$	$2 \cdot 10^{-38}$

By taking into account a high anisotropy of the diffusion in the 123 matrix (Table 1), and the above mentioned orientation of the SFs with respect to 211 precipitates in single-domain samples[1], one can predict the diffusion supply of copper and oxygen in the ab plane of the matrix. This is consistent with TEM data[1] that the SFs propagate easier along the ‹100› direction, and the shear component of their associated displacement vectors is exchanged between the a and b axis directions of the 123 matrix at every twin boundary.

According to data[15] on a strong anisotropy of the oxygen diffusion in the ab plane of the 123 matrix, the quantity for the b axis direction ($D_{O(123)b}$) is much larger than for the a axis direction ($D_{O(123)a}$). Hence, for randomly twinned samples there is $D_{O(123)ab} \approx 0.1\ D_{O(123)b}$, because oxygen atoms diffuse preferably along the b axis direction (Fig. 13, in reference[15]).

From these two facts, one can conclude that the rate-controlling stage of the process[1] is the oxygen diffusion supply, which is characterized by a decrease of several orders of magnitude of the diffusion coefficient. On the other hand, the copper diffusion supply is, obviously characterized by a several orders' enhancement of the diffusion coefficient.

In this respect, it can be noted that the oxygen diffusion supply through SFs areas of 124 or 247 can be neglected (due to the relatively small diffusion coefficient ($D^*_{O(124)ab}$, Table 1). It is also relevant to emphasize that (as it is seen from Table 1) the diffusion redistribution of barium and yttrium atoms in the 123-matrix (which is necessary for flowing of step (3)) is possible only in the close vicinity of the 211 precipitates.

Results[1] indicate that the 123 matrix undergoes a local severe plastic deformation, mainly, in the 211 vicinity, when the composite is submitted to the oxygenation treatment. The most apparent features of the treated microstructure is a drastic increase of the dislocation density within the 123 matrix up to 10^{10} cm^{-2}, as well as the dislocation-twin interaction modes. Samples[1] are also characterized by both a high density of low-angle grain boundaries, and a high concentration of homogeneously distributed fine 211 precipitates (31-36 vol. %), which provide a high effective 211/123 interface area, as well as a high density of microcracks in the matrix at the interfaces.

There is a basis[17] to assume that in the studied samples[1] both the oxygen diffusion decrease, and the copper diffusion enhancement are caused by the influence of the co-segregation at dislocations. This is also consistent with the fact pointed in study[15] that twin boundaries in the 123 matrix do not contribute apparently to the effective bulk oxygen diffusion.

The local deformation, cracking and the dislocation formation in the composites[1] under the oxygenation treatment, obviously, occur at the expense of the energies of the internal reactions[17].

By using Fig. 1, the free energy change per mole of the ceramics, for instance, for step (3) can be evaluated as:

$$\Delta G_{(3)} = RT \ln [(P_{O2(3)}/P_{O2}^{eq})^{(2x-1-1.5y)/4} (a_{Oy}/a_{Ox}^{eq})^{3/4} /(a_{Ox}/a_{Oy}^{eq})], \quad (8)$$

where P^{eq}_{O2} can be found from the extrapolated line 3 in Fig. 1; R is the gas constant; thermodynamic activities of oxygen (a_O) can be found by using data[16]; the internal stresses can be estimated (10^2-10^3 bar, as it is obtained in study[17]).

If the SFs (phase) concentration (ρ_{SFP}, cm^{-1}) is obtained from the TEM observation[3], then the volume percentage of SFs (phase) can be evaluated as:

$$Vol.\ \%\ (SFs) \approx \rho_{SFP}\, h_{SFP}\, 100, \quad (9)$$

where $h_{SFP} \approx 1 \cdot 10^{-7}$ cm. By using stoichiometric coefficients of reaction ((2) or (6)), and taking into account 31-36 vol. % of the pre-existing 211 phase, the phase composition of the treated samples[1-5] can be evaluated.

The plausibility of the concepts developed above can be confirmed by results of such an analysis of data[2-4,13,14], see Fig. 1.

The results of the data analysis show the possibility of a manifestation of a phase fluctuation-like effect with respect to physical properties of HTSC cuprates, which can be evaluated for different oxygenation regimes.

ACKNOWLEDGMENTS

The author is grateful to his collaborators, in particular J. Ashkenazi, J.G. Hirschberg, D.V. Iourtchenko, L.L. Song and T.N. Veziroglu for their contributions. He is thankful to J. Karpinski for a valuable discussion, and also to the Fulbright Scholar Program.

REFERENCES

1. F. Sandiumenge, N. Vilata, S. Pinol, B. Martinez, X. Obradors. *Phys. Rev. B*, **51**, 6645 (1995).
2. F. Sandiumenge, N. Vilata, Y. Maniette, X. Obradors. *Appl. Phys. Lett.* **70**, 1 (1997).
3. P.X. Zhang, H.W. Weber, L. Zhou. *Supercond. Sci. Technol*. **8,** 701, 15 (1995).
4. J. Plain, F. Sandiumenge, J. Rabier, M.F. Denanot, X. Obradors. *Phil. Mag. A*, **82**, 337 (2002).
5. F. Sandiumenge, J. Rabier. *Studies of High Temperature Superconductors*, edited by A. Narlikar, New York: Nova Science (1999) 43.
6. Yu.S. Nechaev, P. Sandiumenge, X. Obradors. *The Abstract Booklet of the International Workshop DIFTRANS'98*, Ukraine (1998) 72.
7. Yu.S. Nechaev, P. Sandiumenge, X. Obradors. *The Abstract Booklet of the International Workshop DSS-02*, Moscow (2002) 72.
8. S.A. Degterev, G.F. Voronin. *Russin J. Phys. Chem.* **67,** 2393 (1993).
9. T.B. Lindemer, F.A. Washburn, C.S. Mac Dougall, R. Feenstra, O.B. Cavin. *Physica C*, **178**, 93 (1991).
10. K. Conder, J. Karpinski, E. Kaldis, S. Rusiecki, E. Jilek. *Physica C*, **196,** 164 (1992).
[11]. R.V. Kumar, D.J. Fray, J.E. Evetts, H.W. Williams, A. Misson. *J. Electrochem. Soc*., **140**, 2895 (1993).
12. R.K. Williams, K.B. Alexander, J. Brynestad, T.J. Henson, D.M. Kroeger, T.B. Lindemer, G.C. Marsh, J.O. Scarbrough, E.D. Specht. *J. Appl. Phys*., **70**, 906 (1991).
13. B. Martinez, F. Sandiumenge, T. Puig, X. Obradors, L. Richard, J. Rabier. *App. Phys. Lett.*, **74,** 73 (1999).
14. T.A. Prikhna, W. Gawalek, F. Sandiumenge, V.E. Moshchil, V.S. Melnikov, S.N. Dub, T. Habisreuther, A.B. Surzhenko, P.A. Nagorny. *J. Mater. Sci*., **35**, 1607 (2000).
15. J.L. Routbort, S.J. Rothman. J. Appl. Phys., **76**, 5615 (1994).
16. Yu.S. Nechaev, V.A. Lykhin, K.N. Zhangozin, D.B. Kargin, N.V. Khromova. *Russian J. Phys. Chem*., **68,** 1535, 1542 (1994).
17. Yu.S. Nechaev. *Defect and Diffusion Forum*, **194-199**, 1713 (2001).

PSEUDOGAP BEHAVIOR IN UNDERDOPED CUPRATES

David Pines
Institute for Complex Adaptive Matter, University of California Office of the President, Physics Dept., UIUC, and Los Alamos National Laboratory

Abstract: I review some of the experimental evidence and theoretical arguments that suggest that pseudogap matter is a new form of matter that coexists with coherent electron matter in the normal state and with superconducting matter below the superconducting transition temperature. I describe work in progress on a phenomenological two-fluid description of the evolution of pseudogap behavior that offers an explanation for the unexpectedly simple scaling behavior for the uniform magnetic susceptibility found in the underdoped cuprates and use this to propose a physical picture of the underdoped cuprates and to estimate the fraction of quasiparticles that become superconducting in underdoped superconductors.

Key words: Cuprates, superconductivity, pseudogap matter, two-fluid model

1. INTRODUCTION

For those of us who predicted d-wave superconductivity in the cuprates, the discovery of d-wave symmetry has meant that the key question in the cuprates has shifted from "What is the mechanism for high Tc? (our answer, " It is electronic and magnetic in origin") to fundamental questions about an unexpected new state of matter, pseudogap matter, that is found well above the superconducting transition temperature in underdoped cuprate superconductors. What is the physical origin of pseudogap behavior, and what is its onset temperature? What does experiment tell us about the resulting transformation of coherent electron states to pseudogap states and

J. Ashkenazi et al. (eds.), New Challenges in Superconductivity: Experimental Advances and Emerging Theories, 97-104.

the description of pseudogap matter? What is the evidence that pseudogap behavior competes with superconductivity, and that this competition can lead to the existence of a quantum critical point?

In this talk, I review briefly some of the experimental evidence and theoretical arguments that suggest that pseudogap matter is a new form of matter that coexists with coherent electron matter in the normal state and with superconducting matter below the superconducting transition temperature. I describe work in progress on a phenomenological two-fluid description of the evolution of pseudogap behavior that offers an explanation for the unexpectedly simple scaling behavior found by Nakano, Johnston, et al for the uniform magnetic susceptibility in the underdoped cuprates and use their results to estimate the fraction of quasiparticles that become superconducting in underdoped superconductors.

2. THE PSEUDOGAP STATE

Measurements of the uniform spin susceptibility of the 1-2-3 materials by Alloul and his colleagues in 1989 showed that in underdoped samples it possessed a maximum at a doping-dependent temperature, T*. The fall-off in that susceptibility below T* was attributed by Friedel to a gap in the quasiparticle spin spectrum, which he called a pseudogap. Subsequent experiments showed that a similar pseudogap phenomenon was present in all cuprate superconductors, while Johnston and Nakano showed in the 2-1-4 materials that when one plotted the ratio of the temperature dependent part of the uniform magnetic susceptibility to that at T*, as a function of T/T*, its temperature evolution displayed simple scaling behavior. Further insight into the pseudogap phenomenon came from NMR and ARPES experiments which suggested that in the underdoped cuprates an energy gap formed for the hot or antinodal quasiparticles (those near pi,0) in momentum space, while from their analysis of the antiferromagnetic component of the Cu spin-lattice relaxation rate and spin-echo decay rate, Barzykin and Pines argued that T* is the temperature at which the AF correlation length associated with the hot quasiparticles is of order 1 to 2 times the lattice spacing, a.

STM experiments suggested that in these materials at low temperatures one had intrinsic electronic spatial inhomogeneity. This conclusion is consistent with a proposal by Slichter on how one might reconcile the results of NMR experiments (a local probe) that seemed to require commensurate spin fluctuation peaks and INS experiments (a global probe) that show an incommensurate peak; Slichter proposed that one is observing discommensuration in the 2-1-4 (and possibly other cuprates), with regions

of commensurate spin fluctuations being separated by small domains that are far less magnetic.

This past October at an Erice workshop, Seamus Davis presented convincing experimental evidence from his STM experiments on underdoped BSCCO that provide direct support for these scenarios (condmat0404005). He finds that pseudogap matter is made up of "hot" or anti-nodal quasiparticles and that it co-exists with superconducting matter at low temperatures, His results were supported by Shin-ichi Uchida in his Erice workshop presentation; along with Davis, Uchida argued that there are two distinct d-wave energy gaps, one associated with superconducting matter, one associated with pseudogap matter, and that the width of the distribution of the large doping dependent energy gaps in the underdoped materials reflects a range of densities in the regions of pseudogap matter. Uchida reported on experiments by Matsuda on the doping dependence of the range of measured energy gaps in the 2-1-4 materials that show this range narrowing as one increases the doping, with a very narrow distribution being measured for a doping level of 0.22. Matsuda's results suggest that for these materials, 0.22 marks the crossover from underdoped to overdoped materials. At Erice, Uchida also reported on experiments that indicate that the decrease in the condensation energy and the superfluid density seen as one goes toward increasingly underdoped materials may simply reflect the volume of the sample that is superconducting.

A simple physical picture that is consistent with the above results is that above T* one has coherent itinerant quasiparticle behavior over the entire Fermi surface, observed as an anomalous Fermi liquid. Below T* one loses that coherent behavior for a portion of the Fermi surface near the antinodes; the hot quasiparticles (those whose spin-fluctuation-induced interaction is strongest) found there enter the pseudogap state; its formation is characterized by a transfer of quasiparticle spectral weight from low to high frequencies that produces the decrease in the uniform spin susceptibility below T*.The remainder of the Fermi surface is largely unaffected.

In the pseudogap state at high temperatures one thus finds the coexistence of two distinct components; pseudogap matter and coherent quasiparticle matter; as the temperature is lowered it is the coherent quasiparticles that enter the superconducting state, while the pseudogapped quasiparticles are largely unaffected by the superconducting transition and do not participate in the superconducting behavior. One therefore expects two gaps in the superconducting state; a hot quasiparticle gap characterizing the pseudogap matter , with an energy (of order 2 T*) that increases as the doping is reduced, and the d-wave gap of the superconducting matter (of order 3 kTc), that decreases as the doping is reduced.

What is the physical origin of the formation of pseudogap matter by the hot quasiparticles? It seems plausible that it is the increase in the strength of their antiferromagnetic correlations, as suggested by Barzykin and Pines. Viewed from the perspective of a hot quasiparticle, it is truly difficult for it to continue to be both itinerant and strongly antiferromagnetically correlated over distances somewhat greater than a lattice spacing. So a hot quasiparticle opts for the pseudogap state in which it is effectively localized and so finds no difficulty in becoming increasingly antiferromagnetically correlated as the temperature is lowered. Being effectively localized, it may also become spatially ordered. Quite importantly, Ali Yazdani 's group (Vershinin et al, Science 303,1995,2004) has found direct evidence from their STM experiments for such spatial ordering at temperatures above the superconducting transition in the BSCCO materials, while Seamus Davis also reported at Erice on evidence from his group's STM measurements on BSCCO at very low temperatures for the existence of periodic structures, presumably associated with regions of pseudogap matter that coexist there with superconductivity.

Pseudogap behavior is most easily identified at temperatures below T* but well above the superconducting transition temperature. A simple expression for the doping dependence of T* for the 2-1-4 materials that is consistent with the Nakano analysis and the Matsuda experiments is

$$T^*=1250\ (1-x/0.22)\ K$$

where x is the hole doping level. To the extent that this extrapolation is correct for very low hole densities, it tells us that in the undoped material, the Mott insulator, at temperatures of order J, one enters the pseudogap state, out of which the Neel antiferromagnet forms at 400K or so. Since T* is of order J, it is plausible that it is a measure of the effective magnetic coupling between nearest neighbor Cu spins which might decrease as the hole density is increased. As one increases the doping above 0.02, one would then expect to find a coherent quasiparticle state coexisting with ordered pseudogap matter until one reaches doping levels above 0.06 or so, where at low temperatures the coherent quasiparticles become superconducting. The very recent optical experiments of the Basov group (Padilla et al, unpublished) provide striking evidence that this is the case. They see two components in the optical absorption, which are distinct at doping levels below 0.06: one is the Drude peak produced by coherent quasiparticles; the second is a mid-IR feature that it seems natural to identify with the pseudogap state. Rather surprisingly the coherent quasiparticle component of the normal state does not change its character appreciably with doping; the observed Drude peak corresponds to quasiparticles whose effective mass is independent of doping;

only the height of the peak, proportional to the density of coherent quasiparticles, varies with doping throughout the entire underdoped region. Since the effective mass is doping independent, it is tempting to identify Basov's low frequency component as representing Fermi liquid islands of approximately constant density whose concentration increases with increasing doping.

A corollary of the above results is that one should expect isotope effects in the quasiparticle spectrum measured in the pseudogap state, since once localized, the hot quasiparticles can become strongly coupled to the lattice. (When not localized, the coupling of the hot quasiparticles to phonons is markedly reduced by vertex corrections associated with their magnetic coupling.) Any coupling of cold quasiparticles to the lattice would be very much smaller. These conclusions appear consistent with the ARPES results reported by Lanzara at this workshop. It leads me to predict that no isotope effect will be found for hot quasiparticles in overdoped materials.

As one increases doping, the above expression suggests that in the absence of superconductivity one would encounter a quantum critical point at a doping level of ~0.22. However this is likely not the case, since we have argued above that the low frequency behavior of the material associated with coherent quasiparticle matter is not affected by the emergence of the pseudogap state; the competition between the pseudogap state and the Fermi liquid state for the hot quasiparticles would therefore not give rise to quantum critical behavior. Put another way, the expected quantum critical point is hidden by the coherent quasiparticles whose behavior goes smoothly through the point in question.

It is worth remarking that the above phenomenology leads one to conclude that the marginal Fermi liquid behavior hypothesized for the optimally doped samples (x~0.16) does not reflect quantum critical behavior.

3. A TWO-FLUID DESCRIPTION OF EMERGENT PSEUDOGAP BEHAVIOR

The transfer of spectral weight from low frequencies to high frequencies that accompanies the formation of pseudogap matter is the inverse of process in heavy electron materials by which at some onset temperature the itinerant coherent heavy electron state emerges out of the local moments that make up the Kondo lattice. It has recently proved possible to develop a two-fluid description that describes this emergent

coherent itinerant electron behavior and, in so doing, uncover fundamental scaling laws (Nakatsuji, Pines, and Fisk , PRL 92, 016401,2004); Curro, Young, Schmalian, and Pines (condmat 0402179). It is natural to inquire whether insight into the evolution of pseudogap matter can be obtained from the measured fall-off in $\chi(T)$below T*, by extending this two-fluid description to the underdoped cuprates, I thus assume that at temperatures below T* some fraction, f(T), of the coherent hole states become part of pseudogap matter, and write the spin susceptibility as

$$\chi(T)= f(T)\, \chi_{PG}(T) + (1-f(T))\, \chi_{COH}\,(T^*)$$

where f(T) may be thought of as an order parameter characterizing the pseudogap state, $\chi_{PG}(T)$ describes the contribution of the pseudogapped quasiparticles to χ, and I have made an assumption consistent with the Basov optical results-- that below T* the coherent quasiparticles cease to evolve so that the contribution of the coherent quasiparticles to χ is temperature independent, and given by their value at T*. To the extent that the transfer of spectral weight to high frequencies for the hot quasiparticles is effective in eliminating their contribution to χ , we may neglect $\chi_{PG}(T)$. We then find

$$\chi(T)/\ \chi(T^*)= \ 1\text{-}f(T)$$

so that the fall-off in χ (T) below T* is explained as the loss of the coherent quasiparticle contribution to χ (T) and provides a direct measure of f(T). If T* sets the scale for the temperature variation of f, ie f(T/T*), one obtains the scaling behavior of χ (T) proposed by Johnston and Nakano et al.

$1\text{-}f(T_c)$ then provides a direct measure of the fraction of the quasiparticles that are coherent and participate in the superconducting state. Assuming that the scaling behavior found for the 2-1-4 materials is universal, we may then use measured (or estimated) values of T* to obtain the following results

Material	T*(K)	$1\text{-}f(T_c)$
1-2-3 O 6.95	175	0.9
1-2-3 O 6.63	420	0.25
2-1-4 Sr 0.15	420	0.25

It will be interesting to see to what extent these results are consistent with the superconducting fraction obtained by other probes.

The much greater relative percentage of pseudogap matter in the 2-1-4 materials might then explain the differences in Tc between the 2-1-4 and 1-2-3 materials. If the superconducting fraction of the 2-1-4 materials behaves just like that in the quite overdoped region of the 1-2-3 materials where Tc increases from zero to, say, 40K, then since at this and lower 2-1-4 hole doping densities, pseudogap matter formation successfully competes with superconductivity, there would be no regions with a Tc greater than 40K.

4. OUTLOOK

The Davis experiments also suggest that in underdoped BSCCO materials, one has islands of local superconductivity embedded in a sea of pseudogap matter, a proposal that has been made by many people. The global result will then be granular d-wave superconductivity, brought about by Josephson coupling between d-wave islands whose hole density is that found near optimal doping , but whose relative fraction (volume) decreases as one decreases the overall doping level. This result is just what one would expect if it is the coherent Fermi liquid islands in the normal state that become superconducting. As noted earlier, a possible corollary of the Uchida results is that the increase in superfluid density with x, as one increases doping from the severely underdoped side, mainly reflects the increase in the relative number of superfluid regions whose average density is pretty much constant, and is of the order of that found near optimal doping. For this scenario to be consistent with a number of experiments that have been successfully interpreted as though one has bulk superconductivity, the Josephson coupling must be sufficiently strong that quasiparticles in the superconducting islands tunnel easily through pseudogap matter, so that at low frequencies there would be no appearance of inhomogeneity. D-wave superconductivity will help being this about, but an intimate relationship between pseudogap and superconducting matter may also be required.

The Hall effect measurements of Balakirev and Boebinger (BB) provide added support for a transition to pseudogap matter, since only that fraction of the Fermi surface that is superconducting would change its character at fields greater than that required to destroy superconductivity, and that fraction should change with doping. As one goes from the overdoped to the underdoped state at very low temperatures in the absence of superconductivity, one would expect to see a jump in the Hall effect whose magnitude would reflect the relative fraction of the quasiparticles that enter the pseudogap state.

The existence of islands of superconductivity that, upon application of a strong enough magnetic field, become “cold” quasiparticle conducting islands embedded in insulating pseudogap matter, might provide a simple explanation of the log dependence on T found in the B B resistivity measurements in fields strong enough to destroy both granular sc and sc in the cold qp matter islands.

Clearly much more work needs to be done before the physical picture presented here is confirmed. Of particular interest is the issue of the order parameter that describes the pseudogap state which, as of this writing, is an open question.

ACKNOWLEDGMENTS

I should like to thank Dmitri Basov, Seamus Davis,Juergen Haase, Alessandra Lanzara, Charlie Slichter, Shin-ichi Uchida, and Ali Yazdani for sharing their experimental results in advance of publication and for stimulating discussions concerning the interpretation of their results, and Artem Abanov, Andrey Chubukov and Steve Kivelson for stimulating discussions on these and related topics, This work has been supported in part by the Institute for Complex Adaptive Matter and the Department of Energy.

REFERENCES

1. J. G. Bednorz and K. A. Müller, *Z. Phys.B* **64**, 189 (1986).
2. D. Pines et al. see the lanl web page for all references

NOTES ON RVB-VANILLA BY ANDERSON ET AL.

C.M. Varma
University of California, Riverside, Ca. 92521

Abstract The claims made for the Resonating Valence Bond ideas for the Cuprates in a recent paper by Anderson et al. on the basis of a variational calculation are discussed.

Keywords: High-T_c cuprates, RVB, phase diagram

1. Introduction

Within weeks of the confirmation of the discovery of high temperature superconductivity in the cuprates by Bednorz and Muller, Anderson[1] suggested an explanation of the phenomena and called it resonating valence bonds (RVB). Despite an enormous theoretical effort by the international scientific community, systematic or consistent theoretical results have been hard to obtain on this idea for the model proposed by Anderson for the cuprates. When some specific predictions were made based on the general ideas or approximate calculations, experiments did not conform.

In a curious recent note Anderson, Lee, Randeria, Rice, Trivedi and Zhang (ALRRTZ) [2]. put forth that the variational calculations that were done over a decade ago based on Anderson's ideas and have been revived [3] recently, support the ideas of RVB for the cuprates. They also reiterate that the Hubbard/t-J model, also proposed by Anderson is a sufficient model for the essential physics of the cuprates.

In this note I point out the following:

(1) The principal result of the variational calculations discussed by ALRRTZ is contrary to a vast array of experimental results. This disagreement is of a fatal nature for ideas which the variational calculation is taken to support.

(2) The properties of the Hubbard/t-J model cannot be adequately studied using the wavefunctions with the limited variational degree of freedom employed by ALRRTZ.

(3) In view of (1) and several other experimental and theoretical results, the Hubbard/t-J model is itself inadequate as a model for the Cuprates.

J. Ashkenazi et al. (eds.), New Challenges in Superconductivity: Experimental Advances and Emerging Theories, 105-115.

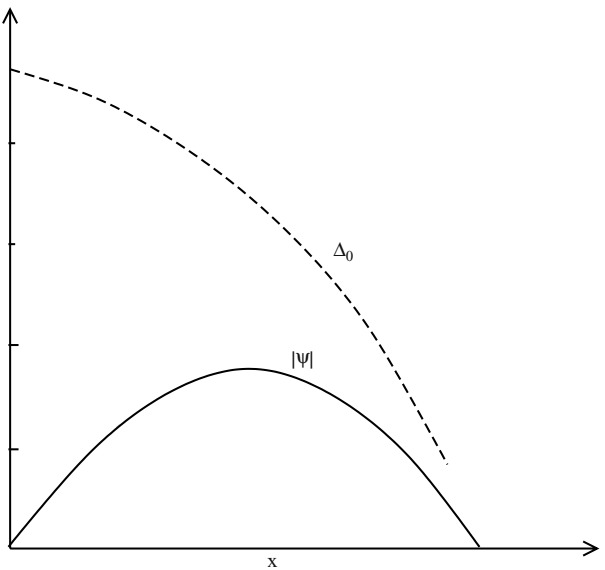

Figure 1. The calculated variation of the parameter Δ_0 in the wavefunction Eq. (1) and the calculated magnitude of the superconducting order parameter with x; adapted from Ref. (2)

2. Experiments and the results from the chosen Wavefunction

The chosen variational wavefunction is the d-wave superconducting wavefunction with projection to remove double occupation:

$$\Phi = \bar{P}\phi_{BCS}(\Delta(\mathrm{k})). \tag{1}$$

$\bar{P}$ is the projection operator and $\Delta(\mathbf{k})$ is the the d-wave BCS order parameter function with a variational parameter of magnitude Δ_0. The principal result of the calculations is that the ground-state energy is minimized when Δ_0 varies with x, the deviation from half-filling as shown schematically in figure (1), while the superconducting long-range order parameter $|\Psi|$ has a dependence with x as also sketched in the figure. Δ_0 is interpreted to represent the magnitude of the experimentally observed pseudogap. A corollary to fig. (1) is a phase diagram sketched in fig. (2), where T_p^A marks the crossover temperature to pseudogap properties. The validity of the argument can be tested by comparing the results of figs. (1) and (2) with experiment. Other comparisons with experiment are not meaningful if this test fails.

The authors acknowledge that the wavefunction does not correctly give the region near $x = 0$, where the model studied as well as the Cuprates have an

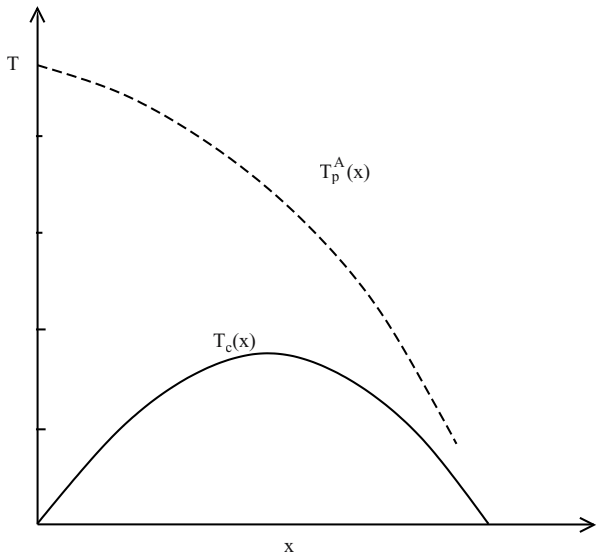

Figure 2. The Phase diagram in the $T - x$ plane implied by calculations reported in Ref. (2)

AFM ground state. An unasked question is : At what x does the chosen RVB variational wavefunction have a lower energy than a wavefunction describing AFM at appropriate wave-vectors $\mathbf{Q}(x)$? They also acknowledge that their approach is no help in understanding the universal normal state properties for compositions near those for the highest T_c. I will return to both these points; first, let us compare the claims made with the experiments.

A crucial feature of Fig. (1) is that the parameter Δ_0 is finite throughout the superconducting region $x_{min} < x < x_{max}$. I summarize evidence below that, in experiments, the pseudogap properties disappear above a critical composition x_c within the superconducting region. Moreover experiments show that a singularity exists at x_c, the Quantum Critical Point (QCP) in the limit $T \to 0$. If T_c is reduced by application of a magnetic field, the normal state anomalies continue to lower temperatures. The pseudogap region as well as the Fermi-liquid region emanate from x_c. Any theory which is smooth across $x = x_c$ can then not be a theory for the Cuprates. The universal phase diagram of the cuprates [4] is as sketched in fig. (3).

The evidence is diverse and mutually consistent:

(1) Tunneling Measurements: The most direct is the measurement of pseudogap by tunneling by Alff et al. [5] in two electron doped superconductors by reducing T_c on applying a magnetic field. The central observations are (a) for $x < x_c$ within the superconducting dome, the characteristic pseudogap feature in tunneling conductance is observed while the superconducting gap feature

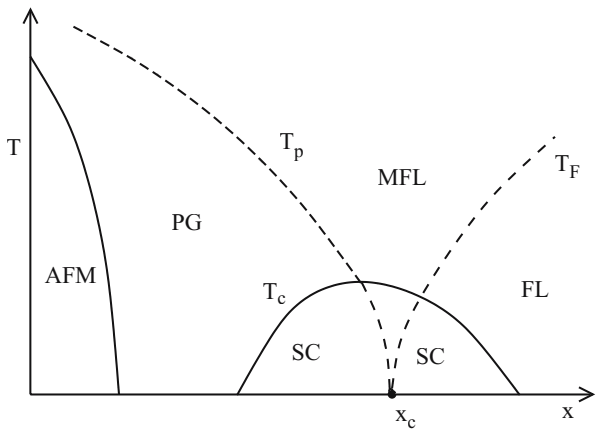

Figure 3. The universal Phase diagram for the Cuprates; from Ref.(4)

disappears as $T_c(H)$ is reduced to 0, (b) This feature appears at a temperature $T_p(x)$ below $T_c(x)$ at $H = 0$, (c) the magnitude of the pseudogap for three different samples with $T_p(x)$ below T_c, and $T_p(x)$ itself, extrapolate to zero at an x_c inside the superconducting dome.

(2) Resistivity near $T = 0$: In the region above $T_c(x)$ and below a temperature characterized by $T_p(x)$, a change in the temperature dependence of the resistivity from linear to a higher power is observed. Similarly below a temperature $T_F(x)$ for $x > x_c$, a change in the power law tending towards the Fermi-liquid value of 2 is observed. This is observed in all the cuprates studied, Fig.(4) organizes the data in a number of compounds [8].

A linear temperature dependence of resistivity at low temperatures cannot occur without a putative singularity in the fluctuation spectra at $T = 0$. Measurements in a large enough magnetic field to drive T_c to 0 show that the linearity persists in an increasingley narrower region of x as T_c is decreased and persists at least down to $40mK$ in one cuprate compound [6] and down to at least 2 K in another [7]. To within the finest composition variation studied, $\delta x = 0.01$, the resistivity power law changes to higher values on either side of x_c.

(3) Hall effect near $T = 0$ [6]: In the case of one of the class of compounds whose T_c is reduced to 0 by a magnetic field, the Hall coefficient has been measured at low temperatures. It shows a singular derivative at $x \approx x_c$.

(4) Transport properties above $T_c(x)$: Actually, it is not necessary to study the properties near $T = 0$ to rule out a pseudogap region beyond an x_c in the superconducting range of x. If fig. (2) were true, the universal normal state anomalies would change to the pseudogap properties for any x for temperatures below $T_p^A(x)$ and above $T_c(x)$. The data does not sustain this point of view.

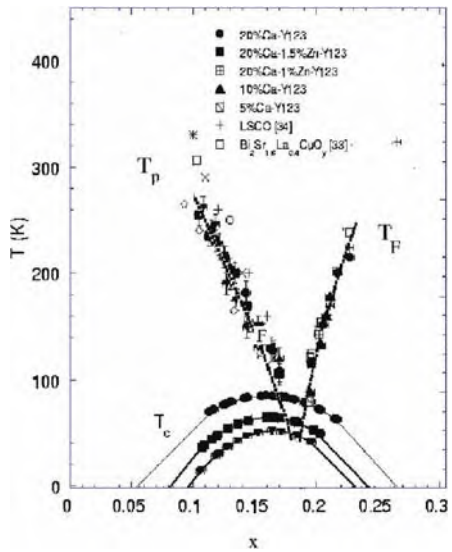

Figure 4. Organization of the Resistivity data for a number of Cuprates: In the region between the set of points indicated by T_c, T_p, T_f, the resistivity is linear in temperature. It has a different dependence in other regions. Figure taken from Ref.(8).

The resistivity data consistent with the phase diagram (3) has been shown in fig. (4). Wuydt et al.[9] have shown that the determination of $T_p(x)$ by thermodynamic measurements, specific heat and magnetic susceptibility as well as the Cu-nuclear relaxation rate is consistent with that from resistivity. Recent measurements of the optical conductivity [10] for various compositions are also consistent with the phase diagram (3).

In a very recent paper, Naqib et al.[11] have measured the resistivity of $Y_{1-x}Ca_xBa_2(Cu1-yZn_y)_3O_{7-\delta}$ over a wide range of x and y and in a magnetic field. Just as a magnetic field, Zn reduces T_c without affecting the pseudogap. They can thereby observe the variation of T_p below the un-Zndoped and zero magnetic field T_c. T_p continues below this T_c, extrapolating to a finite value well within the superconducting dome.

(5) Thermodynamic Measurements: ALRRTZ [2] quote only the thermodynamic measurements and analysis by Loram et al.[12] both in the normal state and for the superconducting condensation energy, and claim not to understand how the conclusions were reached. Actually the conclusions of Loram et al. are consistent with the existence of a QCP and all the experiments quoted above. This is discussed further below in connection with fig.(5).

(6) Raman Susceptibility: Careful measurements of Raman intensity in the compound 123 near $x = x_{opt}$, the composition for the highest T_c, show [13]

that the susceptibility has the scale invariant form

$$\begin{aligned} Im\chi(\omega/T) &\propto \omega/T, \ for\ \omega/T \ll 1 \\ &\propto constant, \ for\ \omega/T \gg 1. \end{aligned} \tag{2}$$

More complete are measurements [14] in the compound 248. At stoichiometry, this compound displays the pseudogap properties with a characteristic change in resistivity from linear to that of the pseudogap behavior below $T_p \approx 200K$ and a T_c of 80 K. Under pressure P, T_c continuously rises to 110 K at a P of 100 kbar; simultaneously T_p decreases and is invisible above a P about 80 kbar [15]. Raman measurements under pressure reveal the form of Eq. (2) near 100 kbar but at lower P one finds a characterstic infra-red cut-off proportional to $T_p(P)$.

In their paper ALRRTZ reproduce the magnitude of a gap deduced from the photoemission experiments [16] which indeed varies with x in the manner similar to fig. (1). This gap is deduced at low temperatures from experiments in the superconducting phase. This may appear reasonable enough. After all the comparison is being made to a parameter in a ground state wavefunction. Actually, this is a specious argument if Δ_0 is understood to represent the pseudogap. A tunneling measurement made below T_c will show a gap which is zero only when both the pseudogap and the superconducting gap are zero because the gap measured is is an appropriate combination of the pseudogap $D(x)$ and the superconducting gap $\Delta_{sc}(x)$; for instance

$$gap = \sqrt{|D(\mathbf{k})|^2 + |\Delta_{sc}(\mathbf{k})|^2} \tag{3}$$

To measure the pseudogap one must kill the superconducting gap as Alff et al. [5] have done, as discussed above. The total gap in zero field and at low temperatures then goes to zero only for $x > x_{max}$. Alternately one may deduce the pseudogap from measurements above T_c. Loram et al. have done this through modelling their thermodyanmic measurements. A comparison of their deduced values of the pseudogap as a function of x with those obtained from tunneling and photoemission at low temperature is shown [17] in fig.(5). The two sets of gaps do follow a relation not inconsistent with Eq. (3) if Δ_{sc0} is proportional to $T_c(x)$.

3. Restricted Variational freedom

The variational results are at odds with the phase diagram for the cuprates. Are they a good representation of the physics of the t-J model? What does the variational parameter Δ_0 really represent? In a model with strong local interactions $U \gg t$, there must be a transfer of the distribution function $n(\mathbf{k})$

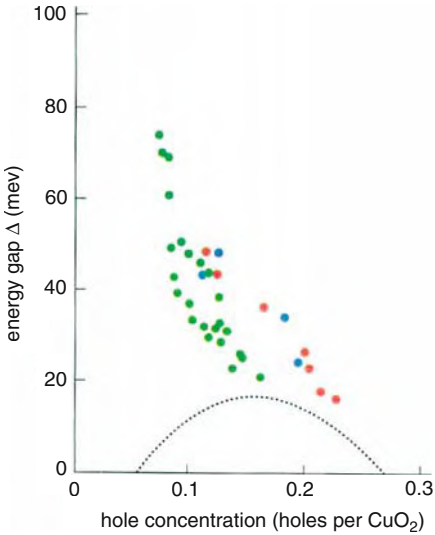

Figure 5. The energy gap in the normal state determined by fitting to the specific heat data with a model density of states by Loram et al. is shown in green. The tunneling experiments well below T_c give the gap shown in red in agreement with ARPES shown in blue.

from below the Fermi-vector to above compared to non-interacting electrons. In the wavefunction, Eq. (1), Δ_0 is the only parameter to accomplish this physics. There is then simply no choice but for the calculations to exhibit a pseudogap. It is put in by hand without comparing the ground state energy with other wavefunctions which accomplish the same physics. The choice of Eq. (1) automatically ensures $\Delta_0 \approx J$ for $x \approx 0$ with a decline to ≈ 0 for large enough x. A Fermi-liquid, accomplishes the same physics with a discontinuity z in $n(\mathbf{k})$ at $\mathbf{k}_F$. z changing smoothly from 0 near $x = 0$ to 1 for large enough x. Much more relevant for the physics of the t-J model would be to compare the ground state energy using Eq. (1) with that for a wavefunction representing AFM order at a wave-vector $\mathbf{Q}(x)$, also projected to remove double-occupation. We know the wavefunction (1) is wrong for the t-J model near $x = 0$ only because the experiments say the region near $x = 0$ is AFM. How far does this problem with the wavefunction persist. Only comparison of the energy with an AFM wavefunction can tell. Based on the results of the mean-field calculations and several numerical calculations, my conjecture is that the regime of AFM for the t-J model is much more extended than in the experiments and that in variational calculations the phase diagram will show AFM followed by a co-existing region of AFM and d-wave superconductivity followed by d-wave superconductivity alone. The physics is much the same as that for d-wave superconductivity

derived from AFM fluctuations with numerical corrections from Fermi-liquid effects [18].

This is not to say that the t-J model has a superconducting ground state above some x. As Anderson et al. point out, numerical evidence on this issue is divided. But, from the perspective of a theory of the cuprate phenomena this issue is incidental. Even if the ground state of the t-J model were to be superconducting, it cannot be a model for the Cuprates unless it can give a phase diagram similar to Fig. (3).

4. Model for Cuprates

It was suggested [19] that a unique property of the cuprates is that the ionization energy of the Cu^{++} ions is very close to the affinity energy of O^{--}. (This is what makes the half-filled Cuprates *charge transfer insulators*[20]). Their difference ϵ_{pd} is similar to the kinetic energy parameter t_{pd} and estimates of the screened nearest neighbor Cu-O ionic interactions V. In this condition, in the metallic phase charge fluctuations exist almost equally on Cu and O ions and that new physics can arise in a model with three dynamic degrees of freedom per unit cell (two Oxygens and one Copper)due to the ionic interactions. Anderson et al. argue instead that as observed in experiments there is only one band near the Fermi-surface and in any case the three orbital model may be reduced to a one effective orbital model by a canonical transformation. In this canonical transformation, they ignore the interactions represented by V. It is easy to show that for $zV \geq t_{pd}$, $\epsilon_p - \epsilon_d$, where z is the number of nearest neighbors, this canonical transformation does not converge.

The argument has never been that there is more than one band near the chemical potential. The relevant question is what is the nature of the wave-functions in this band and the effective interactions among one-particle excitations of the band after the states far from the chemical potential (in band calculations) are eliminated. That new physics arises in the general model (3-orbitals and ionic interactions as well as local interactions) [19] is known from two exact solutions : (a) A local model, which bears the same relation to the general model as the Anderson model for local moments bears to the Hubbard model. A QCP is found in the model with logarithmic singularities unlike the Ground state singlet of the Anderson or Kondo model [21]. (b) Long one-dimensional —Cu-O-Cu-O— chains on which extensive numerical results [22] have been obtained. This model gives new physics including long-rage superconducting correlations not found when the ionic interactions are put to 0.

Mean-field calculations [19] on the general model give a phase diagram similar to fig. (3), with a QCP at x_c and an unusual time-reversal violating phase for the pseudogap region.

5. Concluding Remarks

If fluctuations of the form of Eq. (2) persist down to $T \to 0$, they give that the real part of the susceptibility has the singularity

$$\begin{aligned} Re\chi(\omega.T) &\propto \ln(\omega_c/\omega) \;\; for\; T \ll \omega, \\ &\propto \ln(\omega_c/T) \;\; for\; T \gg \omega, \end{aligned} \tag{4}$$

assuming a high energy cut-off ω_c. I singled out the Raman experiments in Sec. 2, because they directly measure the singularity in the region near x_{opt}. They also show the crossover to fluctuations with an infrared cut-off in the pseudogap region. It is true that the measurements are at present available only above $T_c(x)$. But, given all the other experimental results, can there be any doubt that when measurements are carried out in a magnetic field to reduce T_c to 0, the singularity of Eqs. (2,4) will continue at x_c with an infrared cut-off on both sides of it.

This singularity specifies not only a QCP in the Cuprates inside the superconducting dome but also the critical exponents of the fluctuations about it. This form was predicted [23] in 1989 on phenomenological grounds. Actually what is measured in Raman scattering is only the long wavelength limit of the predicted form. Essentially every normal state anomaly in region I has the marginal Fermi-liquid form which follows from this singularity. The lineshape in single-particle spectra as a function of momentum and energy was predicted and verified in ARPES experiments. From two parameters, obtainable from the ARPES spectra quantitative agreement with transport properties including the Hall effect have been obtained to within a factor of 2.

But what about superconductivity? In any theory based on Cooper pairs, the fluctuations in the normal state and their coupling to the fermions engender the superconducting instability. The high frequency cut-off and the coupling constant of the singular fluctuation obtainable from normal state properties certainly give the right order of magnitude of T_c. This idea can be quantitatively tested in complete detail through an analysis of ARPES experiments in the superconducting state [24] which is an extension to anisotropic superconductors of the Rowell-Mcmillan method of analysing tunneling data for s-wave superconductors [25].

What of the microscopic theory for the singularity and the fluctuations about it? A QCP in more than one-dimension is generally the end-point of a line of phase transitions. From Raman scattering results, as well as lack of any convincing evidence for change of a translational or spin-rotational symmetry, we know that the change of symmetry at this phase transition must occur at $q = 0$ and in the spin-singlet channel. Based on the general model for Cuprates, an unusual Time-reversal violating phase has been predicted for the pseudogap phase [4]. A new experimental technique using ARPES was suggested to look

for this phase [26]. This experiment [27] has been successful. A confirmation of this phase by this or other methods should remove any doubt on what is the minimum model for the Cuprates and what is the nature of the fluctuations responsible for the Cuprate phenomena [28].

Arguments have been given why the fluctuations to this phase in this model produce the specified fluctuations. An exact calculation of the related local model [21] produces precisely the specified form of fluctuations. More work on this issue will be forthcoming.

The vast array of experiments in the cuprates narrows the possible theories for the phenomena. One can be certain that the theories should have a QCP with a phase with a pseudogap ending at it. One can also be certain that in the long wavelength limit, the fluctuations about the QCP must have the form of Eq. (2) because that is what is observed [29].

Unless the ideas of RVB satisfy these requirements, they together with several others which do not, can be excluded as a framework for a theory of the cuprate phenomena. The first paper of Anderson was important for cuprates; it posited the phenomena was due to electron-electron interactions and suggested that quite new physics will be required to understand it. This has turned out to be true. Its direct importance is to physics other than that in cuprates, in the interest it has provoked in search for models in which quantum-mechanics leads to beautiful new states of existence such as RVB. This may have implications for physics yet to come.

References

[1] P.W. Anderson, Science **237**, 1196 (1987).
[2] P.W. Anderson, P.A. Lee, M. Randeria, T.M. Rice, N. Trivedi, F.C. Zhang, arXiv:condmat/-0311467
[3] A. Paramekanti, M. Randeria, N. Trivedi, cond-mat/0305611.
[4] By universal, I mean here the phase diagram drawn on the basis of variation in properties observed in all the cuprates. Such a diagram was first shown in C.M.Varma, Phys. Rev. B **55**, 14554 (1997); Phys. Rev. Letters,**83**, 3538, (1999) and in conference proceedings earlier.
[5] L. Alff et al., Nature, **422**, 698 (2003)
[6] P. Fournier et al., Phys. Rev. Lett. 81, 4720–4723 (1998); Y.Dagan et al., cond-mat/0311041
[7] K.H.Kim and G. Boebinger et al. (unpublished results on 214 compounds)
[8] S.H. Naqib, J.R. Cooper, J.L. Tallon and C. Panagopoulos, cond-mat/0301375
[9] B. Wyuts, V.V. Moschalkov and Y. Bruynseraede, Phys.Rev. B **53**, 9418 (1996)
[10] J. Hwang et al., cond-mat/0306250
[11] S.H. naqib, et al., arXiv.org/cond-mat/0312443
[12] J.L. Tallon and J.W. Loram, Physica **C 349**, 53 (2000).
[13] F.Slakey et al., Phys. Rev. B **43**, 3764 (1991)
[14] T. Zhou et al., Solid State Comm., **99**, 669 (1996).
[15] B. Bucher et al., Physica C bf 157, 478 (1989).

[16] J.C. Campuzano et al., Phys. Rev. Lett, **83**, 3709 (1999)
[17] B. Batlogg and C.M. Varma, Physics World, **13**, 33 (2000).
[18] K.Miyake, S.Schmitt-Rink and C.M. Varma, Phys. Rev. B **34**, 6554, (1986).
[19] C.M. Varma, S. Schmitt-Rink and E. Abrahams, Solid State Comm. **62**, 681 91987). C.M. Varma and T. Giamarchi, in Les Houches Summer School (1991), Edited by B. Doucot. and J.Zinn-Justin, Elsevier (1995).
[20] J. Zaanen, G. Sawatsky and J. Allen, Phys. Rev. Letters, **55**, 418 (1985).
[21] I. Perakis, C.M. Varma and A. Ruckenstein, Phys. Rev. Letters, **70**, 3467 (1993); C. Sire et al., Phys. Rev. Letters, **72**, 2478–2481 (1994)
[22] A.Sudbo et al., Phys. Rev. Lett. **72**, 3292 (1994) E.B. Stechel et al., Phys. Rev. B **51**, 553 (1995).
[23] C.M. Varma, P.B. Littlewood, S. Schmitt-Rink, E. Abrahams, and A. Ruckenstein, Phys. Rev. Letters, **63**, 1996 (1989).
[24] I. Vekhter and C.M. Varma, Phys. Rev. Letters, 90, 237003 (2003)
[25] Since T_c is determined by the spectra at T_c, the analysis of single-particle self-energy just above T_c near x_{opt} does not leave much doubt that the analysis just below T_c will yield that the glue for superconductivity has the fluctuation spectrum of Eq. (2) at essentially all q. Such experiments and analysis should nevertheless be done to be certain.
[26] M.E. Simon and C.M. Varma, Phys.Rev. Letters, **89**, 247003 (2003).
[27] A. Kaminski et al. Nature **416**, 610 (2002).
[28] The principal reason (and a valid one) for scepticism in thinking of the Pseudogap region as one of some broken symmetry is that, although most thermodynamic and transport properties change at $T_p(x)$, there is no observable singularity in the specific heat at $T_p(x)$. Such a situation is not excluded by statistical mechanics. The symmetry change observed in Ref.([27]) belongs to a class of $Z2 \otimes Z2$ models, which in appropriate range of parameters do have a phase transition without a diverging specific heat. This model should however give at least a bump in the specific heat. Since, even that is not observed, I suspect there are some more subtle issues involved.
[29] It is also fairly certain that the momentum dependence of the fluctuations must be much less important than their frequency dependence because that is the only way known to have the transport scattering rates be similar to the single-particle relaxation rates and to understand the NMR experiments on cu in the normal state. A specific form with dyanmical critical exponent of infinity has been proposed.

ENHANCED T_C NEAR THE METAL/INSULATOR TRANSITION: A NEW PERSPECTIVE ON UNCONVENTIONAL SUPERCONDUCTING MATERIALS

M. S. Osofsky, and R. J. Soulen, Jr.
Naval Research Laboratory, Washington, DC 20375

Abstract: Many apparently unrelated systems, including disordered metals and metallic oxides, undergo a metal/insulator transition (MIT) when their carrier concentrations are reduced and/or their disorder is increased. We have found that the superconducting transition temperature, T_c, of such materials is very often enhanced in the vicinity of the MIT. We have constructed superconductivity phase diagrams (T_c vs σ, the conductivity) for many materials whose only common feature is proximity to the MIT and found that they are remarkably similar.

Key words: metal insulator transition; superconductivity; HTS; cuprates; oxides; disordered metals.

1. INTRODUCTION

It is known that many bulk, low-temperature superconductors have dramatically enhanced (sometimes by several orders of magnitude) superconductive transition temperatures, T_c, when they are rendered into a disordered or granular state. Even more striking is the fact that several other systems whose constituents usually have no, or unmeasurably low, T_c's, have been shown to have measurable, and sometimes, even reasonably high T_c's[1-13]

One common feature of these materials is that, when reported, they have resistivities that are considerably higher than those of clean conventional metals.[14-16] Figure 1 is a plot of the normalized T_c versus the log of the resistivity at 4K for several systems. Two features of this plot are noteworthy. The first is that T_c is very low or zero for low and high

J. Ashkenazi et al. (eds.), New Challenges in Superconductivity: Experimental Advances and Emerging Theories, 117-122.

resistivity samples and peaks in between (note that the Nishida SiAu has no data on the low resistivity side). The second feature to note is that these enhancements in T_c occur near the so-called Mott resistivity (0.1-1 mΩ-cm)[17] which is an indication that conventional transport models are not valid. A similar plot can be made for doped $SrTiO_4$, the first known superconductive oxide.[18] These observations suggest that the conventional model of superconductivity should be modified.

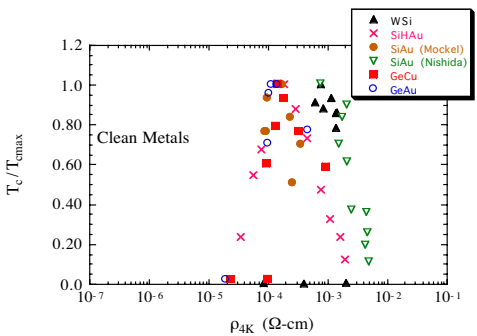

Figure 1. Normalized T_c versus ρ_{4K} for several materials. The data are from references: 19 (WSi), 8 (SiAu Mockel), 9 (SiAu Nishida and SiHAu), and 7 (GeCu and GeAu).

2. THE METAL-INSULATOR TRANSITION

The MIT is a quantum phase transition, i.e. one that occurs at T=0, that demarcates the boundary between materials with electronic states that are extended from those that are localized. In practical terms, such materials can be identified through their electronic transport properties: metals have finite, non-zero conductivity, σ, at T=0 and insulators have σ=0 at T=0. Figure 2 is a schematic diagram showing the temperature dependence of the conductivity for a series of materials spanning the metallic to insulating phases. The region labeled "conventional metal" represents the clean limit where the conductivity is very high and increases as the temperature decreases. In this region the appropriate description of physical behavior is given in terms of a Fermi liquid comprised of long-lived, weakly interacting carriers (quasi-particles) occupying well-defined energy and momentum states. This description remains valid for imperfections at low and moderate concentrations. As these imperfections are added, the conductivity decreases and the temperature dependence weakens. In these regions transport can be described using Boltzmann transport theory. As the disorder is further increased, however, the concept of a Fermi liquid becomes increasingly inaccurate and the conventional description of the normal state is rendered invalid. The transition into this region occurs near the Mott

conductivity ($1/\rho_{Mott}$). In this region (labeled "Scaling" in figure 2), which is still metallic since $\sigma(T=0)>0$, fluctuations begin to become important and the conductivity decreases with decreasing temperature but less dramatically than in an insulator. When the disorder is sufficiently large to induce fluctuations on a length scale comparable with the thermal diffusion length, the system enters the "critical" region. In this region, which lies close to the MIT line in figure 3, fluctuations are so large that the quasi-particle concept is totally invalid. In these two regions physical properties are described by scaling laws. Below the MIT is the insulating phase which is characterized by conductivity that decreases with decreasing temperature and $\sigma(T=0)=0$.

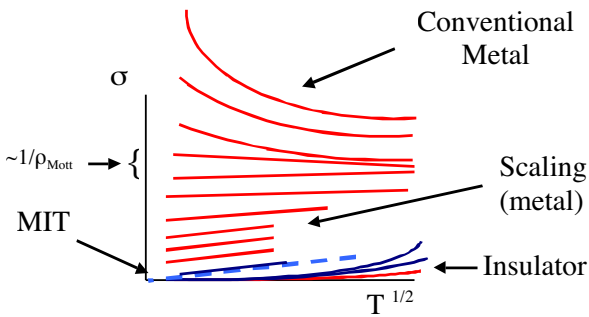

Figure 2. Schematic diagram of the conductivity as a function of $T^{1/2}$ above and below the MIT.

We introduce a coordinate that defines the "distance" from the MIT. The appropriate choice is the inverse of the correlation length, $1/\xi$,[20] which in turn is defined in terms of a measured quantity, p. For instance, p may be the carrier concentration, n, or the doping concentration, x, or σ_{300K}, the value of the conductivity at 300K.[21] This correlation length is negligible in conventional (clean) metals. It becomes important only in the "Scaling" region and is a result of the fact that near the MIT, electron-electron interactions become important causing the carriers within a volume ξ^3 to no longer move independently. By definition, $1/\xi \sim [(p-p_c)/p_c]^{1/\nu}$, where p_c is the value of p at the MIT and where ν is a critical exponent. The expression for $1/\xi$ may be written more precisely as

$$\frac{1}{\xi} = \left(\frac{1}{a}\right)\left(\frac{p-p_c}{p_c}\right)^{\frac{1}{\nu}} = \left(\frac{1}{a}\right)\left(\frac{p}{p_c}-1\right)^{\frac{1}{\nu}} = \left(\frac{1}{a}\right) r^{\frac{1}{\nu}} \qquad (1)$$

where a is a microscopic parameter comparable to the lattice parameter and where ν has been shown to be approximately 1 for many systems.[22] Furthermore, p_c may be determined by an experimental technique *so that r is*

completely defined by experimentally measured quantities.[19] We may also express ξ in terms of $k_F l$, the parameter often used to quantify disorder. That is, if we identity the MIT by the condition, $k_F l = 1$, then $k_F l = r + 1$.

3. MODEL FOR T_c

Since proximity to the MIT controls the normal state transport properties it is natural to assume that it might also influence the superconductive properties. To include these effects in a model, we modified the the Morel-Anderson model for T_c, to span the entire metallic range of an alloy:

$$T_c = 0.85\Theta_D \exp\left[\frac{-1.04(1+\lambda)}{\lambda - 0.15(1+0.62\lambda)}\right] \tag{2a}$$

$$\lambda = N_0\left[1-\exp(-\alpha r)\right]^{\delta}\left[\frac{4\pi e^2}{k_s^2 + q_c^2}\right] \tag{2b}$$

$$k_s^2 \approx \frac{k_{TF}^2}{1+(a/\alpha r)^2} \tag{2c}$$

where Θ_D is the Debeye temperature in the clean limit, α and δ are experimentally determined parameters associated with the "scaling" region, N_o is the single-particle density of states in the clean limit, q_c is a phonon cut-off momentum in the clean limit, k_{TF} the Thomas-Fermi screening wave vector in the clean limit, and a is a fitting parameter.[23] Except for a, all of the parameters in equations 2 are independently determined experimentally.

4. LTS

A search of the literature led us to choose the following alloy systems for analysis[23]: NbTi,[24-27] radiation damaged Nb_3Sn and V_3Si,[28] WSi,[1,2] MoGe and MoSi,[8] Ti and Mo alloys.[29-31] The results are presented in figure 3. Note that the magnitude of the fitting parameter, a, quantifies the extent of the T_c enhancement.

5. HTS

It is well known that HTS are peculiar metals with high resistivity whose transport properties are not consistent with conventional Fermi liquid

behavior. It is also well known that they undergo MIT's as the doping level is reduced. These properties suggest that our model might be applicable for the HTS.[32] Indeed, whenever the data allows us to perform the proper analysis we have found that $T_c(r)$ data can be fit to equation 2.[33]

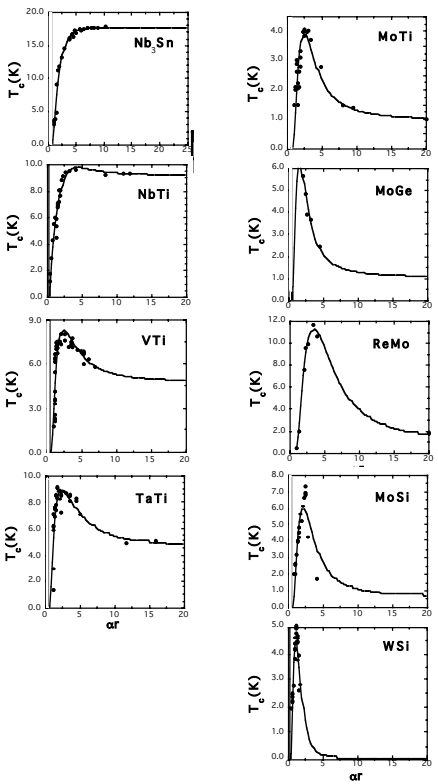

Figure 3. The superconductive transition temperature, T_c, as a function of distance, αr, from the metal/insulator transition ($\alpha r = 0$) for nine alloy systems. The data points are shown as solid circles, and the solid curves represent fits to equations 2. The fitting parameter, a, is given in parentheses for each system: Nb_3Sn (0.01), NbTi (0.69), VTi (1.5), TaTi (2.5), MoTi (6.), MoGe (15), ReMo (11), MoSi (17), and WSi (24.1).

REFERENCES

1. W.L. Bond, A. S. Cooper, K. Andres, G. W. Hull, T. H. Geballe, and B. T. Matthias, Phys. Rev. Lett. **15**, 260 (1965).
2. S. Kondo, J. Mater. Res. **7**, 853 (1992).
3. M. A. Noak, A. J. Drehman, K. M. Wong, A. R. Pelton, and S. J. Poon, Physica **135B**, 295 (1985).
4. S. Kubo, J. Appl. Phys. **63**, 2033 (1988).

5. B. Stritzker, Phys. Rev. Lett. **42**, 1769 (1979).
6. H. L. Luo, T. S. Radhakrishnan, and B. Stritzker, Z. Phys. B-Condensed Matter **49**, 319 (1983) and references therein.
7. B. Stritzker and H. Wuhl, Z. Physik **243**, 361 (1971).
8. D. Mockel and F. Baumann, Phys. Stat. Sol. (a) **57**, 585 (1980).
9. N. Nishida, M. Yamaguchi, T. Furubayashi, K. Morigaki, H. Ishimoto, and K. Ono, Sol. St. Commun. **44**, 305 (1982); M. Yamaguchi, N. Nishida, T. Furubayashi, K. Morigaki, H. Ishimoto, and K. Ono, Physica **117B&118B**, 694 (1983); T. Furubayashi, N. Nishida, M. Yamaguchi, K. Morigaki, and H. Ishimoto, Sol. St. Commun. **55**, 513 (1985);T. Furubayashi, N. Nishida, M. Yamaguchi, K. Morigaki, H. Ishimoto, Sol. St. Commun. **58**, 587 (1986).
10. N. M. Jisrawi, W. L. McLean, N. G. Stoffel, M. S. Hegde, C. C. Chang, D. L. Hart, D. M. Hwang, T. S. Ravi, B. J. Wilkens, J. Z. Sun, and T. H. Geballe, Phys. Rev. B **43**, 7749 (1991).
11. D. B. Kimhi and T. H. Geballe, Phys. Rev. Lett. **45**, 1039 (1980).
12. S. J. Poon and W. L. Carter, Sol. St. Commun. 35, 249 (1980).
13. M. Strongin, O. F. Kammerer, and A. Paskin, Phys. Rev. Lett. 14, 949 (1965).
14. T. Zint, M. Rohde, and H. Micklitz, Phys. Rev. B 41, 4831 (1990).
15. M. Giannouri, E. Rocofyllou, C. Papastaikoudis, and W. Schilling, Phys. Rev. B 56, 6148 (1997).
16. B. I. Belevtsev, Y. F. Komnik, V. I. Odnokozov, and A. V. Fomin, J. Low Temp. Phys. 54, 587 (1984).
17. e.g. $1/\rho_{Mott}=\sigma_{mint}^{3D}$ in P. A. Lee and T. V. Ramakrishnan, Rev. Mod. Phys. **57**, 287 (1985).
18. C. S. Koonce, M. L. Cohen, J. F. Schooley, W. R. Hosler, and E. R. Pfeiffer, Phys. Rev. 163, 380 (1967).
19. M. S. Osofsky, R. J. Soulen, Jr., J. H. Claassen, G. Trotter, H. Kim, and J. Horwitz, Phys. Rev. Lett. **87**, 197004 (2001).
20. NB, the correlation length discussed here is not the superconducting coherence length, which is often identified by the same symbol.
21. M. Osofsky, H. Tardy, M. LaMadrid, and J. M. Mochel, Phys. Rev. B **31**, 4715 (1985); M. Osofsky, H. Tardy, M. LaMadrid, and J. M. Mochel, Phys. Rev. B **32**, 2101 (1985).
22. G. Hertel, D. J. Bishop, E. G. Spencer, J. M. Rowell, and R. C. Dynes, Phys. Rev. Lett. **50**, 743 (1983).
23. R. J. Soulen, Jr., M. S. Osofsky, and L. D. Cooley, PRB **68**, 094505 (2003).
24. Lance Cooley, Peter Lee, and David Larbalestier, in Handbook of Superconducting Materials, edited by David A. Cardwell and David S. Ginley (Institure of Physics, London, 2003).
25. A. Mani, L. S. Valdhyanathan, Y. Hariharan, M. P. Janawadkar, and T. S. Radhakrishnan, Cryogenics, **36**, 937 (1996).
26. James Charles McKinnell, Ph. D. thesis, Univerity of Wisconsin (1990).
27. J. K. Hulm and R. D. Blaugher, Phys. Rev. **123**, 1569 (1961).
28. A. K .Ghosh and Myron Strongin, Superconductivity in d- and f-band Metals, p. 305-315.
29. F. J. Morin and J. P. Mita. Phys. Rev. 129, 1115 1963).
30. E. W. Collings, A Source book of titanium alloy superconductivity, Plenum Press, New York (1983).
31. T. G. Berlincourt and R. R. Hake, Phys. Rev **131**,140 (1963).
32. M. S. Osofsky, R. J. Soulen, Jr., J. H. Claassen, G. Trotter, H. Kim, and J. Horwitz, PRB **66**, 020502(R) (2002); M. S. Osofsky, R. J. Soulen, Jr., W. Si, X. H. Zeng, A. Soukiassian, and X. Xi, Phys. Rev. B **66**, 060501 (R) (2002); M. S. Osofsky, R. J. Soulen, Jr., W. Si, X. H. Zeng, A. Soukiassian, and X. Xi, IEEE Trans. Supercond. **13**, 2799 (2003).
33. R. J. Soulen, Jr. and M. S. Osofsky, unpublished.

ELECTRON-LATTICE INTERACTION IN HTSC CURATES

T. Egami
University of Tennessee, Dept. of Matrials Science and Engineering and Dept. of Physics and Astronomy, Knoxville, TN 37996, and Oak Ridge National Laboratory, Oak Ridge, TN 37831

Abstract: While the majority opinion in the field of high-temperature superconductivity has been that the electron-phonon coupling is irrelevant to the mechanism of superconductivity, recent experimental results suggest otherwise. We show that in the cuprates the electron-phonon coupling is unconventional, and suggest that the Cu-O bond-stretching LO phonons may play a crucial role in superconductivity through formation of a vibronic bound state.

Key words: Electron-lattice coupling, phonons, spin-phonon interaction, vibronic state, neutron scattering

1. INTRODUCTION

When the high temperature superconductivity (HTSC) was discovered[1] it was clear that this phenomenon could not be explained by the conventional BCS theory. Thus it was natural that nearly everyone became convinced that the mechanism involves something other than phonons, most likely spins. However, experimental results indicating the participation of lattice and phonons in the HTSC persisted[2], and the recent ARPES results[3] made it difficult to deny the importance of the electron-phonon (*e-p*) coupling. In addition the recent STM/STS observation[4,5] suggests that the local lattice distortion and electronic inhomogeneity may be intrinsic to the cuprates. It is likely that the negative opinion on the role of the lattice and the phonon mechanism is based upon the conventional view of the electron-phonon coupling, while in the cuprates certain phonon modes show unconventional

J. Ashkenazi et al. (eds.), New Challenges in Superconductivity: Experimental Advances and Emerging Theories, 123-128.

e-p coupling. We suggest that the Cu-O bond-stretching LO phonons that show anomalous temperature dependence[6] play a crucial role in the HTSC mechanism through formation of a vibronic bound state.

Because the undoped cuprates are charge-transfer insulator, optical phonons that modify the Cu-O bond length induce charge transfer between O and Cu. Due to strong on-site Coulomb repulsion these transferred charges are spin polarized, resulting in an unconventional *e-p* coupling. This dynamic charge transfer could create a localized dynamic electronic state in-phase with LO phonons, the so-called vibronic state. We discuss the possible experimental evidence of such a localized state in the results of inelastic neutron scattering.

2. ELECTRON-PHONON COUPLING IN THE CUPRATES

The electron-phonon coupling is usually described by the model of deformation potential in the Fermi sea. The motion of an ion is completely screened by the screening charge except for the Friedel oscillation, and the interaction is well described by the Holstein model with localized Einstein oscillator. This picture, however, needs some modification when we describe transition metal oxides including the cuprates. Firstly the electronic screening is so weak that even in the metallic state atoms are ionic. Thus most of the valence electrons move with the nuclei, and phonons modify the overlap of the atomic orbitals and thus the transfer integral, and this modification results in charge transfer. This interaction is best described by the Su-Schrieffer-Heeger (SSH) model[7],

$$H_{e-p} = \sum_{i,j,\sigma} \left(t_{ij} + \frac{\alpha}{a}\left(u_i - u_j\right) \right) \left(c^{+}_{i,\sigma} c_{j,\sigma} + c^{+}_{j,\sigma} c_{i,\sigma} \right) \tag{1}$$

where u_i is the displacement of the i-th ion, a is the inter-atomic distance and σ denotes spin.

The most widely known case of phonon-induced charge transfer may be that in ferroelectric oxides, such as $BaTiO_3$. In the classic picture of ferroelectricity polarization is produced by positive and negative ions displaced in opposite directions. The polarization is given by uZ, where u is the atomic displacement and Z is the ionic charge. In reality, however, the actual polarization is much larger because of charge transfer;

$$P = Zu + \Delta Z a = Z^{*} u \tag{2}$$

where ΔZ is the amount of charge transfer, a is the distance between the atoms, and Z^* is called the Born effective charge. For Ti^{4+} the effective charge is often more than twice the nominal charge. An elegant Berry phase theory was developed to calculate the Born effective charge[8,9].

In the cuprates the phonon modes that modulate the Cu-O bondlength induce similar charge transfer. It was found[10], however, that the direction of the electronic polarization was opposite of the ionic polarization when the cuprates are doped with holes, and the electronic polarization is strongly dependent on the wavevector q. Fig. 1 shows the effective charge of oxygen as a function of q, calculated for the two-band Hubbard model with a frozen phonon,

$$H = \sum_{i,j,\sigma}\left(t_{ij} + \frac{\alpha}{a}\left(u_i - u_j\right)\right)\left(c^+_{i,\sigma}c_{j,\sigma} + c^+_{j,\sigma}c_{i,\sigma}\right) + \sum_{i,}\left[\varepsilon_i n_i + U n_{i\uparrow} n_{i\downarrow}\right]. \qquad (3)$$

where $n_i = c_i^+ c_i$. Deviation from the ionic value (Z = -1.9) represents electronic polarization due to charge transfer. While the charge transfer at q = 0 is small, it is quite large in the middle of the Brillouin zone.

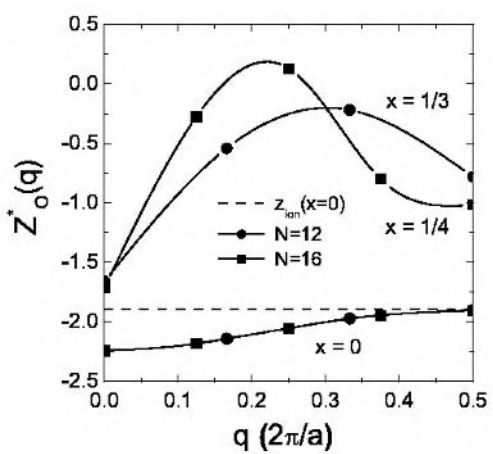

Figure 1. The q dependence of the effective charge of oxygen in the 1-*d* Hubbard model due to the LO phonon monde, calculated for the ring of N = 12 sites with doping level x = 0, 1/3 and for N = 16 with x = 0, 1/4. The dashed line indicates the ionic value (static charge)[10].

It is usually assumed that the *e-p* coupling perturbs only the electronic states near the Fermi surface within the energy $\hbar\omega$, where ω is the phonon frequency. However, this is true only for the Holstein coupling. In the SSH

couling it extends further, as shown in Fig. 2. The optical conductivity is profoundly changed by the phonon up to several eV[10]. This is because of the SSH coupling (2) modifies the transfer integral, thus all parts of the band structure. Phonons are strain waves, and even at $\omega = 0$, the static strain affects the band structure at all energy scales. The SSH coupling describes this effect more effectively. In other words the SSH coulping results in strong **multi-phonon effects**.

It was found that the optical conductivity of the cuprates changes up to 0.5 eV or so upon transition to the superconducting state, and this was used as an argument for an electronic mechanism rather than the phononic mechanism[11-13]. The result shown in Fig. 2 suggests that the phonon mechanism is completely consistent with the observation with the optical conductivity. Similarly in the result of the angle-resolved photoelectron spectroscopy (ARPES) the real part of the electron self-energy was found to be modified up to high energies[3], and was argued to be the evidence of electronic coupling. This, again, must be the consequence of the multi-phonon effect of the SSH coupling.

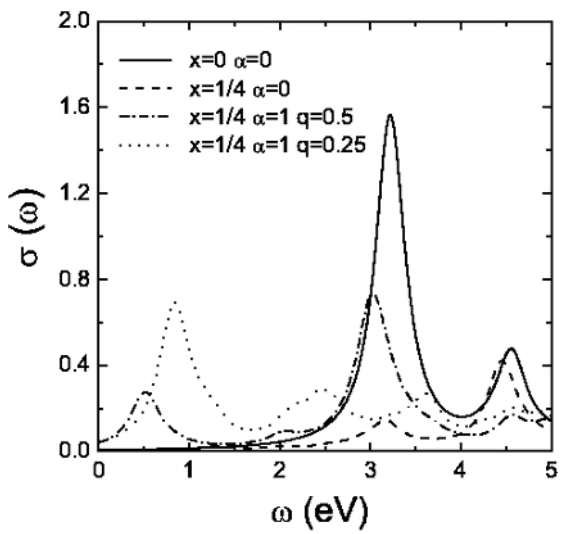

Figure 2. Optical conductivity calculated for the $N = 16$ ring with $x = 0$, 1/4, without phonon ($\alpha = 0$), and with phonon ($\alpha = 1$) with $q = 0.5$ (breathing mode), and with $q = 0.25$ mode[10].

In the Hubbard model it was found that phonon-induced charge transfer is spin polarized because of strong electron correlation. The dynamics of spins is strongly modified by the Cu-O bond-stretching phonons, and the spin excitations are generally greatly softened by phonons[10]. This must be related

to formation of the spin-charge stripes. The results above illustrate the fact that the *e-p* coupling in the cuprates is quite different from the *e-p* coupling in simple metals: It should be characterized as unconventional.

3. IMPLICATIONS TO THE MECHANISM OF HIGH-TEMPERATURE SUPERCONDUCTIVITY

While it is clear that the conventional BCS mechanism does not explain the high-temperature superconductivity, the unconventional nature of the *e-p* coupling suggests that the phonon mechanism cannot be discarded without careful examination. In addition the electronic inhomogeneity observed by the STM/STS measurement[4,5] suggests that the inhomogeneity may be an intrinsic nature of the HTSC phenomenon, and any theory on the mechanism has to incorporate this aspect in a fundamental manner. At present no theory can explain both simultaneously.

The STM/STS measurement also made clear that there are three groups of electrons present in the cuprates[14]. The first group is the $(\pi,0)$ quasi-particles (QP) that become superconducting below T_C. The second is the $(\pi,0)$ electrons that form the pseudo-gap (PG) below the pseudo-gap temperature T_{PG}. The third is the (π,π) electrons that have a long mean-free-path, and do not get scattered by the electronic inhomogeneity of the $(\pi,0)$ electrons. As the hole density is decreased the PG matter increases in volume. The PG matter develops charge ordering (CDW) consistent with the Fermi surface nesting[15]. At the same time below T_{PG} the electron dispersion determined by ARPES develops a clear gap in the $\boldsymbol{k}$-space close to the $(\pi,0)$ point.

A possible scenario to describe these complex developments is the formation of two-hole spin-singlet vibronic bound states made of waves around four $\{\pi,0\}$ points and corresponding two wavepackets of $\{\pi,0\}$ LO phonons. The judicious choice of the envelope makes it possible for these waves to couple effectively. Such a vibronic coupling will greatly enhance the *e-p* coupling, and can lead to high values of T_C. Strong anisotropy in the coupling can stabilize the d-wave superconductivity, while the anisotropic s-wave superconductivity is close in energy. A model calculation based upon the electronic dispersion consistent with the ARPES results and the dielectric function determined from the phonon dispersion demonstrated that such a scenario would results in the d-wave superconductivity with the value of T_C over 100 K[16]. Experimental confirmation of formation of such vibronic states will greatly advance our understanding of the HTSC phenomenon.

ACKNOWLEDGMENTS

The author is grateful to his collaborators, in particular P. Piekarz, J.-H. Chung, H. Mook, M. Tachiki and M. Arai, for their contributions. He is thankful to K. A. Müller, L. P. Gor'kov, A. R. Bishop, J. C. Phillips, A. Bussmann-Holder, A. Lanzara, A. Bianconi, D. Mihailovic, P. Bourge, J. C. Davis and R. Resta for valuable discussions. This work was supported by the National Science Foundation through DMR01-02565.

REFERENCES

1. J. G. Bednorz and K. A. Müller, *Z. Phys.B* **64**, 189 (1986).
2. T. Egami and S. J. L. Billinge, in *Physical Properties of High Temperature Superconductors V*, ed. D. Ginsberg (Singapore, World Scientific, 1996) p. 265.
3. A. Lanzara P. V. Bogdanov, X. J. Zhou, S. A. Keller, D. L. Feng, E. D. Lu, W. J. Zheng, G. Gu, J.-I. Shimoyama, K. Kishio, H. Ikeda, R. Yoshizaki, Z. Hussain, and Z.-X. Shen, *Nature* (*London*), **412**, 510 (2001).
4. S. H. Pan, J. P. O'Neal, R. L. Badzey, C. Chamon, H. Ding, J. R. Engelbrecht, Z. Wang, H. Eisaki, S. Uchida, A. K. Gupta, K.-W. Ng, E. W. Hudson, K. M. Lang and J. C. Davis, *Nature* **413**, 282 (2001).
5. K. M. Lang, V. Madhavan, J. E. Hoffman, E. W. Hudson, H. Eisaki, S. Uchida and J. C. Davis, *Nature* **415**, 412 (2002).
6. J.-H. Chung, T. Egami, R. J. McQueeney, M. Yethiraj, M. Arai, T. Yokoo, Y. Petrov, H. A. Mook, Y. Endoh, S. Tajima, C. Frost, and F. Dogan, *Phys. Rev. B*, **67**, 014517 (2003).
7. W. P. Su, J. R. Schrieffer and A. J. Heeger, *Phys. Rev. Lett*. **42**, 1698 (1979).
8. R. D. King-Smith and D. Vanderbilt, *Phys. Rev. B* **47**, 1651 (1993).
9. R. Resta, *Rev. Mod. Phys.* **66**, 899 (1994).
10. P. Piekarz and T. Egami, *unpublished.*
11. D. N. Basov, E. J. Singley and S. V. Dordevic, *Phys. Rev. B* **65**, 054516 (2002).
12. H. J. A. Molegraaf, C. Presura, D. van der Marel, P. H. Kes and M. Li, *Science* **295**, 2239 (2002).
13. F. Santander-Syro, R. P. S. M. Lobo, N. Bontemps, Z. Konstantinovic, Z. Z. Li, H. Raffy, *Eur. Phys. Lett*. **62**, 568 (2003).
14. K. McElroy, R. W. Simmonds, J. E. Hoffman, D.-H. Lee, J. Orenstein, H. Eisaki, S. Uchida and J. C. Davis*, Nature* **422**, 592 (2003).
15. M. Vershinin, S. Misra, S. Ono, Y. Abe, Y. Ando and A. Yazdani*, Science* **303**, 1995 (2004).
16. M. Tachiki, M. Machida and T. Egami, *Phys. Rev. B* **67**, 174506 (2003).

HIGH-TEMPERATURE SUPERCONDUCTIVITY OF OXIDES

John D. Dow
Arizona State University, Tempe, AZ 85287 USA

Dale R. Harshman
*Physikon Research Corporation, Lynden, WA 98264 USA**
Arizona State University, Tempe, AZ 85287 USA
University of Notre Dame, Notre Dame, IN 46556 USA

Abstract Evidence is presented that high-temperature superconductivity does not necessarily originate in the cuprate-planes. In the cuprates such as $YBa_2Cu_3O_7$, i is argued that the superconductivity resides in the BaO layers. This superconductivity is s-wave, not d-wave, in the bulk. The trio of ruthenate compounds, Cu-doped Sr_2YRuO_6, $GdSr_2Cu_2RuO_8$, and $Gd_{2-z}Ce_zSr_2Cu_2RuO_{10}$ all superconduct in their SrO layers, which is why they have almost the same ∼45 K onset temperatures for superconductivity. Ba_2GdRuO_6, whether doped or not, does not superconduct, because the Gd breaks Cooper-like pairs. $Bi_2Sr_2CaCu_2O_8$ $YBa_2Cu_3O_7$, $Nd_{2-z}Ce_zCuO_4$ homologues, and the $Pb_2Sr_2(RE)_{1-x}Ca_xCu_3O_8$ compounds that superconduct (where RE is a rare-earth) are all s-wave, p-type superconductors.

Keywords: Theories and models of the superconducting state; Type II superconductivity; High-T_c compounds.

1. Locus of high-temperature superconductivity

Most workers in the field of high-temperature superconductivity have *assumed* that the superconducting hole condensate resides primarily in the cuprate-planes based on two papers: (i) work by Cava *et al.* claiming that the Cu charge in the cuprate-planes jumps discontinuously with composition x in $YBa_2Cu_3O_x$ just below the onset of superconductivity at $x < 6.5$ [1], and (ii) data by Jorgensen *et al.* which claimed to confirm the Cava work [2]. However, a close examination of the Cava data reveals that there is only a single datum (and a single composition x) in the jump (all other data are basically

J. Ashkenazi et al. (eds.), New Challenges in Superconductivity: Experimental Advances and Emerging Theories, 129-134.

on a straight line), and that no such jump occurs in the Jorgensen data (all of which lie essentially on a line). (See Fig. 1.) In brief, the most-cited evidence supporting the notion that the cuprate-planes superconduct does not support cuprate-plane superconductivity, as claimed.

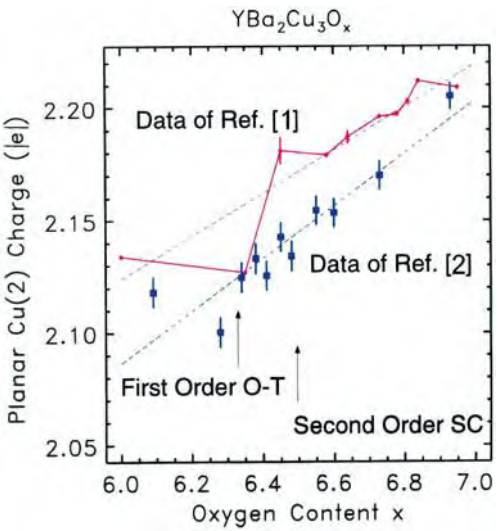

Figure 1. Cuprate-planar Cu charge extracted from the data, versus oxygen content x for $YBa_2Cu_3O_x$, as reported by Cava *et al.* (Ref. [1]) and by Jorgensen *et al.* (Ref. [2]). The two data sets do not follow the same line, because of calibration differences. The jump in the data of Ref. [1] occurs for only one datum, and is not reproduced in Ref. [2]. This calls into question claims that high-temperature superconductivity originates in the cuprate-planes.

2. The cuprate-planes do not superconduct

There is a great deal of evidence that the cuprate-planes do not superconduct, not the least of which is that the cuprate-planes are sometimes adjacent to a *magnetic* (J≠0) pair-breaking rare-earth with L=0, such as Gd^{+3}, which is unsplit by the crystal fields (because it has L=0). In such a case, as in the compound $Gd_{2-z}Ce_zCuO_4$ (which contains a CuO_2 plane, a Gd layer, an O_2 layer, and a Gd layer) the Gd does break Cooper-like pairs and does destroy superconductivity in the adjacent layers (/Gd/O_2/Gd/). (An interstitial oxygen may also occupy a Gd layer.)

But Gd does not destroy superconductivity in $GdBa_2Cu_3O_7$, despite being adjacent to a cuprate-plane, because the cuprate-plane does not superconduct and the superconductivity occupies the BaO layer. This pair of facts alone, that $Gd_{2-z}Ce_zCuO_4$ does not superconduct and $GdBa_2Cu_3O_7$ does,

suggests that the superconducting hole condensate of $GdBa_2Cu_3O_7$ is not in the cuprate-planes adjacent to the Gd (as widely believed) but is in a layer more distant from Gd, namely the BaO layer. It is confirmed by the fact that $(Gd_{1-u}La_u)_{2-z}Ce_zCuO_4$, which unquestionably has a bond-length long enough to superconduct, nevertheless does not superconduct. So $Gd_{2-z}Ce_zCuO_4$, like $(Gd_{1-u}La_u)_{2-z}Ce_zCuO_4$, does not superconduct because Gd is a pair-breaker with J$\neq$0 (and L=0).

3. Doped Sr_2YRuO_6

Sr_2YRuO_6 superconducts when it is doped with only 1% Cu on Ru sites [4]. While the onset of superconductivity occurs at about 45 K, full bulk superconductivity is not observed until 23 K, corresponding to the spin-freezing temperature, T_N, of the fluctuating Ru moments. (Above this temperature, near 30 K, a narrow spin-glass phase has been detected.) Doped Sr_2YRuO_6 demonstrates that fluctuating magnetic moments tend to break pairs, thereby suppressing the superconductivity above 23 K [5].

The Sr_2YRuO_6 compound superconducts at 1% Cu-doping, and is a robust superconductor with only 5% Cu. This suggests that cuprate-planes are not needed for $Sr_2YRu_{1-u}Cu_uO_6$ to superconduct. The material has only two layers per unit cell, a $\frac{1}{2}(YRuO_4)$ layer and a SrO layer. It is clear that the $YRuO_4$ layer features a significant magnetic moment, that lies (almost) in the a-b plane and reverses direction every $YRuO_4$ layer along the c-axis. Therefore the material is an antiferromagnet, whose $YRuO_4$ planes are individually ferromagnetic, but stacked antiferromagnetically. Clearly the superconductivity of Cu-doped Sr_2YRuO_6 lies in its SrO layers.

This raises two questions: (1) are the SrO layers (or the cuprate planes) of other superconducting materials the hosts of superconductivity; and (2) do Sr_2YRuO_6's sister compounds, $GdSr_2Cu_2RuO_8$ and $Gd_{2-z}Ce_zSr_2Cu_2RuO_{10}$, superconduct in their cuprate planes or in their SrO layers?

4. $GdSr_2Cu_2RuO_8$ and $Gd_{2-z}Ce_zSr_2Cu_2RuO_{10}$

The onset temperatures for superconductivity in both $GdSr_2Cu_2RuO_8$ and $Gd_{2-z}Ce_zSr_2Cu_2RuO_{10}$ are also near $\sim$45 K, and so it does appear that doped Sr_2YRuO_6, $GdSr_2Cu_2RuO_8$, and $Gd_{2-z}Ce_zSr_2Cu_2RuO_{10}$ are all members of the same class of superconducting materials, and that they all superconduct in their SrO layers.

This viewpoint is bolstered by the fact that both compounds, $GdSr_2Cu_2RuO_8$ and $Gd_{2-z}Ce_zSr_2Cu_2RuO_{10}$, show magnetism (associated with their cuprate-planes) at low temperatures, which strongly suggests that their superconductivity is in their SrO layers [6], and not in their cuprate-planes.

5. Ba_2GdRuO_6 does not superconduct

It is rather interesting that Ba_2GdRuO_6 does *not* superconduct, even when doped with Cu, because Ba_2GdRuO_6 is virtually the same as Sr_2YRuO_6 (and is certainly in the same class as Sr_2YRuO_6), and is expected to superconduct, except for the fact that Gd has J$\neq$0 (even though it does have L=0). This occurs because Ba_2GdRuO_6 doped with Cu on Ru sites *does not superconduct* on account of J$\neq$0 Gd being a pair-breaker which kills the superconductivity. Therefore, Cu-doped Sr_2YRuO_6 superconducts, Cu-doped Ba_2GdRuO_6 does not superconduct (because it has L=0, J$\neq$0 Gd in it), and $GdSr_2Cu_2RuO_8$ and $Gd_{2-z}Ce_zSr_2Cu_2RuO_{10}$ both superconduct. The three materials that superconduct begin superconducting at about $\sim$45 K, but the superconductivity of Cu-doped Sr_2YRuO_6 becomes full at $\sim$23 K. The superconductivity occurs in the SrO layers, not in the cuprate-planes.

6. $Bi_2Sr_2CaCu_2O_8$

Recent scanning tunneling microscopy (STM) measurements of the cuprate-planes of $Bi_2Sr_2CaCu_2O_8$ by Misra *et al.* [7] show a band gap in excess of 10 mV, with little or no conductivity throughout most of the gap. Those authors have imaged a sub-surface cuprate-plane (the second one below the BiO surface, *sticking out of the side of the crystal*), and have reported negligible conductivity in that plane. Then they have assumed that the protruding cuprate-plane is representative of a cuprate-plane in the bulk, and have argued that their data are evidence of d-wave superconductivity in that cuprate-plane. (Note the absence of any visible states within the gap, opening the possibility of insulating behavior.) Their data definitely are not evidence for s-wave superconductivity at the surface of their protruding plane. However, muon spectroscopy, which senses the superconductivity in the bulk not just in a protruding surface layer, does show that the superconductivity is consistent with s-wave pairing [8]. Klemm and co-workers have also found $Bi_2Sr_2CaCu_2O_8$ to be s-wave in character [9]. Clearly the bulk superconductivity of $Bi_2Sr_2CaCu_2O_8$ is s-wave and (to be consistent with other high-temperature superconductors) it should be in the SrO layers.

7. $YBa_2Cu_3O_7$

$YBa_2Cu_3O_7$ is clearly an s-wave superconductor as demonstrated convincingly by the measurements of Harshman *et al.* [10]. Once temperature-activated and field-dependent flux-line disorder are accounted for, the data are fully consistent with s-wave pairing. These data also rule out d-wave pairing.

8. There are no n-type high-temperature superconductors

Many people in the field believe that some high-temperature superconductors, most notably of the $Nd_{2-z}Ce_zCuO_4$ class, are n-type. But since most high-temperature superconductors rely on oxygen to superconduct, and since at least some oxygen in these materials is already in the O^{-2} state, to dope them n-type requires forming O^{-3}, which does not form.

The situation becomes more complex when one considers $Nd_{2-z}Ce_zCuO_4$ because Ce purportedly dopes the material n-type [11]. But the Madelung potential at the Ce site is about 7 V too weak to ionize Ce to Ce^{+4} (which requires 36.8 V), as needed for this n-type doping viewpoint to be correct. To overcome this $\sim$7 V problem, we have proposed that the Ce is *not an isolated dopant,* but is accompanied by an interstitial oxygen, forming a (Ce,$O_{interstitial}$) pair, which dopes the material p-type rather than n-type. (Oxygen has a charge between O^{-1} and O^{-2}.) Consequently, $Nd_{2-z}Ce_zCuO_4$ superconducts when it is doped p-type by (Ce,$O_{interstitial}$) pairs, not when it is doped n-type by isolated Ce.

This behavior is easy to understand, because O^{-2} can be doped p-type to, say O^{-1}; but it cannot be doped n-type to, say O^{-3}, because the maximum negative charge on oxygen is approximately -2. Hence the claimed n-type simple doping cannot occur; the doping must be more complex and also must be p-type. There are no n-type high-temperature superconductors.

9. PSYCO compounds: either p-type and superconducting, or n-type and non-superconducting

The (rare-earth)-PSYCO compounds [12], $Pb_2Sr_2(RE)_{1-x}Ca_xCu_2O_8$, in which RE is a rare-earth ion or Y, superconduct for all the common rare-earth ions (for which the material is p-type) except for RE=Ce, which naturally becomes Ce^{+4} in its crystal-field and then dopes the material n-type, and the material *does not superconduct* [13]. The same happens for Am^{+4} doping. Clearly, the PSYCO compounds superconduct when doped p-type, but not when doped n-type.

This lends support to the contention that the $(\text{rare-earth})_{2-z}Ce_zCuO_4$ compounds must be p-type when they superconduct, not n-type.

10. Summary

The superconducting hole condensate resides in the SrO or BaO planes of most high-temperature superconductors, and in the interstitial oxygen regions of many of the rest, such as $Nd_{2-z}Ce_zCuO_4$. All of these superconductors are p-type, s-wave superconductors.

Acknowledgments

We are grateful to the TRIUMF Cyclotron Facility staff for their help and expertise, and we thank the U. S. Office of Naval Research for their financial support (Contract No. N00014-03-1-0375).

* Permanent address.

References

1. R. J. Cava, A. W. Hewat, E. A. Hewat, B. Batlogg, M. Marezio, K. M. Rabe, J. J. Krajewski, W. F. Peck, Jr., and L. W. Rupp, Jr., Physica **C 165**, 419 (1990).
2. J. D. Jorgensen, B. W. Veal, A. P. Paulikas, L. J. Nowicki, G. W. Crabtree, H. Claus, and W. K. Kwok, Phys. Rev. **B 41**, 1863 (1990).
3. J. D. Dow and D. R. Harshman, Intl. J. Mod. Phys. **B17**, 3310 (2003).
4. S. M. Rao, J. K. Srivastava, H. Y. Tang, D. C. Ling, C. C. Chung, J. L. Yang, S. R. Sheen, and M. K. Wu, J. Crystal Growth **235,** 271 (2002).
5. J. D. Dow, H. A. Blackstead, and D. R. Harshman, "High-temperature superconductivity is charge-reservoir superconductivity," pages 403-412 (2001), published in "Phase transitions and self-organization in electronic and molecular networks." Ed. by J. C. Phillips and M. F. Thorpe. Kluwer Academic/Plenum Publishers, 2001; D. R. Harshman, W. J. Kossler, A. J. Greer, D. R. Noakes, C. E. Stronach, E. Koster, M. K. Wu, F. Z. Chien, J. P. Franck, I. Isacc, and J. D. Dow, Phys. Rev. **B 67**, 054509 (2003).
6. J. D. Dow, H. A. Blackstead, Z. F. Ren, and D. Z. Wang, "Magnetic resonance of Cu and of Gd in insulating $GdSr_2Cu_2NbO_8$ and in superconducting $GdSr_2Cu_2RuO_8$," to be published.
7. S. Misra, S. Oh, D. J. Hornbaker, T. DiLuccio, J. N. Eckstein, and A. Yazdani, Phys. Rev. Lett. **89**, 087002 (2002).
8. D. R. Harshman, R. N. Kleiman, M. Inui, G. P. Espinosa, D. B. Mitzi, A. Kapitulnik, T. Pfiz, and D. Ll. Williams, Phys. Rev. Lett. **67**, 3152 (1991).
9. A. Bille, R. A. Klemm, and K. Scharnberg, Phys. Rev. **B 64**, 174507 (2001); Qiang Li, Y. N. Tsay, M. Suenaga, R. A. Klemm, G. D. Gu, and N. Koshizuka, Phys. Rev. Lett. **83**, 4160 (1999).
10. D. R. Harshman, W. J. Kossler, X. Wan, A. T. Fiory, A. J. Greer, D. R. Noakes, C. E. Stronach, E. Koster, A. Erb, and J. D. Dow, Intl. J. Mod. Phys. **B 17,** 3582 (2003); D. R. Harshman, W. J. Kossler, X. Wan, A. T. Fiory, A. J. Greer, D. R. Noakes, C. E. Stronach, E. Koster, and J. D. Dow, "Nodeless pairing state in single-crystal $YBa_2Cu_3O_7$," Phys. Rev. **B**, in press.
11. Y. Tokura, J. B. Torrance, T. C. Huang, and A. I. Nazzal, Phys. Rev. **B 38**, 7156 (1988); Y. Tokura, H. Takagi, and S. Uchida, Nature **337**, 345 (1989); Y. Tokura, A. Fujimori, H. Matsubara, H. Watabe, H. Takagi, S. Uchida, M. Sakai, H. Ikeda, S. Okuda, and S. Tanaka, Phys. Rev. **B 39**, 9704 (1989).
12. M. Lehmann, J.D. Dow, and H. A. Blackstead, Physica **C 341-348**, 309 (2000); Blackstead and J. D. Dow, J. Low Temp. Phys. **117**, 557 (1999).
13. S. Skanthakumar and L. Soderholm, Phys. Rev. **B 53**, 920 (1996); L. Soderholm, C. Williams, S. Skanthakumar, M. R. Antonio, and S. Conradson, Z. Physik **B 101**, 539 (1996).

BOSE-EINSTEIN CONDENSATION IN A BOSON-FERMION MODEL OF CUPRATES

T.A. Mamedov* and M. de Llano**
*Baskent University, Engineering Faculty, 06530 Ankara, Turkey. **Instituto de Investigaciones en Materiales, UNAM, 04510 Mexico DF, Mexico.

Abstract: **By relating the Cooper/BCS model inter-electron interaction dimensionless coupling λ with doping concentration, the familiar T_c "dome-shaped" behavior observed in many cuprates is obtained from a boson-fermion (BF) binary gas mixture model of unpaired electrons and bosonic Cooper pairs (CPs). This is done by deriving an analytic relation between a Bose-Einstein condensation (BEC) temperature T_c and the fermion chemical potential which varies with CP formation.**

Key words: Superconductivity; cuprates; boson-fermion model; Bose-Einstein condensation.

To describe superconductors it is argued Refs. [1-9] that a system of electrons with energies ε such that $\varepsilon_F - \hbar\omega_D \le \varepsilon \le \varepsilon_F + \hbar\omega_D$ in 2D (or within a spherical shell in k-space in 3D) may be divided into two coexisting dynamically interacting subsystems: a) *fermions* (pairable but unpaired) and b) *boson* CPs made up of two bound fermions. Here ε_F is the Fermi energy of the ideal Fermi gas (IFG) and $\hbar\omega_D$ the Debye energy. The Hamiltonian describing the binary BF mixture with BF interactions is [1,4]

$$H = \sum_{\mathbf{k},\sigma} \varepsilon_{\mathbf{k}} a^{+}_{\mathbf{k}\sigma} a_{\mathbf{k}\sigma} + \sum_{\mathbf{K}} E(\mathbf{K}) b^{+}_{\mathbf{K}} b_{\mathbf{K}} + H_{\rm int}, \tag{1}$$

$$H_{\rm int} = \frac{f}{L^{d/2}} \sum_{\mathbf{q},\mathbf{K}} (b^{+}_{\mathbf{K}} a_{\mathbf{q}+\frac{1}{2}\mathbf{K},\uparrow} a_{-\mathbf{q}+\frac{1}{2}\mathbf{K},\downarrow} + b_{\mathbf{K}} a^{+}_{-\mathbf{q}+\frac{1}{2}\mathbf{K},\downarrow} a^{+}_{\mathbf{q}+\frac{1}{2}\mathbf{K},\uparrow}), \tag{2}$$

where $a^{+}_{\mathbf{k}\sigma}$ and $a_{\mathbf{k}\sigma}$ are fermion creation and annihilation operators for individual electrons, and $b^{+}_{\mathbf{K}}$ and $b_{\mathbf{K}}$ are similar operators for 2e-CPs of total, or center-of-mass, momentum (CMM) $\mathbf{K}$. Here $\varepsilon_k \equiv \hbar^2 k^2 / 2m$ with m the effective electron mass and $E(\mathbf{K})$ is the CP energy while L and d are the size and dimensionality of the system. Finally, the BF form factor f in (2) is

J. Ashkenazi et al. (eds.), New Challenges in Superconductivity: Experimental Advances and Emerging Theories, 135-138.

a phenomenological parameter responsible for 2e-CP formation/disintegration processes; it is related to the Cooper/BCS model attractive inter-electron interaction $V > 0$ via $f = \sqrt{2\hbar\omega_D V}$ [4]. The total number N of electrons is $N = N_1 + N_2$ where N_1 is the number of unpairable (i.e., non-interacting) electrons while N_2 is the number of pairable (i.e., active) electrons. By pairing into CPs, electrons leave the Fermi subsystem and enter the Bose one. That is, at fixed V and temperature T, N_2 includes the number N_{20} of unpaired (but pairable) electrons as well as the paired ones $N_2 - N_{20}$ within the interaction shell of energy width $2\hbar\omega_D$. A change in the number N_F of *unpaired electrons* must be accompanied by a corresponding opposite change in the number N_B of CPs. Hence, the total electron number N conservation law is $N = N_F + 2N_B \equiv N_1 + N_{20} + 2N_B$ and the total number of CPs at any T is $N_B = (N_2 - N_{20})/2$. To consider variations in N_F and N_B due to CP formation, (1) is recast in the form $\mathrm{H} = H - \mu_2 N$ where μ_2 is defined by demanding that N be fixed. We write the CP energy $E(\mathbf{K})$ in H as $E(\mathbf{K}) - 2\mu_2 = 2(\varepsilon_F - \mu_2) + 2\Delta + \xi_{\mathbf{K}}$ where $\xi_{\mathbf{K}} = c_d \hbar v_F K$ (d = 2 or 3) is a non-negative CP excitation energy with c_d a numerical coefficient, and $\Delta = \hbar\omega_D / \sinh(1/\lambda)$. Both relations follow from Refs. [8,9] where the Bethe-Salpeter equation in the ladder approximation yields a *linear* dispersion relation for *moving* (i.e., with *nonzero* CMM) CPs.

In the RPA approximation, below a certain depairing temperature T^* one finds [10] $n_k = \left(e^{E_k/k_BT} + 1\right)^{-1}$ for the number of electrons n_k in a k-state (see also Ref. [4]), and $n_{B,\mathbf{K}} = \left(e^{\Omega_{\mathbf{K}}/k_BT} - 1\right)^{-1}$ for the boson number $n_{B,K}$ in a state with CMM $\mathbf{K}$. Here E_k and Ω_K are

$$E_k = \sqrt{(\varepsilon_k - \mu_2)^2 + f^2 n_{B,0}}\ , \quad \Omega_{\mathbf{K}} = E(\mathbf{K}) - 2\mu_2 - \frac{f^2}{L^d}\sum_{\mathbf{q}} \frac{n_{\mathbf{q}+\frac{\mathbf{K}}{2},\uparrow} + n_{\mathbf{q}+\frac{\mathbf{K}}{2},\downarrow}}{E(\mathbf{K}) - (\varepsilon_{\mathbf{q}+\frac{\mathbf{K}}{2}} + \varepsilon_{-\mathbf{q}+\frac{\mathbf{K}}{2}})}, \quad (3)$$

(see also Refs. [10,11]) where $n_{B.0} \equiv N_B / L^d$ is the number density of condensed bosons in the $K = 0$ state. Because of mutual transitions of electrons from the Fermi to the Bose system and vise versa, as caused by H_{int}, the electron N_{20} and boson N_B numbers become λ- *and T-dependent*. In analogy with $\varepsilon_F = (\hbar^2/2m)(3\pi^2 N/L^3)^{2/3}$ of the 3D IFG we introduce $\tilde{\mu}$ where instead of N one has the total number $N_F \equiv N_1 + N_{20}$ of *unpaired* electrons in a 3D BF mixture and assume that the main contribution to the change in ε_F that occurs by switching on H_{int} is associated with variations in the fermion number by $N_2 - N_{20}$. We thus set $\mu_2 = \tilde{\mu}$, a choice that keeps N_2 constant. This may be done by adding N_{20}, determined from $\tilde{\mu}$, to $2N_B$, and noting that the sum equals N_2. That is, the change in the number of unpaired fermions is accompanied by a corresponding change in N_B such that $N_2 = N_{20} + 2N_B$ so that $N = N_1 + N_2$ remains constant. In the 2D BF case we relate μ_2 to the density n of unpaired electrons $n = (N_1 + N_{20})/L^2$ through $\mu_2 = \pi\hbar^2 n/m$. We then substitute $N_{20} = N_2 - 2N_B$ into μ_2 and get

$$\varepsilon_F - \mu_2 = \frac{4\varepsilon_F}{3}\frac{N_B}{N} \quad \textbf{in } 3D \quad \textbf{and} \quad \varepsilon_F - \mu_2 = \frac{2\varepsilon_F N_B}{N} \quad \textbf{in } 2D\,. \tag{4}$$

In 2D the result is *exact,* while *i*n 3D it is good to first-order in the binomial expansion of μ_2 for small N_B/N. Equations (4) relate N_B in the mixture to the change in $\varepsilon_F - \mu_2$ due to pair formations.

The total number of bosons in the system is $N_B \equiv \sum_{\mathbf{K}} \left(e^{\Omega_{\mathbf{K}}/k_BT} - 1\right)^{-1}$. When $\Omega_{\mathbf{K}} \to 0$ a singularity occurs in N_B that defines the BEC transition temperature T_c, in analogy with the pure boson gas [12]. Putting $\mathbf{K} = 0$ and $\Omega = 0$ in N_B, replacing the sum over $\mathbf{q}$ by integration over ε of the density-of-states (DOS) $N(\varepsilon)$ (taken as a constant, exactly in 2D and to good approximation in 3D provided that $\hbar\omega_D << \varepsilon_F$) leaves

$$\varepsilon_F - \mu_2 = -\Delta + \frac{\lambda\hbar\omega_D}{2}\int_{-\hbar\omega_D}^{\hbar\omega_D} \frac{\tanh[(x + \varepsilon_F - \mu_2)/2T_c]}{x - \Delta}dx\,. \tag{5}$$

Now $\varepsilon_F - \mu_2$ depends both on Δ, interpreted as a CP formation energy above the Fermi sea, and on the *redistribution* of the single-electron levels due to CP formation. For the linear dispersion law $\xi_{\mathbf{K}} = c_d\hbar v_F K$ [8] and spherical symmetry in $\mathbf{K}$, the integration over $\mathbf{K}$ in N_B is readily performed (see e.g., Ref. [12]) and yields

$$T_c = c_2\frac{2\sqrt{3}}{\pi^{1/2}}\frac{\hbar v_F}{k_B}n_B^{1/2} \quad \textbf{in } 2D \quad \textbf{and} \quad T_c = c_3\frac{\pi^{2/3}}{(1.202)^{1/3}}\frac{\hbar v_F}{k_B}n_B^{1/3} \quad \textbf{in } 3D. \tag{6}$$

Putting (4) into (6) then gives

$$k_BT_c/\varepsilon_F = 0.7(1 - \mu_2/\varepsilon_F)^{1/2} \quad \textbf{in } 2D \quad \textbf{and} \quad k_BT_c/\varepsilon_F = 0.3(1 - \mu_2/\varepsilon_F)^{1/3} \textbf{ in } 3D. \tag{7}$$

Simultaneous solution of (5) and (7) determines BEC T_cs as functions of λ. We first express $\varepsilon_F - \mu_2$ through (7) in terms of T_c; then (5) gives a single equation the numerical solution of which yields T_c. We display T_c as a function of λ for the 2D case in Fig. 1 for two values of ω_D typical in cuprates. As λ increases from zero T_c increases, it then maximizes, and finally *decreases*. Indeed, a superconducting state emerges in this model if $\mu_2 < \varepsilon_F$. The first term Δ on the rhs of (5) increases with λ, and gives rise to an increase in μ_2 over ε_F. Therefore, CPs excited much above ε_F, *i.e.*, associated with larger values of Δ, are less likely to satisfy both $\varepsilon_F - \mu_2 \geq 0$ and (5) simultaneously, than CPs formed with smaller λ. On the other hand, the second term on the rhs of (5), which depends on Δ as well on the redistribution of the single-electron levels due to CP formation, considerably reduces the value of μ_2. Competition between these two effects determines T_c. Contributions from different terms in (5) compensate each other considerably at large λ, leading to $\varepsilon_F - \mu_2 \leq 0$ and thus extinguishing superconductivity. Finally, it should be noted that if in the relation $\lambda = N(0)V$ the

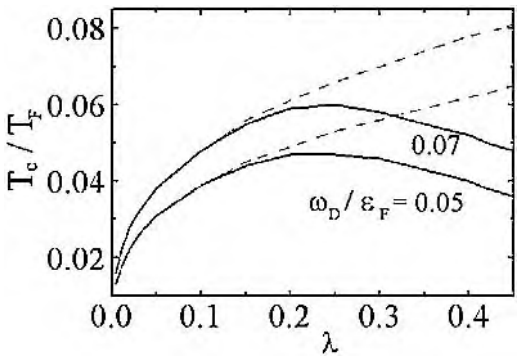

Figure 1. T_c / T_F as a function of λ. Dashed curves show monotonic increase that would result if the CP (linear) dispersion law were not gapped, i.e., if in (5) Δ was artificially deleted.

parameter V is assumed *independent* (or *weakly-dependent*) of the concentration of charge carriers x, then, due to charge density dependence of $N(0)$, λ becomes proportional to x, *i.e.*, $\lambda \propto x^{\alpha}$, with α some positive constant, *at least in 3D*. The T_c *vs* λ behavior shown in Fig. 1 thus reproduces the T_c *vs* x behavior found experimentally in many high-T_c cuprates.

To conclude, in a BF mixture model of superconductivity we have extracted an analytic relation between a BEC T_c and the electron chemical potential that varies with the degree of CP formation. The BEC T_c formula contains contributions from both varying electron number as well as from the redistribution of free-electron states caused by boson formation. As a result T_c *vs* λ exhibits non-monotonic behavior, so that superconductivity emerges only for a limited range of coupling-parameter and doping-concentration values.

Acknowledgements T.A.M. thanks TUBITAK and MdeLl thanks UNAM-DGAPA-PAPIIT (Mexico) grant # IN106401 and CONACyT (Mexico) grant # 27828 E for partial support.

References

1. R. Friedberg and T.D. Lee, Phys. Rev. B **40** (1989) 6745.
2. R. Mićnas *et al.*, Rev. Mod. Phys. **62** (1990) 113.
3. R. Friedberg *et al.*, Phys. Lett. A **152** (1991) 417.
4. V.V. Tolmachev, Phys. Lett. A **266** (2000) 400.
5. M. de Llano and V.V. Tolmachev, Physica A **317** (2003) 546.
6. J. Batle *et al.*, Cond. Matter Theories **18** (2003) 111. Also in cond-mat/0211456.
7. M. Casas *et al.,* Physica A **295** (2001) 425.
8. M. Fortes *et al.*, Physica C **364-365** (2001) 95; V.C. Aguilera-Navarro *et al.*, Sol. St. Comm. **129** (2004) 577.
9. M. de Llano, in *Horizons in Superconductivity Research* (Nova, NY, 2004) (in press).
10. T. Mamedov, J. Low Temp. Phys. **131** (2003) 217.
11. T. Mamedov, Physica C (2004) (in press).
12. M. Casas *et al.*, Phys. Lett. A **245** (1998) 55.

OXYGEN-RELATED BAND-FEATURES OF THE EXTENDED EMERY MODEL FOR THE HTS CUPRATES

Ivana Mrkonjić
Department of Physics, University of Zagreb, Bijenicka 32, POB 331, 10002 Zagreb, Croatia
ivanam@phy.hr

Slaven Barišić
Department of Physics, University of Zagreb, Bijenicka 32, POB 331, 10002 Zagreb, Croatia
sbarisic@phy.hr

Abstract

We examine the band properties of the extended Emery model, parameterized by Cu-O charge transfer energy Δ_{pd}, copper-oxygen overlap t_0, oxygen-oxygen overlap t' and Coulomb interaction U on the copper site. In the charge-transfer limit $U \gg \Delta_{pd} > t, t'$, it retains realistic three band structure, unlike the usually used Hubbard model. Neglecting the ordering of spin degrees of freedom, infinite U slave boson mean field approximation is used to calculate at small doping δ the renormalization trends of the effective band parameters Δ_{pf} and t, replacing Δ_{pd} and t_0, while t', related exclusively to oxygens, remains unchanged. It is shown that small, negative t' expands the range of stability of the metallic phase, changing, through the higher order corrections in t', the thermodynamical nature of the metal-insulator transition point. In the nonperturbative limit, t' modifies qualitatively the renormalization of Δ_{pf} at zero doping, making it saturate at the value of $4|t'|$ and keeping thus the system in the regime of strong correlations. Finite doping δ suppresses the insulating $t = 0$ state approximately symmetrically with respect to its sign. The regime $\Delta_{pf} \approx 4|t'|$ fits very well the ARPES spectra of LSCO and also explains the evolution of the FS with doping accompanied by the spectral weight- transfer from the oxygen to the resonant band. Additionally, the values of the band- parameters Δ_{pf}/t' and t/t' are allowed to vary freely, in order to describe the ARPES data on LSCO, thus providing the direct insight in the role of oxygens, underestimated in the magnetic t-J limit of the large U Emery model. The important role in this theory is played by the effective Cu-O overlap t, very small in the underdoped HTS cuprates and evolving to the values of the order of t' at larger doping.

Keywords: High-T_c cuprates, effective band-structure, slave boson method, $La_{2-\delta}Sr_{\delta}CuO_4$

J. Ashkenazi et al. (eds.), New Challenges in Superconductivity: Experimental Advances and Emerging Theories, 139-144.

Introduction

Most of the many-body theories [1] of the high T_c superconductors, which attribute the peculiar properties of these materials to the CuO_2 conducting planes, are based on the extended Emery model [2]. This model is parameterized by the Cu-O site energy splitting Δ_{pd}, the Cu-O overlap t_0, oxygen-oxygen overlap t' and the Coulomb interaction U on the Cu site. The extended Emery model can be analyzed within various limits. If Δ_{pd} is taken to be the largest parameter, this model reduces to the extended Hubbard model, which retains one site per unit CuO_2 cell [1]. In the opposite case, when $U \gg \Delta_{pd} \gg t_0, t'$, so called charge transfer (CT) [3] limit is reached, where doped holes go on oxygen. Thus the physical properties of the system are governed also by the oxygen band, possibly close to the Fermi level. This particular fact seems to be supported by the ARPES data on the HTS cuprates, exhibiting oxygen-like symmetry of the FS, either in the whole range of doping, as in $Bi_2Sr_2CaCuO_{8+\delta}$ (Bi2212)[4] and $YBa_2Cu_3O_{7-\delta}$ (Y123)[5], or at low doping in $La_{2-\delta}Sr_\delta CuO_4$ (LSCO) [6]. In particular, the evolution of the FS upon doping in LSCO is accompanied by the transfer of the spectral weight from the lower to the conducting band.

In this paper, we show that the observed band-properties can be described within the CT limit of the Emery model, taking into account, beyond the perturbation level, the direct oxygen-oxygen overlap t', treated by the infinite U paramagnetic slave boson method.

1. Slave boson method

When the interaction U is taken to be infinite, within the mean field procedure, two allowed states on the Cu atom can be represented by auxiliary boson and fermion fields [7]. This constraint automatically implies the renormalization of the band-parameters Δ_{pd} and t_0 related to Cu, while t', related exclusively to oxygen, does not change. Thus the problem of the strong renormalization on Cu is mapped to the problem of finding the renormalization functions of the effective parameters $\Delta_{pf}(\Delta_{pd}, t_0, \delta)$ and $t(\Delta_{pd}, t_0, \delta)$, depending strongly on the underlying band-structure [8]. The physical content of this approximation can be understood from the single-hole propagator between Cu-sites [9]

$$\begin{aligned} G^d(\omega, \mathbf{k}) &\approx c\delta\, G^f(\omega, \mathbf{k}) \\ &+ (1 - c\delta) \int \frac{d\mathbf{k}}{(2\pi)^2} \frac{m_k(\mathbf{k})^2}{\omega - (\varepsilon(\mathbf{k}) - \varepsilon_f - \varepsilon_d) - i\eta}, \end{aligned} \tag{1}$$

where constant $c \ll 1$, showing that the spectral weight of the physical hole is distributed between the resonant band at ε_f close to the oxygen energy at ε_p and the copper level at ε_d. One hole ($c \ll 1$!), residing on the Cu level, can

in spin-dependent calculations be related with localized magnetic moments, while both charge and spin fluctuations occur in the resonant band with δ holes, mostly on oxygens ($\varepsilon_f \approx \varepsilon_p$).

2. Anderson's lattice-like limit of the Emery model

It was shown that there exist various limits of the effective parameters, resulting either in strongly correlated regime involving copper [10] or in the non-renormalized all oxygen regime [8]. However, the ARPES measurements point to the limit where the oxygen band is close to the resonant band. This is the case where the bandwidth of the oxygen band $4|t'|$ is close to the Δ_{pf}. At the half filling, Δ_{pf} does not go to zero, as in the $t' = 0$ case [10], but saturates at the value of $4|t'|$ [8]

$$\Delta_{pf} = 4|t'| + 2|t'|e^{-\frac{|t'|\Delta_{pd}}{4\pi t_0^2}} \tag{2}$$

deferring strongly from the physical picture associated with $t' = 0$ t-J model [11]. Nevertheless, the system thus remains in the regime of strong correlations. When small doping δ is added, a situation similar to the heavy-fermion system is obtained: the bandwidth of the resonant band is obtained through the spectral weight-transfer from the oxygen band, resulting in the Anderson lattice-like case where narrow Cu band "interacts" with the broad O band. The transferred oxygen states are thus responsible for the oxygen-like symmetry of the FS, observed by ARPES. When the doping is increased, Δ_{pf} remains close to $4|t'|$, while $t \sim \sqrt{\delta}$, raising upon doping to the value comparable to the value of t'. Through the increase of t, the symmetry of the resonant band is changed from hole-like to electron-like, characteristic of the usual Cu-O lattice.

3. Neighborhood of the Brinkmann-Rice point

The influence of finite t' is also important in the neighborhood of the Brinkmann-Rice (BR) metal-insulator transition point [10] at $\Delta_{pd} \sim 2t_0$, where it can be treated [8] on the perturbation level. It can be shown that small t' does not suppress metal-insulator transition, but only shifts the position of the critical point on Δ_{pd} scale and the corresponding critical value of Δ_{pf}. The introduction of finite small t' expands the range of stability of metallic phase with respect to the insulating one, if the sign of t'/Δ_{pf} is negative, and vice-versa. Concerning the nature of the BR point, it remains tricritical point of the second order phase transition in the lowest order perturbation theory. However, logharitmical terms transform the BR point into bicritical one, in this case associated with one first order and one second order phase transitions.

4. Symmetries

It is also important to note that the slave boson method itself possess two different types of symmetry with respect to doping. From the doping dependence of the effective copper-oxygen overlap t for Δ_{pd}/t_0 large enough, symmetry with respect to zero doping emerges [8], since

$$t \sim \sqrt{|\delta|} \tag{3}$$

which can be related to the overall symmetry of the phase diagram of the single-layer cuprates [12].

The second symmetry is the consequence of the local symmetry of the density of the states of the resonant band. Finite, small t' modifies strongly the dispersion of the conducting band in the vicinity of the van Hove singularities, adding extra states below the Fermi level. The Fermi energy at the half-filling is therefore shifted from the van Hove singularity towards the (π, π) point when $t' < 0$.

Thus the band-properties have the symmetry with respect to the doping δ_c [8] required to bring the Fermi energy back to the van Hove singularity, as observed in the transport data.

5. Experiments

To relate the above results to the physical systems, we now give the comparison of the calculated band structure in the Anderson lattice-like limit of the Emery model with the ARPES data on LSCO [6]. The regime of the bare parameters is $\Delta_{pd}/t_0 \gg 1$, resulting in $\Delta_{pf} \approx 4|t'|$ (and $t' < 0$).

In the underdoped regime, since t is small, i.e. proportional to $\sqrt{\delta}$, dominant propagation axis is the zone-diagonal, which gives the hole-like FS. The value of t raises upon doping to the value of $2|t'|$, resulting finally in the electron-like FS, associated with the propagation along the main axes (Fig.1).

This is accompanied [8, 9] by the transfer of the spectral density from the top of the oxygen band to the resonant band upon doping, as shown on Fig 2.

The observed evolution of the shape of the band-structure upon doping satisfies the Luttinger sum rule [9]. It should be noted that only in the Anderson lattice-like limit of the Emery model it is possible to obtain the observed evolution of the FS upon doping. In all other cases, the oxygen symmetry of the FS can be attributed to the (non-renormalized) oxygen band and therefore the strong doping dependence of the band structure cannot be expected.

The same limit also successfully explains the change of the FS topology in the strained LSCO films data [13], implying the increase of nominal doping with strain, in agreement with [14].

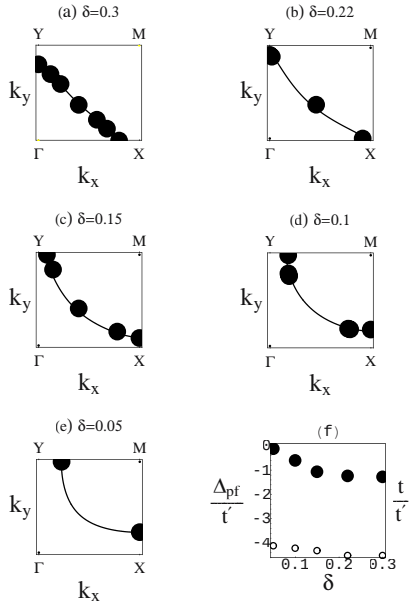

Figure 1. (a-e) Experimentally measured Fermi surfaces for LSCO[6] (dots) and the three band model fits (solid). (f) fitting parameters in the regime $\Delta_{pf} \approx 4|t'|$; circles: values of Δ_{pf}/t', dots: values of t/t'.

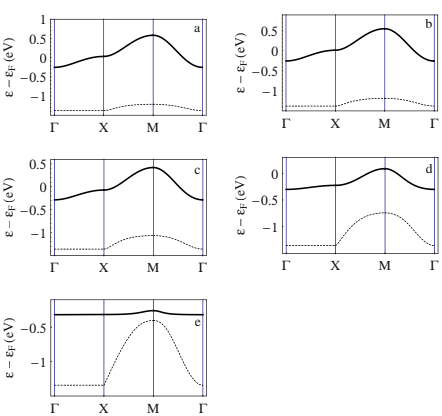

Figure 2. Band-fits for the conducting band of LSCO of [6], corresponding to the Fermi surfaces of Fig.1, illustrating the spectral weight transfer from the lower (oxygen) band to the resonant band upon doping

References

[1] P. W. Anderson,The Theory of Superconductivity in the High T_c Cuprates, (Princeton, New Jersey) 1997;

[2] V. J. Emery, Phys. Rev. Lett **58**, 2794 (1987)

[3] J. Zaanen, G. A. Sawatski and J. W. Allen, Phys. Rev. Lett. **55** 418 (1985);

[4] M. R. Norman, M. Randeria, H. Ding and J. C. Campuzano, Phys.Rev.B**52**,615(1995);

[5] M. C. Shabel, C. -H. Park, A. Matsuura, Z.-X. Shen, D. A. Bonn, Ruixing Liang and W. N. Hardy, Phys. Rev .B **57**, 6090 (1998);

[6] A. Ino, C. Kim, M. Nakamura, T. Yoshida, T. Mizokawa, Z.-X. Shen, A. Fujimori, T. Kakeshita, H. Eisaki and S. J. Uchida, Phys. Rev. B **65**, 94504 (2002);

[7] S. E. Barnes, J. Phys. F **6**, 1375 (1976);

[8] I. Mrkonjic and S. Barisic, Eur. Phys. J. B **34**, 69 (2003);

[9] I. Mrkonjic and S. Barisic, Eur. Phys. J. B **34**, 441 (2003);

[10] B. G. Kotliar, P. A. Lee and N. Read , Physica C **153-155** 538 (1989);

[11] F. C. Zhang and T. M. Rice, Phys. Rev. B **37** 3759 (1987);

[12] A. Damascelli, Z-X Shen and Z. Hussain, Rev. Mod. Phys. **57** 6107 (1998)

[13] I. Mrkonjic and S. Barisic, Phys. Rev. Lett. **92** 129701 (2004),

[14] I. Bozovic, G. Longvenov, I Belca, B. Narimbetov and I Sveklo, Phys. Rev. Lett. **89**, 107001 (2002).

CONDENSATION ENERGY FOR SPIN FLUCTUATIONS MECHANISM OF PAIRING IN HIGH-T_c SUPERCONDUCTORS

Sergei Kruchinin

Bogolyubov Institute for Theoretical Physics, Kiev, Ukraine

Abstract: The condensation energy for the antiferromagnetic spin fluctuations mechanism of pairing are considered. For the calculation the method of functional integrals was used. It has been shown that the condensation energy in high-Tc superconductors is highly sensitive to the doping level, and is greatly reduced in underdoped region.We consider that this effect is due to the decreasing of the number of hot quasiparticles, which are responsible for the interaction with antiferromagnetic spin fluctuations. It is in qualitative agreement with experiment.

Key words: Condensation energy, spin fluctuation mechanism of pairing, thermodynamic, underdoped region, pseudogap

1. INTRODUCTION

The condensation energy is fundamental property of cuprate superconductors. During last years many experiments investions of the condensation energy in high-Tc superconductors. One of the puzzling features of high-Tc cuprates is that the superconducting condesation energy at T=0 , U_0 is greatly reduced in underdoped region [1,2]. This issue has been considered a clue to understanding the mechanism of high-Tc superconductivity and problem of pseudogap. The main problem of theory of superconductivity is the determining of the mechanism of electron

J. Ashkenazi et al. (eds.), New Challenges in Superconductivity: Experimental Advances and Emerging Theories, 145-150.

pairing. In this report we will discuss some thermodynamics properties of the high T_c superconductors on basis of the conception of spin-fluctuations mechanism of pairing. Antiferromagnetic spin fluctuations play important role in high-T_c superconductors[3]. Electron scattering on these fluctuations may cause of electron pairing [4].

In this present paper we'll calculated the condensation energy on basis of antiferromagnetic spin fluctuation mechanism of pairing in high-Tc superconductors.

2. THEORETICAL BACKGROUND

Early was proposed to used the functional integral methods for calculation the thermodynamic properties of high-Tc superconductors including antiferromagnetic spin fluctuations [5].

The antiferromagnetic antiferromagnetic spin fluctuations which result in d-pairing in cuprate superconductor are described by the Lagrangian in lattice representation [5-7]:

$$e^{-\beta\Omega} = N \cdot \int\prod_{n} d\,S_i(n)\, d\,\psi_\alpha^+(n,\tau)\, d\psi_\alpha(n,\tau) \exp\left(-\int_0^\beta d\tau\, \mathrm{L}(\tau) \right), \qquad (1)$$

where L(t) is Lagrangian in lattice representation which are described the spin fluctuations mechanism of pairing [3] :

$$\mathrm{L}(\tau) = \sum_n \psi_\alpha^+(n,\tau)\left(\frac{\partial}{\partial\tau} - \mu \right)\psi_\alpha(n,\tau) - t\sum_{n,p} \psi_\alpha^+(n,\tau)\psi_\alpha(n+p,\tau) +$$

$$+ g\sum_n \psi_\alpha^+(n,\tau)\left(\frac{\sigma^i}{2} \right)_{\alpha,\beta} \psi_\beta(n,\tau) S_i(n,\tau) + \frac{1}{2}\sum\nolimits_{n,m} S_i(n,\tau)\,\chi_{i,j}^{-1}(n,m,\tau)\,S_j(m,\tau)\,, \qquad (2)$$

where the summation is made over all knots of infinite lattice, where Ω – is the thermodynamical potential, $\beta=1/kT$, L – is the Lagrangian in the lattice representation , p – is a unit vector, which connects the neighboring knots, S_i – is the spin of spin fluctuations in the lattice representation , N – is a normalization multiplier, t – is a band halfwidth , μ – is a chemical potential, $\chi_{i,j}(m, n,\tau)$ – is the spin correlation function in lattice representation., which is modulated by

$$\chi(q,\omega) = \frac{\chi_Q}{1 + \xi^2 (q - Q)^2 - i\omega/\omega_{SF}}, \tag{3}$$

$$q_x > 0, \quad q_y > 0,$$

where χ_Q is the static spin susceptibility at wave vector $Q = (\pi/a, \pi/a)$, ξ -is the temperature-dependent antiferromagnetic correlation length, ω_{SF} is the paramagnon energy[8]. All these parameters are taken from NMR experiments .The strong antiferromagnetic fluctuations cause $\chi(q,\omega)$ to peak at Q=(π , π). This has led to distinguish two classes of quasiparticle: hot quasiparticle which are located near (π, 0) and (0, π) which highly anomalous and strongly ccoupled with antiferromagnetic spin fluctuations and cold quasiparticles , those near the diagonals from (0,0) and (π , π) which are not strongly connected by antiferromagnetic spin fluctuations .

Paramagnon energy is connected with antiferromagnetic correlation length:

$$\omega_{SF} = A/\xi^z, \tag{4}$$

where z=1 for pseudogap regime, z=2 for mean field behavior [3].

It was shown that the temperature dependence of the specific heat of the spin-fluctuations mechanism in cuprate superconductors proportional to square the temperature, which correspond d wave pairing [6,9]

Detailed calculations of the big statistical sum are given [5-7]

We have obtained the following expression for the jump of the thermodynamical potential :

$$\Omega(\Delta) = \frac{V}{8}\int \frac{d^2k}{(2\pi)^2}\left\{\begin{array}{l} -\frac{2}{\beta}\ln\frac{ch\frac{\beta}{2}\left(\sqrt{(\varepsilon(\vec{k})-\mu)^2+\Delta(\vec{k})^2}\right)}{ch\frac{\beta\varepsilon}{2}} + \\ \frac{\Delta(\vec{k})^2}{2\sqrt{(\varepsilon(\vec{k})-\mu)^2+\Delta(\vec{k})^2}}\, th\frac{\sqrt{(\varepsilon(\vec{k})-\mu)^2+\Delta(\vec{k})^2}}{2} \end{array}\right\}, \tag{5}$$

where Ω – the jump in thermodynamical potential, $\varepsilon(\vec{k})$– the spectrum of two-dimensional electrons, V – the square of cuprate layer , $\Delta(\vec{k})$– the order parameter , $\vec{k}$ – impulse of electron.

3. CONDENSATION ENERGY

We can evaluate the superconducting condensation energy U_0 by integrating the entropy difference
Sn-Sc, between T=0 and T_c [10-12]:

$$U_0 = \int_0^{T_c} \left(S_n - S_s\right) dT \,, \tag{6}$$

where the subscripts “s” and “n” stand for the superconducting and the normal state , respectively.

$$S_{s,n} = \int_0^{T_c} \left(\frac{C_n}{T}\right)_{s,n} dT = \int_0^{T_c} \gamma_{s,n} dT, \tag{7}$$

where specific heat :

$$\begin{gathered} \gamma_s = \frac{C_s}{T}; \quad \gamma_n = \frac{C_n}{T}; \\ C_s = -T\frac{\partial^2 \Omega_s}{\partial T^2}; \; C_n = -T\frac{\partial^2 \Omega_n}{\partial T^2}; \end{gathered} \tag{8}$$

and thermodynamical potential

$$\Omega_s = \Omega(\Delta), \quad \Omega_n = \Omega(0). \tag{9}$$

We have a numerically calculated the dependence of the condensation energy U_0 on the doping level using formula (6-9) and (5).We have carried out computer calculations of the condensation energy for the compounds $Y_{0.8}Ca_{0.2}.Ba_2 Cu_3O_{7-x}$ as a function of doping x. For our calculation we used the parameters ω_{SF} and χ depended on the doping x, which we took from the Refs. [3, 13, 14].

4. SUMMARY AND CONCLUSIONS

The results of the numerical calculation of U_0 versus the doping level x are shown in Fig. 1(+ - theory). There are also shown the experimental values of U_0 (*- experiment- solid curve) taken from [1]. It can be seen that the condensation energy is greatly reduced in the underdoped region (right hand side of the figure) condensation energy

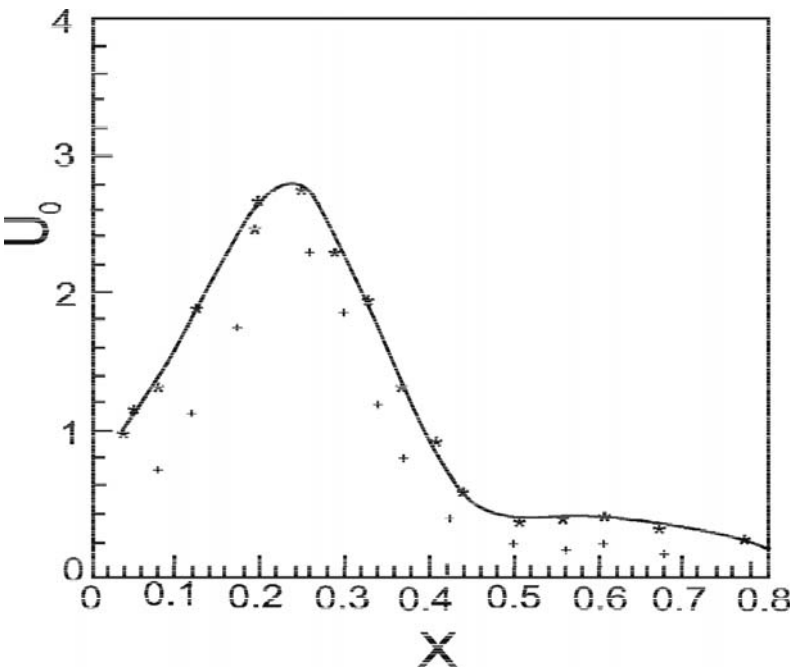

Figure 1. T_c, U_0 the condensation energy (J/g-at.K) vs. doping level x in $Y_{0.8}Ca_{0.2}Ba_2 Cu_3O_{7-x}$ (underdoped side is right hand side of the diagram): + - theory , *- experiment- solid curve.

We consider that this effect is due to the decreasing of the number of hot quasiparticles [3], which are responsible for the interaction with antiferromagnetic spin fluctuations in the underdoped region. It is qualitative agreement with the experiment [1,2]. Important that we can explain the condensation energy for underdoped region which connected with pseudogap region. The theory of pseudogap was successfully developed [2,3]. There were proposed the following models: the model involving preformed pair [16], the model based on microstripes [15] and our model of antiferromagnetic spin fluctuations [3,4]. We can explain the condensation energy as for suerconducting and pseudogap region using interaction hot electron with antiferromagnetic spin fluctuations.

In conclusion, it was shown that the condensation energy in cuprate superconductors is highly sensitive to the doping level and is greatly reduced in underdoped region.

I thank D.Pines, J.W.Loram, M.Oda, W.Y.Liang, N.Momono for stimulating discussion .

This work was supported by INTAS-01-0654 grant.

5. REFERENCES

1. J.W.Loram et al., *Phys.Rev.Let.*71 (1993) 1740.
2. T.Timusk, B.Statt, *Rep.Prog.Phys.* 62 (1999) 61.
3. D.Pines, *Physica C* 341-348 (2000) 59.
4. T.Moriya, K.Ueada, *Advances in Physics* 49 (2000) 555.
5. S.P.Kruchinin, *Modern.Phys.. Lett. B* 9 (1995) 209.
6. S.P.Kruchinin, *Physica C* 282-287 (1997) 1397.
7. S.P.Kruchinin and S.K.Patapis, *J. Low Temp. Phys.* 105 (1996) 717.
8. A.Millis,H.Monien,D.Pines. *Phys.Rev.B* 42 (1990) 67.
9. C.C.Tsuei , Kirtley.*Rev.Mod.Phys.*172 (2000) 969.
10. N.Momono, M.Oda, M.Ido, *Jour.Phys.Soc.Japan.* 71 (2002) 2832.
11. D.Marel, A.J.Leggett , J.W.Loram, J.R.Kirley , cond-mat/0208545 (2002).
12. D.J.Scalapino, S.R.White . *Phys.Rev.B* 48(1998) 8222.
13. J.R.Schmalian, D.Pines, et al., *Phys. Rev. Lett.*80 (1998) 839.
14. S.P.Kruchinin . *Physica C* 341-348 (2000) 901.
15. J.Ashkenazi.*J.Phys. Chem. Sol.* 63 (2002), 2333.
16. P.W.Anderson . *Science* 235 (1996) 1196.

EFFECTS OF DISORDER WITH FINITE RANGE ON THE PROPERTIES OF *D*-WAVE SUPERCONDUCTORS

Carsten T. Rieck, Kurt Scharnberg, and Simon Scheffler
I. Institut für Theoretische Physik,
Fachbereich Physik der Universität Hamburg,
scharnberg@physnet.uni-hamburg.de

Abstract It has long been established that disorder has profound effects on unconventional superconductors and it has been suggested repeatedly that observation and analysis of these disorder effects can help to identify the order parameter symmetry. In much of the relevant literature, including very sophisticated calculations of interference and weak localization effects, the disorder is represented by δ-function scatterers of arbitrary strength. One obvious shortcoming of this approximation is that resonant scattering resulting from the wavelength of the scattered quasiparticle matching the spatial extent of the defect is not included. We find that the mitigation of the Tc-reduction, expected when d-wave scattering is included, is very sensitive to the average strength of the scattering potential and is most effective for weak scatterers. Disorder with finite range not only has drastic effects on the predicted density of states at low energies, relevant for transport properties, but affects the spectral function at all energies up to the order parameter amplitude. The gap structure, which does not appear to be of the simplest d-wave form, should show a defect-dependent variation with temperature, which could be detected in ARPES experiments.

Keywords: Unconventional superconductivity, disorder, non-*s*-wave scattering, ARPES

Introduction

The driving force behind the study of disorder effects in superconductors is the hope that such investigations will give information on the pairing state and the pairing interaction. Indeed, qualitative differences are expected between conventional and unconventional superconductors, the latter being defined by a vanishing Fermi surface average of the order parameter. Potential scattering in an anisotropic conventional superconductor would at high enough concentration lead to a finite, isotropic gap, while unconventional superconductors would acquire midgap states before superconductivity is destroyed. Conventional superconductors show this kind of behavior in the presence of spin-flip scattering. [Abrikosov and Gor'kov, 1961] Because of the innate magnetism

J. Ashkenazi et al. (eds.), New Challenges in Superconductivity: Experimental Advances and Emerging Theories, 151-158.

in high temperature superconductors, nonmagnetic impurities can induce local moments and thus blur the seemingly clear distinction between potential and spin-flip scattering.

Here, we shall assume that we are dealing with d-wave superconductors. Since for unconventional superconductors there is no qualitative difference between these two types of scattering, we shall confine ourselves to the study of potential scattering. Even with this limitation there is a wide range of theoretical predictions as regards T_c-suppression, density of states, transport properties etc, depending on the way disorder is modelled and depending on the analytical and numerical approximations employed to derive experimentally verifiable conclusions. [Atkinson et al., 2000]

In much of the published work, the scattering centers are assumed to be short ranged (s-wave scattering). Even for defects within the CuO_2-planes it seems rather doubtful, that their effect is limited to a single site. Defects due to oxygen nonstoichiometry and cation disorder, which reside on lattice sites away from the conducting CuO_2-planes, are only poorly screened and hence are certainly long ranged. We generalize the selfconsistent T-matrix approximation (SCTMA) to scattering potentials of arbitrary range and then calculate single particle selfenergy correction in 2D d-wave superconductors. First application is to the T_c-suppression and the angle dependent density of states as seen in ARPES.

1. Model assumptions

We start from a two-dimensional free electron gas. The Fermi surface in this model is circular and the band width is infinite. Superconducting properties are described in a Fermi surface restricted approach, so that the weak coupling selfconsistency equation reads

$$\Delta(\varphi) = \pi N_F T \sum_{\omega_n} \int \frac{d\psi}{2\pi} \mathcal{V}(\varphi, \psi) g^1(\psi, i\omega_n), \tag{1}$$

where $g^1(\psi, i\omega_n)$ is the energy integrated anomalous Green function (8). If the pairing interaction is separable such that $\Delta(\varphi) = \Delta(T)e(\varphi)$, the amplitude and the ratio $2\Delta(0)/T_c$ depend sensitively on details of disorder. The variation with φ, however, is completely unaffected by the introduction of disorder. This changes when the pairing interaction is nonseparable as in the spin fluctuation model.[Monthoux and Pines, 1993; Dahm et al., 1993] To elucidate the effects of disorder it is sufficient to consider a two-component order parameter

$$\Delta(\varphi) = \Delta_2\, 2\cos 2\varphi + \Delta_6\, 2\cos 6\varphi. \tag{2}$$

The pairing interaction that gives such an order parameter is of the form

$$N_F \mathcal{V}(\varphi, \psi) = -2 \sum_{\{\nu,\mu\}=\{2,6\}} \cos\nu\varphi \Lambda_{\nu\mu} \cos\mu\psi. \tag{3}$$

This could be diagonalized to give two states, each with its own transition temperature, when both eigenvalues are positive. We shall show that momentum dependent scattering mixes the two eigenstates even at T_c.

For a specific example of an impurity potential with finite range we choose a Gaussian. Taking matrix elements between plain wave states $\vec{k}_F$ and $\vec{k}'_F$ gives

$$v(\varphi) = v_0 \frac{e^{\gamma \cos\varphi}}{I_0(\gamma)} = v_0 \sum_{n=-\infty}^{+\infty} \frac{I_n(\gamma)}{I_0(\gamma)} \cos n\varphi = v_0 \sum_{n=-\infty}^{+\infty} u_n e^{in\varphi}. \tag{4}$$

φ is the angle between $\vec{k}_F$ and $\vec{k}'_F$. v_0 is the average of $v(\varphi)$ over the Fermi surface so that $u_0 = 1$. Below, we parametrize v_0 in terms of an s–wave scattering phase shift $\delta_0 : \pi N_F v_0 = \tan\delta_0$. The last equality in (4) defines the expansion coefficients u_n, which are often treated as free parameters.

2. Selfconsistent *T*–matrix approximation (SCTMA)

Within the Fermi surface restricted approach, the impurity averaged Green function has the form

$$\hat{G}(\boldsymbol{k}, \omega) = \left[\omega\hat{\sigma}_0 - \varepsilon(\boldsymbol{k})\hat{\sigma}_3 - \Delta(\varphi)\hat{\sigma}_1 - \hat{\Sigma}(\varphi, \omega)\right]^{-1}, \tag{5}$$

where $\hat{\Sigma}(\varphi, \omega) = n_{\text{imp}}\, \hat{t}(\varphi, \varphi; \omega)$ is proportional to the single defect $\hat{T}$–matrix:

$$\hat{t}(\varphi, \phi; \omega) = v(\varphi - \phi)\hat{\sigma}_3 + \pi N_F \int \frac{d\psi}{2\pi} v(\varphi - \psi)\hat{\sigma}_3 \hat{g}(\psi, \omega)\hat{t}(\psi, \phi; \omega). \tag{6}$$

Expanding $\hat{t}$ and $\hat{g}$ in terms of Pauli matrices σ^ℓ and the unit matrix we obtain four coupled one-dimensional integral equations for the components $t^\ell(\varphi, \phi)$ of the matrix $\hat{t}$, which contain the energy integrated normal and anomalous retarded Green functions

$$g^0(\psi, \omega_+) = -\frac{\omega - \Sigma^0(\psi, \omega_+)}{\sqrt{[\Delta(\psi) + \Sigma^1(\psi, \omega_+)]^2 - [\omega - \Sigma^0(\psi, \omega_+)]^2}} \tag{7}$$

$$g^1(\psi, \omega_+) = -\frac{\Delta(\psi) + \Sigma^1(\psi, \omega_+)}{\sqrt{[\Delta(\psi) + \Sigma^1(\psi, \omega_+)]^2 - [\omega - \Sigma^0(\psi, \omega_+)]^2}} \tag{8}$$

$g^3(\psi, \omega_+)$ is assumed to vanish, because it is an odd function of energy.

The t^ℓ's are expanded in Fourier series' and the coefficients are collected in the form of matrices $\tilde{t}^\ell$ with elements:

$$t^\ell_{nm} = \pi N_F \int_0^{2\pi} \frac{d\varphi}{2\pi} \int_0^{2\pi} \frac{d\phi}{2\pi} t^\ell(\varphi, \phi)\, e^{-in\varphi + im\phi}. \tag{9}$$

For an order parameter with $d_{x^2-y^2}$–symmetry, $g^l(\psi;\omega)$ has the general form

$$g^\ell(\psi;\omega) = \sum_{m=-\infty}^{+\infty} g^\ell_{q,q+|4m-2\ell|}(\omega)\cos\left[(4m-2\ell)\psi\right] \qquad \ell = 0, 1. \tag{10}$$

The expansion coefficients are independent of q, but have been written in this form to define matrices $\tilde{g}^\ell$ corresponding to $\tilde{t}^\ell$. When the Fourier coefficients $u_n \tan\delta_0$ of the potential (4) are written in the form of a diagonal matrix $\tilde{v}$, the four integral equations are transformed to four equations for $\tilde{t}^\ell$. From these, $\tilde{t}^2$ and $\tilde{t}^3$ can be eliminated, so that we finally obtain.

$$\tilde{t}^0 \pm \tilde{t}^1 = \left[1 - \tilde{v}(\tilde{g}^0 \mp \tilde{g}^1)\tilde{v}(\tilde{g}^0 \pm \tilde{g}^1)\right]^{-1} \tilde{v}(\tilde{t}^0 \mp \tilde{t}^1)\tilde{v} \tag{11}$$

In general, a selfconsistent solution of these two equations can only be obtained numerically.

3. Transition Temperature T_c

In order to calculate T_c, the selfconsistency equation (1) is linearized, which implies that the Green functions (7,8) are to be replaced by

$$g^0 = -i\ \mathrm{sgn}\ \omega_n \quad \text{and} \quad g^1(\psi, i\omega_n) = -\frac{\Delta(\psi) + \Sigma^1(\psi, i\omega_n)}{|i\omega_n - \Sigma^0(\psi, i\omega_n)|}. \tag{12}$$

Σ^0 is required to zeroth order in the order parameter, so that $\tilde{t}^0$ in (11) is diagonal and both $\tilde{t}^1$ and $\tilde{g}^1$ can be neglected. Together with (9) we obtain

$$\Sigma^0(i\omega_n) = -i\ \mathrm{sgn}\ \omega_n \Gamma_N^{\mathrm{el}} \sum_{m=-\infty}^{\infty} \frac{u_m^2}{\cos^2\delta_0 + u_m^2 \sin^2\delta_0}. \tag{13}$$

Here, $\Gamma_N^{\mathrm{el}} = \frac{n_{\mathrm{imp}}}{\pi N_F}\sin^2\delta_0$ is a scattering rate that determines the impurity limited normal state d.c. conductivity.[Hensen et al., 1997] This normal state selfenergy is isotropic, as was to be expected because in our model rotational symmetry is broken only by the superconducting order. Note, that taking the unitary limit $\delta_0 \to \pi/2$ would cause problems with the convergence of this series.
$\hat{t}^1$ and $\hat{g}^1$ are non-diagonal, but since we can neglect products of these matrices we obtain equally easily (11)

$$\Sigma^1(\psi, i\omega_n) = \sum_{\ell=-\infty}^{\infty} g^1_{q,q+4\ell-2}\ \lambda^1_{4\ell-2}\ \cos\left[(4\ell-2)\psi\right], \tag{14}$$

where

$$\lambda^1_{4\ell-2} = -\Gamma_N^{\mathrm{el}} \sum_{m=-\infty}^{\infty} \frac{u_m u_{m+4\ell-2}\,(1 + u_m u_{m+4\ell-2}\tan^2\delta_0)}{(\cos^2\delta_0 + u_m^2\sin^2\delta_0)\,(1 + u_{m+4\ell-2}^2\tan^2\delta_0)}. \tag{15}$$

This, too, would seem to diverge for $\delta_0 = \pi/2$. From (12) we find by inserting the expansions (1), (8), (13), (14):

$$g^1_{q,q+4\ell-2} = -\frac{\Delta_{4\ell-2}}{|\omega_n| + \pi T_c \lambda_{4\ell-2}}, \tag{16}$$

where the pair breaking parameters are given by

$$\lambda_{4\ell-2} = \frac{\Gamma^{e\ell}_N}{\pi T_c} \frac{1}{2} \sum_{m=-\infty}^{\infty} \frac{(u_m - u_{m+4\ell-2})^2}{(\cos^2\delta_0 + u_m^2 \sin^2\delta_0)(1 + u^2_{m+4\ell-2}\tan^2\delta_0)}. \tag{17}$$

Special cases: For an isotropic order parameter, u_{m+4l-2} has to be replaced by u_m and pair breaking from defect scattering is absent, irrespective of the exact form of the scattering potential. For δ–functions scatterers, only $u_0 \neq 0$. Then the pair breaking is equally effective whatever the exact form of the $d_{x^2-y^2}$ order parameter: $\lambda_{4\ell-2} = \frac{1}{\pi T_c}\Gamma^{\rm el}_N$.

Taking the unitary limit in (17) it would appear as if every term in the series vanishes. However, when the series is terminated at $m = \pm m_0$ [Kulić and Dolgov, 1999], one finds $\lambda_{4\ell-2} = \frac{1}{\pi T_c}\Gamma^{\rm el}_N(4\ell - 2)$, independent of m_0. The approach to this limit, however, is sensitive to the choice of m_0. In summary, strong scatterers are more effective in breaking pairs when they have a finite range.

In the Born limit, (17) can be expressed in terms of the square of the potential:

$$\lambda^{\rm Born}_{4\ell-2} = \frac{\Gamma}{\pi T_c}(\pi N_F)^2 \int_0^{2\pi} \frac{d\varphi}{2\pi} v^2(\varphi)\{1 - \cos([4\ell - 2]\varphi)\} > 0. \tag{18}$$

This can become arbitrarily small and would vanish for $v^2(\varphi) \propto \delta(\varphi)$. For the Gaussian model potential (4) the integral can be evaluated

$$\lambda^{\rm Born}_{4\ell-2} = \frac{\Gamma^{\rm el}_N}{\pi T_c} \frac{1}{I_0^2(\gamma)} [I_0(2\gamma) - I_{4\ell-2}(2\gamma)]. \tag{19}$$

If we had normalized the potential such that the average of $v^2(\varphi)$ were kept constant, this would be a monotonically decreasing function of γ, approaching zero for $\gamma \to \infty$. When only a few terms are kept in the Born limit of Eq. (17), a qualitatively different behavior can result. This discrepancy arises because in the Born limit $v^2(\varphi)$ rather than $v(\varphi)$ is approximated.

In order to calculate T_c, we choose the pairing interaction (3). This leads to two coupled linear equations for the two order parameter amplitudes Δ_2 and Δ_6 in (2). From these we obtain Δ_6/Δ_2 and two real solutions for T_c:

$$\begin{aligned} \ln \frac{\omega_D}{2\pi T_c} = {} & \frac{1}{2}\left[\frac{1}{\lambda_+} + \frac{1}{\lambda_-} + \psi_2 + \psi_6\right] \pm \frac{1}{2}\left[\left(\frac{1}{\lambda_+} - \frac{1}{\lambda_-}\right)^2 + \right. \\ & \left. + (\psi_2 - \psi_6)^2 - 2(\psi_2 - \psi_6)\left(\frac{1}{\lambda_+} + \frac{1}{\lambda_-}\right)\frac{\Lambda_{22} - \Lambda_{66}}{\Lambda_{22} + \Lambda_{66}}\right]^{\frac{1}{2}}. \end{aligned} \tag{20}$$

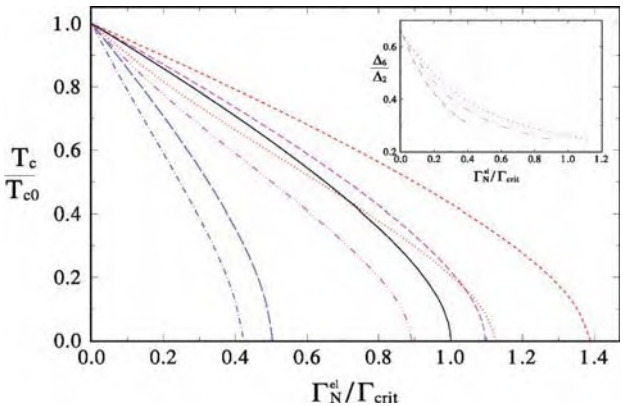

Figure 1. Critical temperature versus $\Gamma_N^{\rm el}$ for the Gaussian potential with width $\gamma = 5$ for $\delta_0 = 0.05\pi, 0.3\pi, 0.3\pi$ full line: Abrikosov-Gorkov, dashed lines: one-component OP, dot-(dash) lines: two-component OP (2). Inset: Δ_6/Δ_2 versus $\Gamma_N^{\rm el}$ for the same three values of δ_0 with the parameters of the pairing interaction chosen such that $T_c^+ = 90$ K, $T_c^- = 30$ K and $\Lambda_{26}/\Lambda_{22} = 0.1$.

with $\psi_i = \psi\left(\frac{1}{2} + \frac{\lambda_i}{2}\right)$. $\lambda_\pm = \frac{1}{2}(\Lambda_{22} + \Lambda_{66}) \pm \frac{1}{2}\sqrt{(\Lambda_{22} - \Lambda_{66})^2 + 4\Lambda_{26}^2}$ are the eigenvalues of the matrix $(\Lambda_{\nu\mu})$ Only when both λ_+ and λ_- are positive, do we have two transition temperatures. The solution found for $\lambda_- < 0$ is an artefact. For the case of pure *s*-wave scattering this equation reduces to

$$\ln \frac{\omega_D}{2\pi T_c} = \psi\left(\frac{1}{2} + \frac{\Gamma_N^{\rm el}}{2\pi T_c}\right) + \frac{1}{\lambda_\pm}. \tag{21}$$

This is the famous and well-known Abrikosov-Gorkov result. [Abrikosov and Gor'kov, 1961] We have now shown that this is independent of the exact form of the order parameter when the scattering is isotropic.

In the limit $\lambda_- \to 0^+$, (20) reduces to

$$\ln \frac{T_c}{T_{c0}} = \frac{\Lambda_{22}}{\Lambda_{22} + \Lambda_{66}}\left[\psi\left(\frac{1}{2}\right) - \psi_2\right] + \frac{\Lambda_{66}}{\Lambda_{22} + \Lambda_{66}}\left[\psi\left(\frac{1}{2}\right) - \psi_6\right]. \tag{22}$$

In both these special cases, Δ_6/Δ_2 is independent of disorder.[Haas et al., 1997] A variation of Δ_6/Δ_2 can, therefore, only be expected for $\lambda_2 \neq \lambda_6$ and $\Lambda_{66}^2 \neq \Lambda_{22}\Lambda_{66}$. However, since Δ_6/Δ_2 depends only on $\psi_2 - \psi_6$ the variation remains modest even for $T_c \to 0$. The inset of Fig. 1 gives an example of the variation of Δ_6/Δ_2 with $\Gamma_N^{\rm el}$ and δ_0. The main panel shows the transition temperature normalized to its clean limit value as function of the scattering rate, normalized to the critical scattering rate for pure *s*-wave scattering $\Gamma_{\rm crit} = 0.882 T_{c0}$, for three values of the scattering phase shift. In the case of

the single component order parameter $\propto \cos 2\varphi$, $\ln \frac{T_c}{T_{c0}} = \psi\left(\frac{1}{2}\right) - \psi\left(\frac{1}{2} + \frac{\lambda_2}{2}\right)$ (dashed lines) shows deviations from (21) that were to be expected from the variation of the pair breaking parameter λ_2 with δ_0, which arises from the finite range of the scattering potential. The reduction in slope observed in electron-irradiated samples [Rullier-Albenque et al., 2003] is compatible only with the assumption of weak scattering. By the same token one concludes that Zn-impurities are strong scatterers. The regime of linear variation can be increased only if the order parameter is some general basis function of the B_1 irreducible representation of the point group C_{4v} and if the scattering is weak. In the example shown in Fig. 1 this change is accompanied by an increase in slope. Finally, we note that an equation formally identical to (22) has been obtained in the Born approximation for arbitrary singlet order parameters and an anisotropic scattering potential of the form $v(\varphi, \phi) = v_i + v_a f(\varphi) f(\phi)$ [Harań and Nagi, 1996].

4. Density of States

The normalized angle dependent DoS, which is measured in ARPES experiments [Borisenko et al., 2002], can be obtained directly from (7): $\frac{N(\omega,\psi)}{N_F} = -\mathcal{I}m\, g^0(\varphi, \omega_+)$. Results for strong scatterers and a single component OP $\propto \cos 2\varphi$ are shown in Fig. 2.

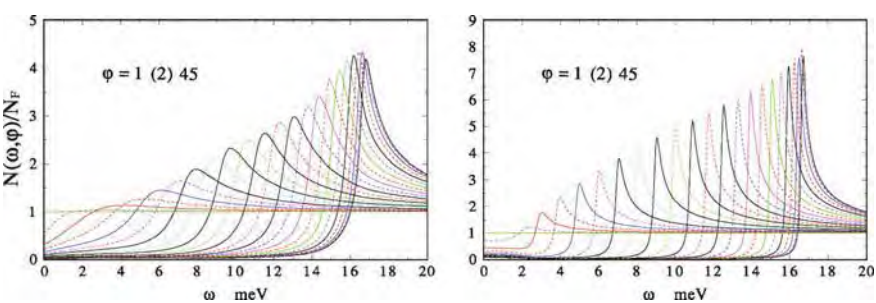

Figure 2. Left panel: Gaussian potential with $\gamma = 5$. Right panel: Point like scatterers. Note the difference in scale. $\delta_0 = 0.49\pi$, $\Gamma_N^{\rm el} = 0.2$ MeV

In the clean limit, we would have square root singularities at $\omega = \Delta \cos 2\varphi$. Defects causing pronounced forward scattering broaden and reduce these singularities much more strongly than point like scatterers. The leading edge gap (LEG), as measured in ARPES, is much less clearly defined. The angle dependence of the LEG, differs substantially from the angle dependence $\cos 2\varphi$ of the OP, being rather *U*-shaped near the node. In this respect, forward scattering would have the same effect as the admixture of a $\cos 6\varphi$ component to the order parameter.

At very low frequencies, the angle integrated DoS is reduced by invoking forward scattering. Details depend sensitively on the choice of the coefficients u_n in (4). This change in the DoS would greatly affect the thermal conductivity and the microwave conductivity.

5. Summary

In the kind of theory developed here, the observed variation in the slope of the disorder-induced T_c-degradation can be attributed to different strengths of the scattering potentials. A mitigation of this T_c-degradation occurs only for strong forward scattering by weak potentials. This could explain why high temperature superconductivity is rather insensitive to cation disorder and disorder associated with oxygen non-stoechiometry. A qualitative change of the dependence of T_c on the scattering rate is found only when the d-wave order parameter has a more complicated angular dependence than $\cos[(4m - 2\ell)\varphi]$. The angle dependent DoS reflects details of the defect potential which could be measured for varying defect concentration n_{imp} by ARPES. Sufficiently low temperatures to eliminate inelastic scattering and high resolution are, of course a precondition. Comparison with $T_c(n_{\mathrm{imp}})$ would provide clues to the form of the pairing interaction $\mathcal{V}(\varphi, \psi)$.

References

Abrikosov, A. A. and Gor'kov, L. P. (1961). Contribution to the theory of superconducting alloys with paramagnetic impurities. *Sov. Phys. JETP*, 12:1243.

Atkinson, W. A., Hirschfeld, P. J., MacDonald, A. H., and Ziegler, K. (2000). Details of disorder matter in 2d d-wave superconductors. *Phys. Rev. Lett.*, 85:3926.

Borisenko, S. V., Kordyuk, A. A., Kim, T. K., Legner, S., Nenkov, K. A., Knupfer, M., Golden, M. S., Fink, J., Berger, H., and Follath, R. (2002). Superconducting gap in the presence of bilayer splitting in underdoped $(Pb,Bi)_2Sr_2CaCu20_{8+\delta}$. *Phys. Rev. B*, 66:140509.

Dahm, T., Erdmenger, J., Scharnberg, K., and Rieck, C. T. (1993). Superconducting states from spin-fluctuation mechanisms. *Phys. Rev. B*, 48:3896.

Haas, S., Balatsky, A. V., Sigrist, M., and Rice, T. M. (1997). Extended gapless regions in disordered $d_{x^2-y^2}$ wave superconductors. *Phys. Rev. B*, 56:5108.

Harań, G. and Nagi, A. D. S. (1996). Role of anisotropic impurity scattering in anisotropic superconductors. *Phys. Rev. B*, 54:15463.

Hensen, S., Müller, G., Rieck, C. T., and Scharnberg, K. (1997). In-plane surface impedance of epitaxial $YBa_2Cu_3O_{7-\delta}$ films: Comparison of experimental data taken at 87 GHz with d- and s-wave models of superconductivity. *Phys. Rev. B*, 56:6237.

Kulić, M. L. and Dolgov, O. V. (1999). Anisotropic impurities in anisotropic superconductors. *Phys. Rev. B*, 60:13062.

Monthoux, P. and Pines, D. (1993). $YBa_2Cu_3O_7$: A nearly antiferromagnetic Fermi liquid. *Phys. Rev. B*, 47:6069.

Rullier-Albenque, F., Alloul, H., and Tourbot, R. (2003). Influence of pair breaking and phase fluctuations on disordered high t_c cuprate superconductors. *Phy. Rev. Lett.*, 91:047001.

SUPERCONDUCTIVITY IN THE BACKGROUND OF TWO-DIMENSIONAL STRIPE SUPERSTRUCTURE

Boris V. Fine
Max Planck Institute for the Physics of Complex Systems
Noethnitzer Str. 38, 01187 Dresden, Germany
fine@mpipks-dresden.mpg.de

Abstract I propose a superconductivity model, which is based on the assumption that stripes in high-T_c cuprates (a) exist and (b) organize themselves in a two-dimensional superstructure. The model describes hole states, which are localized either inside the stripes or in the antiferromagnetic domains between the stripes. The superconductivity in this model emerges due to the interaction, which is, presumably, mediated by the transverse fluctuations of stripes. The tunnelling density of states obtained from the mean field solution of the model is asymmetric with respect to the chemical potential, has Van Hove singularity identified as a superconducting peak, and, in one of the model regimes, has linear functional form in the vicinity of the chemical potential. The relation between the critical temperature and the zero-temperature superfluid density has "fish-like" form, which quantitatively resembles experimental data. The superconducting order parameter obtained from this model has two components exhibiting non-trivial phase and sign change under translations in real space.

Keywords: Stripes, high temperature superconductivity

If energetically *deep* stripes absorbing most of the charge carriers are present in a superconducting (SC) material, then it is likely that the SC mechanism operating in this material would not be operational without stripes. If one further accepts that deep stripes exist in the $La_{2-x}Sr_xCuO_4$ (LSCO) family of high-T_c cuprates, then it implies that the SC mechanism in LSCO is not operational without stripes. Finally, if one also assumes that the SC mechanism is the same in all families of high-T_c cuprates, then the unavoidable conclusion is that stripes, or, at least strong local inhomogeneities exist in all families of high-T_c cuprates and play a crucial role in the mechanism of superconductivity.

In LSCO, the basic evidence of (dynamic) stripes comes in the form of the well-known four-fold splitting of magnetic (π, π) peak, which is observed by inelastic neutron scattering[1], and corroborated by the observation of the elastic response with similar peak pattern in Nd-doped LSCO[2]. The above four-fold splitting has been generally interpreted in the "stripe community" as the

J. Ashkenazi et al. (eds.), New Challenges in Superconductivity: Experimental Advances and Emerging Theories, 159-164.

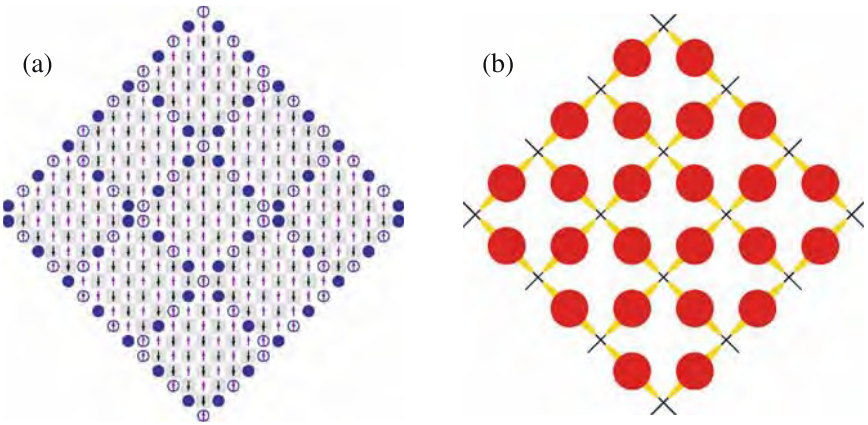

Figure 1. (a) 2D configuration of diagonal stripes. (b) Checkerboard pattern formed by b-states. Circles represent the regions, where b-states are localized.

evidence for two stripe domains, each characterized by a one-dimensional array of stripes running along one of the principal lattice directions. This picture, however, runs into many difficulties, given numerous manifestly two-dimensional (2D) properties of high-T_c cuprates. An alternative interpretation of the four-fold peak pattern, which has been discussed in the literature (see, e.g., Ref. [3]) but never pursued very far, would be based on the 2D arrangement of stripes shown in Fig. 1. The purpose of the present work is to show that the above 2D picture is compatible with superconductivity in general, and with the phenomenology of high-T_c cuprates in particular. This manuscript constitutes a compressed version of a longer paper (Ref. [4]).

The 2D stripe background shown in Fig. 1 implies the existence of two kinds of hole states: a-states — localized inside the antiferromagnetic (AF) domains, and b-states — localized inside the stripes. The on-site energies associated with a- and b-states will be denoted as ε_a and ε_b, respectively. In underdoped cuprates, the expectation is that $\varepsilon_a > \varepsilon_b$. The typical value of the difference $\varepsilon_a - \varepsilon_b$ should then be identified with the pseudogap. The stripe superstructure should strongly suppress the transport of holes. Therefore, in the zeroth-order approximation, it is reasonable to neglect the direct hopping between both a-states and b-states belonging to different units of the stripe superstructure and also exclude all interaction terms, which shift the center of mass of the hole subsystem.

Here, I introduce, perhaps, the most simple model, which satisfies the above "selection rule". The model configuration includes one a-state per AF domain, and two b-states per stripe element having opposite orientations of spins.

(Stripe element is a piece of a stripe confi ned between two subsequent intersections with perpendicular stripes.) The model Hamiltonian is:

$$\mathcal{H} = \varepsilon_a \sum_i a_i^+ a_i \; + \; \varepsilon_b \sum_{i,j(i),\sigma}^{\eta_i=1} b_{ij,\sigma}^+ b_{ij,\sigma} + \; g \sum_{i,j(i)}^{\eta_i=1} (b_{ij,+}^+ b_{ij,-}^+ a_i a_j + \text{h. c.}), \quad (1)$$

where single index i or j labels AF domains; notation $j(i)$ implies, that the jth AF domain is the nearest neighbor of the ith domain; a_i is the annihilation operator of a hole inside the ith AF domain; $b_{ij,\sigma}$ is the annihilation operator of a hole inside the stripe element separating the ith and the jth AF domains; σ is the spin index, which can have two values "+" or "−"; ε_a and ε_b are position-independent on-site energies for a- and b-states, respectively, counted from the chemical potential; and, fi nally, g is the coupling constant. The spin wave function of a-states alternates together with the AF order parameter, i.e. a-states belonging to neighboring AF domains always have opposite spins. The spins of a-states are tracked by index η_i, which can have values 1 or -1. The supercells corresponding to $\eta_i = 1$ and $\eta_i = -1$ are to be called "even" and "odd," respectively. The sum superscript "$\eta_i = 1$" in Eq.(1) indicates that the summation extends only over even supercells. Each transition corresponding to the interaction term in the Hamiltonian (1) can be described either as "two holes from the opposite sides of a given stripe element hopping simultaneously into that element", or as the reverse process. This kind of interaction is, presumably, mediated by the transverse fluctuations of stripe elements.

The mean-fi eld solution of the above model consists of (i) making the Fourier transform of even a-operators and odd a-operators *separately*, which gives, respectively, $a_{\mathrm{e}}(\mathbf{k})$ and $a_{\mathrm{o}}(\mathbf{k})$; and (ii) introducing the following Bogoliubov transformations:

$$a_{\mathrm{e}}(\mathbf{k}) \;\; = \;\; u(\mathbf{k}) A_{\mathrm{e}}(\mathbf{k}) + v(\mathbf{k}) e^{i\phi_a(\mathbf{k})} A_{\mathrm{o}}^+(-\mathbf{k}), \quad (2)$$

$$a_{\mathrm{o}}(-\mathbf{k}) \;\; = \;\; u(\mathbf{k}) A_{\mathrm{o}}(-\mathbf{k}) - v(\mathbf{k}) e^{i\phi_a(\mathbf{k})} A_{\mathrm{e}}^+(\mathbf{k}), \quad (3)$$

$$b_{ij+} = sB_{ij+} \; + \; we^{i\varphi_{ij}} B_{ij-}^+; \quad (4)$$

$$b_{ij-} = sB_{ij-} \; - \; we^{i\varphi_{ij}} B_{ij+}^+, \quad (5)$$

where $A_{\mathrm{e}}(\mathbf{k})$, $A_{\mathrm{o}}(\mathbf{k})$ and $B_{ij,\sigma}$ are the annihilation operators of new Bogoliubov quasiparticles; $\phi_a(\mathbf{k})$ and φ_{ij} are the phases of these transformations; and $u(\mathbf{k})$, $v(\mathbf{k})$, s and w are the real numbers obeying the following normalization conditions: $u^2(\mathbf{k}) + v^2(\mathbf{k}) = 1$; $s^2 + w^2 = 1$. Phases $\varphi_{ij} \equiv \varphi(\mathbf{r}_j - \mathbf{r}_i)$ are chosen to be the same for all translationally equivalent stripe elements. Four kinds of translationally non-equivalent stripe elements correspond to four possible even-to-odd nearest neighbor translation vectors $\mathbf{R}_1 = (1,1)\, l/\sqrt{2}$; $\mathbf{R}_2 = (-1,1)\, l/\sqrt{2}$; $\mathbf{R}_3 = (-1,-1)\, l/\sqrt{2}$; and $\mathbf{R}_4 = (1,-1)\, l/\sqrt{2}$. (Here l

is the length of a stripe element.) Correspondingly, there exist four independent phases $\varphi_\alpha = \varphi(\mathbf{R}_\alpha)$.

Below I consider two most promising cases: Case I — characterized by $\varepsilon_b = 0$, and Case II — characterized by $\varepsilon_a = 0$. In Case I, the standard variational scheme leads to the following equations for the critical temperature (T_c):

$$T_c = \frac{g^2 \left[\exp\left(\frac{|\varepsilon_a|}{T_c}\right) - 1\right]}{8|\varepsilon_a| \left[\exp\left(\frac{|\varepsilon_a|}{T_c}\right) + 1\right]}, \tag{6}$$

and for the zero-temperature energies of A- and B- quasiparticles :

$$\varepsilon_A(\mathbf{k}) = \sqrt{\varepsilon_a^2 + \frac{1}{4} g^2 |V(\mathbf{k})|^2}, \tag{7}$$

$$\varepsilon_B = \frac{g^2}{8N} \sum_{\mathbf{k}} \frac{|V(\mathbf{k})|^2}{\varepsilon_A(\mathbf{k})}, \tag{8}$$

where N is the total number of supercells, and $V(\mathbf{k}) = \sum_\alpha e^{-i\varphi_\alpha - i\mathbf{k}\mathbf{R}_\alpha}$. The four phases φ_α are only constrained by condition $(\varphi_2 + \varphi_4 - \varphi_1 - \varphi_3)/2 = \pi/2 + \pi n,$, where n is an integer number. The density of B-states thus consists of two symmetric δ-function peaks located at $\pm\varepsilon_B$. The density of A-states, is continuous but asymmetric with respect to the chemical potential. It has Van Hove singularities at $\varepsilon_{A0} = \pm\sqrt{\varepsilon_a^2 + g^2}$, and a gap extending between $-\varepsilon_a$ and ε_a.

In Case II, the analogous results are:

$$T_c = \frac{g^2 \left[\exp\left(\frac{|\varepsilon_b|}{T_c}\right) - 1\right]}{8|\varepsilon_b| \left[\exp\left(\frac{|\varepsilon_b|}{T_c}\right) + 1\right]}. \tag{9}$$

$$\varepsilon_A(\mathbf{k}) = \frac{g^2 \, |V(\mathbf{k})| \, C_{a0}}{8\varepsilon_B}, \tag{10}$$

$$\varepsilon_B = \sqrt{\varepsilon_b^2 + \, g^2 \, C_{a0}^2/16}, \tag{11}$$

where $V(\mathbf{k})$ is the same as in Case I, and $C_{a0} \equiv \frac{1}{N} \sum_{\mathbf{k}} |V(\mathbf{k})| = 0.958...$. In this case, the density of A-states is symmetric and has Van Hove singularities at $\varepsilon_{A0} = \pm\frac{g^2 C_{a0}}{4\varepsilon_B}$, while the δ-peaks, corresponding to B-states are asymmetric. Unlike the result for Case I, the density of A-states in Case II has no gap around the chemical potential. Instead, it equals zero at the chemical potential and then increases linearly.

In order to interpret the experimental tunnelling data, it is necessary to assume, that the observed spectra are those of A-states, which means that ε_{A0}

corresponds to the energy of the experimentally observed SC peak. The B-states are, perhaps, more difficult to observe. However, B-states (in the SC state), or b-states (in the normal state) form a checkerboard pattern shown in Fig. 1(b). Therefore, they may be responsible for the checkerboard patterns seen by scanning tunnelling microscopy[5–7].

The superfluid properties of this model are unusual because of the unusual form of the current operator. Fundamental to this model is the internal current operator, which describes the particle flow between a- and b-states. For the ith supercell, the internal current operator can be obtained as follows:

$$J_{ab(i)} \equiv -\frac{d}{dt}(a_i^+ a_i) = -\frac{ig}{\hbar}\sum_{j(i)}(b_{ij,+}^+ b_{ij,-}^+ a_i a_j - \text{h.c.}). \tag{12}$$

Operator (12) sums over four possible transitions, each transferring a hole from ith AF domain to one of the four surrounding stripe elements. When the direction of each of the above transitions is taken into account, the following expression for the translational current operator can be obtained:

$$\mathbf{J}_i^t = -\frac{ig}{2\hbar}\sum_{j(i)} \hat{\mathbf{n}}_{ij} \left(b_{ij,+}^+ b_{ij,-}^+ a_i a_j - \text{h.c.}\right), \tag{13}$$

where $\hat{\mathbf{n}}_{ij}$ is the unit vector in the direction from the ith to the jth supercell.

The internal *supercurrent* corresponding to operator (12) emerges, when the SC solution is modified by adding an extra phase ϕ_{ab} to φ_{ij} in the Bogoliubov transformation for b-states. If the phase ϕ_{ab} is the same for all stripe elements, then the translational supercurrent equals zero. However, when ϕ_{ab} has a weak position dependence, the zero-temperature density of translational supercurrent can be expressed as:

$$\mathbf{j} = \frac{e}{lz_0}\langle \mathbf{J}_i^t \rangle = S_\phi \nabla \phi_{ab}, \tag{14}$$

where, in Case I,

$$S_\phi = \frac{eg^2}{16N\hbar z_0}\sum_{\mathbf{k}} \frac{|V(\mathbf{k})|^2}{\varepsilon_A(\mathbf{k})}; \tag{15}$$

and, in Case II,

$$S_\phi = \frac{eg^2 C_{a0}^2}{32\ \hbar\ z_0\ \varepsilon_B}. \tag{16}$$

Here, z_0 is the transverse distance per one SC plane, and S_ϕ is the SC phase stiffness (frequently referred to as superfluid density).

As the doping concentration changes, the value of $\varepsilon_a - \varepsilon_b$ (characterizing the pseudogap) should, in relative terms, change stronger than the coupling constant g. Therefore, an approximate relation between T_c and S_ϕ within one

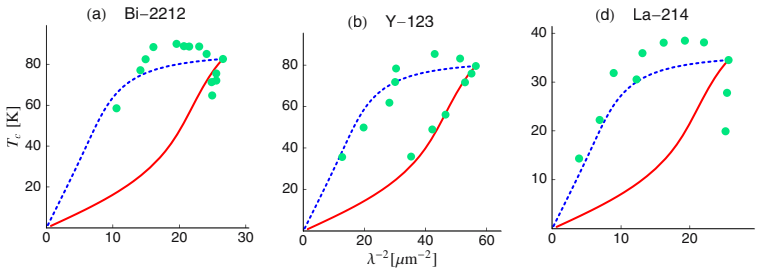

Figure 2. T_c vs. S_ϕ (presented as $1/\lambda^2$, where λ is the in-plane penetration depth of magnetic field): solid line —Case I; dashed line —Case II, circles —experimental points from Ref. [8]. Each plot contains the same pair of theoretical curves, which, initially, were calculated in arbitrary units as described in the text, and then rescaled in such a way that the experimental critical points (evident in every plot) match the theoretical critical point corresponding to $\varepsilon_a = \varepsilon_b = 0$.

family of high-T_c cuprates can be obtained by fi xing the value of g and then calculating T_c and S_ϕ as functions of ε_a (in Case I), or ε_b (in Case II). The resulting theoretical relation is compared with experiments in Fig. 2.

In conclusion, I have shown that superconductivity is compatible with 2D stripe superstructure. The specifi c model presented in this work has the following qualitative features resembling the phenomenology of high-T_c cuprates: (i) emergence of the quasiparticle coherence in k-space only at temperatures below T_c (see $\varepsilon_A(k)$); (ii) linear density of states in the vicinity of the chemical potential (in Case II); (iii) asymmetry in the tunnelling characteristics; (iv) Van Hove singularity in the tunnelling density of states (ε_{A0}); (v) real space checkerboard pattern in the density of states; (vi) low superfluid density having universal "fi sh-like" dependence on T_c. Although not discussed in this paper, the Bogoliubov transformations (2-5) imply a very unconventional symmetry of the SC order parameter, which, in particular, includes the sign change of at least one of the two SC components under translations in real space [4]. A similar prediction has also been made by Ashkenazi in Ref. [9].

References

[1] K. Yamada *et al. Phys. Rev. B*, 57:6165, 1998.

[2] J. M. Tranquada *et al. Phys. Rev. B*, 54:7489, 1996.

[3] G. Seibold and M. Grilli. *Phys. Rev. B*, 63:224505, 2001.

[4] B. V. Fine. *Eprint:* cond-mat/0308428

[5] J. E. Hoffman *et al. Science*, 295:466–469, 2002.

[6] C. Howald *et al. Phys. Rev. B*, 67:014533, 2003.

[7] M. Vershinin *et al. Science*, 303:1995–1998, 2004.

[8] J. L. Tallon *et al. Phys. Rev. B*, 68:180501, 2003.

[9] J. Ashkenazi. *Eprint:* cond-mat/0308153

THEORY FOR KEY EXPERIMENTS IN CUPRATE SUPERCONDUCTORS

Fingerprints of the Pairing Interaction: Resonance Peak and Kink

D. Manske
Max-Planck-Institute for Solid State Research (MPI-FKF)
Heisenbergstr. 1, D-70569 Stuttgart, Germany
d.manske@fkf.mpg.de

I. Eremin
Free University of Berlin, Institute for Theoretical Physics
Arnimallee 14, D-14195 Berlin, Germany
ieremin@physik.fu-berlin.de

K.H. Bennemann
Free University of Berlin, Institute for Theoretical Physics
Arnimallee 14, D-14195 Berlin, Germany
khb@physik.fu-berlin.de

Abstract We argue that a Scalapino-Schrieffer-Wilkins analysis of the elementary excitations is possible in high-T_c cuprates. We demonstrate this by considering the resonance peak in inelastic neutron scattering (INS) experiments and the kink in angle-resolved photoemission (ARPES) data. Both properties contain characteristic features of the superconducting gap function $\Delta(\mathbf{k},\omega)$ that reflect the pairing interaction. We can qualitatively explain the experiments by using a generalized Eliashberg theory for the one-band Hubbard model based on spin-fluctuation-mediated Cooper-pairing in which $\Delta(\mathbf{k},\omega)$ is calculated self-consistently. This gives strong evidence for Cooper-pairing due to spin excitations in the high-T_c cuprates.

Keywords: high-T_c superconductivity, spin-fluctuation mechanism

J. Ashkenazi et al. (eds.), New Challenges in Superconductivity: Experimental Advances and Emerging Theories, 165-176.

Introduction

More than 15 years after the discovery of high-T_c superconductivity in layered cuprates its mechanism is still under debate. This has to do with the asymmetry of physical properties between the electron-doped and hole-doped side of the complex phase diagram, temperature vs. doping, $T(x)$, and with the fact that no consensus has been reached about the question what are the key experiments a theory of high-T_c superconductivity must be able to explain. In this paper we argue that the elementary excitations and their interdependence with spin excitations in the cuprates are of central interest in order to learn more about the correlations in general and, in particular, about the mechanism for Cooper-pairing in these systems.

For comparison we discuss first the key experiments in conventional (strong-coupling) phonon-induced superconductors like niobium or lead. In general, neutron scattering data can be used in order to determine the phonon density of states, and I-V characteristics of superconducting tunnel junctions yield also informations about the electron-phonon coupling. Assuming that the exchanged phonon can be described by a spectral function $F(\mathbf{q},\omega)$ and that it couples to the electrons via a vertex function $\alpha(\mathbf{k},\omega)$, one arrives at the effective pairing potential

$$V_{eff} = \alpha^2_{\mathbf{k},\mathbf{k}'} F(\omega) \quad . \tag{1}$$

Then, employing the conventional strong-coupling, i.e. ω- dependent, Eliashberg-theory and using V_{eff} as an input, one obtains a superconducting gap function $\Delta(\omega)$ that can be tested experimentally. In a pioneering work Scalapino, Schrieffer, and Wilkins used $\Delta(\omega)$ in the general expression for tunneling density of states, $N_T(\omega)$, (normalized by the density of states at the Fermi level $N(0)$)

$$\frac{N_T(\omega)}{N(0)} = \mathrm{Re}\left[\frac{\omega}{\sqrt{\omega^2 - \Delta^2(\omega)}}\right] \tag{2}$$

and found very good agreement with experimental data [1]. Therefore, in short, the understanding of the elementary excitations, in particular, their charge degrees of freedom, were most important in accepting the picture of electron-phonon mediated superconductivity.

Similarly, in the high-T_c cuprates many experiments reveal characteristic fingerprints of the superconducting gap function $\Delta(\mathbf{k},\omega)$ where also the $\mathbf{k}$-dependence becomes important. For example, phase sensitive measurements in hole- and electron-doped cuprates show a d-wave symmetry of the superconducting order parameter [2], $\Delta(\mathbf{k}) = \frac{\Delta_0}{2}\,[\cos(k_x) - \cos(k_y)]$, where Δ_0 is the maximum of the superconducting gap function for $T \to 0$. In addition, an large number of experiments using different techniques are compatible with nodes and thus with the d-wave interpretation [3, 4]. Hence, in short, a theory for Cooper-pairing in the high-T_c cuprates should be able to explain a d-wave

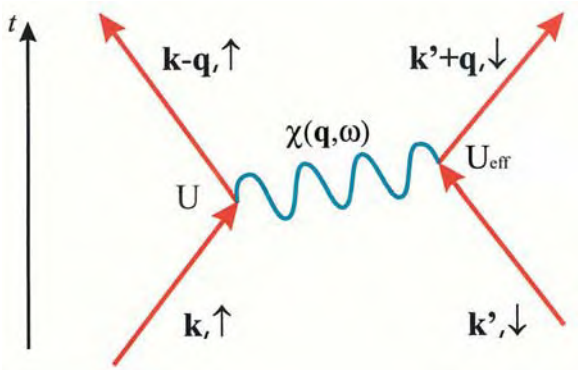

Figure 1. Illustration of singlet Cooper-pairing due to spin excitations. They are described by a spin susceptibility $\chi(\mathbf{q},\omega)$ and interact with electrons via a (renormalized) vertex U (U).

order parameter on both sides of the phase diagram. This is possible for theories based on the exchange of antiferromagnetic spin fluctuations because a simple Ornstein-Zernicke form for the spin susceptibility $\chi(\mathbf{q},\omega)$ [5],

$$\chi(\mathbf{q},\omega) = \frac{\chi_{\mathbf{Q}}}{1+\xi^2(\mathbf{q}-\mathbf{Q})^2 - i\frac{\omega}{\omega_{sf}}}. \tag{3}$$

allows for a sharp enhancement of fluctuations near the antiferromagnetic wave vector $\mathbf{Q} = (\quad)$. In this case, in analogy to the conventional picture, the process for Cooper-pairing is described by the Feynman diagram shown in . 1 in which spin excitations are exchanged. In Eq. (3), $\chi_{\mathbf{Q}}$ is the value of the static spin susceptibility at the wave vector $\mathbf{Q}$, ξ is the magnetic correlation length, and ω_{sf} is the characteristic frequency of spin fluctuations. Based on weak-coupling arguments one can show on general ground that (repulsive) spin excitations described by this $\chi(\mathbf{q},\omega)$ yield d-wave pairing [6, 7]. However, note, in an electronic theory the physical properties ξ and ω_{sf} should follow from a self-consistent calculation.

But what about the important frequency-dependent fingerprints of the superconducting gap $\Delta(\omega)$ in analogy to Scalapino, Schrieffer, and Wilkins? In the past it was shown by several groups that the so-called peak-dip-hump structure observed in angle-resolved photoemission spectroscopy (ARPES) below T_c can be explained in terms of a feedback effect of superconductivity arising from the frequency-dependent gap function $\Delta(\omega)$ [8–10]. Moreover, it has been argued that this structure reflects the effective pairing interaction and points towards a spin-fluctuation-mediated Cooper-pairing. We consider this as an important first step to compare fingerprints of $\Delta(\omega)$ in the charge channel, however, we argue that the spin degrees of freedom should mainly to be analyzed, if Cooper-pairing is mediated by spin excitations.

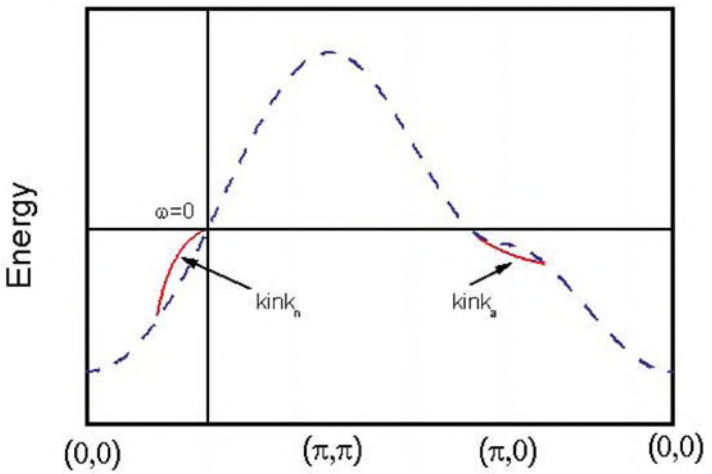

Figure 2. Illustration of the kink in both the nodal (k_n) and antinodal (k_a) direction (solid lines) that is a result of many-body interactions described by $\omega_{\mathbf{k}} = \epsilon_{\mathbf{k}} + \mathrm{Re}\,\Sigma(\mathbf{k},\omega)$ (Σ is the quasiparticle self-energy). The dashed line refers to the bare tight-binding band structure $\epsilon_{\mathbf{k}}$. While the kink in the nodal direction is present above and below T_c reflecting mainly the normal state excitations, the kink in the $((0,\pi) \rightarrow (\pi,\pi))$ direction occurs only in the superconducting state and thus is directly reflecting $\Delta(\omega)$.

Recently, due to an improved ARPES resolution, another fingerprint of $\Delta(\omega)$ has been observed: an abrupt change of the Fermi (or group) velocity of the quasiparticles along the antinodal $((0,\pi) \rightarrow (\pi,\pi))$ direction that results in a 'kink' in the dispersion occurring only in the superconducting state. Such a kink is also present in the nodal $((0,0) \rightarrow (\pi,\pi))$ direction above and below T_c. Both kinks are illustrated in Fig. 2. In Ref. [11] we have shown that the existence as well as its temperature- and momentum-anisotropy can be well described by spin fluctuation-mediated Cooper-pairing. Here, we focus on the relation of the kink to the resonance peak.

In order to discuss the the spin susceptibility we illustrate $\mathrm{Im}\,\chi(\mathbf{q},\omega)$ at the antiferromagnetic wave vector $\mathbf{Q} = (\pi,\pi)$ for $YBa_2Cu_3O_{6.7}$ (YBCO), for example. The normal state data, although in experiment difficult to extract from the background, can be described by Eq. (3). On the other hand, below T_c a strong feedback of superconductivity occurs: a strong suppression for small frequencies accompanied by a resonating peak structure. Thus, one has to answer the important question: is this behavior a characteristic fingerprint of the superconducting gap function $\Delta(\mathbf{k},\omega)$ in analogy to the conventional study by Scalapino, Schrieffer, and Wilkins [1]? In the following we will argue that such an analysis is indeed possible.

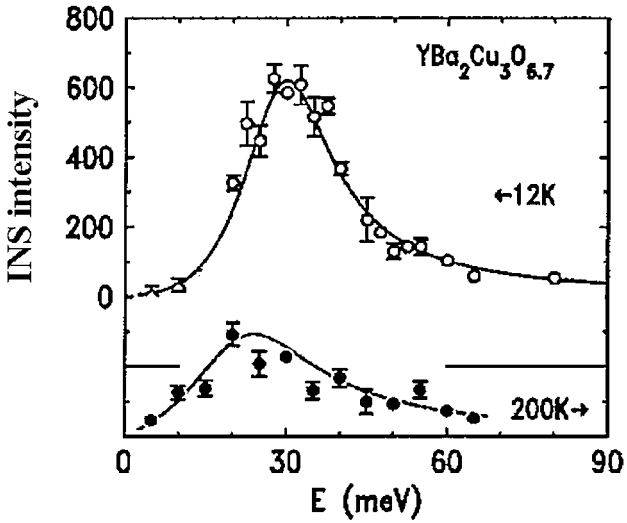

Figure 3. Illustration of the resonance peak at the antiferromagnetic wave vector $\mathbf{Q} = (\pi, \pi)$ for hole-doped cuprates (after [12]). While the normal-state data (lower curve) may be described by an Ornstein-Zernicke form (see Eq. (3)), in the superconducting state a strong suppression for small frequencies occurs followed by a large peak at $\omega_{res} \simeq 2\Delta_0$.

1. Generalized Eliashberg theory

What is a minimum model for describing the main physics of a single CuO_2-plane? In this paper we employ an effective one-band Hubbard Hamiltonian:

$$H = -\sum_{\langle ij \rangle \sigma} t_{ij} \left(c^+_{i\sigma} c_{j\sigma} + c^+_{j\sigma} c_{i\sigma} \right) + U \sum_i n_{i\uparrow} n_{i\downarrow} \quad , \tag{4}$$

where $c^+_{i\sigma}$ creates an electron with spin σ on site i, U denotes the on-site Coulomb interaction, and t_{ij} is the hopping integral. This one-band approach seems to be justified because upon hole doping antiferromagnetism disappears due to Zhang-Rice singlet formation and quenching of Cu-spins. In this one-band picture the Coulomb interaction between the quasiparticles refers to an effective interaction (i.e. the Hubbard U) within the conduction band. Then, further doping increases the carrier mobility and a system of strongly correlated quasiparticles occurs. In the overdoped case less magnetic activity is present yielding usual Fermi liquid (FL). It is perhaps interesting to note that, as we will discuss below, in our approach we are not considering the half-filled case (or close to it). We assume here the conventional FL picture rather than

the view of a doped Mott insulator. Thus, for simplicity, we assume $U \simeq W/2$ ($W =$ bandwidth) independent of the doping concentration.

After diagonalization of the first term, one arrives at the bare tight-binding energy dispersion $\epsilon_{\mathbf{k}} = -2t\,(\cos k_x + \cos k_y) + 4t' \cos k_x \cos k_y - \mu$. Here, t and t' refer to the hopping of a hole (electron) between nearest, next-nearest sites on the square lattice, and μ is the chemical potential that defines the doping. We also set the lattice constant to unity. Then, the description of the electron- and hole-doped cuprates within a one-band approximation is possible if one takes into account different parameters and quasiparticle dispersion. Note that in the case of electron doping the electrons occupy the copper d-band, while in the hole-doped case holes refer mainly to the oxygen p-states yielding different dispersion parameters.

How to calculate the important $\mathbf{k}$- and ω-dependence of the superconducting gap? In this one-band model, we assume that the *same* electrons (holes) are participating in the formation of antiferromagnetic fluctuations and in Cooper-pairing due to the exchange of these fluctuations. Thus, both the magnetic susceptibility and the quasiparticle self-energy must be calculated self-consistently. This is possible in the FLEX approximation [11, 13–16]. In this approach the dressed one-electron Green's function are used to calculate the charge and spin susceptibilities. These susceptibilities are then used to construct an effective Berk-Schrieffer-like [17] pairing interaction reflecting the exchange of spin fluctuations on an RPA level which is a generalization of Fig. 1 and of Eq. (3). Note that the FLEX approximation ignores the fact that cuprates are doped Mott insulators and, secondly, is only based on perturbation theory. On the other hand, in defending this approach, we argue that for optimally doped or overdoped cuprates the Mott physics is no longer dominant. And, in addition, this method allows to calculate the important frequency dependence of the superconducting gap in a controlled way which enables us to employ a Scalapino-Schrieffer-Wilkins analysis to the spin spectrum in the superconducting state (resonance peak), for example.

Like in conventional Eliashberg theory, due to the central role of the superconducting gap function Δ which can be understood as the off-diagonal part of the quasiparticle self-energy, it is convenient to formulate the theory in terms of self-energy components. In a short-hand notation, the generalized Eliashberg equations for a repulsive spin fluctuation-mediated pairing can be written down in terms of the quasiparticle self-energy components Σ_ν ($\nu = 0, 3, 1$) with respect to the Pauli matrices τ_ν in the Nambu representation[18, 19], *i.e.* $\Sigma_0 = \omega(1 - Z)$ (mass renormalization), $\Sigma_3 = \xi$ (energy shift), and $\Sigma_1 = \phi$ (gap parameter). They are given by

$$\Sigma_\nu(\mathbf{k}, \omega) = \sum_{\mathbf{k}'} \int_0^\infty d\Omega\, V_{\text{eff}}(\mathbf{k} - \mathbf{k}', \Omega) \int_{-\infty}^{+\infty} d\omega' I(\omega, \Omega, \omega')\, A_\nu(\mathbf{k}', \omega') \quad (5)$$

with the effective pairing interaction

$$V_{\text{eff}} = \left[P_s(\mathbf{k}-\mathbf{k}',\Omega) - (\delta_{\nu 1} - \delta_{\nu 0} - \delta_{\nu 3})\, P_c(\mathbf{k}-\mathbf{k}',\Omega)\right]. \qquad (6)$$

P_s and P_c denote the spectral density of the spin and charge excitations, respectively, and are treated within RPA, $P_s = (2\pi)^{-1} U^2 \,\text{Im}\,(3\chi_s - \chi_{s0})$ with $\chi_s = \chi_{so}(1 - U\chi_{s0})^{-1}$ and $P_c = (2\pi)^{-1} U^2 \,\text{Im}\,(3\chi_c - \chi_{c0})$ with $\chi_c = \chi_{c0}(1 + U\chi_{c0})^{-1}$. The kernel I and the spectral functions of the one-particle Green's function in Eq. (5), A_ν, read

$$I(\omega,\Omega,\omega') = \frac{f(-\omega') + b(\Omega)}{\omega + i\delta - \Omega - \omega'} + \frac{f(\omega') + b(\Omega)}{\omega + i\delta - \Omega - \omega'}, \qquad (7)$$

$$A_\nu(\mathbf{k},\omega) = -\pi^{-1}\text{Im}\ \left[a_\nu(\mathbf{k},\omega)/D(\mathbf{k},\omega)\right], \qquad (8)$$

and

$$D = [\omega Z]^2 - [\epsilon^0_{\mathbf{k}} + \xi]^2 - \phi^2, \qquad (9)$$

$$a_0 = \omega Z(\mathbf{k},\omega), \quad a_3 = \epsilon^0_{\mathbf{k}} + \xi(\mathbf{k},\omega), \quad a_1 = \phi(\mathbf{k},\omega). \qquad (10)$$

The superconducting gap function can be written as $\phi = Z\Delta$. In Eq. (7), f and b are the Fermi and Bose distribution function, respectively. In short, within our generalized Eliashberg approach the dressed one-electron Green's function are used to calculate the charge and spin susceptibilities. Thus, for example, no input parameters in Eq. (3) are needed because ξ and ω_{sf} are calculated self-consistently for fixed values of U, t, t', and μ. These susceptibilities are then used to construct an effective Berk-Schrieffer-like [17] pairing interaction V_{eff} describing the exchange of charge and spin fluctuations. More details on this theory can be found in Ref. [11]. These generalized Eliashberg equations allow us to calculate all the properties of the system self-consistently like the elementary excitations and their interdependence with the dynamical spin susceptibility and the resulting $\mathbf{k}$- and ω-dependent superconducting order parameter, for example.

2. Results and discussion

While the original analysis of the elementary excitations made by Scalapino, Schrieffer, and Wilkins was done on tunneling experiments (i.e. on the charge channel) we argue that, if spin excitations are responsible for Cooper-pairing in the cuprates, one has first to analyze the *spin susceptibility* (spin channel) in order to see fingerprints of the superconducting gap function $\Delta(\omega)$. In other words, for high-T_c cuprates Eq. (2) has to be replaced by the RPA expression for the spin susceptibility (in our case for the one-band Hubbard model)

$$\text{Im}\,\chi(\mathbf{Q},\omega) = \frac{\text{Im}\,\chi_0(\mathbf{Q},\omega)}{(1 - U\,\text{Re}\,\chi_0(\mathbf{Q},\omega))^2 + U^2\,(\text{Im}\,\chi_0(\mathbf{Q},\omega)^2} \quad , \qquad (11)$$

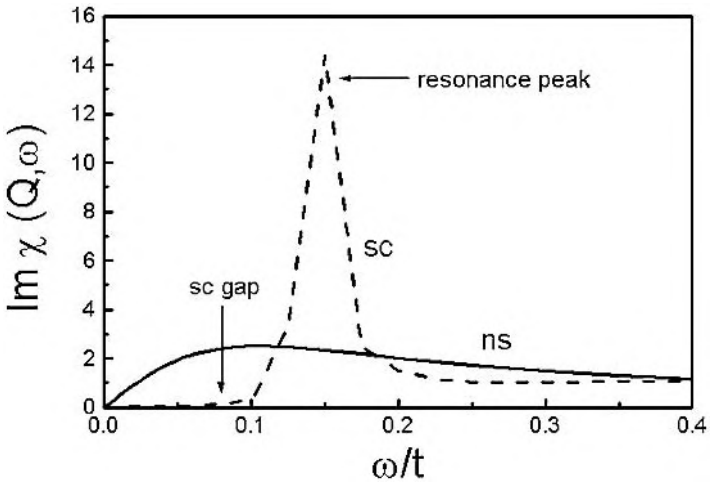

Figure 4. Calculated feedback of superconductivity on the spin susceptibility Im $\chi(\mathbf{q},\omega)$ for hole-doped cuprates at optimal doping (x=0.15) for wavevector $\mathbf{q} = \mathbf{Q}$ using $U = 4t$ and $t' = -0.45t$. The solid curves refer to the normal state ($T = 1.5T_c$), while the dashed curves denote the renormalized spin susceptibility in the superconducting state at $T = 0.7T_c$.

that contains the self-consistently calculated gap function. For simplicity we focus here on the antiferromagnetic wave vector $\mathbf{Q} = (\pi, \pi)$. Note that usually Im $\chi_0(\mathbf{Q},\omega)$ yields the dominating structure in Eq. (11), except if a resonance condition towards a spin-density-wave collective mode is satisfied (or close to it):

$$\frac{1}{U_{cr}} = \text{Re}\ \chi_0(\mathbf{q} = \mathbf{Q}, \omega = \omega_{res}) \quad . \tag{12}$$

Our results for the spin susceptibility Im $\chi(\mathbf{Q},\omega)$ are shown on Fig. 4. Note that the suppression of Im $\chi(\mathbf{Q},\omega)$ for low frequencies is a result of both the d-wave symmetry of the gap and also its frequency dependence [20]. Then, in addition, if Eq. (12) is fulfilled, the spin excitations *may* become resonant reflecting in particular the frequency dependence of the superconducting gap (and its overall magnitude, of course). Because, in general, $\Delta(\mathbf{k},\omega)$ reflects the structure of the actual pairing interaction yielding a renormalized spin susceptibility below T_c, we safely conclude that a detailed Scalapino-Schrieffer-Wilkins-like analysis has to be done on the spin susceptibility in order to proove that spin excitations are responsible for Cooper-pairing in cuprates. This is possible within our theory and our calculation using model parameters already yields fair agreement with experiment.

So far, we have discussed our results only for the important antiferromagnetic wave vector $\mathbf{Q} = (\pi, \pi)$, but what is the dispersion of resonance peak?

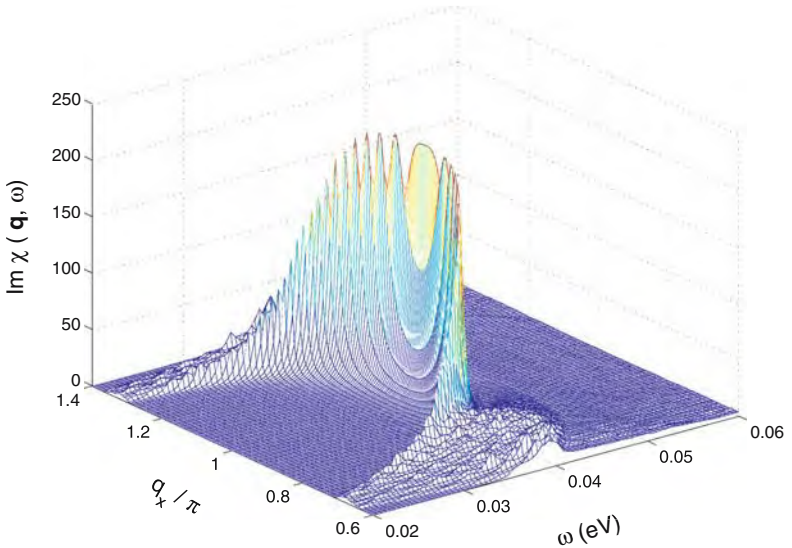

Figure 5. Lower branch of the dispersion of the resonance peak using $q_y = \pi$ and the same parameters as in Fig. 4.

To a good approximation the RPA expression for $\mathrm{Im}\,\chi(\mathbf{Q},\omega)$ (see Eq. (11)) can be expanded around its resonance condition yielding two quadratic dispersions of the resonance peak. Our results are shown in Fig. 5 in which for simplicity only the lower branch is displayed. One clearly sees a parabola-like envelope which is in good agreement with experiment [21]. A closer inspection shows that for frequencies smaller than $\omega \simeq 35$meV a strong decrease of the resonance peak occurs. In such a situation, the nominator of Eq. (11) may become dominant yielding four peaks around (π,π). This seems to be case in $La_{2-x}Sr_xCuO_4$ (LSCO) in which the gap is too small to generate a resonance peak. Recently Tranquada *et al.* measured $\chi(\omega)$ at one of these $\mathbf{q}$-points and have found only a rearrangement of spectral weight, but no resonance peak [22]. This scenario has been theoretically discussed in connection with Fig. 10(a) in Ref. [11].

Finally, we return to the charge degrees of freedom. Although the above Scalapino-Schrieffer-Wilkins-like analysis of the spin channel might already be enough to identify the pairing interaction, an independent fingerprint in the elementary excitations directly would be extremely helpful. In contrast to the early work on conventional superconductors, where only the $\mathbf{k}$-integrated density of states was analyzed, in the case of high-T_c cuprates the *local* density of states, i.e. the $\mathbf{k}$-resolved spectral density $N(\mathbf{k},\omega)$, can be analyzed directly due to a highly improved resolution in angle-resolved photoemission

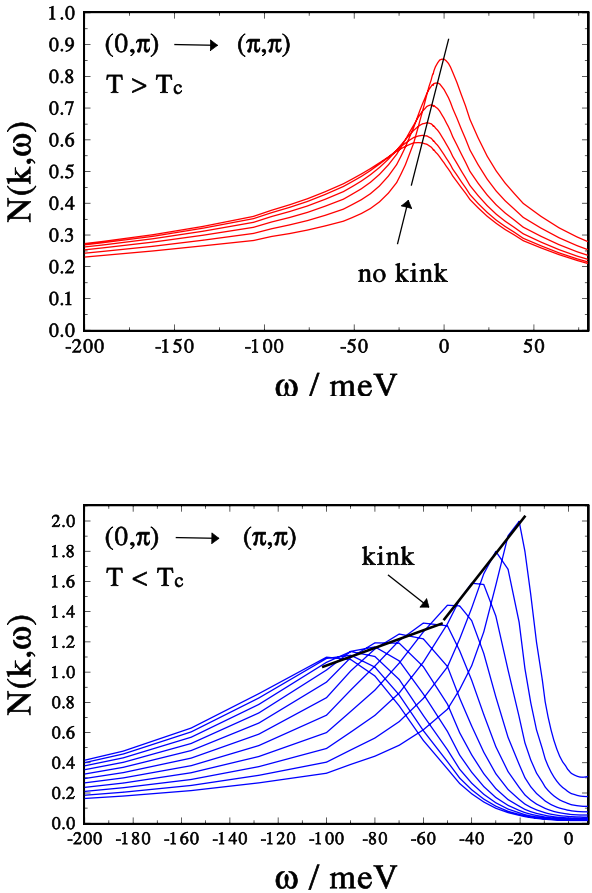

Figure 6. Calculated spectral density $N(\mathbf{k},\omega)$ along the antinodal $(\pi,0) \rightarrow (\pi,\pi)$ direction as a function of frequency in the first BZ in the normal (a) and superconducting (b) state. We use the same parameters as in Fig. 4. Due to the flat band close to the Fermi level the spectral density shows no kink structure in the normal state. Below T_c the superconducting gap $\Delta(\omega)$ opens yielding a kink structure in the spectral density.

(ARPES) experiments. Therefore, it is important to compare the above theory with ARPES data that reveal a sudden change ('kink') in the Fermi (or group) velocity close to the Fermi level for all hole-doped cuprates.

While the kink in the nodal direction is theoretically discussed in Ref. [11], we focus here on the antinodal ($(0,\pi) \rightarrow (\pi,\pi)$) direction, in which superconducting gap function is clearly seen [23, 24]. In Fig. 6 we show our results for this direction above (a) and below T_c (b). In the normal state no kink occurs due to the flat part of the band dispersion around $(\pi,0)$ as illustrated by the

dashed line in Fig. 2. In agreement with experiment we obtain a kink only in the superconducting state. This again, is only possible due to the important frequency-dependent gap function $\Delta(\mathbf{k},\omega)$ that leads to structure in the self-energy and thus to a renormalized energy dispersion $\omega_{\mathbf{k}}$:

$$\omega_{\mathbf{k}} = \epsilon_{\mathbf{k}} + \mathrm{Re}\,\Sigma(\mathbf{k},\omega) \tag{13}$$

yielding a renormalized Fermi velocity close to the antinodal point (see solid line in Fig. 2). Because the same superconducting gap function $\Delta(\mathbf{k},\omega)$ (in our case calculated self-consistently) is entering both the resonance condition (Eq. (12)) and the renormalized dispersion (Eq. (13)), the kink in the antinodal direction is intimately related to the resonance peak. Hence, in short, both the kink in the antinodal direction and the resonance peak below T_c contain the information of the momentum and frequency dependence of the gap function and thus reflect the pairing interaction. Then, what is needed is a detailed comparison with experiment as Scalapino, Schrieffer, and Wilkins had done.

Finally, we comment on the doping dependence of the resonance peak and kink [25]. In our view, the kink in hole-doped cuprates in the nodal direction is a result of the coupling of quasiparticles (holes) to spin excitations in the normal state, and, if strong enough for generating a high T_c, should thus be present for almost every doping concentration. This is a quite general effect and is also expected in other unconventional superconductors [11]. On the other hand, both the kink in the antinodal direction and the important resonance peak are only possible, if $\Delta(\mathbf{k},\omega)$ is large enough and reveals a robust structure in order to change significantly the self-energy of the quasiparticles. In addition, in the case of the resonance peak, Eq. (12), i.e. the resonance condition, must be fulfilled. Thus, we expect in overdoped cuprates where $T_c \propto \Delta_0$ is valid, that no resonance peak might be seen in INS experiments while the kink in the antinodal direction might be still observable for ARPES. For larger overdoping even this kink should vanish.

3. Summary

To summarize, we argue that the resonance peak observed in INS and the kink in ARPES experiments are key experiments when a Scalapino-Schrieffer-Wilkins analysis the to high-T_c cuprates is applied. While in many experiments the d-wave symmetry is observed, a closer inspection is needed for identifying the frequency dependence of the superconducting gap function. Within a generalized Eliashberg theory using the one-band Hubbard Hamiltonian and a Berk-Schrieffer-like paring due to spin fluctuations, we are able to account qualitatively for the main features in both INS and ARPES experiments, if $\Delta(\mathbf{k},\omega)$ is calculated self-consistently. For a quantitative comparison between theory and experiment further detailed analysis is needed.

Acknowledgments

We wish to thank S. Borisenko, V. Hinkov, C. Honerkamp, and B. Keimer for helpful discussions. This work is supported by INTAS grant 001-0654.

References

[1] D. J. Scalapino, J. R. Schrieffer, and J. W. Wilkins, Phys. Rev. **148**, 263 (1966).

[2] C. C. Tsuei and J. R. Kirtley, in *The physics of superconductors*, Eds.: K. H. Bennemann and J. B. Ketterson, Vol. 1, chapter 9, Springer (Heidelberg), 2003.

[3] J. Zasadzinski, in *The physics of superconductors*, Eds.: K. H. Bennemann and J. B. Ketterson, Vol. 1, chapter 8, Springer (Heidelberg), 2003.

[4] D. Einzel and R. Hackl, J. Raman Spektroscopy **27**, 307 (1996).

[5] A. J. Millis, H. Monien, and D. Pines, Phys. Rev. B **42**, 167 (1990).

[6] D. J. Scalapino, Phys. Rep. **250**, 329 (1995).

[7] D. Manske, I. Eremin, and K. H. Bennemann, in *The physics of superconductors*, Eds.: K. H. Bennemann and J. B. Ketterson, Vol. 2, chapter 9, Springer (Heidelberg), 2004.

[8] T. Dahm, D. Manske, and L. Tewordt, Phys. Rev. B **58**, 12454 (1998).

[9] M. Eschrig and M. R. Norman, Phys. Rev. Lett. **85**, 3261 (2000).

[10] A. V. Chubukov, D. Pines, and J. Schmalian, in *The physics of superconductors*, Eds.: K. H. Bennemann and J. B. Ketterson, Vol. 1, chapter 7, Springer (Heidelberg), 2003.

[11] D. Manske, I. Eremin, and K.H. Bennemann, Phys. Rev. B **67**, 134520 (2003).

[12] H. F. Fong *et al.*, Phys. Rev. B **61**, 14773 (2000).

[13] N. E. Bickers, D. J. Scalapino, and S. R. White, Phys. Rev. Lett. **62**, 961 (1989); N. E. Bickers and D. J. Scalapino, Annals Phys. **193**, 206 (1989); P. Monthoux and D. J. Scalapino, Phys. Rev. Lett. **72**, 1874 (1995).

[14] T. Dahm and L. Tewordt, Phys. Rev. Lett. **74**, 793 (1995).

[15] M. Langer, J. Schmalian, S. Grabowski, and K. H. Bennemann, Phys. Rev. Lett. **75**, 4508 (1995).

[16] St. Lenck, J.P. Carbotte, and R. C. Dynes, Phys. Rev. B **50**, 10149 (1994).

[17] N. F. Berk and J. R. Schrieffer, Phys. Rev. Lett. **17**, 433 (1966).

[18] Y. Nambu, Phys. Rev. **117**, 648 (1960).

[19] J. R. Schrieffer, *Theory of Superconductivity*, Addison-Wesley (Redwood City, 1964).

[20] D. Manske, I. Eremin, and K.H. Bennemann, Phys. Rev. B **63**, 054517 (2001).

[21] P. Bourges *et al.*, Science **288**, 1234 (2000).

[22] J. Tranquada *et al.*, cond-mat/0310231 (unpublished).

[23] A. D. Gromko *et al.*, Phys. Rev. B **68**, 174520 (2003).

[24] S. V. Borisenko *et al.*, Phys. Rev. Lett. **90**, 207001 (2003); T. K. Kim *et al.*, Phys. Rev. Lett. **91**, 167002 (2003).

[25] The possible reason why for electron-doped cuprates neither a kink nor a resonance peak is observed has been discussed in Ref. [11].

DYNAMICAL SPIN SUSCEPTIBILITY IN SINGLET-CORRELATED BAND MODEL

M.V. Eremin
Physics Department, Kazan State University, 420008 Kazan, Russian Federation
Mikhail.Eremin@ksu.ru

I.Eremin
Institut fur Theoretische Physik, Freie Universitat Berlin, Arnimallee 14, D-14195 Berlin, Germany
ieremin@physik.fu-berlin.de

Abstract Starting from the three-band p – d Hubbard Hamiltonian we derive the effective single-correlated model Hamiltonian including electron-phonon interaction of quasiparticles with optical phonons and strong electron correlations. Within an effective Hamiltonian we analyze their influence on the dynamical spin susceptibility in layered cuprates. We find an isotope effect on resonance peak in the magnetic spin susceptibility, Im $\chi(\mathbf{q}, \omega)$, seen by inelastic neutron scattering. It results from both the electron-phonon coupling and the electronic correlation effects taken into account beyond random phase approximation(RPA) scheme.

Keywords: High-T_c cuprates, spin susceptibility, electron-phonon interaction

Introduction

An understanding of the elementary and the spin excitations in high-T_c cuprates is of central significance. For example, it is known that the Cooper-pairing scenario via the exchange of antiferromagnetic spin fluctuations was quite successful in explaining the various features of superconductivity in hole-doped cuprates such as $d_{x^2-y^2}$-wave symmetry of the superconducting order parameter and its feedback on the elementary and spin excitatitions[1]. Most importanly, in this scenario the dynamical spin susceptibility, $\chi(\mathbf{q}, \omega)$, controls mainly the superconducting and normal state properties of the layered cuprate [1]. One of the key experimental fact in the phenomenology of high-T_c cuprates is the occurrence of a so-called resonance peak in the inelastic neutron scattering(INS) experiments[2, 3]. It occurs below T_c in the dynamical spin susceptibility, $\chi(\mathbf{q}, \omega)$, at the antiferromagnetic wave vector $\mathbf{Q} = (\pi, \pi)$ and $\omega \approx \omega_{res}$ which is of the order of 40meV in the optimally doped cuprates. Its

J. Ashkenazi et al. (eds.), New Challenges in Superconductivity: Experimental Advances and Emerging Theories, 177-186.

feedback in various electronic properties like optical conductivity, Raman response function, and elementary excitations has been observed experimentally by various techniques[1]. Furthermore, its successful explanation within spin-fluctuation-mediated Cooper-pairing together with $d_{x^2-y^2}$-wave symmetry of the superconducting order parameter favors this scenario as a basic one for superconductivity in the cuprates. On the other hand, recent experiments indicate that also electron-phonon interaction influences strongly their behavior[4–7]. In particular, the observation of the relatively large isotope effect in various characteristics of cuprates like penetration depth[4], 'kink'-structure seen by ARPES[8] still raises a question: what is the role of phonons in determining the superconducting properties of cuprates?

Here, we derive an effective $t-J$ Hamiltonian where both the hopping integral, t, and the superexchange interaction between neighboring spins, J, are renormalized by phonons. We analyze the influence of the electron-phonon interaction on the dynamical spin susceptibility in layered cuprates. In particular, we find an isotope effect on the resonance peak in the magnetic spin susceptibility, $\mathrm{Im}\chi(\mathbf{q},\omega)$. It results from both the electron-phonon coupling and the electronic correlation effects taken into account beyond random phase approximation(RPA) scheme. We show that even if the superconductivity is driven by the magnetic exchange the characteristic energy features of cuprates can be significantly renormalized by the strong electron-phonon interaction.

1. Effective Hamiltonian

We start from the atomic limit of the three-band $p-d$ Hamiltonian

$$H_0 = \sum \epsilon_d d_{i\sigma}^\dagger d_{i\sigma} + \sum \epsilon_p p_{i\sigma}^\dagger p_{i\sigma} + \sum U_d n_{d\uparrow} n_{d\downarrow} + \sum U_p n_{p\uparrow} n_{p\downarrow} + \sum \hbar\omega_{\mathbf{q}} f_{\mathbf{q}}^\dagger f_{\mathbf{q}} \tag{1}$$

where ϵ_d and ϵ_p are the on-site energies of the copper and the oxygen holes, $n_{d\sigma} = d_{i\sigma}^\dagger d_{i\sigma}$ and $n_{p\sigma} = p_{i\sigma}^\dagger p_{i\sigma}$ are the copper $3d$ and oxygen $2p$ hole densities for site i, respectively. U_d and U_p refer to the on-site copper and oxygen Coulomb repulsion, respectively, $f_{\mathbf{q}}^\dagger$ denotes the phonon creation operator and $\hbar\omega_{\mathbf{q}}$ is a phonon energy dispersion. The hopping term between copper and oxygen

$$H_1 = \sum_\sigma t_{pd} \left(d_{a\sigma}^\dagger p_{b\sigma} + h.c. \right), \tag{2}$$

and the electron-phonon interaction

$$H_2 = \sum_{l=d,p} g_l n_l \left(f_{-\mathbf{q}}^\dagger + f_{\mathbf{q}} \right), \tag{3}$$

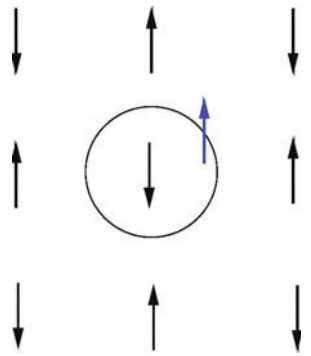

Figure 1. Illustration of the copper-oxygen singlet formation on the square lattice. The additional doped hole cannot go to the copper site due to strong on-site Coulomb repulsion and is distributed among four oxygen sites forming together with the copper spin a Zhang-Rice singlet.

we consider as a perturbation. Here, t_{pd} is a hopping term between copper and oxygen, g_l is a electron-phonon coupling strength at the site l. This notation is similar to the simplified Holstein model where the migrating charge interacts locally with breathing phonon modes forming electron-vibrational states.

To derive an effective t–J Hamiltonian we employ the canonical Schrieffer-Wolf-like transformations $e^{-S}He^{S}$ [9, 10]. The matrix of the unitary transformation for the initial Hamiltonian is found by excluding the odd terms with respect to the hopping integral with an accuracy up to the sixth order perturbation theory and the details are published elsewhere[11]. Note, in the second order perturbation the effective hopping integral, t_{ij}, appears. It is further renormalized by the electron-phonon interaction in the fourth order term where we introduce the average over the phonons. Similarly, the superexchange interaction occurs in the fourth order perturbation theory and its renormalization takes place in the sixth order term. Finally, the relevant effective Hamiltonian is given by

$$H = \sum_{ij} t_{ij} \Psi_i^{pd,\sigma} \Psi_j^{\sigma,pd} + \sum_{i>j} J_{ij} \left[(\mathbf{S}_i \mathbf{S}_j) - \frac{n_i n_j}{4} \right]. \tag{4}$$

The index pd corresponds to a Zhang-Rice singlet formation with one hole placed on the copper site whereas the second hole is distributed on the neighboring oxygen sites [12]. Namely, $\Psi_i^{pd,\sigma} = \frac{1}{\sqrt{2}} \left[X_i^{\uparrow,\downarrow} P_i^{\uparrow,0} - X_i^{\uparrow,\uparrow} P_i^{\downarrow,0} \right]$ is the copper-oxygen creation operator in terms of copper (X) and oxygen

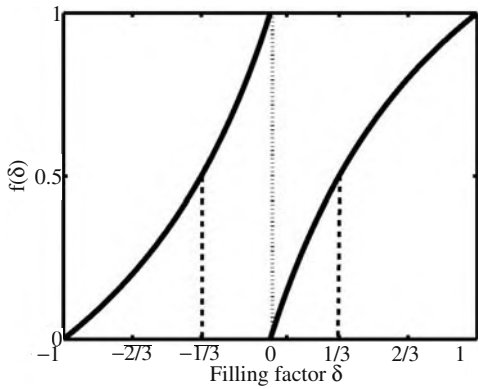

Figure 2. The spectral weight of the lower Hubbard (copper) band ($-1 < \delta < 0$) and the singlet-correlated (copper-oxygen) band ($0 < \delta < 1$). Note, the optimal doping corresponds to the half-filled copper-oxygen band which is reached for $\delta = 1/3$.

(P) projecting operators. One can check that copper-oxygen exchange term $J_{pd}\left[\left(\mathbf{S}_p\mathbf{S}_d\right) - \frac{n_d n_p}{4}\right]$ is diagonal by introducing $\Psi^{pd,\sigma}$ and $\Psi^{\sigma,pd}$ operators, i.e. $i\hbar\frac{\partial\Psi_i^{pd,\sigma}}{\partial t} = \frac{J_{pd}}{2}\Psi_i^{pd,\sigma}$.

Note, in general case the effective Hamiltonian contains also the Coulomb interaction between doped holes and the interaction of quasiparticles via the phonon field. We dropped these terms here, because they do not contribute directly to the spin susceptibility. The hopping matrix element is $t_{ij} = t_{ij}^0\, e^{-\gamma E_i^*/\hbar\omega_i^*}\left[\frac{1+\delta}{2} + \frac{2}{1+\delta} < S_i S_j >\right]$ where t_{ij}^0 is the bare hopping integral. The exponential factor takes into account electron-phonon interaction, $E_i = (g_i^*)^2/\hbar\omega_i^*$ is the so-called polaron stabilization energy of the copper-oxygen singlet state and $0 < \gamma < 1$. From the experimental data[13] the whole exponential factor was estimated to be $\gamma E_i^*/\hbar\omega_i^* \approx 0.92$ around the optimal doping. Note, its value is increasing upon decreasing doping. The effect of the copper spin correlations is described by the square brackets. In particular, one sees that for the antiferromagnetic square lattice the hopping between nearest neighbors vanishes. This is illustrated in Fig. 1. As one sees the oxygen hole cannot move between the copper sites with antiparallel spin orientation. Furthermore, there is no more than one oxygen hole per each unit cell. Then, the spectral weight of the singlet-correlated band changes upon doping similar to that of the upper Hubbard band. The half-filling is already reached at $\delta = 1/3$. This doping level we will refer to the optimal doping. We show in Fig.2 the doping evolution of the spectral weight for the lower Hubbard (copper) band and singlet-correlated (copper-oxygen) band. Note, the latter is completely filled for $\delta = 1$.

Similarly the superexchange interaction between nearest copper spins is given by

$$J = J_0 \left\{ 1 + \frac{3\hbar}{\Delta_{pd}^2} \left[E_p \omega_p \coth\left(\frac{\hbar\omega_p}{2k_B T}\right) + E_d \omega_d \coth\left(\frac{\hbar\omega_d}{2k_B T}\right) \right] \right\}, \tag{5}$$

where $\Delta_{pd} = \epsilon_p - \epsilon_d + U_p - U_d$ is the energy transfer from copper to oxygen and is known to be of the order of 1.5eV in the cuprates. Here, J_0 is the superexchange interaction of copper spins via the intermediate oxygen atom in the absence of phonons. We took the phonon frequency of the order of $\omega^* \approx \omega_p \approx \omega_d = 50$meV which roughly corresponds to the energy of the longitudinal optical(LO) bond stretching phonon mode in cuprates. According to the recent experiments[5, 6] it may play an essential role in the physics of cuprates. The so-called polaronic stabilization energy $E^* \approx E_p \approx E_d$ was estimated of the order of 0.5eV in accordance with the measurements of the isotope effect in cuprates[14].

2. Dynamical spin susceptibility

To derive the dynamical spin susceptibility in the superconducting state we use the method suggested by Hubbard and Jain[15] that allows to take into account strong electronic correlations. First we add the external magnetic field applied along c-axis into the effective Hamiltonian

$$H_i = h_{-\mathbf{q}} e^{i(\omega t - \mathbf{q}\mathbf{R_i})} + h_{\mathbf{q}} e^{-i(\omega t - \mathbf{q}\mathbf{R_i})}. \tag{6}$$

Then we write an equation of motion for the Ψ operators using the Roth-type of the decoupling scheme[16] and expanding the $P_{pd}^{\sigma} = \left\{ \Psi_i^{\sigma,pd} \Psi_i^{pd,\sigma} \right\} = \frac{1+\delta_i}{2} + \sigma \mathrm{Re} \sum_{\mathbf{q}} \left[S_{\mathbf{q}}^z e^{i(\mathbf{q}\mathbf{R_i} - \omega t)} \right]$ up to the first order in $S_{\mathbf{q}} = \chi^{zz}(\mathbf{q}, \omega) h_{\mathbf{q}}$. In particular,

$$i\hbar \frac{\partial \Psi_{\mathbf{k}}^{-\sigma,pd}}{\partial t} = (\epsilon_{\mathbf{k}} - \mu)\Psi_{\mathbf{k}}^{-\sigma,pd} + \Delta_{\mathbf{k}} \Psi_{-\mathbf{k}}^{pd,\sigma} + \left[\left(\frac{J_{\mathbf{q}}}{2} - t_{\mathbf{k}-q} \right) S_{\mathbf{q}} - \frac{h_{\mathbf{q}}}{2} \right] \Psi_{\mathbf{k}-\mathbf{q}}^{-\sigma,pd} e^{-i\omega t} \tag{7}$$

and the similar expression occurs for $\Psi_{-\mathbf{k}}^{pd,\sigma}$. Here, $\Delta_{\mathbf{k}} = \frac{\Delta_0}{2}(\cos k_x - \cos k_y)$ is $d_{x^2-y^2}$-wave superconducting gap, $J_{\mathbf{q}} = J(\cos k_x - \cos k_y)$ is the Fourier transform of the superexchange interaction on a square lattice.

The expression for the longitudinal component of the dynamical spin susceptibility can be obtained from the relation

$$\langle \Psi_i^{pd,\uparrow} \Psi_i^{\uparrow,pd} \rangle - \langle \Psi_i^{pd,\downarrow} \Psi_i^{\downarrow,pd} \rangle = 0, \tag{8}$$

and using the Bogolyubov-like transformations to the new quasiparticle states

$$\begin{aligned} X_k^{-\sigma,pd} &= u_k \psi_k^{-\sigma,pd} + v_k \psi_{-k}^{pd,\sigma}, \\ X_k^{pd,\sigma} &= u_k \psi_k^{pd,\sigma} - v_k \psi_{-k}^{pd,\sigma}. \end{aligned} \tag{9}$$

Here, $u_{\mathbf{k}}^2 = \frac{1}{2}\left(1 + \frac{\epsilon_{\mathbf{k}} - \mu}{E_{\mathbf{K}}}\right)$ and $v_{\mathbf{k}}^2 = \frac{1}{2}\left(1 - \frac{\epsilon_{\mathbf{k}} - \mu}{E_{\mathbf{K}}}\right)$ are the Bogolyubov coefficients, μ is a chemical potential, and $E_{\mathbf{k}} = \sqrt{(\epsilon_{\mathbf{k}} - \mu)^2 + \Delta_{\mathbf{k}}^2}$ is the energy dispersion in the superconducting state. Substituting Eq.(9) in Eq.(8) and using the equations of motion (7) one obtains the expression for the dynamical spin susceptibility in the form

$$\chi(\mathbf{q}, \omega) = \frac{\chi_0(\mathbf{q}, \omega)}{J_{\mathbf{q}} \chi_0(\mathbf{q}, \omega) + \Pi(\mathbf{q}, \omega) + Z(\mathbf{q}, \omega)}. \tag{10}$$

This is a central result of our paper. Here, $\chi_0(\mathbf{q}, \omega)$ is the usual BCS-like Lindhard response function, $\Pi(\mathbf{q}, \omega)$ and $Z(\mathbf{q}, \omega)$ result from the strong electronic correlation effects. In the normal state the expression for $\Pi(\mathbf{q}, \omega)$ has been obtained by Hubbard and Jain [15]. In the superconducting state it is given by

$$\begin{aligned} \Pi(\mathbf{q}, \omega) = \frac{P_{pd}}{N} \sum_{\mathbf{k}} & \\ & u_{\mathbf{k}} u_{\mathbf{k+q}} (u_{\mathbf{k}} u_{\mathbf{k+q}} + v_{\mathbf{k}} v_{\mathbf{k+q}}) \frac{t_{\mathbf{k}} f_{\mathbf{k}} - t_{\mathbf{k+q}} f_{\mathbf{k+q}}}{\omega + i0^+ + E_{\mathbf{k}} - E_{\mathbf{k+q}}} \\ & + v_{\mathbf{k}} v_{\mathbf{k+q}} (v_{\mathbf{k}} v_{\mathbf{k+q}} + u_{\mathbf{k}} u_{\mathbf{k+q}}) \frac{t_{\mathbf{k}} (1 - f_{\mathbf{k}}) - t_{\mathbf{k+q}} (1 - f_{\mathbf{k+q}})}{\omega + i0^+ - E_{\mathbf{k}} + E_{\mathbf{k+q}}} \\ & + u_{\mathbf{k}} v_{\mathbf{k+q}} (u_{\mathbf{k}} v_{\mathbf{k+q}} - u_{\mathbf{k+q}} v_{\mathbf{k}}) \frac{t_{\mathbf{k}} f_{\mathbf{k}} - t_{\mathbf{k+q}} (1 - f_{\mathbf{k+q}})}{\omega + i0^+ + E_{\mathbf{k}} + E_{\mathbf{k+q}}} \\ & + u_{\mathbf{k+q}} v_{\mathbf{k}} (v_{\mathbf{k}} u_{\mathbf{k+q}} - u_{\mathbf{k}} v_{\mathbf{k+q}}) \frac{t_{\mathbf{k}} (1 - f_{\mathbf{k}}) - t_{\mathbf{k+q}} f_{\mathbf{k+q}}}{\omega + i0^+ - E_{\mathbf{k}} - E_{\mathbf{k+q}}}. \end{aligned} \tag{11}$$

The function $Z(\mathbf{q}, \omega)$ is written as follows

$$Z(\mathbf{q}, \omega) = \frac{1}{N} \sum_{\mathbf{k}} \frac{\omega + i0^+}{\omega + i0^+ + \epsilon_{\mathbf{k}}^{(1)} - \epsilon_{\mathbf{k+q}}^{(1)}}. \tag{12}$$

Here, $f_{\mathbf{k}}$ is the Fermi distribution function, $\epsilon_{\mathbf{k}}^{(1)} = \frac{1-\delta}{2} t_{\mathbf{k}}$, $\epsilon_{\mathbf{k}} = P_{pd} t_{\mathbf{k}}$ is the energy dispersion in the normal state, and $t_{\mathbf{k}} = 2t(\cos k_x + \cos k_y) +$

$4t'\cos k_x \cos k_y + 2t''(\cos 2k_x + \cos 2k_y)$ is the Fourier transform of the hopping integral on a square lattice including nearest, next- and next-next-nearest neighbor hopping, respectively. The origin of the terms $\Pi(\mathbf{q}, \omega)$ and $Z(\mathbf{q}, \omega)$ relates to the no double occupancy constraint. In particular, for the Coulomb repulsion $U = \infty$ and $J = 0$ the dynamical spin susceptibility does not reduce to the standard Lindhard response function but is renormalized by the electronic correlation effects[17]. For the $\Delta_{\mathbf{k}} = 0$ Eq.(10) agrees with the normal state result for the dynamical spin susceptibility[15, 18, 19].

3. Results and Discussion

Inelastic neutron scattering(INS) measurements probe directly the imaginary part of the dynamical spin susceptibility. Therefore, it is of interest to analyze the role played by the electronic correlations in connection with the 'resonance' peak seen by INS[3]. This feature is well understood using various approaches[20, 21] as a result of the spin density wave(SDW) collective mode formation at $\omega = \omega_{res,}$ *i.e.* when the denominator of the RPA spin susceptibility at the antiferromagnetic wave vector $\mathbf{Q}$ is close to zero.

Let us first concentrate on the influence of the electronic correlations beyond RPA on the resonance peak formation at $\mathbf{Q} = (\pi, \pi)$ In Fig. 3(a) we show results of our calculations for the Im $\chi(\mathbf{Q}, \omega)$ from Eq. (10) as a function of frequency and $q_x(q_y = \pi)$ in the superconducting state. Here, we use $t = 200, t' = -20$, and $t'' = 4$ (in meV) at optimal doping. For comparison we also put RPA results using the same parameters in Fig.3(b). Clearly, additional electronic correlations beyond RPA (Π and Z terms) affect significantly the Imχ behavior in the superconducting state. First, in contrast to the RPA the position of the resonance peak obtained from Eq.(10) is shifted to a lower frequencies. The main reason is that due to Π and Z–terms the resonance condition can be satisfied easily in a more wide range of parameters. Furthermore, its intensity is also much higher than in the RPA case. In addition, the upper branch of the resonance peak dispersion away from ω_{res} and $\mathbf{Q}_{AF}$ is much more pronounced. Note, these dispersion curves $\propto \mathbf{q}^2$ are in good agreement with experiment[22, 23]. Finally, we discuss the influence of the electron-phonon interaction on the resonance peak formation by changing the isotope mass of ^{16}O by ^{18}O. This shifts the average frequency of the LO phonon mode and consequently renormalizes the hopping integral t and the superexchange coupling constant, J. Most importantly, the electron-phonon interaction changes most dramatically the hopping integral t rather than the superexchange coupling J. In particular, as can be seen from Eq.(5) the superexchange coupling constant J changes less than 1% upon substituting the isotopes[24] which agrees well with experimental data[25]. Therefore, there is almost no influence of the isotope substitution on the resonance peak determined from RPA, since

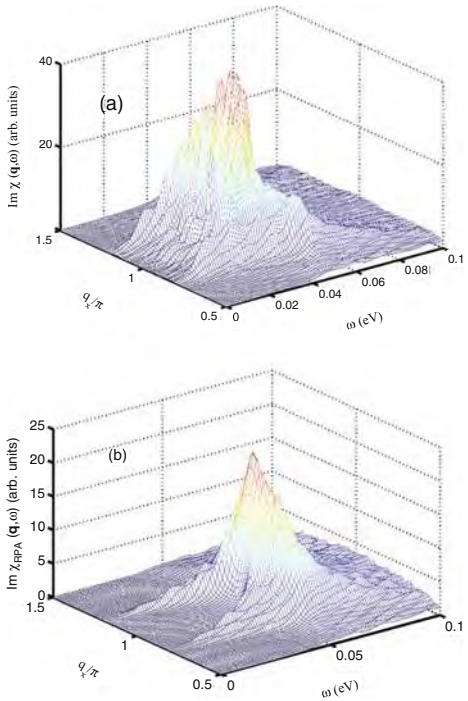

Figure 3. Dispersion of the resonance peak calculated from Eq.(10)(a) as a function of frequency and q_x away from (π, π). Two branches of the dispersion curves are in good agreement with recent experimental data [23]. For comparison we also put the RPA results(b) using the same parameters.

in this approximation its formation is determined mainly by J. In particular, we find *within* **RPA** no change in the ω_{res} value upon changing the isotopes. in the case of Eq.(10) the most important contribution to the isotope effect on the resonance peak appears due to $\Pi(\mathbf{q}, \omega) \propto t_k$. In particular, using our estimation given above we find that at optimal doping the hopping integral changes by 6% upon replacing ^{16}O by ^{18}O. This results in the lowering of the resonance frequency at (π, π) from 41meV for the ^{16}O isotope towards 39meV for the ^{18}O sample. This leads to $\alpha_{res} = -\frac{d\ln \omega_{res}}{d\ln M} \approx 0.4$ for optimally-doped cuprates. This effect is beyond the experimental error and can be further tested experimentally. Furthermore, in the underdoped cuprates one may expect larger isotope effect due to a larger value of $\gamma E_i^*/\hbar\omega_i^*$[13]. At the same time the superconducting transition temperature which is determined by J shows much weaker isotope effect and is around $\alpha_{T_c} \approx 0.05$ [24]. Therefore, even if the superconductivity is driven by the magnetic exchange the resonance peak formation can be significantly renormalized by the strong electron-phonon interaction.

4. Summary

To summarize, we analyze the influence of the electronic correlations and the electron-phonon interaction on the dynamical spin susceptibility in layered cuprates. The electronic correlations taken beyond RPA redistribute the spectral weight of the resonance peak away from (π, π) leading to the pronounced dispersion. This is in good agreement with recent INS data[22, 23]. Furthermore, we find the isotope effect on the resonance peak due to strong coupling of the carriers to LO phonon mode. It results from both electron-phonon coupling and electronic correlation effects. In contrast to the small isotope effect on the superconducting transition temperature we find larger isotope coefficient on the resonance peak $\alpha_{res} \approx 0.4$ in optimally-doped cuprates. We also would like to note that the value of the isotope coefficient depends strongly on the value of the exponential factor. Therefore, the experimental verification of our prediction is desirable. In particular, it would put a strong constraint on the ingredients the theory of cuprates must contain.

It's pleasure to thank Ph. Bourges and P. Meier for useful discussions. The work of I.E. is supported by INTAS grant No. 01-0654. M.V.E. is supported by the RFBR Grant No. 03-02-16550 and RSP "Superconductivity" 98014-3.

References

[1] Chubukov A.V., Pines D., and Schmalian J., (2003). "A Spin Fluctuation Model for d-wave Superconductivity" in *The Physics of Conventional and Unconventional Superconductors* eds. by Bennemann K.H. and Ketterson J.B., Vol. 1 (Springer-Verlag).

[2] He H., Bourges P., Sidis Y., Ulrich C., Regnault L.P., Pailhes S., Berzigiarova N.S., Kolesnikov N.N., and Keimer B., (2002). Magnetic Resonant Mode in the Single-Layer High-Temperature Superconductor $Tl_2Ba_2CuO_{6+\delta}$. *Science* 295:1045–1047.

[3] See for review Bourges P., (1998). "From Magnons to the Resonance Peak: Spin Dynamics in High-T_c Superconducting Cuprates by Inelastic Neutron Scattering" in *The Gap Symmetry and Fluctuations in High Temperature Superconductors* edited by Bok J., Deutscher G., Pavuna D., and Wolf S.A. (Plenum Press), pp.349–371.

[4] Khasanov R., Eshchenko D.G., Luetkens H., Morenzoni E., Prokscha T., Suter A., Garifianov N., Mali M., Roos J., Conder K., and Keller H., (2003). The oxygen-isotope effect on the in-plane penetration depth in underdoped $Y_{1-x}Pr_xBa_2Cu_3O_{7-\delta}$ as revealed by muon-spin rotation. *J. Phys.: Condens. Matter* 15:L17–L24.

[5] McQueeney R.J., Sarrao J.L., Pagliuso P.G., Stephens P.W., and Osborn R., (2001). Mixed Lattice and Electronic States in High-Temperature Superconductors. *Phys. Rev. Lett.,* 87:077001.

[6] Pintschovius L., Endoh Y., Reznik D., Hiraka H., Tranquada J.M., Reichardt W., Uchiyama H., Masui T., Tajima S., (2003). Evidence for Dynamic Charge Stripes in the Phonons of Optimally Doped YBCO. cond-mat/0308357 (unpublished).

[7] For review of earlier results see Kulic M., (2000). Interplay of electron-phonon interaction and strong correlations: the possible way to high-temperature superconductivity. *Phys. Rep.* 338:1–264.

[8] Lanzara A., private communication.
[9] Schrieffer J.R., and Wolf P.A., (1966). Relation between the Anderson and Kondo Hamiltonians. *Phys. Rev.* 149:491–492.
[10] Kugel K.I., and Khomskii D.L., (1980). Polaron effects and exchange interaction in magnetic insulators with Jahn-Teller ions. *Zh. Eksp. Teor. Fiz.* 79:987–1005 [*Sov. Phys. JETP* 52:501–515].
[11] Eremin I., Kamaev O., and Eremin M.V., (2004). Possible isotope effect on the resonance peak formation in high-T_c cupraes. Phys. Rev. B 69:094517.
[12] Zhang F.C., and Rice T.M., (1988). Effective Hamiltonian for the superconducting Cu oxides. *Phys. Rev. B* 37:3759–3761.
[13] Zhao G.-M., Hunt M.B., Keller H., and Mueller K.A., (1997). Evidence for polaronic supercarriers in the copper oxide superconductors $La_{2-x}Sr_xCuO_4$. *Nature* 385:236–239.
[14] Zhao G.-M., Keller H., and Conder K., (2001). Unconventional isotope effects in the high-temperature cuprate superconductors. *J. Phys.: Condens. Matter* 13:R569–R587.
[15] Hubbard J., and Jain K.P., (1968). Generalized spin susceptibility in the correlated narrow-energy-band model. *J. Phys. C (Proc. Phys. Soc.), Ser. 2* 1:1650–1657.
[16] Plakida N.M., Hayn R., and Richard J.L., (1995). Two-band singlet-hole model for the copper oxide plane. *Phys. Rev. B* 51:16599–16607.
[17] Note, the term $Z(\mathbf{q}, \omega)$ in the dynamical spin susceptibility occurs in the higher order decoupling scheme for the Green's function. It originates from the spin fluctuations in the singlet *pd*-band and lower Hubbard (copper) band, which is in hole-doped cuprates is completely filled.
[18] Zavidonov A.Yu., and Brinkmann D., (1998). Evolution of antiferromagnetic short-range order with doping in high-T_c superconductors. *Phys. Rev. B* 58:12486–12494.
[19] Eremin M., Eremin I., and Varlamov S., (2001). Dynamical charge susceptibility in layered cuprates: Beyond the conventional random-phase-approximation scheme. *Phys. Rev. B* 64:214512. Eremin I., (1997), *Physica (Amsterdam) B*, **234–236**, 792.
[20] Onufrieva F., and Pfeuty P., (2002). Spin dynamics of a two-dimensional metal in a superconducting state: Application to the high-T_c cuprates *Phys. Rev. B* 65:054515; Manske D., Eremin I., and Bennemann K.H., (2001). Analysis of the resonance peak and magnetic coherence seen in inelastic neutron scattering of cuprate superconductors: A consistent picture with tunneling and conductivity data. *Phys. Rev. B* 63:054517.
[21] Norman M.R. (2001). Magnetic collective mode dispersion in high-temperature superconductors. *Phys. Rev. B* 63:092509.
[22] Arai M., Nishijima T., Endoh Y., Egami T., Tajima S., Tomimoto T., Shiohara Y., Takahashi M., Garrett A., and Bennington S.M., (1999). Incommensurate Spin Dynamics of Underdoped Superconductor $YBa_2Cu_3O_6.7$. *Phys. Rev. Lett.* 83:608–612.
[23] Reznik D., Bourges P., Pintschovius L., Endoh Y., Sidis Y., Shiokara Y., and Tajima S., (2003). Dispersion of Magnetic Excitations in Superconducting Optimally Doped $YBa_2Cu_3O_{6.95}$. cond-mat/0307591 (unpublished).
[24] Eremin M.V., Eremin I.M., Larionov I.A., and Terzi A. V., (2002). Polaron Effects on Superexchange Interaction: Isotope Shifts of T_N, T_c, and T^* in Layered Copper Oxides. *Pis'ma Zh. Eksp. Teor. Fiz.* 75:467–470 [*JETP Lett.* 75:395–398].
[25] Zhao G.-M., Singh K.K., and Morris D.E., (1994). Oxygen isotope effect on Neel temperature in various antiferromagnetic cuprates. *Phys. Rev. B* 50:4112–4117.

STRIPE-LIKE INHOMOGENEITIES, COHERENCE, AND THE PHYSICS OF THE HIGH T_C CUPRATES

J. Ashkenazi
Physics Department, University of Miami, P.O. Box 248046, Coral Gables, FL 33124, U.S.A.
jashkenazi@miami.edu

Abstract The carriers in the high-T_c cuprates are found to be polaron-like "stripons" carrying charge and located in stripe-like inhomogeneities, "quasi-electrons" carrying charge and spin, and "svivons" carrying spin and some lattice distortion. The anomalous spectroscopic and transport properties of the cuprates are understood. The stripe-like inhomogeneities result from the Bose condensation of the svivon field, and the speed of their dynamics is determined by the width of the double-svivon neutron-resonance peak. The connection of this peak to the peak-dip-hump gap structure observed below T_c emerges naturally. Pairing results from transitions between pair states of stripons and quasi-electrons through the exchange of svivons. The pairing symmetry is of the $d_{x^2-y^2}$ type; however, sign reversal through the charged stripes results in features not characteristic of this symmetry. The phase diagram is determined by pairing and coherence lines within the regime of a Mott transition. Coherence without pairing results in a Fermi-liquid state, and incoherent pairing results in the pseudogap state where localized electron and electron pair states exist within the Hubbard gap. A metal-insulator-transition quantum critical point occurs between these two states at $T = 0$ when the superconducting state is suppressed. An intrinsic heterogeneity is expected of superconducting and pseudogap nanoscale regions.

Keywords: High-T_c, cuprates, stripes, inhomogeneities, pairing symmetry, Mott transition

1. Introduction

It is suggested that the anomalous physics of cuprates, including the existence of high-T_c superconductivity, can be understood as the result of a behavior typical of their structure within the regime of a Mott transition. Theoretical calculations, and a variety of experimental data, support the assumption that their microscopic structure, within this regime, is often characterized by dynamic stripe-like inhomogeneities.

To study this regime, a combination of large-U and small-U orbitals is considered, where major aspects within the CuO_2 planes are approached by the $t-t'-J$ model. The large-U electrons, residing in these planes, are treated by the "slave-fermion" method [1]. Such an electron in site i and spin σ is created by $d^\dagger_{i\sigma} = e^\dagger_i s_{i,-\sigma}$, if it is in the "upper-Hubbard-band", and by $d'^\dagger_{i\sigma} = \sigma s^\dagger_{i\sigma} h_i$, if it

J. Ashkenazi et al. (eds.), New Challenges in Superconductivity: Experimental Advances and Emerging Theories, 187-212.

is in a Zhang-Rice-type "lower-Hubbard-band". Here e_i and h_i are ("excession" and "holon") fermion operators, and $s_{i\sigma}$ are ("spinon") boson operators. These auxiliary operators have to satisfy the constraint: $e_i^\dagger e_i + h_i^\dagger h_i + \sum_\sigma s_{i\sigma}^\dagger s_{i\sigma} = 1$.

An auxiliary space is introduced within which a chemical-potential-like Lagrange multiplier is used to impose the constraint on the average. Physical observables are projected into the physical space by expressing them as combinations of Green's functions of the auxiliary space. Since the time evolution of Green's functions is determined by the Hamiltonian which obeys the constraint rigorously, it is not expected to be violated as long as justifiable approximations are used.

The reader is referred to previous publications by the author [2, 3] which include technical details concerning the work discussed here.

2. Auxiliary Fields

Uncoupled auxiliary fields are considered at the zeroth order, where the spinon field is diagonalized by applying the Bogoliubov transformation for bosons [4]:

$$s_\sigma(\mathbf{k}) = \cosh(\xi_{\sigma\mathbf{k}})\zeta_\sigma(\mathbf{k}) + \sinh(\xi_{\sigma\mathbf{k}})\zeta_{-\sigma}^\dagger(-\mathbf{k}). \tag{1}$$

Spinon states created by $\zeta_\sigma(\mathbf{k})$ have "bare" energies $\epsilon^\zeta(\mathbf{k})$, having a V-shape zero minimum at $\mathbf{k} = \mathbf{k}_0$. Bose condensation results in an antiferromagnetic (AF) order of wave vector $\mathbf{Q} = 2\mathbf{k}_0 = \left(\frac{\pi}{a}, \frac{\pi}{a}\right)$. Within the lattice Brillouin zone (BZ) there are four inequivalent possibilities for $\mathbf{k}_0$: $\pm\left(\frac{\pi}{2a}, \frac{\pi}{2a}\right)$ and $\pm\left(\frac{\pi}{2a}, -\frac{\pi}{2a}\right)$, thus introducing a broken symmetry. One has [4]:

$$\begin{aligned}
\cosh(\xi_\mathbf{k}) &\to \begin{cases} +\infty, & \text{for } \mathbf{k} \to \mathbf{k}_0, \\ 1, & \text{for } \mathbf{k} \text{ far from } \mathbf{k}_0, \end{cases} \\
\sinh(\xi_\mathbf{k}) &\to \begin{cases} -\cosh(\zeta_\mathbf{k}), & \text{for } \mathbf{k} \to \mathbf{k}_0, \\ 0, & \text{for } \mathbf{k} \text{ far from } \mathbf{k}_0. \end{cases}
\end{aligned} \tag{2}$$

The dynamic stripe-like inhomogeneities are approached adiabatically, treating them statically with respect to the electrons dynamics. Their underlying structure is characterized [5] by narrow charged stripes forming antiphase domain walls between wider AF stripes. Within the one-dimensional charged stripes it is justified to use the spin-charge separation approximation under which two-particle spinon-holon (spinon-excession) Green's functions are decoupled into single-auxiliary-particle Green's functions. Holons (excessions) within the charged stripes are referred to as "stripons" (of charge − e), created by $p_\mu^\dagger(\mathbf{k})$.

Localized stripon states are assumed at the zeroth order, due to the disordered one-dimensional nature of the charged stripes. Their k wave vectors present

k-symmetrized combinations of localized states to be treated in a perturbation expansion when coupling to the other fields is considered.

Away from the charged stripes, creation operators of approximate fermion basis states of coupled holon-spinon and excession-spinon pairs are constructed [2]. Together with the small-U states they form, within the auxiliary space, a basis to "quasi-electron" (QE) states, created by $q^{\dagger}_{\iota\sigma}(\mathbf{k})$. The bare QE energies $\epsilon^{q}_{\iota}(\mathbf{k})$ form quasi-continuous ranges of bands within the BZ.

When the cuprates are doped, such QE states are transferred from the upper and lower Hubbard bands to the vicinity of the Fermi level (E_{F}). The amount of states transferred is increasing with the doping level, moving from the insulating to the metallic side of the Mott transition regime.

Hopping and hybridization terms introduce strong coupling between the QE, stripon and spinon fields, which is expressed by a coupling Hamiltonian of the form (for p-type cuprates):

$$\begin{aligned}\mathcal{H}' = \frac{1}{\sqrt{N}} \sum_{\iota\lambda\mu\sigma} \sum_{\mathbf{k},\mathbf{k}'} \{ & \sigma \epsilon^{qp}_{\iota\lambda\mu}(\sigma\mathbf{k}, \sigma\mathbf{k}') q^{\dagger}_{\iota\sigma}(\mathbf{k}) p_{\mu}(\mathbf{k}') \\ & \times [\cosh(\xi_{\lambda,\sigma(\mathbf{k}-\mathbf{k}')}) \zeta_{\lambda\sigma}(\mathbf{k}-\mathbf{k}') \\ & + \sinh(\xi_{\lambda,\sigma(\mathbf{k}-\mathbf{k}')}) \zeta^{\dagger}_{\lambda,-\sigma}(\mathbf{k}'-\mathbf{k})] + h.c.\}. \end{aligned} \tag{3}$$

Using the formalism of Green's functions ($\mathcal{G}$), the QE, stripon and spinon propagators are couples by a vertex introduced through $\mathcal{H}'$ [6].

The stripe-like inhomogeneities are strongly coupled to the lattice, and it is the presence of stripons which creates the charged stripes within them. Consequently, processes involving transitions between stripon and QE states (which, through $\mathcal{H}'$, are followed by the emission and/or absorption of spinons) involve also lattice displacements. Since the hopping and hybridization terms depend on the atomic positions [7], the effect of these lattice displacements can be expressed by modifying $\mathcal{H}'$ in Eq. (3), adding to each of the spinon creation and annihilation operators there a term in which the spinon operator is multiplied by a lattice displacement operator. This introduces a new vertex due to which the spinons are renormalized, becoming "dressed" by phonons, and thus carry some lattice distortion in addition to spin. Such phonon-dressed spinons are referred to as "svivons", and the physical effect of the new vertex, which is most relevant here, is assumed to be the replacement the spinons by svivons in the $\mathcal{H}'$ vertex.

The physical signature of the auxiliary fields, within the t–t'–J model, is demonstrated in Fig. 1, where an adiabatic "snapshot" of a section of a CuO_2 plane, including a stripe-like inhomogeneity, is shown. Within the adiabatic time scale a site is "spinless" either if it is "charged", removing the spinned electron/hole on it (as in "stripon sites" in Fig. 1), or if the spin is fluctuating on a shorter time scale (due to, *e.g.*, being in a singlet spin pair). In this description,

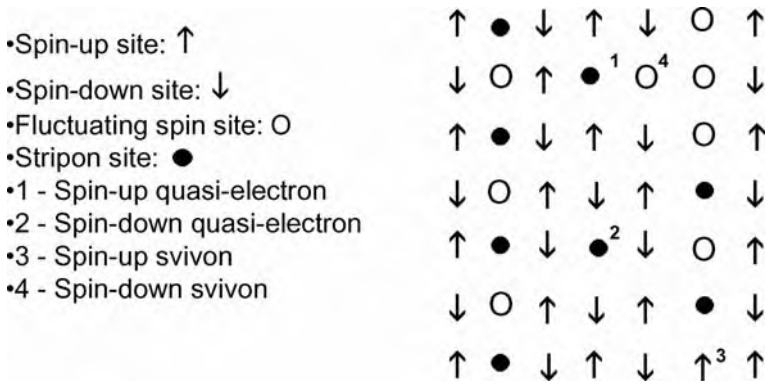

Figure 1. An adiabatic "snapshot" of a stripe-like inhomogeneity and carriers within a CuO_2 plane.

a site stripon excitation represents a transition between these two types of a spinless site within the charged stripes, a site svivon excitation represents a transition between a spinned site and a fluctuating-spin spinless site, and a site QE excitation represents a transition between a spinned site and a charged spinless site within the AF stripes. The dynamics of these sites is ignored in Fig. 1 for demonstration purposes.

3. Auxiliary Spectral Functions

Self-consistent expressions are derived [2] for the spectral functions A^q, A^p, and A^ζ for the QE's, stripons, and svivons, respectively [$A(\omega) \equiv \Im\mathcal{G}(\omega - i0^+)/\pi$], including the scattering rates Γ^q, Γ^p, and Γ^ζ[$\Gamma(\omega) \equiv 2\Im\Sigma(\omega - i0^+)$], and the real parts of the self-energies $\Re\Sigma^q$, $\Re\Sigma^p$ and $\Re\Sigma^\zeta$. Since the stripon bandwidth turns out to be considerably smaller than the QE and svivon bandwidths, a phase-space argument could be used, as in the Migdal theorem, to ignore vertex corrections to the $\mathcal{H}'$ vertex.

The expressions are derived for the intermediary energy range (and the $T \to 0$ limit), where the high energy range ($\gtrsim 0.5$ eV) is treated by introducing cut-off integration limits at $\pm\omega_c$ (resulting in spurious logarithmic divergencies at $\pm\omega_c$), and the low energy range ($\lesssim 0.02$ eV) introduces non-analytic behavior at "zero-energy". The **k** dependence is omitted in the expressions for simplicity, and all the coefficients appearing in them are positive. The expressions for the auxiliary spectral functions are:

$$A^q(\omega) \cong \begin{cases} a^q_+\omega + b^q_+, & \text{for } \omega > 0, \\ -a^q_-\omega + b^q_-, & \text{for } \omega < 0, \end{cases} \tag{4}$$

$$A^q(\omega) \cong \delta(\omega), \tag{5}$$

$$A^{\zeta}(\omega) \cong \begin{cases} a^{\zeta}_{+}\omega + b^{\zeta}_{+}, & \text{for } \omega > 0, \\ a^{\zeta}_{-}\omega - b^{\zeta}_{-}, & \text{for } \omega < 0. \end{cases} \tag{6}$$

Analyticity is restored in the low-energy range, and specifically $A^{\zeta}(\omega = 0) = 0$. Special behavior occurs for svivons around $\mathbf{k}_0$. The expressions for the QE and svivon scattering rates are:

$$\frac{\Gamma^{q}(\omega)}{2\pi} \cong \begin{cases} c^{q}_{+}\omega + d^{q}_{+}, & \text{for } \omega > 0, \\ -c^{q}_{-}\omega + d^{q}_{-}, & \text{for } \omega < 0, \end{cases} \tag{7}$$

$$\frac{\Gamma^{\zeta}(\omega)}{2\pi} \cong \begin{cases} c^{\zeta}_{+}\omega + d^{\zeta}_{+}, & \text{for } \omega > 0, \\ c^{\zeta}_{-}\omega - d^{\zeta}_{-}, & \text{for } \omega < 0, \end{cases} \tag{8}$$

and those for the real parts of their self energies are:

$$\begin{aligned} -\Re\Sigma^{q}(\omega) \;\cong\; & \omega_c(c^{q}_{+} - c^{q}_{-}) + (d^{q}_{+} \ln|\frac{\omega - \omega_c}{\omega}| - d^{q}_{-} \ln|\frac{\omega + \omega_c}{\omega}|) \\ & + \omega(c^{q}_{+} \ln|\frac{\omega - \omega_c}{\omega}| + c^{q}_{-} \ln|\frac{\omega + \omega_c}{\omega}|), \end{aligned} \tag{9}$$

$$\begin{aligned} -\Re\Sigma^{\zeta}(\omega) \;\cong\; & \omega_c(c^{\zeta}_{+} + c^{\zeta}_{-}) + (d^{\zeta}_{+} \ln|\frac{\omega - \omega_c}{\omega}| + d^{\zeta}_{-} \ln|\frac{\omega + \omega_c}{\omega}|) \\ & + \omega(c^{\zeta}_{+} \ln|\frac{\omega - \omega_c}{\omega}| - c^{\zeta}_{-} \ln|\frac{\omega + \omega_c}{\omega}|). \end{aligned} \tag{10}$$

The logarithmic divergencies at $\omega = 0$ are truncated by analyticity in the low-energy range.

For the case of p-type cuprates the following inequalities exist between the coefficients:

$$a^{q}_{+} > a^{q}_{-},\ b^{q}_{+} > a^{q}_{-},\quad c^{q}_{+} > c^{q}_{-},\quad d^{q}_{+} > d^{q}_{-}, \tag{11}$$

$$a^{\zeta}_{+} > a^{\zeta}_{-},\ b^{\zeta}_{+} > b^{\zeta}_{-},\quad c^{\zeta}_{+} > c^{\zeta}_{-},\quad d^{\zeta}_{+} > d^{\zeta}_{-}. \tag{12}$$

For "real" n-type cuprates, in which the stripons are based on excession and not holon states, the direction of the inequalities is reversed for the QE coefficients (11), but stays the same for the svivon coefficients (12). Deviations from these inequalities, especially for the $a\pm$ and $b\pm$ coefficients, could occur due to band-structure effects, and at specific $\mathbf{k}$ points; by Eq. (2) they almost disappear for svivons close to point $\mathbf{k}_0$.

The auxiliary-particle energies are renormalized (from ϵ to $\bar{\epsilon}$) through: $\bar{\epsilon} = \epsilon + \Re\Sigma(\bar{\epsilon})$. This renormalization is particularly strong for the stripon energies, and their bandwidth drops down to the low energy range [thus having a δ-function for $A^{p}(\omega)$ in Eq. (5)].

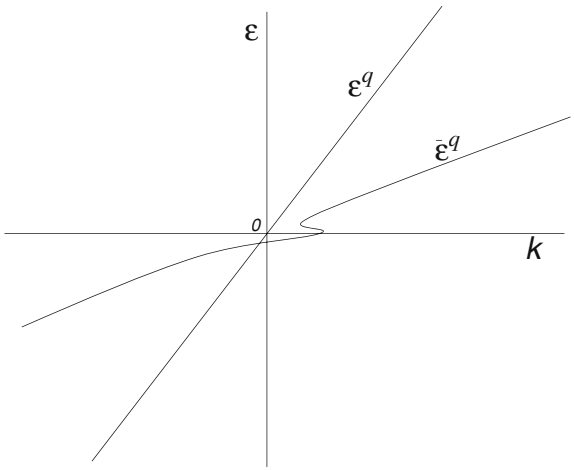

Figure 2. A typical self-energy renormalization of the QE energies, for p-type cuprates.

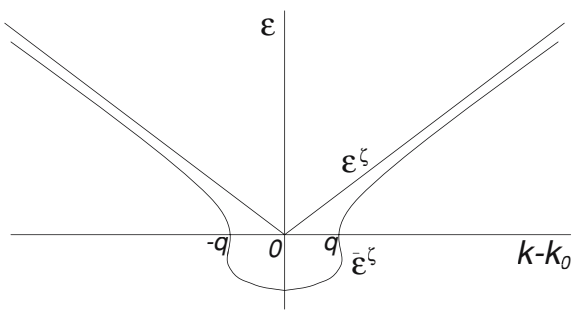

Figure 3. A typical self-energy renormalization of the svivon energies around the minimum at k_0.

A typical renormalization of the QE energies (for p-type cuprates), around zero energy, is shown in Fig. 2. The kink-like behavior around zero energy is a consequence of the logarithmic singularity at $\omega = 0$ (truncated in the low energy range) in the $(d_+^q - d_-^q)$ In $|\omega|$ term in Eq. (9) for $\Re\Sigma^q$. The asymmetry between positive and negative energies is a consequence of inequality (11), and this asymmetry is expected to be inverted for real n-type cuprates.

A typical renormalization of the svivon energies, around the V-shape zero minimum of ϵ^ζ at $\mathbf{k}_0$, is shown in Fig. 3. The significant effect results from the $(d_+^\zeta + d_-^\zeta)\ln|\omega|$ term in Eq. (10) for $\Re\Sigma^\zeta(\omega)$, contributing a logarithmic singularity at $\omega = 0$ (which is truncated in the low-energy range). By Eq. (8) $\bar{\epsilon}^\zeta$ is expected to have a considerable linewidth around $\mathbf{k}_0$ (except where it crosses zero). But the existence of a pairing gap in the low-energy QE and stripon

states, coupled by svivons around $\mathbf{k}_0$, disables the scattering processes causing the linewidth near the negative minimum of $\bar{\epsilon}^{\zeta}$ at $\mathbf{k}_0$.

This renormalization of the svivon energies changes the physical signature of their Bose condensation from an AF order to the observed stripe-like inhomogeneities (including both their spin and lattice aspects). The structure of $\bar{\epsilon}^{\zeta}$ around its minimum at $\mathbf{k}_0$ determines the structure of these inhomogeneities, and their dynamics depends on the linewidth of $\bar{\epsilon}^{\zeta}$ around $\mathbf{k}_0$, becoming slower (and thus detectable) in a pairing state.

As was mentioned above, the stripon states are based on localized states in the charged stripe-like inhomogeneities (see Fig. 1), to which some itineracy is introduced by coupling to the QE and svivon states through $\mathcal{H}'$. This implies that their translational symmetry is lower than that of the basic lattice, resulting in a mixture of $\mathbf{k}$ values of the lattice BZ. Since the charged stripes (where the bare stripon states reside) occupy about a quarter of the CuO_2 plane, the number of stripon states should be about a quarter of the number of states in this BZ.

The BZ $\mathbf{k}$ values mostly contributing to the stripon states reflect the structural nature of the stripe-like inhomogeneities, on one hand, and the minimization of free energy due to the $\mathcal{H}'$-coupling, on the other hand. Such a minimization is achieved when the stripon $\mathbf{k}$ values are mainly at BZ areas where the energetic effect of their coupling is the strongest. This would occur for optimal stripon coupling with svivons around $\mathbf{k}_0$ (see the behavior of $\bar{\epsilon}^{\zeta}$ there in Fig. 3), and with QE's at BZ areas of highest density of states (DOS) close to E_{F}, which are found in most of the cuprates around the "antinodal" points $(\frac{\pi}{a}, 0)$ and $(0, \frac{\pi}{a})$.

If (from its four possibilities) $\mathbf{k}_0$ were chosen at $(\frac{\pi}{2a}, \frac{\pi}{2a})$, then in order to minimize free energy, the BZ areas (in most of the cuprates) which the $\mathbf{k}$ values contributing to the stripon states should mostly come from, would be at about a quarter of the BZ around $\pm\mathbf{k}^p = \pm(\frac{\pi}{2a}, -\frac{\pi}{2a})$ (thus the antinodal points are at $\mathbf{k}^p \pm \mathbf{k}_0$). Stripon states corresponding to an equal mixture of $\mathbf{k}^p$ and $-\mathbf{k}^p$ states are created by:

$$p_{\mathrm{e}}^{\dagger}(\pm\mathbf{k}^p) \propto \sum_i p_i^{\dagger} \cos\left[\frac{\pi}{2a}(x_i - y_i)\right],$$
$$p_{\mathrm{o}}^{\dagger}(\pm\mathbf{k}^p) \propto \sum_i p_i^{\dagger} \sin\left[\frac{\pi}{2a}(x_i - y_i)\right]. \tag{13}$$

In the stripe-like inhomogeneity shown in Fig. 1 (where the stripes are directed in the y-direction), one has $(x_i, y_i) = (4am, an)$, where m and n are integers, and thus $p_{\mathrm{e}}^{\dagger}(\pm\mathbf{k}^p)$ creates a state with non-zero amplitudes in the even n points, while $p_{\mathrm{o}}^{\dagger}(\pm\mathbf{k}^p)$ creates a state with non-zero amplitudes in the odd n points. A similar result would be obtained also in lattice areas where the stripes are

directed in the x-direction. It will be shown below that pairing occurs between stripon states close to the ones in Eq. (13).

4. Electron Spectrum

Spectroscopic measurements (as in ARPES) based on the transfer of electrons into, or out of, the crystal, are determined by the electron's spectral function A_e. Projecting the spectral functions from the auxiliary to the physical space [2], A_e is expressed in terms of QE (A^q) and convoluted stripon-svivon ($A^q A^\zeta$) terms. From the quasi-continuum of QE bands, only few, closely related to those of physical electron, contribute "coherent" bands, while the others contribute an "incoherent" background to A_e.

The electron bands are specified by **k** vectors within the lattice BZ, though the stripe-like inhomogeneities introduce a perturbation of lower periodicity, reflected *e.g.* in "shadow bands". These bands (as well as the incoherent background in A_e) include hybridized contributions of QE states and convoluted stripon–svivon states. As in Eq. (7) for Γ^q, the electronic bandwidths have a $\propto \omega$ and a constant term, in agreement with experiment.

A significant stripon–svivon contribution to A_e close to E_F (at energies around $\epsilon^{-p} \pm \bar{\epsilon}^\zeta$) is obtained with svivons around their energy minimum at $\mathbf{k}_0$ (see Fig. 3). As was discussed above, such a contribution should be found (in most cuprates) in BZ areas around the antinodal points, as has been widely observed (see e.g. Ref. [8]).

Such type of a stripon-svivon contribution is not expected close to "nodal" Fermi surface (FS) crossing points, in the vicinity of $\pm(\frac{\pi}{2a}, \pm\frac{\pi}{2a})$. Thus the behavior of the electron bands there should be similar to that of the QE bands ϵ^{-q} (see Fig. 2), having a kink closely below E_F, as has been observed in ARPES [9, 10]. The observed kink has been attributed to the coupling of electrons to phonons [9] or to the neutron scattering resonance mode [10]. However, such a coupling would generally result in two opposite changes in the band slope (below and above the coupled excitation energy) below E_F, while the experimental kink looks more consistent with one change in slope below E_F, as in Fig. 2.

This kink was not found in measurements in the n-type cuprate NCCO [11], which is consistent with the prediction here (suggested by the author earlier [3]) that in real n-type cuprates this kink should be above, and not below E_F (where ARPES measurements are relevant). Also, there appears to be a sharp upturn in the ARPES band in NCCO [11] very close to E_F (believed there to be an artifact), which is expected here as the kink is approached from the other side of E_F (see Fig. 2).

Measurements of the doping-dependence of the slopes of the electron bands around the nodal points [12] show almost no change with doping of the slope

very close to E_F from below (thus including the kink effect). Here this low-energy slope depends on the nature of the low-energy truncation of the logarithmic singularity in Eq. (9); thus it depends of the width ω^p of the stripon band. Our analysis for the thermoelectric power [3], discussed below, predicts $\omega^p \sim 0.02$ eV, with very weak decrease with doping, which is consistent with the observed slope behavior.

The nodal kink, discussed above, shows almost no change when the temperature is lowered below T_c, as is expected here. A different type of a kink has been observed around the antinodal points [13, 14], showing a very strong temperature dependence, where its major part appears only below T_c. Within the present analysis, the temperature dependent part of this antinodal kink originates from the stripon–svivon contribution to the electron bands (discussed above), while the temperature-independent part is of the same origin as the nodal kink (thus due to the QE contribution to the electron bands).

As will be discussed below, the opening of a superconducting (SC) gap causes a decrease in the svivon linewidth around the energy minimum at $\mathbf{k}_0$, resulting in the narrowing of the stripon–svivon contribution to the antinodal electron bands below T_c. This is expressed by the appearance of the temperature-dependent antinodal kink, as well as a peak-dip-hump structure, below T_c (see discussion below). The appearance of this antinodal kink away from the nodal point on the FS is viewed in ARPES studies, above and below T_c [15], of FS crossings between the nodal point and half way towards the antinodal point.

The existence of high electron DOS close to E_F around the antinodal points is actually a consequence of the hybridization between QE's and convoluted stripon–svivon states of svivons around $\mathbf{k}_0$. This has been viewed in ARPES [16] as "an extra low energy scattering mechanism" around the antinodal points. As was discussed above, this could occur when the stripons reside around points $\pm\mathbf{k}^p$, which by Eq. (13) is consistent with "vertical stripes" (as those shown in Fig. 1). And indeed, in ARPES measurements in LSCO [17], including both high and low (non-SC) doping levels (which are characterized by "diagonal stripes"), a contribution of A_e close to E_F is observed around the nodal points for all doping levels, while around the antinodal points it is observed only for doping levels where the stripes are vertical.

As was demonstrated in Ref. [2], t' hopping processes (between next-nearest-neighbor sites – along the diagonal) in a CuO_2 plane, can take place without disrupting the AF order, and thus are only weakly affected by stripes and stripons, while in order for t hopping processes (between nearest-neighbor sites) to occur without the disruption of the AF order, it is essential for stripons in vertical stripes of $4a$ separation (as in Fig. 1) to be involved. The existence of nodal electron states close to E_F is mainly due to t' processes, while the existence of antinodal electron states close to E_F is mainly due to t processes.

5. The Neutron Resonance Mode

The imaginary part of the spin susceptibility $\chi''(\mathbf{q}, \omega)$ (at wave vector $\mathbf{q}$ and energy ω) has a major contribution from double-svivon excitations which can be expressed [2] as:

$$\chi''(\mathbf{q}, \omega) \sim \sum_{\mathbf{k}} \sinh(2\xi_{\mathbf{k}}) \sinh(2\xi_{\mathbf{q}-\mathbf{k}}) \int d\omega' A^{\zeta}(\mathbf{k}, \omega') \times \{A^{\zeta}(\mathbf{q}-\mathbf{k}, -\omega-\omega') - A^{\zeta}(\mathbf{q}-\mathbf{k}, \omega-\omega)' + 2A^{\zeta}(\mathbf{q}-\mathbf{k}, \omega'-\omega)[b_T(\omega'-\omega) - b_T(\omega']\}. \quad (14)$$

Due to the sinh (2ξ) factors, and Eq. (2), large contributions to χ'' are obtained when both $\mathbf{k}$ and $\mathbf{q}-\mathbf{k}$ are close to $\mathbf{k}_0$. The effect of the negative minimum of $\bar{\epsilon}^{\zeta}(\mathbf{k})$ at $\mathbf{k}_0$, (see Fig. 3), and specifically in the SC state, where its linewidth is often small, is the existence of a peak in $\chi''(\mathbf{q}, \omega)$ at $\mathbf{q} = 2\mathbf{k}_0 = \mathbf{Q}$ (the AF wave vector) and $\omega = -2\bar{\epsilon}^{\zeta}(\mathbf{k}_0)$. This peak is consistent with the neutron resonance mode [of energy $E_{\rm res} = -2\bar{\epsilon}^{\zeta}(\mathbf{k}_0)$], often found in the high-T_c cuprate at ~ 0.04 eV [18, 19]. It is expected here that the energy of this resonance mode has a local maximum, as a function of $\mathbf{k}$, at $\mathbf{k} = \mathbf{Q}$ [since $\bar{\epsilon}^{\zeta}$ has a minimum at $\mathbf{k}_0$]; however, also a branch of the mode with energy rising with $\mathbf{k} - \mathbf{Q}$ is expected due to the range where $\bar{\epsilon}^{\zeta}(\mathbf{k})$ is positive and rising. And indeed, measurements in YBCO [18, 19] show a neutron-scattering peak branch dispersing downward (from the $\mathbf{k} = \mathbf{Q}$ value), and also one dispersing upward [19]. An approximate circular symmetry around $\mathbf{k} = \mathbf{Q}$ is obtained [19], as is expected here.

The incommensurate low-energy neutron-scattering peaks, corresponding to the stripe-like inhomogeneities [5], occur at points $\mathbf{Q} \pm 2\mathbf{q}$, where the slope of the low-energy $\bar{\epsilon}^{\zeta}(\mathbf{k})$ is not too steep (see Fig. 3). In the LSCO system the resonance energy at $\mathbf{k} = \mathbf{Q}$ is higher than the maximal SC gap, and thus a sharp peak is not observed there, being too wide (see discussion below); however, sharp peaks have been observed [20–22] at incommensurate $\mathbf{Q} \pm 2\mathbf{q}$ points, where the energy is lower than the maximal SC gap. In the LBCO system, the energy dependence of the peak (whether it is sharp or wide) with $\mathbf{q}$ was also found [23] to have branches dispersing both downward and upward around $\mathbf{k} = \mathbf{Q}$. A similar behavior was observed in $YBCO_{6.6}$ [24].

Thus, both the resonance mode at $\mathbf{k} = \mathbf{Q}$, and the excitations at incommensurate $\mathbf{Q} \pm 2\mathbf{q}$, are double-svivon excitations, around its energy minimum at $\mathbf{k}_0$, shown in Fig. 3. These are excitations towards the destruction of the stripe-like inhomogeneities; their width determines the speed of the inhomogeneities dynamics, and they exist for stoichiometries where SC exists [21]. Because of the lattice dressing of svivons, these double-svivon excitations are expected to be lattice-dressed spin excitations, and indeed, Cu–O optical phonon modes have been found to be involved in such excitations [25].

Spin excitations in bilayer cuprates are expected [2] to have either odd or even symmetry, with respect to the layers exchange. For odd symmetry one gets results similar to those obtained in the single-layer approach discussed above, while for even symmetry one gets a mode whose energy has a minimum at $\mathbf{k} = \mathbf{Q}$, in agreement with experiment [26].

6. Transport Properties

Transport properties, unlike *e.g.* ARPES, measure the electrons *within* the crystal, and thus can detect the small energy scale of the stripons, without convoluting them with svivons.

Normal-state transport expressions, *not* including the effect of the pseudogap (PG), were derived [3] using linear response theory, where the zero-energy singularities in the auxiliary spectral functions in Eqs. (4–6) are smoothened in the low-energy range, through Taylor expansion [imposing $A^{\zeta}(\omega = 0) = 0$]. In this derivation it was taken into account that the electric current can be expressed as a sum $\mathbf{j} = \mathbf{j}_0^q + \mathbf{j}_0^p$ of contributions of bare QE and stripon states, respectively, and that $\mathbf{j}_0^p \cong 0$ since the bare stripon states are localized. Thus the contributions to the current of both the QE and the stripon dressed (thus coupled) states originate from $\mathbf{j}_0^q$.

Results for the electrical resistivity ρ, the Hall constant R_{H}, the Hall number $n_{\mathrm{H}} = 1/eR_{\mathrm{H}}$, the Hall angle θ_{H} (through $\cot\theta_{\mathrm{H}} = \rho/R_{\mathrm{H}}$), and the thermoelectric power (TEP) S, are presented in Fig. 4. Their anomalous temperature dependencies result both from the low-energy-range stripon band [Eq. (5)], modeled by a "rectangular" shape A^p of width ω^p and fractional occupancy n^p, and from those of the scattering rates $\Gamma^q(T, \omega = 0)$ and $\Gamma^p(T, \omega = 0)$ (see Ref. [3]), including also impurity scattering temperature independent terms.

The transport results in Fig. 4 correspond to five stoichiometries of p-type cuprates, ranging from $n^p = 0.8$, corresponding to the underdoped (UD) regime, to $n^p = 0.4$, corresponding to the overdoped (OD) regime. The parameter N_e^q corresponds to the QE contribution to the electrons DOS at E_{F}. It is assumed to increase with the doping level x, reflecting transfer of QE spectral weight from the upper and lower Hubbard bands towards E_{F}, while moving from the insulating to the metallic side of the Mott transition regime. Consequently ω^p is assumed to decrease somewhat with doping, due to stronger renormalization of the stripon energies [3].

The parameters n_{H}^q and $n_{\mathrm{H}}^{\mathrm{p}}$ represent effective QE and stripon contributions to the density of charge carriers (reflected in the Hall number). Since they both contribute through the current $\mathbf{j}_0^q$ of the bare QE states, they are expected to have same sign (corresponding to these states). The values of these parameters are assumed to increase with x (for the same reason that N_e^q does). Since the coupling between QE's and stripons grows with x, and the increase of N_e^q with

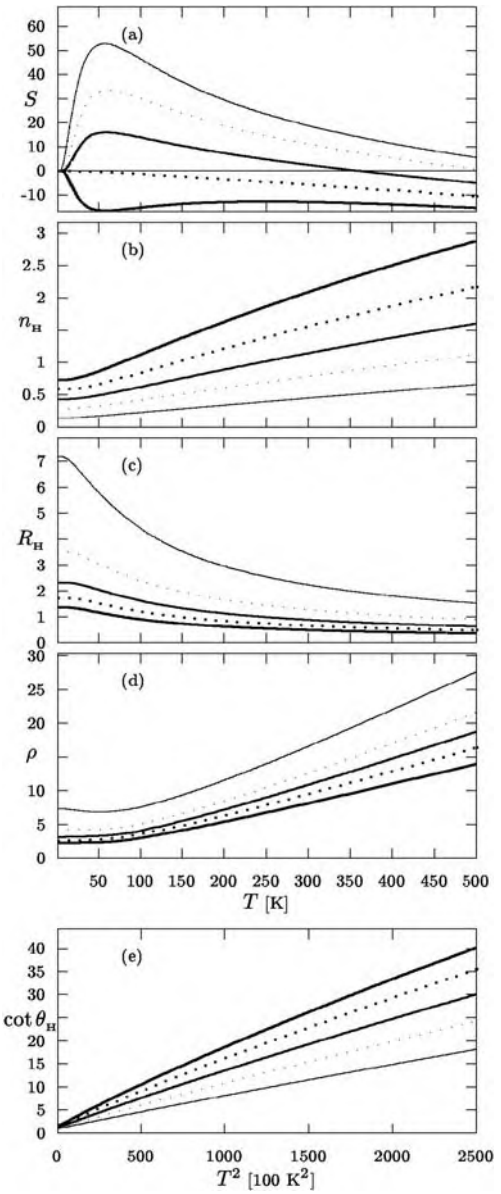

Figure 4. The transport coefficients, in arbitrary units and $\mu V/K$ units for S (a)], for: $n^p = 0.8, 0.7, 0.6, 0.5, 0.4$; $10000N_e^q = 20, 23, 26, 29, 32$; $\omega^p[\mathrm{K}] = 200, 190, 180, 170, 160$; $n_{\mathrm{H}}^p = 0.1, 0.2, 0.3, 0.4, 0.5$; $n_{\mathrm{H}}^q = 6, 7, 8, 9, 10$; $S_1^q = -0.025$; $\gamma_0^p = 500$; $\gamma_2^p = 0.03$; $\gamma_0^q = 5$; $\gamma_1^q = 0.2$. The last values correspond to the thickest lines.

x is slower than that of $1 - n^p$, it is assumed that the increase of $n_{\rm H}^p$ with x is faster than that of $1 - n^p$, which is faster than that of $n_{\rm H}^q$.

Doping-independent values are assumed for the QE TEP parameter S_1^q [3] [which is normally negative for p-type cuprates by the inequality (11)], and for the stripon and QE scattering rate parameters γ_0^p, γ_2^p, γ_0^q, and γ_1^q [3].

The TEP results depend strongly on n^p, and reproduce very well the doping-dependent experimental behavior [27, 28]. The position of the maximum in S depends on the choice of ω^p, and it may occur below or above T_c (the existence of a PG may shift it to a higher temperature than predicted here).

Also the results for the Hall coefficients in Fig. 4 reproduce very well the experimental behavior [29, 30]. The anomalous temperature dependence of the $n_{\rm H}$ is due to the growing role of $n_{\rm H}^q$ in its determination with increasing T, being dominantly determined by $n_{\rm H}^p$ at $T = 0$.

The temperature dependence of the resistivity in Fig. 4(d) is linear at high T, becoming "sublinear" at low T (for all stoichiometries), while experimentally [31] the low-T behavior crosses over from "superlinarity" in the UD regime, to sublinearity in the OD regime (being linear at low T for optimally doped cuprates). The superlinear behavior is being generally understood as the effect of the PG (not considered here), and the crossover to sublinear behavior (predicted here) in the OD regime is a natural consequence of the disappearance of the PG with increasing x.

The TEP in real n-type cuprates is normally expected [3] to behave similarly to the TEP in p-type cuprates, but with an opposite sign and slope. Results for NCCO [32] show such behavior for low doping levels, but in SC doping levels the slope of S changes from positive to negative, and its behavior resembles that of OD p-type cuprates, shown in Fig. 4(a). This led [3] to the suggestion that NCCO may be not a real n-type cuprate, its stripons being based on holon states (like in p-type cuprates). More recent measurements on the n-type infinite-CuO_2-layer SLCO [33] do show TEP results for an SC cuprate which have the opposite sign and slope than those of Fig. 4(a) (for p-type cuprates), as is expected for real n-type cuprates (thus with stripons based on excession states).

As was discussed above, the absence of a kink in the nodal band below $E_{\rm F}$ [11] in NCCO, supports the possibility that it is also a real n-type cuprate. It is possible that the change in the sign of the TEP slope in NCCO with doping is an anomalous band-structure effect, probably associated with the peculiar evolution of its FS with doping, detected in ARPES [34]. The position of the kink (below or above $E_{\rm F}$) is determined by the inequality (11) between d_+^q and d_-^q, which is less susceptible to band-structure effects than the inequality (11) between b_+^q and b_-^q, determining the sign of the TEP slope. Anomalous behavior is observed also in the Hall constant of NCCO [32], which changes

its sign with temperature in the stoichiometries where the sign of the slope of the TEP has changed.

7. Hopping-Induced Pairing

As was demonstrated in Ref. [2], the $\mathcal{H}'$ vertex enables inter-stripe stripon hopping, through intermediary QE–svivon states. This vertex was also demonstrated [2] to enable inter-stripe hopping of pairs of neighboring stripons through intermediary states of pairs of opposite-spin QE's, obtained by the exchange of svivons. The pair hopping was shown to result in a gain in inter-stripe hopping energy (compared to the hopping of two uncorrelated stripons), avoiding intermediary svivon excitations. Furthermore, the hybridization of the QE's with orbitals, beyond the $t-t'-J$ model, results in further gain in both intra-plane and inter-plane hopping energy.

This provides a pairing scheme based on transitions between pair states of stripons and QE's through the exchange of svivons. The inter-plane pair hopping, introduced within this scheme, is consistent with *c*-axis optical conductivity results [35], revealing (in addition to the opening of the SC gap), the increase of the spectral weight in the mid-IR range (well above the gap) below T_c. This effect has been observed both in bilayer and single-layer cuprates, and proposed [35] to be the signature of a *c*-oriented collective mode emerging (or sharpening) below T_c. The existence of such a mode below T_c is due to the hopping of pairs in the *c*-direction, during their QE-pair stages, while above T_c, *c*-axis hopping of stripons (through intermediary QE-svivon states) is, at the most, limited to adjacent CuO_2 planes.

The pairing diagram (sketched in Ref. [6]) provides Eliasherg-type equations, of coupled stripon and QE pairing order parameters. Coherent pairing occurs [2] between two subsets of the QE and stripon states. For QE's these subsets are, naturally, of the spin-up ($\uparrow$) and spin-down ($\downarrow$) QE's. Since the stripons are spinless, their subsets should be determined according to a different criterion.

As was illustrated in Fig. 1, for a CuO_2 plane within the $t-t'-J$ model, the $\uparrow$ QE's can reside on $\downarrow$ sites, and the $\downarrow$ QE's can reside on $\uparrow$ sites of the stripe-like inhomogeneities. In Fig. 5 an adiabatic snapshot of an extended section of a stripe-like inhomogeneity is shown, including an expected crossover between stripe segments directed in the *a* and the *b* directions. Denoted are the *available* sites for the $\uparrow$ and $\downarrow$ QE subsets. Since the QE subsets have a spatial interpretation in the CuO_2 planes (within the adiabatic time scale) it is natural to choose the stripon subsets also on a spatial basis, in a manner which optimizes the coupled pairing.

Since the pairing is optimal between neighboring stripons along the charged stripes [2], the stripon pairing subsets are chosen such that the nearest neighbors

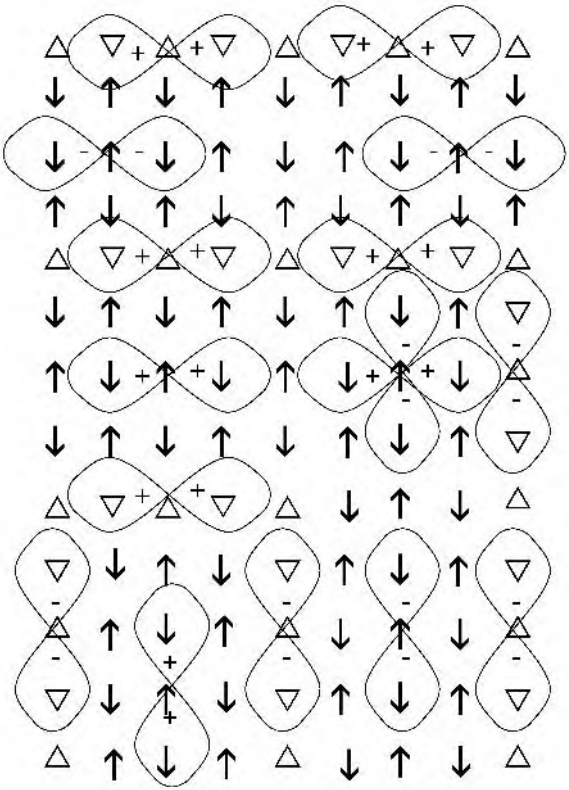

Figure 5. An adiabatic snapshot of an extended section of a stripe-like inhomogeneity, where the available sites for the QE and stripon pairing subsets are illustrated, as well as sketches demonstrating the local symmetry of the pairing order parameters Φ^q and Φ^p.

of a site corresponding to one subset are sites corresponding to the other subset. These subsets are denoted by $\triangle$ and ∇, and the sites *available* for them are shown in Fig. 5 too. Note that each of the stripon states created by $p_e^\dagger(\pm\mathbf{k}^p)$ and $p_o^\dagger(\pm\mathbf{k}^p)$, defined in Eq. (13), belongs to a different subset. This indicates that combinations of stripon states around points $\pm\mathbf{k}^p$ in the BZ are consistent with this pairing scheme. The required degeneracy of the QE and stripon paired subsets is restored by stripes dynamics.

The QE and stripon pair-correlation functions (pairing order parameters) are defined, within in the position (r) representation, as:

$$\Phi^q(r_1, r_2) \equiv \langle q_\uparrow(r_1) q_\downarrow(r_2)\rangle, \tag{15}$$

$$\Phi^p(r_1, r_2) \equiv \langle p_\triangle(r_1) p_\nabla(r_2)\rangle. \tag{16}$$

They are coupled to each other through Eliashberg-type equations, which can be expressed, in the position and the Matzubara (ω_n) representations, as:

$$\Phi^q(\mathbf{r}_1, \mathbf{r}_2, i\omega_n) = \sum_{n'} \int d\mathbf{r}'_1 \int d\mathbf{r}'_2 K^{qp}(\mathbf{r}_1, \mathbf{r}_2, n; \mathbf{r}'_1, \mathbf{r}'_2, n') \times \Phi^p(\mathbf{r}'_1, \mathbf{r}'_2, i\omega'_n), \tag{17}$$

$$\Phi^p(\mathbf{r}_1, \mathbf{r}_2, i\omega_n) = \sum_{n'} \int d\mathbf{r}'_1 \int d\mathbf{r}'_2 K^{pq}(\mathbf{r}_1, \mathbf{r}_2, n; \mathbf{r}'_1, \mathbf{r}'_2, n') \times \Phi^q(\mathbf{r}'_1, \mathbf{r}'_2, i\omega'_n). \tag{18}$$

Expressions for the kernel functions K^{qp} and K^{pq} are obtained from the pairing diagrams; they depend on Φ^q and Φ^p up to the temperature where the latter vanish. The combination of Eqs. (17) and (18) results in BCS-like equations for both the stripon and the QE order parameters. The coupling between Φ^q and Φ^p results in maximal pairing between nearest neighbors in the stripe direction, both for stripons and QE's. The resulting local symmetry of $\Phi^q(\mathbf{r}_1, \mathbf{r}_2)$ and $\Phi^p(\mathbf{r}_1, \mathbf{r}_2)$ (within the adiabatic time scale) is illustrated in Fig. 5, where point r_1 is fixed on selected sites (of the $\uparrow$ and $\triangle$ QE and stripon subsets), while point r_2 is varied over the space including the nearest neighbors.

As is illustrated in Fig. 5, the sign of Φ^q reverses between the two sides of a charged stripe. This is expected because when two QE sites on different sides of a charged stripe have a stripon site midway between them, then one of them is of $\uparrow$ and the other is of $\downarrow$, and since the exchange of the two fermion operators in the definition of Φ^q in Eq. (15) results in sign reversal, there must be sign reversal in Φ^q between the two sites. A similar sign reversal has been proposed recently by Fine [36].

The sign of both Φ^q and Φ^p is expected to be reversed between *a*-oriented and *b*-oriented stripe segments meeting in a "corner" (shown in Fig. 5). This provides optimal pairing energy, yielding maximal $|\Phi^q(\mathbf{r}_1, \mathbf{r}_2)|$ when $\mathbf{r}_1$ and $\mathbf{r}_2$ are at nearest neighbor QE sites, and zero $\Phi^q(\mathbf{r}_1, \mathbf{r}_2)$ when $\mathbf{r}_1$ and $\mathbf{r}_2$ are at next nearest neighbor sites (where the QE's have the same spin and thus do not pair). Away from the corner regions, $|\Phi^q(\mathbf{r}_1, \mathbf{r}_2)|$ is maximal when $\mathbf{r}_1$ and $\mathbf{r}_2$ are at nearest neighbor QE sites along the stripe direction, but it does not vanish when they are at nearest neighbor sites perpendicular to the stripe direction (which is not implied from Fig. 5).

These symmetry characteristics of Φ^q and Φ^p are reflected in the symmetry of the physical pairing order parameter. The overall symmetry is expected to be of a $d_{x^2-y^2}$ type; however, the sign reversal of Φ^q through the charged stripes, and the lack of coherence in the details of the dynamic stripe-like inhomogeneities between different CuO_2 planes, is expected to result in features different from those of a simple $d_{x^2-y^2}$-wave pairing (especially when the

c-direction is involved). There is a strong experimental support in the existence of features of $d_{x^2-y^2}$-wave pairing, though different features have been reported too.

8. Pairing and Coherence

The pairing mechanism here depends on the stripe-like inhomogeneities, and is expected to be stronger when the AF/stripes effects are stronger, thus closer to the insulating side of the Mott transition regime. Consequently one expects the pairing temperature T_{pair} to decrease with the doping level x, as is sketched in the pairing line in Fig. 6.

The existence of SC requires the existence of not only pairing, but also of phase coherence of the pairing order parameters. Under conditions satisfied for low x values, within the phase diagram of the cuprates, pairing occurs below T_{pair}, while SC occurs only below $T_{\text{coh}}(< T_{\text{pair}})$, where phase coherence sets in. The normal-state PG, observed in the cuprates above T_c (except for high x values) is a pair-breaking gap at $T_{\text{coh}} < T < T_{\text{pair}}$ (see Fig. 6). Its size and symmetry are similar to those of the SC gap, and specific heat measurements [37] imply that it accounts for most of the pairing energy. The pairs in the PG state behave similarly to localized bipolarons, and do not contribute to electrical conductivity at low temperatures.

Pairing coherence requires energetic advantage of itineracy of the pairs. Thus T_{coh} is expected to increase with x, as is sketched in the coherence line in Fig. 6, due to moving towards the metallic side of the Mott transition regime. Such a determination of the pairing coherence temperature is consistent with a phenomenological model [38] evaluating T_{coh} on the basis of the phase "stiffness". It yields $T_{\text{coh}} \propto n_s^*/m_s^*$, where m_s^* and n_s^* are the effective SC pairs mass and density, in agreement with the "Uemura plots" [39] in the PG doping regime.

Similarly, the existence of single-electron coherence in the normal state, namely the existence of a Fermi liquid, depends on the advantage of itineracy of the electronic states near E_{F}, resulting in the increase of T_{coh} with x (due to moving towards the metallic side of the Mott transition regime), as is sketched in Fig. 6. Within the non-Fermi-liquid approach used here, the stripe-like inhomogeneities are treated adiabatically. But their dynamics becomes faster above T_{pair}, resulting (for $T_{\text{pair}} < T < T_{\text{coh}}$) in a Fermi-liquid state where fast stripe fluctuations may still exist.

ARPES measurements in the OD regime [40] confirm the appearance of coherence effects for $T_{\text{pair}} < T < T_{\text{coh}}$. They are found in the nodal and antinodal peaks, and consist of the existence of sharp peak edges and resolved bilayer-split bands. The existence of a coherent three dimensional FS in this regime has been demonstrated through polar angular magnetoresistance oscillations [41].

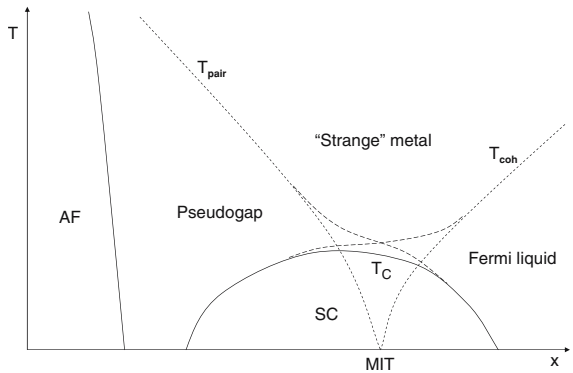

Figure 6. A schematic phase diagram for the cuprates. The T_c line is determined by the pairing line (T_{pair}), decreasing with x, and the coherence line (T_{coh}), increasing with x. Broken lines should not be regarded as sharp lines (except when $T \to 0$), but as crossover regimes. The MIT point is where a metal-insulator transition occurs at $T = 0$ when SC is suppressed.

Measurements of the in-plane optical conductivity through T_c [42], show a BCS-type behavior in the OD regime, supporting the existence of Fermiliquid normal state there (as shown in Fig. 6). On the other hand, in the UD regime these measurements reveal the transfer, below T_c, of spectral weight from high energies (extending over a broad range up to at least 2 eV), to the infrared range. This behavior has been associated with the establishment of coherence [43]. Within the present approach the PG state consists of localized pairs (and unpaired carriers) within the Hubbard gap, while the establishment of pair coherence in the SC state requires moving states from the upper and lower Hubbard bands into this gap, to contribute to Bloch-like states, explaining the observed transfer of spectral weight.

ARPES measurements on LSCO thin films [44] show that T_c rises under strain, while the bands close to E_{F} become wider. Such a change in the bands is consistent with a move towards the metallic side of the Mott transition regime. Thus we predict that the increase in T_c under that strain is due to an increase in T_{coh}, and that T_{pair} (where the PG state sets in) may have decreased in this case.

As is sketched in Fig. 6, there is an increase in the values of T_{pair} and T_{coh} in the regime where pairing and coherence coexist, compared to their extrapolated values from the regimes where only one of them exists. This is due to the energy gain in the SC state, compared to both the PG and the Fermi-liquid normal states.

If the SC state is suppressed, the occurrence of a metal-insulator transition (MIT) is expected here at $T = 0$, at the MIT point in the phase diagram (see Fig. 6), where the metallic phase is of the Fermi-liquid regime, and the insulating phase is of the PG regime of localized electrons and electron pairs within the Hubbard gap. And indeed, experiments where the SC state is suppressed by

a magnetic field [45], or by doping [46], show an MIT at $T \to 0$, at $x \simeq 0.19$. This stoichiometry corresponds here to a fractional stripon occupancy of $n^p \simeq \frac{1}{2}$, as was determined from the TEP results above (see Fig. 4). The existence of the MIT close to this stoichiometry is plausible, because for higher doping levels inter-atomic Coulomb repulsion destabilizes the dynamic charged stripes, essential for the PG state (though the energy gain in the SC state helps maintaining them for higher x).

The MIT point in Fig. 6 is a quantum critical point (QCP), and there have been various theoretical approaches addressing the existence of such a QCP. Such approaches often consider different mechanisms for the SC pairing and for the driving force of the PG state, and consequently predict (in difference with the present approach) the existence different regimes of different symmetries, within the SC phase [47]. This has not been confirmed by experiment, in agreement with the present approach. The existence of an intrinsic nanoscale heterogeneity of SC and PG regions [48] will be addressed below.

The connection between SC and an MIT (where the insulating state is due to localization) in the cuprates, as well as in other systems with a similar phase diagram, has been pointed out by Osofsky *et al*. [49]. The conclusion from the present approach is that if a pairing interaction exists, and the insulating state is characterized by the existence of localized pairs at low temperatures, then an SC phase, based on the same pairing interaction, ought to exist around the MIT regime.

9. Pairing Gap, Excitations, and the Resonance Mode

The QE and stripon pairing gaps $2\Delta^q$ and $2\Delta^p$ are closely related to the order parameters Φ^q and Φ^p [see Eqs. (15) and (16)], and have the same symmetries. Thus Δ^q vanishes at the nodal points and has its maximum $\Delta^q_{\max}$ at the antinodal points. Since the stripons reside in about a quarter of the BZ around $\pm\mathbf{k}^p$ [see Eq. (13)], $|\Delta^p|$ does not vary much from its mean value $\bar{\Delta}^p$, and it is greater than the stripon bandwidth ω^p, except for the heavily OD regime.

Since the coupled pairing equations (17) and (18) yield in the second order BCS-like equations for both Φ^q and Φ^p, the QE and stripon single-auxiliary-particle (Bogoliubov) energy bands in a pairing state can be expressed as:

$$E^q_{\pm}(\mathbf{k}) = \pm\sqrt{\bar{\epsilon}^q(\mathbf{k})^2 + \Delta^q(\mathbf{k})^2}, \tag{19}$$

$$E^p_{\pm}(\mathbf{k}) = \pm\sqrt{\bar{\epsilon}^p(\mathbf{k})^2 + \Delta^p(\mathbf{k})^2} \tag{20}$$

(where $E^p_{\pm} \simeq \pm\Delta^p$ in the UD regime), and the pairing gaps scale with T_{pair}, approximately according to the BCS factors, with an increase due to strong-coupling. The relevant factors are of s pairing for Δ^p, and of d pairing [50] for

Δ^q:

$$2\bar{\Delta}^p \gtrsim 3.5 k_{\rm B} T_{\rm pair}, \quad 2\Delta^q_{\rm max} \gtrsim 4.3 k_{\rm B} T_{\rm pair}. \tag{21}$$

In the PG state the pairs lack phase coherence, and thus Eq. (19) does not yield a coherence peak in the QE gap edge. Furthermore, in this state the low-energy svivon states are wide, due to incoherence and scattering, and thus the gap is filled with unpaired convoluted stripon–svivon states (see discussion below). Consequently the PG is just a depression of width:

$$2\Delta^{\rm PG}(\mathbf{k}) = 2\Delta^q(\mathbf{k}) \tag{22}$$

in the DOS, as has been observed, *e.g.* by tunneling spectroscopies [51, 52].

Pairing coherence sets in below T_c, and the structure of the pair-breaking excitations is determined by the scattering between QE, stripon, and svivon states. This scattering is strong when $E^q \simeq E^p \pm \overline{\epsilon}^\zeta$, and particularly for svivon states close to $\mathbf{k}_0$, where the cosh ($\xi_{\mathbf{k}}$) and sinh ($\xi_{\mathbf{k}}$) factors, appearing in the coupling terms, are large [see Eqs. (2) and (3)]. When there are unpaired convoluted stripon–svivon states within the QE gap, paired QE states are scattered to them, resulting in the widening of the QE coherence peak [due to Eq. (19)], at the QE gap edge, to a hump.

The existence of a pairing gap, and especially of the SC gap, limits the scattering of the svivon states around $\mathbf{k}_0$, resulting in a decrease in their linewidth. Let $\mathbf{k}_{\rm min}$ be the points of small svivon linewidth, for which $\overline{\epsilon}^\zeta(\mathbf{k}_{\rm min})$ is the closest to the energy minimum $\overline{\epsilon}^\zeta(\mathbf{k}_0)$ (see Fig. 3). Often one has $\mathbf{k}_{\rm min} = \mathbf{k}_0$, but there are cases, like that of LSCO, where the linewidth of $\overline{\epsilon}^\zeta$ is small not at $\mathbf{k}_0$, but at close points $\mathbf{k}_{\rm min} = \mathbf{k}_0 \pm \mathbf{q}$. The resonance mode energy $E_{\rm res}$ is taken here as $-2\overline{\epsilon}^\zeta(\mathbf{k}_{\rm min})$, accounting both for the generally observed "commensurate mode" at $\boldsymbol{Q} = 2\mathbf{k}_0$, and for cases of an "incommensurate mode", as observed in LSCO at $\mathbf{Q} \pm 2\mathbf{q}$ [20–22].

The determination of $\mathbf{k}_{\rm min}$ is through the limitation of the scattering of a double-svivon excitation of energy $-2\overline{\epsilon}^\zeta(\mathbf{k}_{\rm min})$ to a QE pair-breaking excitation of at least the SC gap $2|\Delta^{\rm SC}|$, by exchanging a stripon. If $2\tilde{\Delta}^{\rm SC}$ (which is somewhat smaller than the maximal SC gap $2\Delta^{\rm SC}_{\rm max}$) is the minimal energy necessary to break a pair of QE's which are coupled to stripons around $\pm\mathbf{k}^p$ through a svivon at $\mathbf{k}_{\rm min}$, then this condition can be expressed as:

$$\frac{E_{\rm res}}{2} = |\overline{\epsilon}^\zeta(\mathbf{k}_{\rm min})| \leq \tilde{\Delta}^{\rm SC}. \tag{23}$$

Consequently the svivon energies $\overline{\epsilon}^\zeta$ have a small linewidth within the range $|\overline{\epsilon}^\zeta| \leq |\overline{\epsilon}^\zeta(\mathbf{k}_{\rm min})|$, and for $\overline{\epsilon}^\zeta$ within this range, the convoluted stripon–svivon states of energies $E^p_+ \pm |\overline{\epsilon}^\zeta|$ and $E^p_- \pm |\overline{\epsilon}^\zeta|$ from spectral peaks around

$$\pm E_{\rm peak}(\mathbf{k}) = E^p_\pm(\mathbf{k} \pm \mathbf{k}_0), \tag{24}$$

where to the "basic" peak width:

$$W_{\rm peak} = 2|\overline{\epsilon}^{\zeta}(\mathbf{k}_{\rm min})| = E_{\rm res} \tag{25}$$

one has to add the effects of the svivon and stripon linewidth, and of the dispersion of $E^{p}_{\pm}(\mathbf{k} \pm \mathbf{k}')$ when $\overline{\epsilon}^{\zeta}(\mathbf{k}_{\rm min}) \lesssim \overline{\epsilon}^{\zeta}(\mathbf{k}') \lesssim 0$ (see Fig. 3). The size of the SC gap is experimentally determined by the spacing between the closest maxima on its two sides. Thus, in the BZ ranges around the antinodal points where $E_{\rm peak}(\mathbf{k})$ exists, it often determines the SC gap:

$$|2\Delta^{\rm SC}(\mathbf{k})| = 2\,\min[|\Delta^{q}(\mathbf{k})|, E_{\rm peak}(\mathbf{k})]. \tag{26}$$

[Actually, since the peak lies on the slope of the QE gap, its maximum may be shifted to an energy slightly above $E_{\rm peak}(\mathbf{k})$.] $\Delta^{\rm SC}$ equals Δ^{q} around its zeroes at the nodal points, which is consistent with the observation by STM [48] that the low energy excitations near the SC gap minimum are not affected by heterogeneity, while the excitations near the gap edge (where it equals $E_{\rm peak}$) are affected by it (see discussion below). Note that there remain within the SC gap, below the peak, some unpaired convoluted stripon–svivon states corresponding to svivon states of large linewidth and of positive energies $\overline{\epsilon}^{\zeta}$ at $\mathbf{k}$ points farther from $\mathbf{k}_0$ (see Fig. 3).

As a result, one gets below T_c a peak-dip-hump structure (on both sides of the gap), where the peak is largely contributed by the convoluted striponsvivon states around $E_{\rm peak}(\mathbf{k})$, the dip results from the sharp descent at the upper side of this peak, and the hump above them is of the QE gap edge and other states, widened due to scattering to the peak states. Such a structure has been widely observed, *e.g.* by tunneling measurements [51, 52], where the evolution of the gap from a depression in the PG state to a peak-dip-hump structure in the SC state has been viewed. The appearance of the resonance mode energy $E_{\rm res}$ in the peak width in Eq. (25) has been observed in tunneling measurements as the energy separation between the SC gap edge, and the dip for different doping levels [53].

By Eqs. (21), (22), and (26), $\Delta^{\rm PG}$ and $\Delta^{\rm SC}$ scale with $T_{\rm pair}$, and thus decrease with x, following the pairing line in Fig. 6, as has been observed. Since $-\overline{\epsilon}^{\zeta}(\mathbf{k}_0)$ is zero for an AF, its value (and thus $E_{\rm res}$) is expected to increase with x, distancing from an AF state. However, by Eq. (23) its linewidth cannot remain small if it crosses the value of $\tilde{\Delta}^{\rm SC}$, which decreases with x. Thus the energy $E_{\rm res}$ of a *sharp* resonance mode is expected to cross over from an increase to a decrease with x when it approaches the value of $2\tilde{\Delta}^{\rm SC}$, as has been observed [18]. This crossover could be followed by a shift of the resonance wave vector $2\mathbf{k}_{\rm min}$ from the AF wave vector $\mathbf{Q}$ to incommensurate wave vectors.

Studies of the gap structure by ARPES give information about its $\mathbf{k}$ dependence, confirming the above features. In bilayer cuprates, the QE bands are

split around the antinodal points into a bonding band (BB) and an antibonding band (AB). On the other hand, the convoluted stripon–svivon peak given by Eqs. (24) and (25) is *not* split and extends over a range of the BZ around the antinodal points. As x is increased, $\Delta^{q}_{\max}$ is decreased, and in the OD regime it is exceeded by $E_{\rm peak}(\mathbf{k})$, at least in a part of the antinodal BZ range [see Eqs. (20) and (24)].

The AB lies very close to $E_{\rm F}$, on the SC gap edge, and consists of Bogoliubov quasiparticles [54] through the antinodal BZ range. In the UD regime the stripon–svivon peak lies within the QE AB gap, reflected in the observation [55] of an AB hump above the peak. On the other hand, in the OD regime the peak lies on the QE AB, or even above it, and consequently the strong scattering which widens the QE band edge coherence peak into a hump is missing. Thus the reported observation is either of one AB peak [13], including the unresolved QE and stripon–svivon contributions, or of two barely resolved peaks [56], where the QE contribution is referred to as an "AB peak", and the stripon–svivon contribution, lying slightly above it, is referred to as a "BB peak".

The BB, on the other hand, crosses $E_{\rm F}$, and disperses up to over 0.1 eV from it. Below T_c, when its distance from $E_{\rm F}$ is greater than that of the stripon–svivon peak, it contributes a (QE) hump, referred to [13, 55, 56] as a "BB hump" (though in much of this range its nature is close to that of a normal-state band). In the range where the QE BB overlaps the stripon–svivon peak, the fact that the electron band is formed by their hybridized contributions results in the appearance of the antinodal kink [13–15], due to the narrowing of the peak, as the temperature is lowered below T_c. This narrowing slows down the stripes dynamics, and widens the "hump states" above the peak. As has been observed [15], this widening (and the resulting band renormalization) has an isotope effect due to the significance of lattice effects in the stripe-like inhomogeneities and in the svivon dressing.

The peak-dip-hump structure has been also observed in tunneling measurements in single-layer BSCO and BSLCO [52], proving that it is not the result of just bilayer splitting. These measurements show that in the PG state above T_c in BSLCO, the stripon–svivon peak, and the QE hump are merged into one hump. ARPES results in the PG state of BSLCO [57] show an apparent "bilayer splitting" which may indicate that even though the QE and the stripon–svivon contributions to this hump appear merged in tunneling results, they are separated from each other in different $\mathbf{k}$ points.

In the heavily OD regime, where $\Delta^{\rm SC}$ and $E_{\rm res}$ become smaller than ω^{p}, the dispersion of $E_{\rm peak}(\mathbf{k})$ becomes wider than $\Delta^{\rm SC}$ and $W_{\rm peak}$ [see Eqs. (20), (24) and (25)]. This results in the smearing of the peak in spectroscopies where it is integrated over the BZ, though it may still be detected in different k points [where there remains some smearing, as was mentioned below Eq. (25)]. The

apparent disappearance, in the heavily OD regime, of the peak (of width $E_{\rm res}$) observed in optical measurements [58] below T_c may be the result of such smearing (see Ref. [59]). Concerning the question [58]. whether the resonance mode is significant for high-T_c SC, the approach presented here considers svivons in the vicinity of $\mathbf{k}_0$ to be significant for the SC pairing, whether they contribute to the narrow resonance mode peak, or to higher energy excitations [23, 24].

10. Heterogeneity and Pairs Density in the SC Phase

The narrow stripon band splits in the SC state, through the Bogoliubov transformation, into the $E^p_-(\mathbf{k})$ and $E^p_+(\mathbf{k})$ bands, given in Eq. (20). The states in these bands are created, respectively, by $p^\dagger_-(\mathbf{k})$ and $p^\dagger_+(\mathbf{k})$, which are expressed in terms of creation and annihilation operators of stripons of the two pairing subsets [see Eq. (16)] through equations of the form:

$$\begin{aligned} p_-(\mathbf{k}) &= u_{\mathbf{k}} p_\triangle(\mathbf{k}) + v_{\mathbf{k}} p^\dagger_\triangledown(-\mathbf{k}), \\ p^\dagger_+(\mathbf{k}) &= -v_{\mathbf{k}} p^\dagger_\triangle(\mathbf{k}) + u_{\mathbf{k}} p_\triangledown(-\mathbf{k}), \end{aligned} \tag{27}$$

where $|u_{\mathbf{k}}|^2 + |v_{\mathbf{k}}|^2 = 1$.

If all the stripons were paired, then at low temperatures, where the E^p_- band is completely full, and the E^p_+ band empty, then the fractional stripon occupancy n^p should have been equal to $\langle |u_{\mathbf{k}}|^2 \rangle$. However this cannot be fulfilled in the UD regime, where $\bar{\Delta}^p$, is considerably greater than the stripon bandwidth ω^p, and $E^p_\pm \simeq \pm\Delta^p$, resulting in $\langle |u_{\mathbf{k}}|^2 \rangle \simeq \frac{1}{2}$, while $n^p > \frac{1}{2}$ (see Fig. 4).

Consequently, in the UD regime, the PG state should consist of *both* paired and unpaired stripons (as was discussed above), and the SC phase should be *intrinsically* heterogenous with nanoscale SC regions, where, locally, $n^p \simeq \frac{1}{2}$, and PG regions where, locally $n^p > \frac{1}{2}$, such that the correct average n^p for that stoichiometry is obtained. The size of the regions in this nanostructure should be as small as permitted by the coherence length, and it was indeed observed in nanoscale tunneling measurements in the SC phase [48]. There are, however, physical properties which are determined through a larger scale averaging over these regions. This nanostructure would be naturally pinned to defects, and could become dynamic in very "clean" crystals.

For $x \simeq 0.19$, one has $n^p \simeq \frac{1}{2}$, and an SC phase could exist without such a nanostructure. Furthermore, in the OD regime $\bar{\Delta}^p$ becomes comparable, and even smaller than ω^p, and the condition $\langle |u_{\mathbf{k}}|^2 \rangle = n^p$ could be satisfied with all the stripons being paired. Thus the SC phase could exist in the OD regime (especially for $x \gtrsim 0.19$) without the above nanoscale heterogeneity, as has been observed [48].

The Uemura plots [39] give information about the effective density of SC pairs n_s^*. Within the present approach, the pair states are fluctuating between QE and stripon pair states, and thus n_s^* is determined by the smaller one, *i.e.*, the density of stripon pairs. As was discussed above, the stripon band is half full for $x \simeq 0.19$, and consequently n_s^* should be maximal around this stoichiometry, being determined (for p-type cuprates) by the density of hole-like stripon pairs for $x \lesssim 0.19$, and of particle-like stripon pairs for $x \gtrsim 0.19$. This result is not changed by the intrinsic heterogeneity for $x \lesssim 0.19$, since even though the stripon band remains approximately half full within the SC regions, the fraction of space covered by these regions, and thus n_s^*, is *increasing* with x in this regime, while in the $x \gtrsim 0.19$ regime, n_s^* is *decreasing* with x because the occupation of stripon band is decreasing below half filling. This result is consistent with the "boomerang-type" behavior [60] of the Uemura plots around $x \simeq 0.19$.

Low temperature ARPES results for the spectral weight within the SC peak (omitting the background including the hump), integrated over the antinodal BZ area [61], reveal a maximum for $x \simeq 0.19$ (similarly to n_s^*). This is expected here, assuming that the integrated spectral weight counted is dominantly within the stripon–svivon peak (discussed above), and that this peak counts the major part of SC hole-like pair-breaking excitations of stripons within the E_-^p band, as is expected. For the intrinsically heterogenous $x \lesssim 0.19$ regime, the integrated weight within the peak is expected to increase with x because of the increase in the fraction of space covered by the SC regions (keeping the stripon band approximately half full within these region). For the $x \gtrsim 0.19$ regime the integrated weight, measured by ARPES, scales with $\langle |u_{\mathbf{k}}|^2 \rangle$, and is thus decreasing with x below half filling of the stripon band. Note that the contribution of the QE AB to the ARPES peak had to be omitted [61] in order to get the decrease of the peak weight for $x \gtrsim 0.19$, confirming that this behavior is due to the stripon–svivon peak, as is suggested here.

11. Conclusions

The anomalous properties of the cuprates, including the occurrence of high-T_c superconductivity, are found to be a result typical of their electronic and lattice structure, within the regime of a Mott transition. On one hand, hopping-induced pairing, which depends on dynamical stripe-like inhomogeneities, is stronger for low doping levels, closer to the insulating side of the Mott transition regime. On the other hand, phase coherence, which is necessary for superconductivity to occur, is stronger for high doping levels, closer to the metallic side of the Mott transition regime. Pairing without coherence results in the pseudogap state of localized electrons and electron pairs, and coherence without pairing results in a Fermi-liquid normal state. Suppression of superconductivity results

in a quantum critical point of a metal-insulator transition between these two states at $T = 0$. An intrinsic heterogeneity exists of nanoscale superconducting and pseudogap regions.

References

[1] S. E. Barnes, *Adv. Phys.* **30**, 801 (1980).
[2] J. Ashkenazi, *J. Phys. Chem. Solids,* **65**, 1461 (2004); cond-mat/0308153.
[3] J. Ashkenazi, *J. Phys. Chem. Solids*, **63**, 2277 (2002); cond-mat/0108383.
[4] J. Ashkenazi, *J. Supercond.* , 719 (1994).
[5] J. M. Tranquada *et al., Phys. Rev. B* **54**, 7489 (1996); *Phys. Rev. Lett.* **78**, 338 (1997).
[6] J. Ashkenazi, *High-Temperature Superconductivity*, edited by S. E. Barnes, J. Ashkenazi, J. L. Cohn, and F. Zuo (AIP Conference Proceedings 483, 1999), p. 12; cond-mat/9905172.
[7] E. Pavarini, *et al., Phys. Rev. Lett.* **87**, 047003 (2001).
[8] T. Yoshida, *et al., Phys. Rev. B* **63**, 220501 (2001).
[9] A. Lanzara, *et al. Nature* **412**, 510 (2001).
[10] P. D. Johnson, *et al., Phys. Rev. Lett.* **87**, 177007 (2001).
[11] N. P. Armitage, *et al., Phys. Rev. B* **68**, 064517 (2003).
[12] X. J. Zhou, *et al, Nature* **423**, 398 (2003).
[13] A. D. Gromko, *et al., Phys. Rev. B* **68**, 174520(2003).
[14] T. Sato, *et al., Phys. Rev. Lett.* **91**, 157003 (2003).
[15] G.-H. Gweon, *et al., Nature* **430**, 187 (2004); A. Lanzara, *et al.,* these proceedings.
[16] X. J. Zhou, *et al., Phys. Rev. Lett.* **92**, 187001 (2004).
[17] T.Yoshida, *et al., Phys. Rev. Lett.* **91**, 027001 (2003).
[18] Ph. Bourges, *et al. Science* **288**, 1234 (2000); cond-mat/0211227; Y. Sidis, *et al.,* cond-mat/0401328.
[19] D. Reznik, *et al.,* cond-mat/0307591.
[20] J. M. Tranquada, *et al., Phys. Rev. B* **69**, 174507 (2004).
[21] S. Wakimoto, *et al., Phys. Rev. Lett.* **92**, 217004 (2004).
[22] N. B. Christensen, *et al*., cond-mat/0403439.
[23] J. M. Tranquada, *et al.*, *Nature* **429**, 534 (2004).
[24] S. M. Hayden, *et al., Nature* **429**, 531 (2004).
[25] R. J. McQueeney, *et al., Phys. Rev. Lett.* **87**, 077001 (2001); J.-H.Cung, *et al., Phys. Rev. B* **67**, 014517 (2003); L. Pintschoius, *et al*., cond-mat/0308357; T. Cuk, *et al*., cond-mat/0403521; T. Egami, these proceedings, views the lattice effect as the primary one; M. V. Eremin and I. Eremin, these proceedings, consider spin-lattice coupling.
[26] Ph. Bourges, *et al., Phys. Rev. B* **56**, R12439 (1997); S. Pailhes, *et al., Phys. Rev. Lett.* **91**, 23700 (2003); cond-mat/0403609.
[27] B. Fisher, *et al., J. Supercond.* **1**, 53 (1988); J. Genossar, *et al., Physica C* **157**, 320 (1989).
[28] S.Tanaka, *et al., Phys. Soc. Japan* **61**, 1271 (1992); K. Matsuura, *et al., Phys. Rev. B* **46**, 11923 (1992); S. D. Obertelli, *et al., ibid.,* p. 14928; C. K. Subramaniam. *et al., Physica C* **203**, 298 (1992).
[29] Y. Kubo and T. Manako. *Physica C* **197**, 378 (1992).
[30] H. Y. Hwang, *et al., ibid*. **72**, 2636 (1994).
[31] H. Takagi, *et al., Phys. Rev. Lett.* **69**, 2975 (1992).
[32] J. Takeda, *et al., Physica C* **231**, 293 (1994); X.-Q. Xu. *et al., Phys. Rev. B* **45**, 7356 (1992); Wu Jiang, *et al., Phys. Rev. Lett.* **73**, 1291 (1994).
[33] G. V. M. Williams, *et al., Phys. Rev. B* **65**, 224520 (2002).

[34] N. P. Armitage, *et al., Phys. Rev. Lett.* **88**, 257001 (2002).
[35] M. Gruninger, *et al., Phys. Rev. Lett.* **84**, 1575 (2000); D. N. Basov, *Phys. Rev. B* **63**, 134514 (2001); A. B. Kuzmenko, *et al., Phys. Rev. Lett.* **91**, 037004 (2003).
[36] B. V. Fine, cond-mat/0308428; these proceedings.
[37] I. Tifrea, and C. P. Moca, *Eur. Phys. J. B* **35**, 33 (2003).
[38] V. J. Emery, and S. A. Kivelson, *Nature* **374**, 4347 (1995); *Phys. Rev. Lett.* **74**, 3253 (1995); cond-mat/9710059.
[39] Y. I. Uemura, *et al., Phys. Rev. Lett.* **62**, 2317 (1989).
[40] Z. M. Yusof, *et al., Phys. Rev. Lett.* **88**, 167006 (2002); A. Kaminski, *et al., Phys. Rev. Lett.* **90**, 207003 (2003).
[41] N. E. Hussey, *et al., Nature* **425**, 814 (2004); these proceedings.
[42] H. J. A. Molegraaf, *et al., Science* **295**, 2239 (2002); A. F. Santander-Syro, *et al., Europhys. Lett.* **62**, 568 (2003); cond-mat/0405264; C, C. Homes, *et al., Phys. Rev. B* **69**, 024514(2004).
[43] M. R. Norman, and C. Pepin, *Phys. Rev. B* **66**, 100506 (2002); cond-mat/0302347.
[44] M. Abrecht, *et al., Phys. Rev. Lett.* **91**, 057002 (2003); D. Pavuna, *et al*., these proceedings.
[45] G. S. Boebinger, *et al., Phys. Rev. Lett.* **77**, 5417 (1996).
[46] J. L. Tallon, and J. W. Loram, *Physica C* **349**, 53 (2001); C. Panagopoulos, *et al., Phys. Rev. B* **69**, 144510 (2004); S. H. Naqib, *et al*., cond-mat/0312443.
[47] *E.g.*: David Pines, these proceedings; C. M. Varma, these proceedings.
[48] K. McElroy, *et al., Nature* **422**, 592 (2003); cond-mat/0404005.
[49] M. S. Oaofsky, *et al., Phys. Rev. B* **66**, 020502 (2002); these proceedings.
[50] H. Won, and K. Maki, *Phys. Rev. B Phys. Rev. B* **49**, 1397 (1994).
[51] Ch. Renner, *et al.,Phys. Rev. Lett.* **80**, 149 (1998); M. Suzuki, and T. Watanabe, *Phys. Rev. Lett.* **85**, 4787 (2000).
[52] M. Kugler, *et al., Phys. Rev. Lett.* **86**, 4911 (2001);A. Yurgens, *et al., Phys. Rev. Lett.* **90**, 147005 (2003).
[53] J. F. Zasadzinski, *et al., Phys. Rev. Lett.* **87**, 067005 (2001); M. Oda, *et al.*, these proceedings.
[54] H. Matsui, *et al., Phys. Rev. Lett.* **90**, 217002 (2003).
[55] S. V. Borisenko, *et al.,Phys. Rev. Lett.* 90, 207001 (2003); T. K. Kim, *et al., Phys. Rev. Lett.* **91**, 177002(2003).
[56] D. L. Feng, *et al., Phys. Rev. Lett.* **86**, 5550 (2001).
[57] C. Janowitz, *et al., Europhys. Lett.* **60**, 615 (2002); cond-mat/0107089.
[58] J. Hwang, *et al., Nature* **427**, 714 (2004).
[59] T. Cuk, *et al.,* cond-mat/0403743.
[60] Ch. Niedermayer, *et al., Phys. Rev. Lett.* **71**, 1764 (1993).
[61] D. L. Feng, *et al., Science* **289**, 277 (2000); H. Ding, *et al., Phys. Rev. Lett.* **87**, 227001 (2001); R. H. He, *et al., Phys. Rev. B* **69**, 220502 (2004).

SELF-SUPPORTED SUPERCONDUCTIVITY IN LAYERED METALOCHLORONITRIDES

V.Z. Kresin
Lawrence Berkeley Laboratory, University of California, Berkeley, CA 94720, USA
vzkresin@lbl.gov

A. Bill
Laboratory for Neutron Scattering, ETH Zurich & PSI, 5232 Villigen PSI, Switzerland
abill@psi.ch

H. Morawitz
IBM Almaden Research Center, San Jose, CA 95120, USA
morawitz@almaden.ibm.com

Abstract The superconducting state in the novel family of layered metalochloronitrides is provided by electronic collective excitations, the acoustic plasmons. These plasmons are a characteristic feature of layered conductors. This is the first experimentally observed case of self-supported superconductivity.

Keywords: layered superconductors, chloronitrides, electronic pairing mechanism

Introduction

This study has been motivated by the recent discovery and investigations of a new family of superconductors: metal-intercalated chloronitrides. For example, the compound $Li_{0.48}(THF)_yHfNCl$ has a relatively high value of $T_c \sim 25$K [1]-[5]. The mechanism of superconductivity for these materials had remained a puzzle. Indeed, according to theoretical calculations [6] the electron-phonon interaction is not sufficient to provide the observed value of T_c. Analysis of the data on heat capacity [2], based on the dependence $\gamma \sim (1+\lambda)$, see [7], has led to a similar conclusion (γ is the Sommerfeld constant, λ is the electron-phonon coupling constant).

J. Ashkenazi et al. (eds.), New Challenges in Superconductivity: Experimental Advances and Emerging Theories, 213-217.

The absence of magnetic ions rules out the magnetic mechanism. Note also that normal properties are very well described by the Fermi liquid picture, and this excludes the importance of correlation effects.

One can show, and this is the subject of our paper, that we are dealing with the remarkable case of self-supported superconductivity. The pairing is provided by the exchange of unusual acoustic plasmons, that is, by collective excitations of the same electronic system, which undergoes the superconducting transition.

Plasmon Spectrum of Layered Conductors

As is known, the plasmon spectrum in ordinary metals is characterized by the dispersion law: $\omega(\mathbf{q}) = \omega_0 + \alpha q^2$; the value of $\omega_0 \sim 5-10$eV is very high, so that the Coulomb interaction in usual superconductors can be described by a static pseudopotential $\mu^\star$.

The picture in layered conductors is entirely different. The plasmon spectrum of such conductors contains low frequency acoustic branches. Qualitatively, this can be seen in the following way. The plasmons correspond to the solution of the equation: $\epsilon(\kappa, q_z; \omega) = 0$, $\epsilon = 1 + \Pi V$ with $V = e^2/(\kappa^2 + q_z^2)$, κ is the in-plane momentum, the axis z is chosen to be perpendicular to the layers [$\mathbf{q} = (\kappa, q_z)$]. The polarization is provided by the in-plane transport only: $\Pi \equiv \Pi(\kappa, \omega)$. At small κ one can obtain $\Pi \sim -(\kappa/\omega)^2$. As a result, the equation $\epsilon = 0$ at $q_z = 0$ has a root $\omega = \omega_0 = constant$ (this corresponds to the upper branch and is similar to the 3D case. However, for $q_z \neq 0$, including $q_z = \pi/d_c$ (d_c is the interlayer distance), we obtain an acoustic dispersion law $\omega \sim \kappa$. This result has been obtained first in the hydrodynamic approximation in [8]. A general expression for the plasmon band $\omega(\kappa, q_z)$ has the form [9]:

$$\omega = v_F \kappa \sqrt{1 + \frac{\alpha^2}{4(\alpha+1)}}, \qquad \alpha = \frac{4me^2}{\epsilon_M \kappa} \frac{\sinh \kappa d_c}{\cosh \kappa d_c - \cos q_z d_c}. \tag{1}$$

One can show also [10] that the density of states for the plasmon band is peaked at the upper ($q_z = 0$) and the lower ($q_z = \pi/d_c$) branches. As a result, the plasmon band can be modeled as a set of two branches (see Fig. 1). The upper branch is similar to that in the 3D case. The most important factor is the existence of low acoustic branches ("electronic" sound).

Superconducting State

The acoustic branch can contribute to the pairing in a way similar to usual acoustic phonons. Theoretically the pure acoustic plasmon mechanism was studied in [11]. Such a mechanism in conjunction with phonon contribution (phonon-plasmon mechanism) was proposed in [9]. The equation for the order

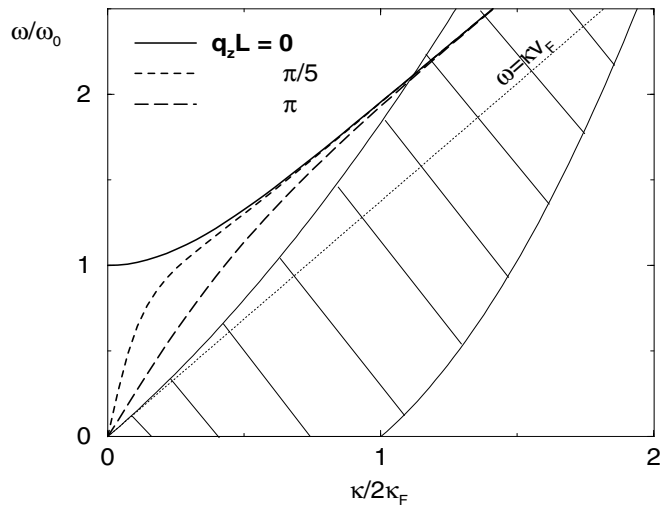

Figure 1. Collective excitations in a layered conductor. At $\omega > v_F\kappa$ there are one optical and $N_c - 1$ acoustic plasmon branches (N_c is the number of conducting planes).

parameter which allows us to evaluate T_c has the form:

$$\Delta(\mathbf{k},\omega_n)Z(\mathbf{k},\omega_n) = T\sum_{m=-\infty}^{\infty}\int \frac{\mathrm{d}^3\mathbf{k}'}{(2\pi)^3}\Gamma(\mathbf{k},\mathbf{k}';\omega_n-\omega_m)F^{\dagger}(\mathbf{k}',\omega_m), \quad (2a)$$

$$Z(\mathbf{k},\omega_n) - 1 = \frac{T}{\omega_n}\sum_{m=-\infty}^{\infty}\int \frac{\mathrm{d}^3\mathbf{k}'}{(2\pi)^3}\Gamma(\mathbf{k},\mathbf{k}';\omega_n-\omega_m)G(\mathbf{k}',\omega_m), \quad (2b)$$

where $F^{\dagger} =< c^{\dagger}_{\mathbf{k},\uparrow}c^{\dagger}_{-\mathbf{k},\downarrow} >$ is the Gor'kov pairing function, $G =< c^{\dagger}_{\mathbf{k},\sigma}c_{\mathbf{k},\sigma} >$ is the usual Green function, and Γ is the total interaction kernel. The total kernel $\Gamma \equiv \Gamma(\mathbf{q},\omega_n-\omega_m)$, with $\mathbf{q} = \mathbf{k} - \mathbf{k}'$, is written in the form

$$\Gamma = \Gamma_{ph} + \Gamma_c + \mu^{\star}\Theta(\omega - \omega_c), \quad (3)$$

The first term on the right hand side of Eq.(2) describes the phonon contribution to the pairing, the third term is the usual static term (it corresponds to the region $\omega < v_F\kappa$), and the second term reflects the dynamic, acoustic plasmon channels of the pairing. The formalism of thermodynamic Green's functions is employed [12]. Let us consider the metalochloronitride $Li_{0.48}(THF)_yHfNCl$. The parameters for this material (see [2–6], are: $d_c = 18.7$A, $\Omega = 60$meV, $m_b = 0.6m_e$, $E_F \sim 1$eV. We have chosen also a reasonable value of $\epsilon_M = 1.75$. Note that the inequality $\epsilon_M > 1$ allows one to justify the use of the RPA, since $\lambda_c \sim \epsilon_M^{-1}$. If we neglect the plasmon term (assume $\lambda_c = 0$), then

we obtain from Eq.(2) the value of $T_c = T_c^{ph}$. which appears to be very low: $T_c^{ph} < 1$K. The presence of the dynamic term makes a great impact. Indeed, with use of the parameters for the compound (see above), we obtain $T_c \simeq 25$K (!), in a good agreement with the observed value. Therefore, the superconducting state in the metal-intercalated chloronitride compound is mainly provided by the exchange of acoustic plasmons. It is essential that the acoustic plasmons are collective excitations of the same electronic system which undergoes the superconducting transition. This case is different from other pairing scenarios. Indeed, usually pairing is provided by some second subsystem (ions for the phonon mechanism, magnetic excitations,etc.) Even the other case where acoustic plasmons arise (the so-called "demons" in the presence of two bands, see the review [13] and [14, 15]) requires the presence of two bands. In our case of layered conductors we are dealing with a single group of electrons for which the acoustic plasmons correspond to their collective excitations. Therefore, we are dealing with the phenomenon of self-supported superconductivity. The electronic mechanisms of superconductivity were introduced first in [16–18]. We think that the layered metalochloronitrides are the first observed systems with electronic nature of the pairing mechanism. The presence of low frequency plasmons is important for other layered conductors as well. The relative contribution of the plasmon mechanism depends on the values of the parameters entering Eq.(2) and is different for various systems. For example, for the organic superconductor κ-$(ET)_2Cu(NCS)_2$ one can calculate $T_c^{ph} \sim 6.3$K and $T_c \sim 10.4$K, that is, about 40% of the pairing is provided by the acoustic plasmons exchange (see Ref. [19]).

Summary

In summary, it is shown that the superconducting state of the novel family of layered superconductors, the metalochloronitrides, is provided by the plasmon mechanism, or more specifically, by the exchange of acoustic plasmons, the existence of which is specific to layered conductors. To the best of our knowledge, this is the first observed system with self-supported superconductivity, that is, with the pairing provided by collective modes of the same electrons as those undergoing the superconducting transition.

References

[1] S. Yamanaka, K-I. Hotehama and H. Kawaji. *Nature*, 392:580, 1998.

[2] H.Tou, Y. Maniwa, T. Koiwasaki, and S. Yamanaka. *Phys. Rev. B* 63:020508 (2000); *Phys.Rev.Lett.* 86:5775, 2001.

[3] H. Tou, Y. Maniwa, and S. Yamanaka. *Phys. Rev. B* 67:100509, 2003.

[4] P. Adelmann, B. Renker, H. Schober, M. Braden, and F.Fernandez-Diaz. *J. Low Temp. Phys.* 117:449, 1999.

[5] A. Cros, A. Cantarero, D. Beltran-Porter, J. Oro -Solet', and A. Fuertes. *Phys. Rev. B* 67:104502, 2003.

[6] R. Weht, A. Filippetti, and W.E. Pickett. *Europhys. Lett.* 48:320, 1999.

[7] G.Grimvall. *The electron-phonon interaction in metals*. North-Holland, Amsterdam, 1981; V.Kresin and G.Zaitsev. *Sov. Phys. JETP*, 47:983, 1978.

[8] A. Fetter. *Ann. Phys. N.Y.*, 88:1, 1974.

[9] V.Z. Kresin and H. Morawitz. *Phys. Lett. A* 145:368, 1990; *Phys. Rev. B* 37:7854, 1988.

[10] H. Morawitz, I. Bozovic, V.Z. Kresin, G. Rietveld, and D. van der Marel. *Z. Phys. B: Condens. Matter* 90:277, 1993.

[11] Y. Takada. *J. Phys. Soc. Jpn.* 45:786, 1977; *Phys. Rev. B* 37:150, 1988; 61:238, 1992.

[12] A.Abrikosov, L.Gor'kov, I.Dzyaloshinskii. *Methods of Quantum Field Theory in Statistical Physics*, Dover, NY, 1963.

[13] J. Ruvalds. *Adv. Phys.* 30:677, 1981.

[14] B.Geilikman. *JETP* 21:796, 1965; E.Pashitskii and V.Chernousenko. *ibid.*, 60:1483, 1971; J.Askenazi and C.Kuper. *Physica C* 153:1315, 1988.

[15] W.A. Little. *Phys. Rev.* 134:A1416, 1964.

[16] V.Ginzburg and D.Kirzhnits, editors. *High temperature superconductivity*. Cons. Bureau, NY, 1987.

[17] B.Geilikman. *Usp.* 16:17, 1973.

[18] A. Bill, H. Morawitz, and V. Z. Kresin. *Phys.Rev.B* 66:100501(R), 2002.

[19] A. Bill, H. Morawitz, and V. Z. Kresin. *Phys.Rev.B* 68:114519, 2003.

FIRST ORDER SUPERCONDUCTING TRANSITION NEAR A FERROMAGNETIC QUANTUM CRITICAL POINT

Dirk K. Morr *
Department of Physics, University of Illinois at Chicago, Chicago IL 60607

Abstract We study the emergence of triplet superconductivity in an electronic system near a ferromagnetic quantum critical point (FQCP). Previous studies found that the superconducting transition is of second order, and T_c is strongly reduced near the FQCP due to pair-breaking effects from thermal spin fluctuations. In contrast, we show that near the FQCP, the system avoids pair-breaking by undergoing a *first order* transition at a much larger T_c. At some distance from the FQCP, a second order superconducting transition emerges at a tricritical point.

Keywords: ferromagnetic superconductors, ferromagnetic quantum critical point, first order transition, tricritical point

Superconductivity near a magnetic instability is a topic of current interest in condensed-matter physics. Magnetically mediated pairing near an antiferromagnetic instability is a candidate scenario for $d-$wave superconductivity in the cuprates and heavy fermions compounds while superconductivity mediated by the exchange of ferromagnetic spin fluctuations is expected near ferromagnetic transitions. Ferromagnetic exchange yields Cooper pairs with $S = 1$ and therefore generally gives rise to triplet pairing [1]. In recent years, an intensive search has focused on superconductivity in compounds which can be tuned to a ferromagnetic quantum critical point (FQCP) by varying either pressure or chemical composition. Examples include MnSi, and the heavy fermion compound UGe_2 [2].

The emergence of superconductivity in electronic systems close to a ferromagnetic instability has recently been studied by solving a linearized gap equation within the Eliashberg formalism [3–5]. In both two- (2D) and three-dimensional (3D) systems, it was found that the superconducting transition temperature, T_c^l ('l' stands for linearized) substantially decreases as the sys-

*This work was done in collaboration with A. V. Chubukov, A. M. Finkel'stein, and R. Haslinger

J. Ashkenazi et al. (eds.), New Challenges in Superconductivity: Experimental Advances and Emerging Theories, 219-224.

tem approaches criticality. The physical origin of this decrease lies in the presence of thermal spin fluctuations which behave like magnetic impurities whose scattering potential diverges as the FQCP is approached [3–5]. This behavior is reflected in the fermionic self-energy in the normal state, $\Sigma(\omega_n) \propto iT\sum_m \mathrm{sign}\,(\omega_n)\chi_L(\omega_m - \omega_n)$, where $\chi_L(\omega) = \int d^{D-1}q\chi(q,\omega)$ is the "local" spin susceptibility. Since $\chi_L(\omega = 0)$ diverges at the FQCP for $D \leq 3$ (assuming $\chi(q,0) = \chi_0/(\xi^{-2} + q^2)$ with $\xi \to \infty$), the dominant contribution to $\Sigma(\omega_n)$ comes from the $n = m$ term in the frequency sum, i.e., from classical, thermal spin fluctuations. This leads to $\Sigma(\omega) = i\gamma \mathrm{sign}\,\omega$ with $\gamma \propto T\xi^{3-D}$ for system dimension $D < 3$ and $\gamma \propto T\log\xi$ for $D = 3$. Inserting this result in the linearized gap equation yields that T_c^l vanishes as $T_c^l \propto \xi^{D-3}$ in $D < 3$, and $T_c^l \propto 1/\log\xi$ for $D = 3$. Numerical solutions of the linearized Eliashberg equations near a FQCP confirm this conclusion [3–5].

We argue below that the behavior of the system is actually different in that close to a FQCP, superconductivity emerges via a *first order phase transition* at $T_c \sim T_{c0}$, where T_{c0} is the transition temperature in the absence of thermal fluctuations. The origin of this first order transition lies in feedback effects from the superconducting pairing on the ferromagnetic spin fluctuations. These effects, which are only accounted for when considering the full set of nonlinear Eliashberg equations, lead to a smooth evolution of the pairing gap from $T = 0$ up to $T \sim T_{c0}$. The much smaller T_c^l is thus the end point of the temperature hysteresis loop at which the normal state becomes unstable.

The physics of the first order transition can be understood by considering the ratio of the divergent terms in the self-energy and the pairing vertex. These terms appear with different signs in the gap equation, hence if the overall factors were the same, the pair-breaking effects would be cancelled out. The overall factors are, however, not equal since the spin factor in the self-energy, $\Sigma_{\alpha\beta} = \Sigma\delta_{\alpha\beta}$, is 3 as $\sum_\gamma \sigma_{\alpha\gamma}\sigma_{\gamma\beta} = 3\delta_{\alpha\beta}$. In contrast, the spin factor in the triplet pairing vertex, $\Gamma_{\alpha\beta} = \Gamma\delta_{\alpha\beta}$, is 1 as $\sum_{\gamma,\delta} \delta_{\gamma\delta}\sigma_{\gamma\alpha}\sigma_{\delta\beta} = \delta_{\alpha\beta}$. The ratio of the divergent terms in the self-energy and in the pairing vertex is then $3/1$, i.e., pair-breaking effects are not cancelled out, and T_c^l vanishes at criticality.

Consider next a triplet superconducting state, which can be either of the A or B type [1, 6]. Since the low-energy fermions acquire a gap, the low-energy part of the spin susceptibility, arising from these fermions, changes. In the A phase, where without loss of generality the spin of the Cooper pair $\vec{S}_{cp}$ lies in the spin XY-plane, feedback effects on the spin susceptibility are different for χ_{zz} and $\chi_\pm$. In particular, $\chi_\pm$ remains massless at the FQCP, but χ_{zz} acquires a mass and becomes non-divergent. When $\chi_\pm$ and χ_{zz} are not equivalent, the spin summation shows that the former $3/1$ ratio of the dangerous terms becomes now $[2\chi_\pm + \chi_{zz}]\,/\,[2\chi_\pm - \chi_{zz}]$ and the divergent terms cancel out in the *nonlinear* gap equation. Thus the superconducting state remains stable well above T_c^l, but only as long as $\Delta(\omega)$ is not small. We then expect that at

the FQCP, the solution with a finite gap survives up to $T_c^{nl} \sim T_{c0} \gg T_c^l$ ('nl' stands for the solution of the nonlinear equation) where it becomes unstable. This is a classic first order transition. The superconducting state therefore remains stable well above T_c^l, but only as long as the gap remains large. In the B phase, the spin susceptibility remains isotropic, but all of its components become massive and thus do not diverge in the superconducting state [6].

In the remainder of this paper we consider the A phase and compute T_c^{nl} from the full set of nonlinear Eliashberg equations. Our starting point is the spin-fermion model, which describes the interaction of low-energy fermions with their own spin degrees of freedom, $\mathbf{S_q}$, whose propagator is peaked at $q = 0$ [7, 3–5, 8]. The model is described by the Hamiltonian

$$\begin{aligned} \mathcal{H} &= \sum_{\mathbf{k},\alpha} \mathbf{v_F}(\mathbf{k}-\mathbf{k}_F) c^\dagger_{\mathbf{k},\alpha} c_{\mathbf{k},\alpha} + \sum_q \chi^{-1}(\mathbf{q}) \mathbf{S_q} \mathbf{S_{-q}} \\ &\quad + g \sum_{\mathbf{q},\mathbf{k},\alpha,\beta} c^\dagger_{\mathbf{k+q},\alpha}\, \sigma_{\alpha,\beta}\, c_{\mathbf{k},\beta} \cdot \mathbf{S_{-q}}\,, \end{aligned} \tag{1}$$

where the spin-fermion coupling, g, the Fermi velocity, v_F (we assume a circular Fermi surface), and the static spin propagator $\chi(q,0)$ are input parameters. While the upper energy cutoff is in general also an input parameter, our results are cutoff independent in $D = 2$ (our conclusions are, however, also valid in $D = 3$). We assume that the static $\chi(q,0)$ has the conventional lorentzian form with a weakly temperature dependent ξ. The dynamical part of $\chi(q,\Omega_m) = \chi_0/[q^2 + \xi^{-2} + \Pi(q,\Omega_m)]$ arises from the interaction with the low-energy fermions and is explicitly calculated. A conventional perturbation theory in the spin-fermion coupling (for which $\Sigma = \Pi = 0$ is the point of departure) holds in powers of $\lambda = g^2\chi_0/(4\pi v_F \xi^{-1})$. Since the quantum-critical region near the FQCP corresponds to the strong coupling limit, we employ the Eliashberg theory [9] whose validity requires certain restrictions that we discuss after presenting the results.

We first consider the situation at the FQCP where $\xi^{-1} = 0$. In the normal state, the dynamical part of the spin polarization operator, $\Pi(q,\Omega_m)$, is independent of the fermionic self-energy, $\Sigma(q,\omega_n)$ (but not vice versa), as the essential momenta for $\Pi(q,\Omega_m)$ are those with $v_F q \gg \Omega_m, \Sigma$. As a result, $\Pi(q,\Omega_m)$ has the same form as for free fermions, i.e., for $|\Omega_m| \ll v_F q$, $\Pi(q,\Omega_m) = F(\Omega_m)/(v_F q)$ where $F(\Omega_m) = \alpha k_F^2 |\Omega_m|$, $\alpha = g^2\chi_0/(2\pi E_F)$, and $E_F = k_F v_F/2$. At the same time, one finds $\Sigma(\omega_m) = \omega_0^{1/3}\, \omega_m^{2/3}$, where $\omega_0 = (3\sqrt{3}/4)\alpha^2 E_F$. The non-Fermi liquid, $\omega^{2/3}$-dependence of the self-energy in 2D is due to the divergence of the perturbation theory at the FQCP [10]. In the superconducting state, the equations for two components of $F(\Omega)$ (F_{zz} and $F_{xx} = F_{yy}$) are coupled to the equation for the pairing gap $\Delta(\omega)$, which need to be self-consistently solved. At the FQCP, the coupled equations

for $\Delta(\omega)$, $F_{zz}(\Omega) = F_-$ and $F_{xx} = F_{yy} = F_+$ are

$$\begin{aligned}\Delta\ (\omega_n) &= \frac{4\pi}{9}\omega_0^{1/3} T \sum_m \frac{1}{\sqrt{\omega_m^2 + \Delta^2(\omega_m)}} \\ &\times \left\{ \frac{2\omega_m}{[F_+(T,\Delta,\omega_m-\omega_n)]^{1/3}} \left[\frac{\Delta(\omega_m)}{\omega_m} - \frac{\Delta\ (\omega_n)}{\omega_n} \right] \right. \\ &\left. - \frac{\omega_m}{[F_-(T,\Delta,\omega_m-\omega_n)]^{1/3}} \left[\frac{\Delta(\omega_m)}{\omega_m} + \frac{\Delta\ (\omega_n)}{\omega_n} \right] \right\} \qquad (2)\end{aligned}$$

and

$$F_\pm(T,\Delta,\omega_m-\omega_n) = \pi T \sum_n \left[1 - \frac{\omega_n(\omega_m) \pm \Delta(\omega_n)\Delta(\omega_m)}{\sqrt{\omega_n^2+\Delta^2(\omega_n)}\sqrt{\omega_m^2+\Delta^2(\omega_m)}} \right] \qquad (3)$$

Since $F_+(T,\Delta,0) = 0$ the corresponding susceptibilities, χ_{xx} and χ_{yy}, describe massless modes. The vanishing of $F_+(T,\Delta,0)$, however, is not dangerous as it is compensated by the simultaneous vanishing of the numerator in Eq.(2). The vanishing of $F_-(T,\Delta,0)$ would be dangerous, but for finite Δ, $F_-(T,\Delta,0) = 2\pi T \sum_n \Delta^2(\omega_n)/\sqrt{\omega_n^2+\Delta^2(\omega_n)}$ is also finite and the longitudinal spin excitations described by χ_{zz} are massive. In contrast, for the linearized gap equation Δ is vanishingly small, $F_-(T,\Delta,0)$ vanishes, and the r.h.s of Eq.(2) diverges. Due to this divergence, the linearized gap equation does not have a solution down to $T = 0$. Since the only energy scale in the Eliashberg equations is ω_0, the gap equation is *fully universal*. In Fig. 1a we present the numerical solution for $\Delta(T)$ at the lowest Matsubara frequency, $\omega_m = \pi T$. As expected for a first order phase transition, the gap changes discontinuously from a finite value to zero at $T_c^{nl} \sim 0.015\omega_0$. The inset shows that the discontinuous jump in Δ occurs for all Matsubara frequencies.

Away from criticality ($\xi^{-1} \neq 0$) the equations for $F_\pm(T,\Delta,\omega_m)$ retain their form, but in the gap equation, the factors $F_\pm(T,\Delta,\omega_m)$ are replaced by $F_\pm(T,\Delta,\omega_m)/I^3(\beta_\pm)$, where $I(\beta_\pm)$ by itself depends on $F_\pm(T,\Delta,\omega_m)$ through

$$I(\beta_\pm) = \frac{3\sqrt{3}}{2\pi} \int_0^\infty dx \frac{x}{1+\beta_\pm x + x^3}\ , \qquad (4)$$

$\beta_\pm = b/[F_\pm(T,\Delta,\Omega_m)/\omega_0]^{2/3}$, and $b = (8/3\sqrt{3})^{2/3}(\alpha k_F \xi)^{-2}$ measures the deviation from the FQCP ($b = 0$ at the FQCP). At finite ξ, the gap equation is divergenceless, even at infinitesimally small Δ, thus both T_c^{nl} and T_c^l are nonzero. In Fig. 1b we plot $\Delta(T, i\pi T)$ for $b = 2$. The temperature dependence of the gap is now continuous, in contrast to Fig. 1a, and the transition is second order for $b > b_c$ (the inset shows that the continuous evolution of Δ holds for all Matsubara frequencies). The tricritical point is located at $b_c \approx 1.2$, where

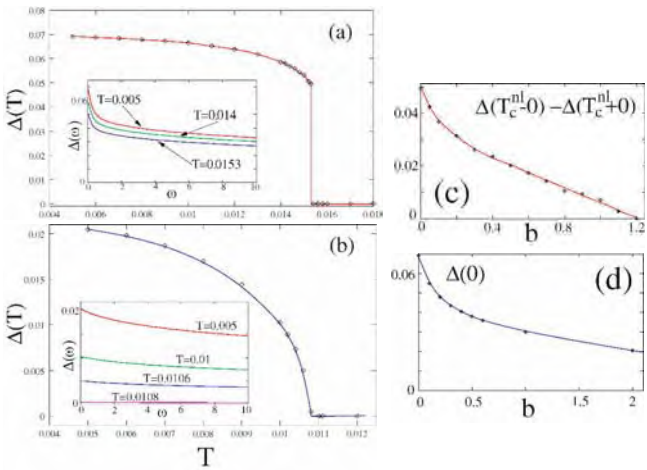

Figure 1. (a) Temperature dependence of $\Delta(T, \omega_m)$ at $\omega_m = \pi T$ for $b = 0$. Δ, T and ω_m are in units of ω_0. The discontinuity of $\Delta(T)$ at 0.015 indicates a first order transition. The inset shows $\Delta(\omega)$ versus frequency at several T. (b) Same away from the FQCP, for $b = 2$. Now the transition is continuous. (c) The jump of $\Delta(T, i\pi T)$ at the instability temperature versus b. All lines are guides to the eye. (d) $\Delta(T, i\pi T))$ at the lowest T versus b.

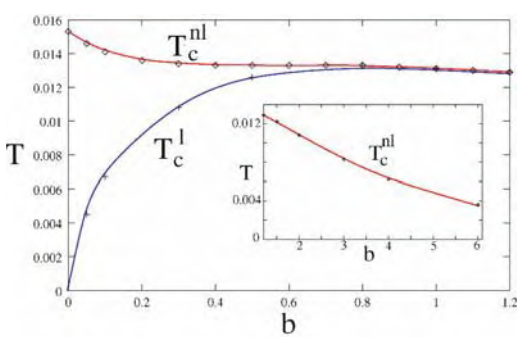

Figure 2. Phase diagram near the FQCP. For $b < b_c$, the superconducting transition is first order, while for $b > b_c$, it is a second order transition. Inset: the reduction of T_c at large b.

the gap discontinuity disappears (the jump of $\Delta(T, i\pi T)$ at T_c^{nl} is plotted in Fig. 1c). The system's phase diagram is presented in Fig. 2. Note that T_c^{nl} and T_c^l are the instability temperatures for the solutions with a large and infinitesimally small gap, respectively. The actual first order transition temperature, T_c, lies between T_c^l and T_c^{nl} and remains *finite* at $b = 0$. The insert shows the reduction of T_c at large b due to the decreased effective coupling.

The validity of the Eliashberg theory requires that three conditions be satisfied. First, typical bosonic momenta q_B should be much larger than typical fermionic $|k - k_F|$, leading to $\Sigma(k, \omega) \approx \Sigma(\omega)$. Since $q_B \sim \alpha k_F$, while the $|k - k_F| \sim \omega_0 / v_F \sim \alpha^2 k_F$, the Eliashberg theory is valid if $\alpha \ll 1$. Hence, $\omega_0 \ll E_F$ and the physical behavior of the system is universally determined by low energy excitations only. Second, vertex corrections should be small. Generally, this is not possible for $q_B \ll k_F$, but for $\alpha \ll 1$, we only need to consider vertex corrections with $\Omega \ll v_F q$ (since $v_F q_B \gg \Omega \sim \omega_0$) in which case they scale as $\log \xi$. They are still non-negligible at the FQCP, where they change the pole in the spin susceptibility into a branch cut [7]. Third, the momentum dependence of the pairing gap should be neglected, while preserving the gap symmetry. This approximation is again justified for $\alpha \ll 1$, since the typical momentum transfers along the Fermi surface $\delta k \sim q_B \sim \alpha k_F$ are much smaller than k_F. The momentum variation of the gap only introduces $O(1)$ corrections to the Eliashberg theory [8], which can be safely neglected.

In summary, we showed that near a FQCP, spin fluctuation exchange gives rise to a strong first order transition into a triplet superconducting state. As a result, T_c saturates at a nonzero value at criticality. The first order transition persists up to a finite distance from the FQCP, where it becomes second order.

Acknowledgments

It is our pleasure to thank A. Abanov, D. Khveschenko, D. Pines, A. Tsvelik and Z. Wang for useful discussions.

References

[1] P.W. Anderson and P. Morel, Phys. Rev **123**, 1911 (1961); for a review see e.g., A.J.Legget Rev. Mod. Phys. **47**, 331, 1975..

[2] C. Pfleiderer, G. J. McMullan, S. R. Julian, and G. G. Lonzarich, Phys. Rev. B **55**, 8330 (1997); S.S. Saxena *et al*, Nature **406**, 587 (2000).

[3] Ph. Monthoux and G.G. Lonzarich, Phys. Rev. B **59**, 14598 (1999).

[4] Z. Wang, W. Mao and K. Bedell, Phys. Rev. Lett. **87**, 257001 (2001); K.B. Blagoev, J.R. Engelbrecht and K. S. Bedell, Phys. Rev. Lett **82**, 133 (1999).

[5] R. Roussev and A. J. Millis, Phys. Rev. B **63**, 140504 (2001).

[6] D. Vollhardt and P. Wolfle, "The superfluid phases of helium3", Taylor and Francis, London, 1990.

[7] A. Abanov, A. V. Chubukov, J. Schmalian, cond-mat/0107421.

[8] Ar. Abanov, A. V. Chubukov, and A. M. Finkel'stein, Europhys. Lett., **54** ,488-494 (2001).

[9] G.M. Eliashberg, Sov. Phys. JETP **11**, 696 (1960); D.J. Scalapino in *Superconductivity*, Vol. 1, p. 449, Ed. R. D. Parks, Dekker Inc. N.Y. 1969; F. Marsiglio and J.P. Carbotte, in 'The Physics of Conventional and Unconventional Superconductors', Eds. K.H. Bennemann and J.B. Ketterson (Springer-Verlag).

[10] B. L. Altshuler, L.B. Ioffe, and A. J. Millis, Phys. Rev. B **52**, 5563 (1995).

STRUCTURES AND SUPERCONDUCTING PROPERTIES OF SODIUM COBALT OXIDES

Kazunori Takada,[1,3] Hiroya Sakurai,[2] Eiji Takayama-Muromachi,[2]
Fujio Izumi,[1] Ruben A. Dilanian,[1] and Takayoshi Sasaki[1,3]

[1]*Advanced Materials Laboratory, National Institute for Materials Science 1-1, Namiki, Tsukuba, Ibaraki 305-0044, Japan*

[2]*Superconducting Materials Center, National Institute for Materials Science 1-1, Namiki, Tsukuba, Ibaraki 305-0044, Japan*

[3]*CREST, Japan Science and Technology Agency*

takada.kazunori@nims.goip

Abstract Since the discovery of high T_C cuprates, superconductivity has been sought in nickel or cobalt oxides, because the elements are neighboring to copper in the periodic table; however the attempts were in vain. We found the first superconductor, $Na_xCoO_2.yH_2O$ ($x \approx 0.35$, $y \approx 1.3$), in cobalt oxides.

Keywords: Sodium cobalt oxide, superconductivity, layered structure, hydrate

1. Introduction

Cobalt oxides with layered structures are attracting a great deal of interest because of their potential for practical applications and their unique physical properties. Li_xCoO_2 has been used as a cathode material in commercialized lithium-ion batteries [1], and Na_xCoO_2 shows large thermoelectric power [2], which is promising for its application to thermoelectric elements. Their unique physical properties are based on spin-frustration or strongly-correlated electrons. Such interest has provoked a number of studies on the layered cobalt oxides; however, superconductivity has never been found in the system. We found that a softchemical modification makes a cobalt oxide superconducting [3]. This finding made the material much more interesting.

2. Softchemical modification of sodium cobalt oxide into a superconducting phase

The superconducting cobalt oxide was prepared from a parent compound, $Na_{0.7}CoO_2$, that has a layered structure comprising of two-dimensional CoO_2 layers and charge-balancing Na^+ ions between them. Partial deintercalation of Na^+ ions by chemical oxidation using an ace-tonitrile solution of bromine and the subsequent insertion of H_2O molecules into the galleries brought about a

J. Ashkenazi et al. (eds.), New Challenges in Superconductivity: Experimental Advances and Emerging Theories, 225-230.

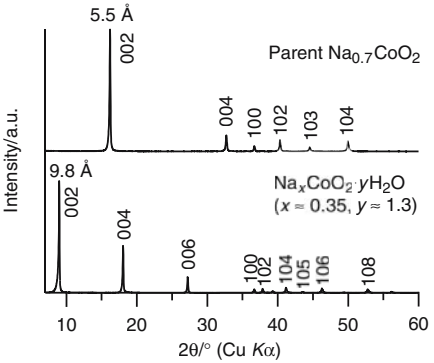

Figure 1. Powder X-ray diffraction patterns of parent $Na_{0.7}CoO_2$ and the bilayer-hydrate phase obtained by the softchemical modification. Miller indices based on space group of $P6_3/mmc$ for strong reflections are labeled.

remarkable change in the XRD pattern as shown in Fig. 1. The basal spacing, or interlayer distance, was increased from 5.5 Å in the parent phase to 9.8 Å. The large separation between the adjacent CoO_2 layers will enhance the two dimensionality. Superconductivity might be found in the new phase with the large interlayer distance, because such strong two-dimensionality is important nature of high T_C cuprates. The magnetic and electric properties of the new phase shown in Fig. 2 were clear evidence for superconducting transition at *ca*. 5 K.

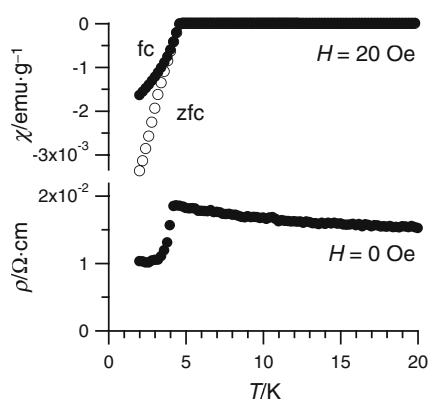

Figure 2. Magnetic susceptibility (χ) and resistivity (ρ) of the bilayer hydrate as a function of absolute temperature T.

3. Crystal structure of the superconducting cobalt oxide

Procedures that formed the superconducting phase were a chemical oxidation with Br_2 and immersion in water. Therefore, conceivable intercalation guest that propped open the interlayer is H_2O molecule. In fact, energy dispersive X-ray spectroscopy evidenced that bromine did not remain in the superconducting phase, and infrared spectrum of the evolved gas from the heated sample revealed the presence of H_2O molecules in the superconducting phase. When the sample of the superconducting phase was dried, a new series of basal reflections with an interlayer distance of 6.9Å appeared with disappearance of the superconductivity [4]. The new reflections disappeared with recovery of the original reflections of the 9.8 Å phase, when humidity, to which the sample was exposed, was increased again. This result suggested that the superconducting phase has H_2O molecules in the galleries and removal and insertion of H_2O molecules controlled its interlayer distance. The interlayer distances of 5.5 Å in the parent oxide, 9.8 Å in the superconducting phase, and 6.9 Å in the dried phase are similar to those found in a manganese oxide system: an anhydrous phase, a bilayer-hydrate (BLH) one called buserite, and a monolayer-hydrate one called birnessite [5], respectively. Therefore, it will be concluded that H_2O molecules were coordinated to the residual Na^+ ions, forming a double layer in the gallery in the superconducting phase. However, positions of H_2O molecules in such BLH structures have not been refined, because the highly-disordered arrangement of H_2O molecules makes the refinement rather difficult. We tried to refine the crystal structure by a Rietveld analysis with aid of a maximum-entropy method (MEM).

Layered sodium cobalt oxides show many polymorphs with different stacking sequences of CoO_2 layers [6,7]. First of all, we should know the stacking sequence. When the reflections were indexed, all of them were indexable based on the same space group as the parent oxide ($P6_3/mmc$), indicating that the superconducting phase has the same stacking sequence of CoO_2 layers as the parent phase. We used MEM to find out the positions of H_2O molecules. We started with a structure model that does not contain H_2O molecules. Structure factors were estimated by a preliminary Rietveld analysis using this model, and electron-density distribution was calculated by MEM from the structure factors, using computer programs, RIETAN-2000 [8] and PRIMA [9], respectively. The MEM analysis gave electron-density distribution displayed in Fig. 3, in which additional electrons coming from H_2O molecules, which were excluded in the structure model, were clearly observed.

When the structure model was modified by taking into account H_2O molecules positioned where the additional electrons were observed, the structure parameters refined by the Rietveld analysis listed in Table 1 gave satisfactorily low *R*-factors.

Table 1. Fractional coordinates, occupancies, g, and isotropic atomic displacement parameters, U, of $Na_xCoO_2{\cdot}yH_2O$ ($x \approx 0.35$, $y \approx 1.3$).

	Site	x	y	z	g	U/Å^2
Co	2*a*	0	0	0	1	0.0063(6)
O	4*f*	1/3	2/3	0.0451(3)	1	0.0162(12)
Na1	2*d*	2/3	1/3	1/4	0.159(4)	= U(O)
Na2	2*b*	0	0	1/4	0.192*	= U(O)
WO1†	12*k*	0.174(13)	= 2x(WO1)	0.1793(2)	0.070(12)	= U(O)
WO2†	12*k*	0.370(12)	= x(WO2)/2	= z(WO1)	0.176(12)	= U(O)

Space group: $P6_3/mmc$ (No. 194); $a = 2.8230(2)$ Å and $c = 19.6207(14)$ Å; $R_{wp} = 11.58\%$ ($S = 2.17$), $R_B = 2.84\%$, and $R_F = 3.53\%$. †WO denotes a virtual chemical species whose atomic scattering factor is set equal to the sum of one O and two H atoms. *Na content was constrained to be 0.351 that was determined by ICP-AES.

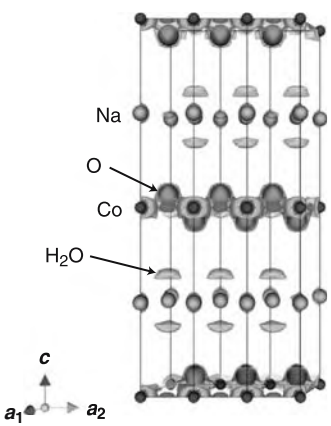

Figure 3. Isosurfaces of electron densities calculated by a MEM analysis using from a preliminary structure model that does not contain H_2O molecules. Balls indicate atoms used in the structure model. Equidensity level: 1.2 Å^{-3}.

In BLH-Na_xCoO_2, the guest species in the galleries are highly disordered. MEM is quite effective for detailed structure analysis of such an intercalation compound. In MEM-based whole-pattern fitting (MPF), crystal structures are expressed not by structure parameters such as fractional coordinates and atomic displacement parameters but by electron densities in the unit cell. Therefore, MPF allows us to represent the disordered atomic configuration in a more appropriate way than conventional Rietveld analysis adopting a split-atom model. The MPF decreased the R-factors from $R_B = 2.84\%$, $R_F = 3.53\%$ to $R_B = 1.84\%$, $R_F = 2.03\%$. Disordered arrangement of H_2O molecules are clearly seen as spread electron-density distribution as shown in Fig. 4.

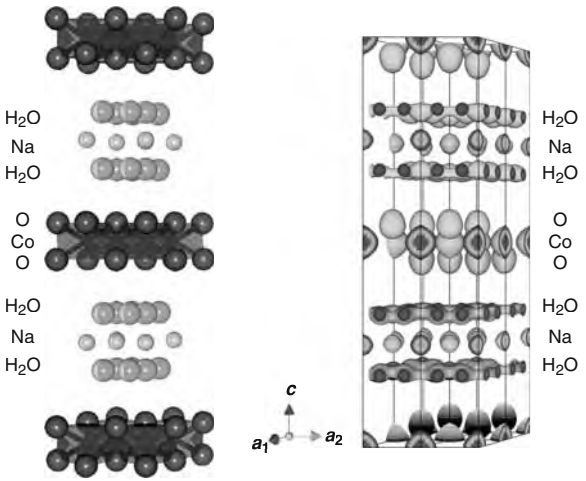

Figure 4. Structure model (left) and isosurfaces of electron densities determined for the sodium cobalt oxide hydrate by MEM analysis (right). Equidensity level: 1.0 $Å^{-3}$.

4. Summary

We have presented the softchemical modification making a cobalt oxide superconducting, and the results of the structure study on the superconducting phase. Although many theoretical studies already have been done to elucidate its superconducting mechanism, its characterization still remains rather difficult owing to its strongly-disordered arrangement of the guest species and non-stoichiometry. For example, conventional X-ray diffraction was used to investigate its crystal structure in the present study. More accurate characterization, e.g. using neutron diffraction, will lead us to better understanding of the material. We have investigated its crystal structure again using synchrotron radiation. The result will be presented in near future.

Acknowledgments

The authors wish to thank Messrs. Y. Yajima, S. Takenouchi, and H. Komori of our institute for IR, ICP-AES, and EDX analyses.

References

[1] Mizushima, K., Jones, P. C., Wiseman, P. J. and Goodenough, J.B. (1980). Li_xCoO_2 ($0 \leq x \leq 1$): A new cathode material for batteries of high energy. *Mat. Res. Bull.*, 15:783–789.

[2] Terasaki, I., Sasago, Y., and Uchinokura, K. (1997). Large thermoelectric power in $NaCo_2O_4$. Phys. *Rev. B*, 56:R12685–R12687.

[3] Takada, K., Sakurai, H., Takayama-Muromachi, E., Izumi, F., Dilanian, R. A., and Sasaki, T. (2003). Superconductivity in two-dimensional CoO_2 layers. *Nature*, 422:53–55.

[4] Takada, K., Sakurai, H., Takayama-Muromachi, E., Izumi, F., Dilanian, R. A., and Sasaki, T. (2004). Structural difference between a superconducting sodium cobalt oxide and its related phase. *J. Solid State Chem.,* 177:372–276.

[5] Chen, R., Zavalij, R., Whittingham, M. S. (1996). Hydrothermal synthesis and characterization of $K_xMnO_2{\cdot}yH_2O$. *Chem. Mater.*, 8:1275–1280.

[6] Fouassier, C., Matejka, G., Reau, J. -M, and Hagenmuller, P. (1973). Sur de nouveaux bronzed oxygénés de formule Na_xCoO_2 ($x \leq 1$), le systém cobalt-oxygéne-sodium. *J. Solid State Chem.*, 6:532–537.

[7] Braconnier, J. -J., Delmas, C., Fouassier, C., and Hagenmuller, P. (1980). Comportment electrochimique des phases Na_xCoO_2. Mat. Res. Bull., 15:1797–1804.

[8] Izumi, F and Ikeda, T. (2000). A Rietveld-analysis program RIETAN-98 and its applications to zeolites. *Mater. Sci. Forum*, 321–324:198–203.

[9] Izumi, F. and Dilanian, R. A. *Recent Research Developments in Physics*, Vol. 3, PartII, pages 699–726. Transworld Research Network, Trivandrumn, 2002.

UPPER CRITICAL FIELD FOR COBALT OXIDE SUPERCONDUCTORS

Maciej M. Maśka and Marcin Mierzejewski
Department of Theoretical Physics, Institute of Physics
University of Silesia, 40–007 Katowice, Poland

Abstract Motivated by the recent discovery of superconductivity in the cobalt oxide superconductors, we calculate the upper critical field for the CoO_2 layer. Using the lattice version of the Gor'kov equations we investigate how applied magnetic field affects superconductivity on a triangular lattice. We demonstrate the possibility of field-induced transition from singlet to triplet superconductivity, explaining the observed temperature dependence of the upper critical field.

The fundamental problem of the influence of the external magnetic field on superconductivity has attracted much interest for several decades. There are two mechanisms responsible for a suppression of conventional superconductivity in an external magnetic field: the Pauli pair breaking and the diamagnetic pair breaking. First of them, the Pauli pair breaking, is connected with the Zeeman coupling. The magnetic field tends to align the spins of the electrons forming the Cooper pair, and the singlet superconductivity disappears at the Chandrasekhar–Clogston (CC) limit [1]. However, this critical field for the majority of type–II systems is found to be above H_{c2} determined by the orbital (diamagnetic) pair–breaking. Especially, this effect is of minor significance in materials with low effective g–factor. Another possibility is the superconductivity with nonhomogeneous order parameter (the Larkin–Ovchinnikov–Fulde–Ferrell state [2]), which can exist above the CC limit. One can also look for high–magnetic–field superconductivity in systems with triplet equal spin pairing.

The second effect, the diamagnetic pair–breaking, usually crucial in determining the upper critical field, is connected with the orbital frustration of the superconducting order parameter in a magnetic field. This frustration enlarges the free energy of the superconducting state, and, when the magnetic field is strong enough, the normal state becomes energetically favorable. The orbital effect can be reduced in layered two–dimensional superconductors, when the applied magnetic field is parallel to the conducting layers. Such a situation has been analyzed theoretically [3] and recently observed experimentally in organic conductors [4].

The upper critical field, i.e., the magnitude of the magnetic field at which superconductivity disappears in the whole sample, can be determined using

J. Ashkenazi et al. (eds.), New Challenges in Superconductivity: Experimental Advances and Emerging Theories, 231-234.

various methods. However, due to the complexity of the Gor'kov equations one usually assumes that the normal–state properties of the system under consideration can properly be described by three– [5] or two–dimensional [6] electron gas. Recently, we have proposed an approach that enables calculation of the upper critical field for a two–dimensional lattice gas [7, 8]. This method has been developed for *s*– and *d*–wave superconductivity on a square lattice. In the present paper we extend it to cover a triplet pairing and a triangular lattice. Such an extension is motivated by the recent discovery of superconductivity in $Na_xCoO_2 \cdot yH_2O$. This systems is made of stacked triangular layers and it is unclear whether its superconductivity originates from singlet or triplet pairing. The temperature dependence of the upper critical field, measured by Yang *et al.* [9], possesses a very large slope and extrapolated to low temperatures goes far above the CC limit. This feature strongly supports the triplet pairing scenario, at least in strong applied field. The superconductivity occurs when the distance between CuO_2 layers is enlarged by hydration. This indicates the crucial role of the dimensionality of the system.

We consider a two–dimensional triangular lattice immersed in a perpendicular uniform magnetic field of magnitude H_z. We assume pairing interactions, V^s and V^t, responsible for singlet and triplet pairing, respectively. The relevant Hamiltonian reads:

$$\begin{aligned} H = & \sum_{\langle ij\rangle\sigma} t_{ij} e^{i\theta_{ij}} c^\dagger_{i\sigma} c_{j\sigma} - \mu \sum_{i,\sigma} c^\dagger_{i\sigma} c_{i\sigma} - g\mu_B H_z \sum_i \left(c^\dagger_{i\uparrow} c_{i\uparrow} - c^\dagger_{i\downarrow} c_{i\downarrow}\right) \\ & + V^s \sum_{\langle ij\rangle} \left(\Delta_{ij} c^\dagger_{i\uparrow} c^\dagger_{j\downarrow} + \text{H.c.}\right) \\ & + V^t \sum_{\langle ij\rangle} \sum_{s_1,s_2=\uparrow\downarrow} \left(\Delta^{s_1 s_2}_{ij} c^\dagger_{i,s_1} c^\dagger_{j,s_2} + \text{H.c.}\right), \end{aligned} \tag{1}$$

where

$$\Delta_{ij} = \langle c_{i\uparrow} c_{j\downarrow} - c_{i\downarrow} c_{j\uparrow}\rangle, \tag{2}$$

is the singlet, and

$$\Delta^{\uparrow\downarrow}_{ij} = \langle c_{i\uparrow} c_{j\downarrow} + c_{i\downarrow} c_{j\uparrow}\rangle, \qquad \Delta^{\uparrow\uparrow}_{ij} = \langle c_{i\uparrow} c_{j\uparrow}\rangle, \qquad \Delta^{\downarrow\downarrow}_{ij} = \langle c_{i\downarrow} c_{j\downarrow}\rangle \tag{3}$$

are the triplet superconducting order parameters. Here, $c^{(\dagger)}_{i\sigma}$ annihilates (creates) an electron with spin σ at the lattice site i, g is the gyromagnetic ratio and μ_B is the Bohr magneton. θ_{ij} describes the phase that an electron acquires when hopping from site i to site j in the presence of magnetic field. According to so called *Peierls substitution* [10] it is given by: $\theta_{ij} = (ie/\hbar c)\int_{\mathbf{R}_j}^{\mathbf{R}_i} \mathrm{A}.d\mathbf{l}$. We restrict our analyzes to the case of nearest–neighbor pairing. However, as the

superconductivity develops on the triangular lattice, at each site we introduce three order parameters in each pairing channel: Δ^1 describing paring along the x axis, Δ^2 and Δ^3 corresponding to the cases when the sites involved in the Cooper pair form an angle of 60° and 120° with the x–axis. Since the applied magnetic filed destroys the translational symmetry, the order parameters are site dependent. However, in the Landau gauge $\mathrm{A} = (-H_z y, 0, 0)$ they depend on the y coordinate only.

In order to determine the upper critical field we follow the procedure described in [7, 8]. We start with the diagonalization of the first term in Eq. (1) for a finite system. Due to translational symmetry along the x axis, the eigenfunctions are of plane–wave character in this direction. Their y–dependence is determined from one-dimensional Harper equation [11]. Using these eigenfunctions we derive the set of selfconsistent equations for the gap functions $(\Delta^1(y), (\Delta^2(y), (\Delta^3(y))$. Next, we solve a linearized version of these equations on 150×150 cluster and get the temperature dependence of H_{c2} for singlet and triplet superconductivity. In the latter case we have investigated separately the paired states $|\downarrow\downarrow\rangle$, $1/\sqrt{2}(|\uparrow\downarrow\rangle + |\downarrow\uparrow\rangle)$ and $|\uparrow\uparrow\rangle$. We refer to these states by the corresponding spin projection $S_z = -1, 0, 1$, respectively. The crucial parameters that determine the shape of $H_{c2}(T)$ are the pairing potentials for singlet and triplet superconductivity and the carrier concentration. In the following we assume the potentials are independent of the applied field and are of comparable magnitude. The former assumption has partially been verified in Ref. [8], whereas the latter one is fulfilled e.g. for nearest–neighbor density–density interaction. If zero field transition temperatures for singlet and triplet types of pairing differ significantly, the highest $H_{c2}(T = 0)$ takes place for pairing with larger T_c. However, if these temperatures are of comparable magnitudes the slope of $H_{c2}(T)$ is always larger for triplet superconductivity. The triplet equal–spin superconductivity is obviously favored in high field regime due to the absence of the Pauli pair–breaking mechanism. However, this feature holds also in the triplet state with $S_z = 0$, indicating that the orbital pair–breaking mechanism is more effective in the singlet state. As a result the external magnetic field may induce the transition from singlet to triplet superconductivity. This transition shows up as a bend of $H_{c2}(T)$, similar to that observed in Refs. [9, 12]. It is illustrated in Fig. 1. We present a reduced critical field $h_{c2} = \Phi(H_{c2})/\Phi_0$, where $\Phi(H)$ is the flux through the lattice cell and Φ_0 is the flux quantum. Here, carrier concentration, $n = 0.67$, has been assumed according to the experimental data [13].

To conclude, we have shown that the specific shape of $H_{c2}(T)$ observed in the cobalt oxide superconductor can be explained in terms of the field–induced transition from singlet to triplet pairing. This scenario assumes a competition between singlet and triplet types of superconductivity, which remains in

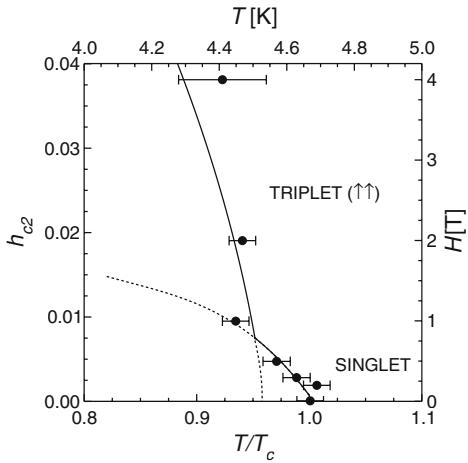

Figure 1. Numerical results for $h_{c2}(T)$ (solid lines, left and bottom axes). We have assumed the model parameters $n = 0.67$ and $V^s = V^t = 0.7t$. The experimental points (top and right axes) are taken from Ref. [9].

agreement with the phase diagram proposed in Ref. [14] for $Na_xCoO_2 \cdot yH_2O$. However, this hypothesis should be verified by phase–sensitive experiments.

References

[1] B. S. Chandrasekhar, Appl. Phys. Lett. **1**, 7 (1962); A. M. Clogston, Phys. Rev. Lett. **9**, 266 (1962).
[2] P. Fulde and R. A. Ferrel, Phys. Rev. **135**, A550 (1964); A. I. Larkin and Yu. N. Ovchinnikov, Zh. Eksp. Teor. Fiz. **47**, 1136 (1964) [Sov. Phys. JETP **20**, 762 (1965)].
[3] A. G. Lebed and K. Yamaji, Phys. Rev. Lett. **80**, 2697 (1998).
[4] S. Uji et al., Nature **410**, 908 (2001).
[5] E. Helfand and N.R. Werthamer, Phys. Rev. Lett. **13**, 686 (1964).
[6] Yu. N. Ovchinnikov and V. Z. Kresin, Phys. Rev. B **52**, 3075 (1995).
[7] M. Mierzejewski and M.M. Maśka, Phys. Rev. B **60**, 6300 (1999).
[8] M. M. Maśka and M. Mierzejewski, Phys. Rev. B **64**, 064501 (2001).
[9] H. D. Yang, *et al.*, cond–mat/0308031.
[10] R. E. Peierls, Z. Phys. **80**, 763 (1933); J.M. Luttinger, Phys. Rev. **84**, 814 (1951).
[11] P.G. Harper, Proc. Phys. Soc. London, Sect. **A68**, 874 (1955).
[12] M. M. Maśka *et al.*, cond-mat/04020503.
[13] R.E. Schaak *et al.*, Nature **424**, 527 (2003).
[14] G. Baskaran, Phys. Rev. Lett. **91**, 097003 (2003).

DISPROPORTIONATION AND SPIN ORDERING TENDENCIES IN Na_xCoO_2 AT $x = \frac{1}{3}$

J. Kuneš,[1,2] K.-W. Lee[1] and W. E. Pickett[1]
[1]*Department of Physics, University of California, Davis CA 95616*
[2]*Institute of Physics, Academy of Sciences,*
Cukrovarnicka 10, CZ-162 53 Prague, Czech Republic

Abstract The strength and effect of Coulomb correlations in the (superconducting when hydrated) $x \approx 1/3$ regime of Na_xCoO_2 have been evaluated using the correlated band theory LDA+U method. Our results, neglecting quantum fluctuations, are: (1) there is a critical $U_c = 3$ eV, above which charge ordering occurs at $x = 1/3$, (2) in this charge-ordered state, antiferromagnetic coupling is favored over ferromagnetic, while below U_c, ferromagnetism is favored; and (3) carrier conduction behavior should be very asymmetric for dopings away from $x = 1/3$. For $x < \frac{1}{3}$, correlated hopping of parallel spin pairs is favored, suggesting a triplet superconducting phase.

1. Introduction

Since the discovery of high temperature superconductivity in cuprates, there has been intense interest in transition metal oxides with strongly layered, (quasi) two-dimensional (2D) crystal structures and electronic properties. For several years now alkali-metal intercalated layered cobaltates, particularly Na_xCoO_2 (NxCO) with $x \sim 0.50 - 0.75$, have been pursued for their thermoelectric properties.[1] Li_xCoO_2 is of course of great interest and importance due to its battery applications. The recent discovery[2] and confirmation[3–5] of superconductivity in this system, for $x \approx 0.3$ when intercalated with H_2O, has heightened interest in the NxCO system.

The crystal structure[6–8] is based on a 2D CoO_2 layer in which edgesharing CoO_6 octahedra lead to a triangular lattice of Co ions. Na donates its electron to the CoO_2 layer, hence x controls the doping level of the layer: $x = 0$ corresponds to Co^{4+}, S $= \frac{1}{2}$ low spin ions with one minority t_{2g} hole, and $x = 1$ corresponds to non-magnetic Co^{3+}. Nearly all reports of non-stoichiometric materials quote values of x in the 0.3–0.75 range, and the materials seem generally to show metallic conductivity. Reports of the magnetic behavior are of particular interest to us. For x in the 0.5–0.75 range, the susceptibility $\chi(T)$ is Curie-Weiss-like (C-W) with reported moment of the order of magnitude 1 μ_B per Co^{4+}[2, 3] which indicates the presence of correlated electron behavior on the Co ions.

J. Ashkenazi et al. (eds.), New Challenges in Superconductivity: Experimental Advances and Emerging Theories, 235-242.

Magnetic ordering at 22 K with very small ordered moment has been reported for $x = 0.75$[9] and Wang *et al*. measured field dependence [4] that indicated the spin entropy of the magnetic Co system is responsible for the unusual thermoelectric behavior. Thus for $x \geq 0.5$ magnetic Co ions and magnetic ordering give evidence of correlated electron behavior.

However, for H_2O intercalated samples with $x \approx 0.3$, (*i.e.* the superconducting phase) C-W behavior of χ vanishes. [3, 5, 10, 11]. It is extremely curious that the appearance of superconductivity correlates with the disappearance of Co moments in the samples. From a single-band strongly interacting viewpoint, the $x = 0$ system corresponds to the half-filled triangular lattice that has been studied extensively for local singlet (resonating valence bond) behavior. [12] The $x \approx 0.3$ region of superconductivity in NxCO is however well away from the half-filled system, and the behavior in such systems is expected to vary strongly with doping level.

There is now a serious need to understand the electronic structure of the normal state of the unhydrated material, and its dependence on the doping level x. The electronic structure of the $x = 1/2$ ordered compound in the local density approximation (LDA) has been described by Singh.[13] Within LDA all Co ions are identical ("$Co^{3.5+}$"), the Co t_{2g} states are crystal-field split (by 2.5 eV) from the e_g states, and the t_{2g} bands are partially filled, consequently the system is metallic consistent with the observed conductivity. The t_{2g} band complex is $W \approx 1.6$ eV wide, and is separated from the 5 eV wide O 2_p bands that lie just below the Co *d* bands. Singh noted that the expected on-site Coulomb repulsion $U = 5$–8 eV on Co gives $U \gg W$ and correlation effects can be anticipated. A value of $U \approx 4$ eV was assumed by Wang, Lee, and Lee [14] to justify a strongly correlated $t - J$ model treatment of this system. While it must be kept in mind that the study of this system is still in its infancy and no clear experimental data plus theoretical interpretation agreement has established the degree of correlation, we also take the viewpoint here that effects of on-site repulsion need to be assessed.

Although the experimental evidence indicates nonmagnetic Co ion in the superconducting material, most theoretical approaches[14–16] consider the strongly interacting limit where not only is U important, it is large enough to prohibit double occupancy, justifying the single band $t - J$ model. Another question to address is whether the single band scenario is realistic: indeed the rhombohedral symmetry of the Co site splits the t_{2g} states into a_g and e'_g representations, but the near-octahedral local symmetry leaves their band centers and widths very similar.

In this paper we begin to address the correlation question using the correlated band theory LDA+U method. We focus on the $x \approx 1/3$ regime where superconductivity emerges. We find that $U \geq U_c = 3$ eV leads to charge ordering

at $x = 1/3$ accompanied by antiferromagnetic (AFM) spin order; of course, the fluctuations neglected in the LDA+U method, the availability of three distinct sublattices for ordering, and the tendency of the Na ions to order[8] (which can mask other forms of ordering at the same wavevector), can account for the lack of ordering (or of its observation).

2. Method of Calculation

Two all-electron full-potential electronic methods have been used. The full-potential linearized augmented-plane-waves (FLAPW) as implemented in Wien2k code [17] and its LDA+U [18] extension were used. Valence and conduction s,p, and d states were treated using the APW+lo scheme [19], while the standard LAPW expansion was used for higher l's. Local orbitals were added to describe Co $3d$ and O $2s$ and $2p$ states. The basis size was determined by $R_{mt}K_{max} = 7.0$. In addition, the full-potential nonorthogonal local-orbital minimum-basis scheme (FPLO) of Koepernik and Eschrig[20] was also used extensively. Valence orbitals included Na $2s2p3s3p3d$, Co $3s3p4s4p3d$, and O $2s2p3s3p3d$. The spatial extension of the basis orbitals, controlled by a confining potential [20] $(r/r_0)^4$, was optimized for the paramagnetic band structure and held fixed for the magnetic calculations. The Brillouin zone was sampled with regular mesh containing 50 irreducible k-points. Both popular forms[21] of the LDA+U functional have been used to assess possible sensitivity to the choice of functional, but in these studies the differences were small. We do not consider interlayer coupling in the work presented here, which allows us to use a single layer cell in the calculations.

3. Results of Self-Consistent Calculations

LDA electronic structure at $x = \frac{1}{3}$.

The crystal field splitting of 2.5 eV puts the (unoccupied) e_g states (1 eV wide) well out of consideration. The trigonal symmetry of the Co site splits the t_{2g} states into one of a_g symmetry and a doubly degenerate e'_g pair. The a_g band is 1.5 eV wide (corresponding to $t = 0.17$ eV in a single band picture) while the e'_g states have nearly the same band center but are only 1.3 eV wide; hence they lie *within* the a_g band. As might be anticipated from the local octahedral environment, there is mixing of the a_g and e'_g bands throughout most of the zone, and the a_g DOS does not resemble that of an isolated band in a hexagonal lattice. For the paramagnetic case $x = \frac{1}{3}$ corresponds to $\frac{8}{9}$ filling of the t_{2g} band complex, resulting in hole doping into the e'_g states as well as in the a_g states.

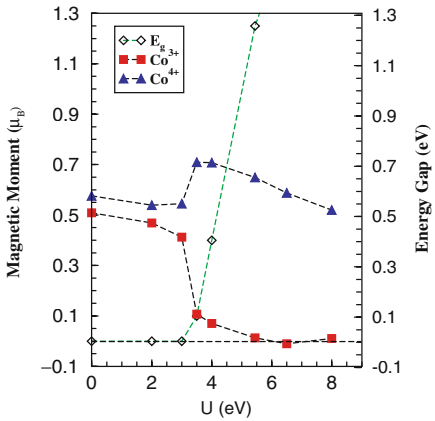

Figure 1. Effect of the intraatomic repulsion U on the magnetic moment of the Co1 and Co2 ions for ferromagnetic order. The LDA+U method in the FPLO code was used. Disproportionation to formal charge states Co^{3+} and Co^{4+} states occurs above $U_c = 3$ eV.

Singh found that ferromagnetic (FM) phases seemed to be energetically favored for all noninteger x [13]. No ferromagnetism is seen in this system, so NxCO becomes another member in small but growing list of compounds[22] whose tendency toward FM is *overestimated* by LDA because they are near a magnetic quantum critical point. We confirm these FM tendencies within LDA for $x = 1/3$, obtaining a half metallic FM state with a moment of $\frac{2}{3}\mu_B$/Co that is distributed almost evenly on the three Co ions, which occupy two crystallographically distinct sites because of the Na position. The exchange splitting of the t_{2g} states is 1.5 eV, and the Fermi level (E_F) lies within the metallic minority bands and just above the top of the fully occupied majority bands. The FM energy gain is about 45 me V/Co. With the majority bands filled, the filling of the minority t_{2g} bands becomes $\frac{2}{3}$, leading to larger e'_g hole occupation than for the paramagnetic phase. We conclude that, in opposition to much of the theoretical speculation so far, $x = \frac{1}{3}$ is necessarily a multiband $(a_g + e'_g)$ system. Our attempts using LDA to obtain self-consistent charge-ordered states, or AFM spin ordering, always converged to the FM or nonmagnetic solution.

LDA+U Magnetic Structure and energies

First the behavior of the LDA+U results versus U were studied (on-site exchange was kept fixed at 1 eV). The dependence of the magnetic moment on U (obtained from the FPLO code) for FM ordering is shown in Fig. 1. Recall that the ordered array of Na ions in our cell gives two crystallographically

Disproportionation in Na_xCoO_2

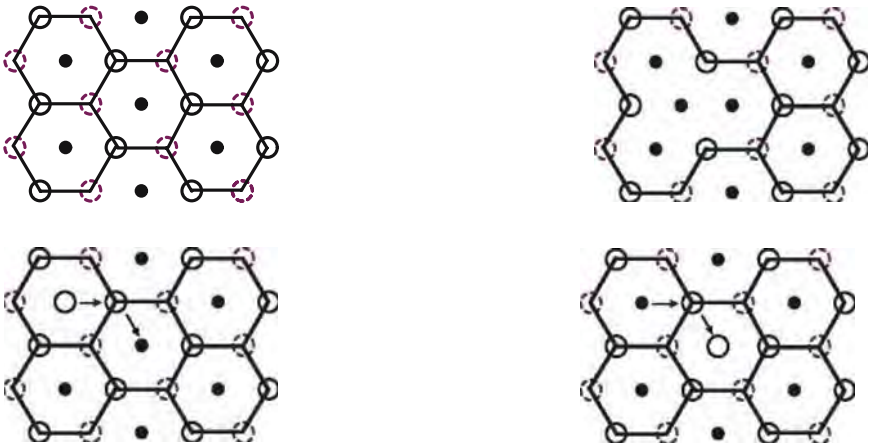

Figure 2. Upper left: The charge ordered triangular Co lattice → honeycomb lattice, with antiferromagnetic spin order designated by solid circles (↑), dashed circles (↓), and filled circles (Co^{3+} $S = 0$ sites). Lines denote nearest neighbor magnetic couplings. *Upper right*: addition of a ↑ electron converts a Co^{4+} $S = \frac{1}{2}$ site to a nonmagnetic site. Hopping of a neighboring hole to this site costs 4J in energy. The lower two panels illustrate the correlated pair hopping process after a ↑ hole is added to the system: hopping of the hole to a neighboring site, followed by refilling of the site by the added hole, results in an identical (but translated) state.

inequivalent Co sites. For $U < U_c \approx 3$ eV, the moments are nearly equal and similar to LDA values (which is the $U \to 0$ limit). Above U_c, charge ordering accompanied by a metal-insulator (Mott) transition occurs by disproportionation into nonmagnetic Co^{3+} and two $S = \frac{1}{2}$ Co^{4+} ions. Nonmagnetic Co^{3+} states lie at the bottom of the 1 eV wide gap, with the occupied Co^{4+} e_g' states 1–2 eV lower. After adding the on-site correlation to LSDA results, the hole on the Co^{4+} ion occupies the a_g orbital A possibility that we have not attempted would be to obtain a solution in which the hole occupies an e_g' orbital, in which case one should then investigate orbital ordering in addition to charge- and spin-ordering.

Reasonable estimates for cobaltates put U at 5 eV or above, so we now concentrate on results for $U = 5.4$ eV, which we expect is near the lower end of reasonable values. For this value of U both FM and AFM spin-ordered solutions are readily obtained, with AFM energy 1.2 mRy/Co lower than for FM order. In terms of nearest neighbor (nn) coupling on the charge-ordered honeycomb lattice, the FM - AFM energy difference corresponds to $J = 11$ meV. Referring to the paramagnetic bandwidth identified above, the corresponding superexchange constant would be $4t^2/U \sim 20$ meV.

Discussion and Comparison with Experiment

These calculations establish that at $x = 1/3$, there is a strong tendency to charge-order, and that there is a nn J of antiferromagnetic sign; hence we consider as reference the $\sqrt{3} \times \sqrt{3}$ charge-ordered AFM state shown in Fig. 2. Considering the charge-ordering energies as dominant over the magnetic energies, the fundamental problem at $x = \frac{1}{3}$ becomes the spin behavior of the half-filled honeycomb lattice. Spin correlations and quantum fluctuations on the honeycomb lattice have been considered by Moessner *et al.*[23] based on the quantum dimer model, where singlet-pairing regimes indeed are found in which the rms magnetization on a site is strongly reduced. Such pairing would strongly suppress the Curie-Weiss susceptibility.

The foregoing discussion neglects (among other aspects) the metallic nature of NxCO. Now we consider "doping" away from $x = 1/3$. Addition of an electron (of, say, spin up) converts a $Co^{4+} \downarrow$ to a Co^{3+}, that is, it destroys a spin down hole which also was a potential carrier (if charge order were lost). This frees up a site for hopping of a neighboring hole, but the energy cost of doing so is 4 J (loss of two favorable J and gain of two unfavorable J) and thus is strongly inhibited. Now we turn to the removal of an $\uparrow$ electron (addition of a hole) corresponding to superconducting region $x < \frac{1}{3}$, which has quite a different effect. This type of doping converts an inert Co^{3+} to a Co^{4+} that is surrounded by six Co^{4+} sites with alternating spins. Single particle hopping is disallowed (strictly speaking, it costs U); however, correlated *parallel-spin pair hopping* as shown in Fig. 2 returns the system to an equivalent state and therefore requires no net energy. This process suggests a tendency toward triplet pairing superconductivity in this regime, although our results are too preliminary to permit serious conclusions. Although some progress on such processes might be made analytically within a single band model, the multi-band nature of NxCO turns even the relatively simple Hubbard model on a triangular or honeycomb lattice into a formidable numerical problem.

4. Summary and Acknowledgments

Now we summarize. We have used the LDA+U method to evaluate the effects of Hubbard-like interactions in NxCO, and find charge disproportionation and a Mott insulating state at $x = \frac{1}{3}$ when fluctuations are neglected. Nearest neighbor coupling $J \approx 11$ meV provides AFM correlations. Indications based on this "mean field" AFM charge-ordered state are for very different behavior for electron or for hole doping relative to $x = \frac{1}{3}$; hole doping from this point tends to favor parallel-spin pair-hopping and thus possible triplet superconductivity. Fluctuation effects may however be substantial.

We acknowledge important communications with R. T. Scalettar, R. R. P. Singh, R. Cava, B. C. Sales, and D. Mandrus. J. K. was supported by National Science Foundation Grant DMR-0114818. K.-W. L. and W. E. P. were supported by DOE Grant DE-FG03-01ER45876.

References

[1] I. Terasaki, Y. Sasago, and K. Uchinokura, Phys. Rev. B **56**, R12685 (1997).
[2] K. Takada, H. Sakurai, E. Takayama-Muroachi, F. Izumi, R. A. Dilanian, and T. Sasaki, Nature **422**, 53 (2003).
[3] H. Sakurai, K. Takada, S. Yoshii, T. Sasaki, K. Kindo, and E. Takayama-Muromachi, Phys. Rev. **B 68**, 132507 (2003); R. Jin, B. C. Sales, P. Khalifah, D. Mandrus, Phy. Rev. Lett. **91**, 217001 (2003).
[4] B. Lorenz, J. Cmaidalka, R. L. Meng, and C. W. Chu, Phys. Rev. B **68**, 132504 (2003); G. Cao, C. Feng, Y. Xu, W. Lu, J. Shen, M. Fang, and Z. Xu, J. Phys.: Condens. Matt. **15**, L519 (2003); T. Waki, C. Michioka, M. Kato, K. Yoshimura, K. Takada, H. Sakurai, E. Takayama-Muromachi, and T. Sasalki, cond-mat/0306036; Y. Wang, N. S. Rogado, R. J. Cava, and N. P. Ong, Nature **423**, 425 (2003); R. E. Schaak, T. Klimczuk, M. L. Foo, and R. J. Cava, Nature **424**, 527 (2003).
[5] F. C. Chou, J. H. Cho, P. A. Lee, E. T. Abel, K. Matan, and Y. S. Lee, cond-mat/0306659.
[6] Y. Ono, R. Ishikawa, Y. Miyazaki, Y. Ishii, Y. Morlii, and T. Kajitani, J. Solid State Chem. **166**, 177 (2002).
[7] J. W. Lynn, Q. Huang, C. M. Brown, V. L. Miller, M. L. Foo, R. E. Schaak, C. Y. Jones, E. A. Mackey, and R. J. Cava, Phys. Rev. B **68**, 214516 (2003).
[8] J. D. Jorgensen, M. Avdeev, D. G. Hinks, J. C. Burely, and S. Short, Phys. Rev. B **68**, 214517 (2003).
[9] R. Motohashi, R. Ueda, E. Naujalis, T. Tojo, I. Terasaki, T. Atake, M. Karppinen, and H. Yamauchi, Phys. Rev. B **67**, 064406 (2003).
[10] The unusual susceptibility observed by Sakurai *et al.*,[3] with $\mathrm{d}\chi/\mathrm{dT}$ positive above 130 K, was interpreted to include a Curie-Weiss term that would imply a Co moment of the order of 0.01 μ_B.
[11] Y. Kobayashi, M. Yokoi, M. Sato, J. Phys. Soc. Jpn. **72**, 2161 (2003).
[12] R. Moessner and S. L. Sondhi, Phys. Rev. Lett. **86**, 1881 (2001).
[13] D. J. Singh, Phys. Rev. B **61**, 13397 (2000); *ibid*. **68**, 20503 (2003).
[14] Q.-H. Wang, D.-H. Lee, and P. A. Lee, Phys. Rev. B **69**, 092504 (2004).
[15] R. Koretsune and M. Ogata, Phys. Rev. Lett. **89**, 116401 (2002); M. Ogata, J. Phys. Soc. Japan **72**, 1839 (2003).
[16] R. Moessner and S. L. Sondhi, Prog. Th. Phys. Suppl. **145**, 37 (2002); B. Kumar and B. S. Shastry, Phys. Rev. B **68**, 104508 (2003); A. Tanaka and X. Hu, Phys. Rev. Lett. **91**, 257006 (2003); C. Honerkamp, Phys. Rev. **B** 68, 104510 (2003); G. Baskaran, Phys. Rev. Lett. **91**, 097003 (2003); cond-mat/0306569
[17] WIEN97: see P. Blaha, K. Schwarz, and J. Luitz, Vienna University of Technology, 1997, improved and updated version of the original copyrighted WIEN code, which was published by P. Blaha, K. Schwarz, P. Sorantin, and S. B. Trickey, Comput. Phys. Commun. **59**, 399 (1990).
[18] P. Novak, F. Boucher, P. Gressier, P. Blaha, and K. Schwarz, Phys. Rev. B **63**, 235114 (2001); A. B. Shick, A. I. Liechtenstein, and W. E. Pickett, Phys. Rev. B **60**, 10763 (1999).

[19] E. Sjesledt, L. Nordstrem, and D. J. Singh, Solid State Commun. **114**, 15 (2000).
[20] K. Koepernik and H. Eschrig, Phys. Rev. B **59** 1743 (1999); H. Eschrig, *Optimized LCAO Method and the Electronic Structure of Extended Systems* (Springer, Berlin, 1989).
[21] V. I. Anisimov, I. V. Solovyev, M. A. Korotin, M. T. Czyzyk, and G. A. Sawatzky, Phys. Rev. B **48**, 16929 (1993); M. T. Czyzyk and G. A. Sawatzky, Phys. Rev. B 49, 14211 (1994).
[22] I. I. Mazin, D. J. Singh, and A. Aguayo, cond-mat/0401563.
[23] R. Moessner, S. L. Songhi, and P. Chandra, Phys. Rev. B **64**, 144416 (2001).

INTERBAND SCATTERING IN MgB_2

R.P.S.M. Lobo,[1] M. Elsen,[1] P. Monod,[1] J.J. Tu,[2] Eun-Mi Choi,[3]
Hyeong-Jin Kim,[3] W. N. Kang,[3] Sung-Ik Lee,[3] R.J. Cava,[4] and G.L. Carr[5]
[1]*Laboratoire de Physique du Solide (UPR5 CNRS) ESPCI, 75231 Paris cedex 05, France*
[2]*Department of Physics, The City College of New York, New York, NY 10031*
[3]*National Creative Research Initiative Center for Superconductivity, Department of Physics, Pohang University of Science and Technology, Pohang 790-784, Korea*
[4]*Princeton University, Princeton, NJ 08544*
[5]*National Synchrotron Light Source, Brookhaven National Laboratory, Upton, NY 11973*
email: lobo@espci.fr

Abstract The scattering process responsible for connecting the bands remains one of the last open questions on the physical properties of MgB_2. Through the analysis of the equilibrium and photo-induced far-infrared properties as well as electron spin resonance of MgB_2 we propose a phonon mediated energy transfer process between the bands based on the coupling of quasiparticles to an E_{2g} phonon.

Keywords: MgB_2, infrared, ESR, pump-probe, interband scattering

1. Introduction

The discovery of superconductivity in MgB_2 [1] triggered a major theoretical and experimental effort to understand its mechanisms. Kortus *et al.* [2] predicted that that MgB_2 should have two metallic bands at the Fermi energy one two dimensional (σ) band along the Γ–A direction and another three dimensional (π) band covering most of the Brillouin zone volume. They also predicted that both bands should undergo the superconducting transition with different energy gaps, the higher being in the σ band. Several experimental studies have found evidence for a double gap in MgB_2 [3, 4]. In particular Giubileo *et al.* STM data [3] showed that these two gaps close at the same T_c. The first attempt to describe a two band superconductor was done as early as 1959 [5], when Suhl *et al.* proposed that when two superconducting bands interact the critical temperature (T_c) of the lowest gap band increases and joins the one of the higest gap band. This is qualitatively the effect observed in STM measurements. Most of the physics behind superconductivity of MgB_2 is now understood [6] and the remaining big question concerns the process responsible for connecting the two bands.

J. Ashkenazi et al. (eds.), New Challenges in Superconductivity: Experimental Advances and Emerging Theories, 243-248.

In this work we address this issue by looking at the far-infrared equilibrium and photo-induced reflectivity of a MgB_2 thin film and at the Electron Spin Resonance (ESR) of powder samples.

2. Experimental

Optical data was taken on a $\sim$ 30 nm thick c-axis oriented film of MgB_2 deposited on a sapphire substrate at Postech [7]. Its T_c of 30 K is suppressed compared to the bulk material (T_c = 39 K). Standard reflectance measurements were performed using the Bruker 66v FTIR spectrometer at beamline U10A of the NSLS, with synchrotron radiation as the IR source. The specimen was solidly clamped with indium gaskets to the copper cold-finger of a heli-tran cryostat, leaving a 3 mm diameter aperture exposed for the IR measurement. The remaining 80% of the sample's surface was available for thermal conduction into the cold finger.

Transient far-infrared photo-reflectance measurements were also performed using the same spectrometer and beamline. Here, we measured the reflectance change due to illuminating the MgB_2 film with 2 ps near-infrared ($\lambda = 760$ nm) pulses from a Ti:sapphire laser. The laser pulses break pairs and weaken the superconducting state for a brief amount of time ($\sim$ 1 ns) [8]. The resulting change in reflectance is sensed with the $\sim$ 1 ns infrared pulses from the synchrotron in a pump-probe configuration [9]. The average laser power was 20 to 50 mW (0.4 to 1 nJ per pulse) so that the MgB_2 film could be maintained at $T = 5$ K. The pulse repetition frequency was 53 MHz, matching the pulsed IR output from the synchrotron. For time-dependent studies, the broadband probe pulses were not spectrally resolved, and the response is an average of the reflectance across the 10 to 100 cm^{-1} spectral range.

ESR data was collected between 40 K and 600 K with a Bruker ESP300E 10 GHz spectrometer equiped with an Oxford ESR He cryostat on MgB_2 powder samples synthesized in Princeton. The powder was mechanically ground to avoid skin depth problems.

3. Results and Discussion

Figure 1(a) shows the ratio of superconducting to normal far-infrared reflectance at equilibrium. The dashed line is a Mattis-Bardeen fit [10] assuming a gap at 43 cm^{-1}. The solid line is obtained using a simple non-interacting carrier model for the conductivity $\sigma = (1-f)\sigma_\sigma + f\sigma_\pi$ where σ_σ and σ_π are Mattis-Bardeen conductivities for each band and f is the fraction of the π band that contributes to the total conductivity. The parameters used for the latter are $2\Delta_\sigma = 56$ cm $^{-1}$ and $2\Delta_\pi = 30$ cm $^{-1}$ ($f = 0.6$). Although the 2 gap model better describes the data at low frequencies, the improvement is not sufficient to conclude that two gaps must exist. In fact, previous data on equilibrium

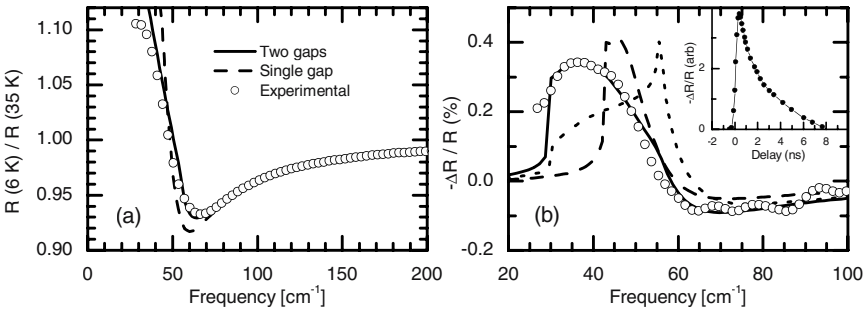

Figure 1. (a) Equilibrium infrared reflectivity of MgB_2 film at 5 K (dots). The lines are fits using the Mattis-Bardeen optical conductivity for systems with one or two gaps. (b) Photo-induced reflectivity of MgB_2 film at 5 K (dots). The lines are attempts to describe the data using the same parameters as those from panel (a). The dashed line assumes a single gap. The dotted and continuous lines are calculations for a two gap system. For the former we assume that in the photo-excited state both bands have excess quasiparticles and for the latter, we assume that all excess quasiparticles find themselves in the lower energy gap band (π). The inset in panel (b) shows the time dependence of the integrated photo-induced signal.

infrared spectra of MgB_2 [11] did not provide any clear cut picture about the presence of two bands in MgB_2, either. However, the data does not seem to follow strictly the BCS theory.

An analysis of the time dependent transient photo-reflectance gives us a good estimate of the effective pair recombination rate [8]. The inset in Fig. 1(b) shows the average reflectance change as a function of the delay between pump and probe pulses at 6 K. In accordance with other BCS superconductors the effective recombination time is found to be a few nanoseconds. One important remark is that, within the experimental time resolution, no evidence of multiple decays is found. In fact, ultra-fast pump-probe measurements on MgB_2 [12, 13] did not find any evidence for a double relaxation down to the ps regime.

Panel (b) in Fig. 1 shows the photo-induced spectra taken with pump and probe at coincidence. The pairs broken by the laser pulse will create an excess quasiparticle population. Owen and Scalapino [14] showed that this excess quasiparticle population weakens the superconducting state. This weakened state can be spectroscopically detected and resolved as a slightly reduced energy gap allowing the transient photo-reflectance data to be analyzed using the same expressions as those for the equilibrium reflectance. The dashed curve in Fig. 1(b) assumes that the system has a single gap at 43 cm^{-1} which is decreased by photo-excitation. Although the amplitude and overall shape of the signal can be reproduced by this simulation, quantitative agreement is not achieved. The dotted line assumes that the system has the same two gaps used in the equilibrium reflectance fit and that in the photo-excited state both gaps

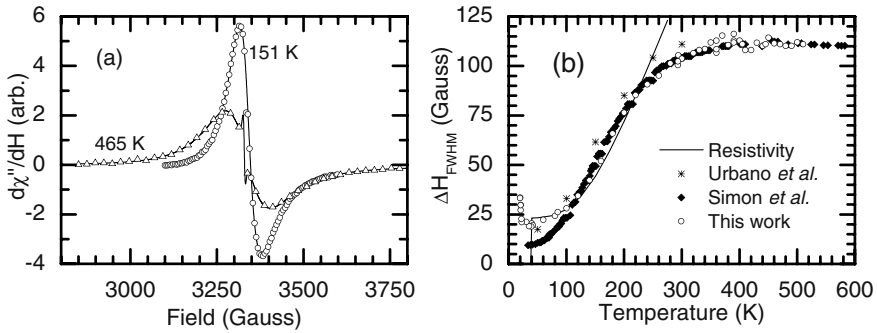

Figure 2. (a) ESR signal for MgB_2 at 151 K (circles) and 465 K (triangles). The solid line are fits with an assymetric Dysonian line. (b) ESR line widths for this work (circles), Ref. [17]. (diamonds) and Ref. [18] (stars). The solid line is the resistivity (normalized to compare with the ESR data) from Ref. [19].

shrink by an amount consistent with a small rise in the electronic temperature. The introduction of this second gap does not improve the data description and, actually, introduces new features absent from the data. Our third approach, depicted by the solid line, assumes that the system does have two gaps but that only the smaller energy gap shrinks in the photo-excited state. This is the behavior one would expect if, after pair-breaking by the laser, the excess quasiparticles are left primarily in the band having the smaller energy gap.

Figure 2(a) shows the ESR signal measured for two temperatures and fits using an assymetric Dysonian line shape. The fit allows us to determine the Lande g factor and the line width (ΔH) gives us a measurement of the spin scattering time τ_s using $(g\mu_B \Delta H)\tau_s = \hbar$.

ESR spectroscopy uses a static magnetic field to lift spin states degeneracies by a Zeeman splitting and probes the magnetic dipole transitions between these states with a small perpendicular rf magnetic field. In metals, the high collision rate of quasi-particles defines a single spin-lattice relaxation time τ_s. The electronic spin-orbit interaction has two consequences on the ESR response: (i) a "static" interaction produces a shift in the g factor from the free electron value and (ii) in the presence of phonons a "dynamic" (time averaged) interaction leads to the Elliott-Yafet relation [15]. The Elliott-Yafet relation states that $(\delta g)^2 \tau_c/\tau_s = \text{const}$, where τ_c is the electronic collision scattering time. In a simple one band model these two relaxation rates are proportional, a fact that has been observed in many metals [16].

Figure 2(b) compares the thermal evolution of the MgB_2 ESR linewidth (this work and Refs. [17, 18]) with its dc resistivity extract from Ref. [19]. The linewidth is measuring the spin scattering rate and the resistivity gives the

electron collision rate. Had Elliott-Yafet been followed, the ESR data should agree with the resistivity. Both quantities agree at low temperatures but this agreement breaks down around room temperature. Formally this implies a g factor unexpectedly varying with temperature. However, if one considers that the σ and π bands have different g factors, a temperature dependent mixing of these bands leads to a temperature dependent effective g.

4. Interband scattering

The photo-induced spectra in the superconducting state and the ESR data in the normal state can be understood in terms of an interband scattering process. When talking about interband scattering, one may think in terms of transfer of quasiparticles or, alternatively, transfer of the energy of quasiparticles. The latter process can be viewed as a process in which excited quasiparticles in one band relax emitting phonons which can excite quasiparticles in the other band. There is no transfer of the actual quasiparticles but rather of their energy.

The recent inelastic X-ray scattering data of Shukla *et al.* [20] shows that the E_{2g} phonon at around 60 meV is anomanously large in the $\Gamma - A$ direction of the Brillouin zone, the same direction as the σ bands. This E_{2g} phonon is the only phonon showing a large linewidth and it is natural to assume that this effect is coming from a strong coupling with σ quasiparticles. However, once created, E_{2g} phonons can scatter quasiparticles in both bands. As the π bands occupy a larger volume of the Brillouin zone, it is natural to assume that more quasiparticles in this band will get excited.

This picture naturally explains our data. The photo excited spectra originates from quasiparticles created by a 1.5 eV laser excitation. When quickly relaxing from high energies, the quasiparticles in the σ band eventually reach energies comparable with that of the E_{2g} phonon. At that time their energy is transfered to the π bands leading to a photo-excited state (at our ns time resolution) that is composed mostly of excess quasiparticles in the π band. The ESR response can be understood in similar terms. In this case we have no excited quasiparticles. At lower temperatures the g factor is a mixture of σ and π bands. When we raise the temperature we give enough energy to the quasiparticles to interact with the E_{2g} phonon. Eventually, this changes the balance between σ and π bands populations inducing a change in the effective g factor.

5. Summary

We looked at the far-infrared equilibrium and photo-induced reflectivity of a MgB_2 thin film and at the ESR spectra of powder samples. The photo-induced response shows one gap at 3 meV and another at 7 meV. However, excess quasiparticles are only found at the edge of the smaller gap. ESR data on the normal state shows a break down, around room temperature, of the

Elliott-Yafet time relaxation behavior observed in virtually any metal. These effects can be described in terms of an interband energy transfer process mediated by the anomanously broadened E_{2g} phonon [20].

Acknowledgments

This work was performed with the support of the U.S. Department of Energy through contract DE-ACO2-98CH10886 at the NSLS. Operation of the synchronized laser system is also supported by DOE through contract DE-FG02-02ER45984 with the University of Florida. We are grateful to P.B. Allen, J. Carbotte, T. Devereaux, M.V. Klein, I.I. Mazin, A.J. Millis, M.R. Norman, E. Nicol and D.B. Tanner, for useful discussions.

References

[1] J. Nagamatsu *et al.*, Nature **410**, 63 (2001).

[2] J. Kortus *et al.*, Phys. Rev. Letters **86**, 4656 (2001).

[3] F. Giubileo *et al.*, Phys. Rev. Letters **87**, 177008 (2001).

[4] J.W. Quilty *et al.*, Phys. Rev. Letters **90**, 207006 (2003). F. Bouquet *et al.*, Phys. Rev. Letters **87**, 047001 (2001). S. Souma *et al.*, Nature **423**, 65 (2003).

[5] H. Suhl, B.T. Matthias, and L.R. Walker, Phys. Rev. Letters **3**, 552 (1959).

[6] H.J. Choi *et al.*, Nature **418**, 758 (2002).

[7] W.N. Kang *et al.*, Science **292**, 1521 (2001) .

[8] G.L. Carr *et al.*, Phys. Rev. Letters **85**, 3001 (2000).

[9] R.P.S.M. Lobo *et al.*, Rev. Sci. Instrum. **73**, 1 (2002).

[10] W. Zimmermann *et al.*, Physica C **183**, 99 (1991).

[11] J. H. Jung *et al.*, Phys. Rev. B **65**, 052413 (2002). R.A. Kaindl *et al.*, Phys. Rev. Letters **88**, 027003 (2002).

[12] Y. Xu *et al.*, Phys. Rev. Letters **91**, 197004 (2003).

[13] J. Demsar *et al.*, Phys. Rev. Letters **91**, 267002 (2003).

[14] C.S. Owen, and D.J. Scalapino, Phys. Rev. Lett. **28**, 1559 (1972).

[15] R.J. Elliott, Phys. Rev. **96** 266 (1954). Y.Yafet, Solid State Phys. **14**, 1 (1963).

[16] P. Monod, and F. Beneu, Phys. Rev. B **19**, 911 (1974).

[17] F. Simon *et al.*, Phys. Rev. Letters **87**, 047002 (2001).

[18] R.R. Urbano *et al.*, Phys. Rev. Letters **89**, 087602 (2002).

[19] Yu. Eltsev *et al.*, Phys. Rev. B **66**, 180504 (2002).

[20] A. Shukla *et al.*, Phys. Rev. Letters **90**, 095506 (2003).

PHONON STRUCTURE IN POINT-CONTACT SPECTRA OF MGB_2

I.K. Yanson

B.I. Verkin Institute for Low Temperature Physicsa and Engineering, National Academy of Sciences, 47 Lenin Ave., 61103, Kharkiv, Ukraine.

yanson@ilt.kharkov.ua

Abstract In strong-coupling superconductors with a short electron mean free path the self-energy effects in the superconducting order parameter play a major role in the phonon manifestation of the point-contact spectra at above-gap energies. We compare the expressions for the nonlinear conductivity of tunnel, ballistic, and diffusive point-contacts and show that these expression are similar and correspond to the measurements of the phonon structure in the point-contact spectra for the π-band of MgB_2.

Keywords: MgB_2, point-contact spectroscopy, two-band/gap superconductivity, electron-phonon interaction

1. Introduction

The inelastic point-contact spectra of phonons in metals are based on expansion of the nonlinear $I - V$ characteristic in terms proportional to d/l_ε, where d is the characteristic size of metallic nanoconstriction connecting two bulk metal half-spaces and l_ε is the inelastic electron mean free path [1, 2].

If d is smaller than the electron mean free path l ($l^{-1} = l_i^{-1} + l_\varepsilon^{-1}$, l_i is the elastic mean free path), the electrons flow through the contact ballistically. In opposite cases ($d \gg l$) they perform a diffusive motion, but if the energy relaxation length $\Lambda_\varepsilon \approx \sqrt{l_i l\varepsilon}$ remains larger than d, their movement inside the constriction is conservative, and the inelastic point-contact spectroscopy is still possible [3, 4].

In the superconducting state a new characteristic length appears: the size of the Cooper pair or the coherence length ξ, and the additional nonlinear features emerge being proportional to the expansion of the so called "excess" current in terms proportional to d/ξ. In all the cases

J. Ashkenazi et al. (eds.), New Challenges in Superconductivity: Experimental Advances and Emerging Theories, 249-258.

considered, the size of the contact is smaller than the corresponding characteristic length scale: ξ, $l_\varepsilon, \Lambda_\varepsilon$ *etc.*

The zero-approximation in expansion of $I(V)$ in d/l_ε is the ohmic current considered by Sharvin [5]. From the Sharvin's formula the characteristic size d of the contact can be determined in the ballistic limit. The second derivative of the first approximation in expansion of $I(V)$ in d/l_ε is directly proportional to the spectral function of electron-phonon interaction (PC EPI) $g_{PC}(\omega) = \alpha^2_{PC}(\omega) F(\omega)$ of the specific point-contact transport both in the normal and in the superconducting states [1, 6, 7]. This term is the basis of the canonical inelastic point-contact spectroscopy (PCS). Here, $\alpha^2_{PC}(\omega)$ is the average electron-phonon matrix element taking into account the kinematic restriction imposed by contact geometry and $F(\omega)$ is the phonon density of states.

In diffusive point contacts ($d \gg l_i$) the role of the scale, where the backscattering inelastic processes become essential, turns from d in l_i and in the case when $l_i/l_\varepsilon \ll 1$ the corresponding contribution becomes negligible [3, 4]. This property will be essential when we consider the phonon structure in point-contact spectra of dirty MgB_2 contacts in the c-direction.

In the superconducting state, due to the Andreev reflections of quasiparticles at the $N - S$ boundary, the excess current appears both in $S - c - N$ and $S - c - S$ contacts (c stands for constriction). Its magnitude is the constant proportional to Δ for the weak-coupling BCS approximation at $eV \gg \Delta$ (Δ is the superconducting energy gap) [8, 9]. In the strong-coupling model of EPI the energy gap depends on the energy of quasiparticles due to phonon retardation effects reflecting the characteristic features of the phonon spectrum at singular van-Hove energies. Hence, even in the zeroth order the nonlinearities appear in $I(V)$ [10]. For the issue of this study it is most important that these nonlinearities are independent of the elastic mean free path (i.e., purity of the contact). In this connection one should keep in mind that for the simple method of a gentle touch between two sharp edges of the electrodes it is not possible to control the elastic mean free path in the constriction. In what follows we show that in spite of this restriction, the satisfactorily reproducible results are obtained not only for the shapes of phonon structure but also for their amplitude.

To conclude this section, we mention that the use of the first approximation in expansion of excess current in powers of d/ξ allows the nonequilibrium effects in the vicinity of the constriction to be developed, which are out of the scope in this paper [11].

2. Theoretical background of zeroth-order elastic component in excess current

In this section we review what has recently become known about the phonon structure in the point-contact spectra [12]. In order to do this, we should refer to the works where the excess current in point contact is considered in terms of the strong-coupling theory. That was first done in the paper of Omel'yanchuk, Beloborod'ko and Kulik for ballistic $S-c-N$ point contact [10]. The first derivative of $I(V)$-characteristic at $T=0$ has the following form in this case:

$$R_N\left(\frac{dI}{dV}\right)_{bal} = 1 + \left|\frac{\Delta(\varepsilon)}{\varepsilon + \sqrt{\varepsilon^2 - \Delta^2(\varepsilon)}}\right|^2, \qquad \varepsilon = eV \tag{1}$$

where R_N is the resistance of the contact in the normal state. This expression implies $d \ll \xi$ to be fulfilled (ξ is the coherence length in pure metal).

For diffusive point contact with the restriction: $l_i \ll d \ll \sqrt{l_i \xi}$, the same quantity takes the form [12]:

$$R_N\left(\frac{dI}{dV}\right)_{dif} = \frac{1}{2}\ln\left|\frac{\varepsilon + \Delta(\varepsilon)}{\varepsilon - \Delta(\varepsilon)}\right| \frac{\Re\frac{\varepsilon}{\sqrt{\varepsilon^2-\Delta^2(\varepsilon)}}}{\Re\frac{\Delta(\varepsilon)}{\sqrt{\varepsilon^2-\Delta^2(\varepsilon)}}}, \qquad \varepsilon = eV \tag{2}$$

We would like to compare these dependences with the expression for the conductance of the tunnel junction due to the self-energy effect in the superconducting energy gap:

$$R_N\left(\frac{dI}{dV}\right)_{tun} = \Re\frac{\varepsilon}{\sqrt{\varepsilon^2 - \Delta^2(\varepsilon)}}, \qquad \varepsilon = eV \tag{3}$$

In the above mentioned formulae $\Delta(\varepsilon)$ is the complex superconducting order parameter

$$\Delta(\varepsilon) = \Delta_1(\varepsilon) + i\Delta_2(\varepsilon), \tag{4}$$

where $\Delta_1(\varepsilon)$ and $\Delta_2(\varepsilon)$ are the $\Re(\varepsilon)$ and $\Im\Delta(\varepsilon)$, respectively. It would be very instructive to express Eqs. (1), (2), (3) as functions of real and imaginary components.

Thus, using the auxiliary expression $A(\varepsilon) = \sqrt{\left(\varepsilon^2 - \Delta_1^2 + \Delta_2^2\right)^2 + 4\Delta_1\Delta_2}$, the results are as follows:

$$R_N\left(\frac{dI}{dV}\right)_{bal} = 1 + \frac{1}{(\Delta_1^2+\Delta_2^2)}\left[\varepsilon^2 + A - \sqrt{2\varepsilon}\sqrt{A+\varepsilon^2-\Delta_1^2+\Delta_2^2}\right], \tag{5}$$

$$R_N\left(\frac{dI}{dV}\right)_{dif} = \frac{1}{2}\ln\left[\frac{\sqrt{\left(\varepsilon^2-\Delta_1^2-\Delta_2^2\right)^2+4\varepsilon^2\Delta_2^2}}{\left(\varepsilon-\Delta_1\right)^2+\Delta_2}\right]\times \tag{6}$$

$$\times\frac{\varepsilon\sqrt{A+\varepsilon^2-\Delta_1^2+\Delta_2^2}}{\Delta_1\sqrt{A+\varepsilon^2-\Delta_1^2+\Delta_2^2}\pm\Delta_2\sqrt{A-\varepsilon^2+\Delta_1^2-\Delta_2^2}},$$

where "plus" and "minus" in the last line stand for $\Delta_1\Delta_2 < 0$ and $\Delta_1\Delta_2 > 0$, respectively.

Finally, for tunnel junction the same quantity reads:

$$R_N\left(\frac{dI}{dV}\right)_{tun} = \frac{\varepsilon\sqrt{A+\varepsilon^2-\Delta_1^2+\Delta_2^2}}{\sqrt{2A}}. \tag{7}$$

Expressions (1), (2), (3) [and (5), (6), (7)] seem quite different but in reality they are very similar. This becomes evident if we compare their asymptotic expressions for the limit $\varepsilon \gg \Delta$. For three extreme regimes of current flow in aforementioned point contacts the corresponding equations take the form:

for a ballistic point contact:

$$R_N\left(\frac{dI}{dV}\right)_{bal} \approx 1 + \frac{\Delta_1^2}{4\varepsilon^2} + \frac{\Delta_2^2}{4\varepsilon^2}, \tag{8}$$

for a diffusive point contact:

$$R_N\left(\frac{dI}{dV}\right)_{dif} \approx 1 + \frac{\Delta_1^2}{3\varepsilon^2}, \tag{9}$$

and for a tunnel junction:

$$R_N\left(\frac{dI}{dV}\right)_{tun} \approx 1 + \frac{\Delta_1^2}{2\varepsilon^2} - \frac{\Delta_2^2}{2\varepsilon^2}. \tag{10}$$

In all these equations $\varepsilon = eV$ and $T = 0$ are implied.

Since $\Delta_2(\varepsilon)$ becomes comparable to $\Delta_1(\varepsilon)$ only at the highest phonon energy, almost in the whole phonon energy range these three extreme

regimes of current flow differ only little, mostly in amplitudes, which decrease in the tunnel→diffusive→ballistic contact row like their prefactors $\frac{1}{2} \to \frac{1}{3} \to \frac{1}{4}$. This derivation is of a key importance to understanding the quite similar phonon point-contact spectra for the different contacts randomly accessible in the experiment.

3. Self-energy effect in *c*-axis oriented MgB_2 films

For two-band superconductor MgB_2 (see the review [13]) the $\Re\Delta(\omega)$ and $\Im\Delta(\omega)$ for π and σ-band are depicted in the upper and lower panel of Fig. (1)[12], respectively. We are interested mostly in the π-band dependences, since for thin films oriented along the *c*-axis only the $\pi-$band part of the Fermi surface has nonzero Fermi velocity for charge carriers (holes) along the contact axis, playing the main role in the contact current. For the σ-band, which is two-dimensional, only holes with the velocity in the *ab*-plane exist. The driving force for superconductivity is the very strong EPI of these holes with the E_{2g}-phonon mode with the energy of about 70 meV. This mode is seen as the strong peak in $\Re\Delta_\sigma$ in the lower panel of Fig. (1) [13]. Note, that the ordinate scale for the latter panel is about three times higher than that for the π-band. For the $\pi-$band all the phonons in the energy range $\sim 30 \pm 100$ meV take part in the $\Re\Delta_\pi$ dependence, but with a lower magnitude as compared with the σ-band. Up to about 80 meV $\Im\Delta(\omega)$ is small, hence, only $\Re\Delta(\omega)$ is important in Eqs. (8), (9), (10). Thus, we expect that up to $\sim$ 80 meV the point-contact spectra differ only in amplitude just like the prefactors in the $[\Re\Delta(\varepsilon)/\varepsilon]^2$ term. This is evident from Fig. (2). We can see that up to the energies $\sim 80 \div 90$ meV the shapes of the calculated spectra are similar (Fig. (2)). The discrepancy is observed only at higher energies, where $\Im\Delta(\omega)$ becomes essential. In the range of biases $80 \div 120$ meV the variations of point-contact spectra are quite appreciable and mirror in the experimental curves. Although the $\Delta(\omega)$ value is of the order of $\Delta_{\max}$ at biases higher than 120 meV, the phonon features on the PC spectra are small enough, due to the factor $1/\varepsilon^2(\omega)$. When we compare theoretical and experimental curves, we consider only the biases up to 120 meV, since for higher biases the experimental results are irreproducible, due to nonequilibrium suppression of the superconducting state in the contact. Comparison of calculated and experimental curves is shown in Fig. (3). For the ordinate scale we use the second harmonic voltage V_2 measured in experiment, which is related to the second derivative of the $I - V$ characteristic as follows:

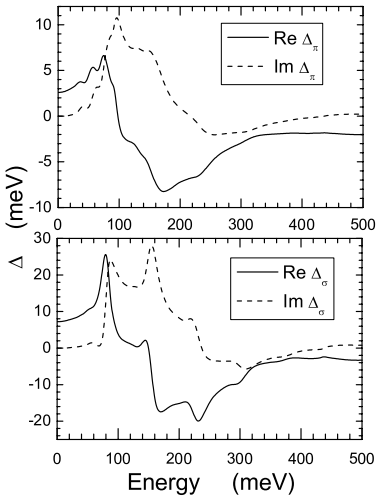

Figure 1 Real and imaginary parts of $\Delta(\varepsilon)$-dependences for π- and σ-bands (upper and lower panels, respectively) of MgB_2 [12].

$$V_2(V) = -\frac{V_1^2}{2\sqrt{2}} \frac{d}{dV} \left(R_N \frac{dI}{dV} \right), \tag{11}$$

where V_1 is the modulation voltage, which is conventionally taken equal to 3 meV (close to the value used in the experiment).

In the upper panel of Fig. (3) three different point-contact spectra are shown. They have similar shape up to 100 meV with a slight increase of average amplitudes in the row $R_N = 49 \rightarrow 36 \rightarrow 80\ \Omega$. In the same sequence the so-called zero-bias maximum in the $dV/dI(V)$ characteristic increases (not shown) , being $R_0/R_N \leq 1$, $\simeq 1$ and ≥ 1, respectively (R_0 is the zero-bias resistance in the superconducting state), for the above mentioned row. One may speculate that in the same direction the contact changes from ballistic towards the tunnel regime[1]. The lower panel of Fig. (3) shows that in the same row the average amplitude of phonon structure increases in the calculated curves. The positions of the maxima of the experimental phonon features roughly correspond to the expected ones taking into account that the orientation of experimental junction is approximately along the c-axis, since the spreading behavior of current in direct conductivity point contact embraces a wide solid angle near the contact axis. The alignment of our contacts along the c-axis is inferred indirectly by measuring the Andreev reflection spectra in the

[1]One should be cautioned to ascribe the case $R_0/R_N \simeq 1$ to the ballistic regime with the tunnel barrier having Z parameter of about 0.5. In most cases this value of Z in the BTK [9] fitting corresponds to the diffusive regime of current flow. This happens in many cases, where the same Z value have many junctions with quite different materials as dissimilar electrodes.

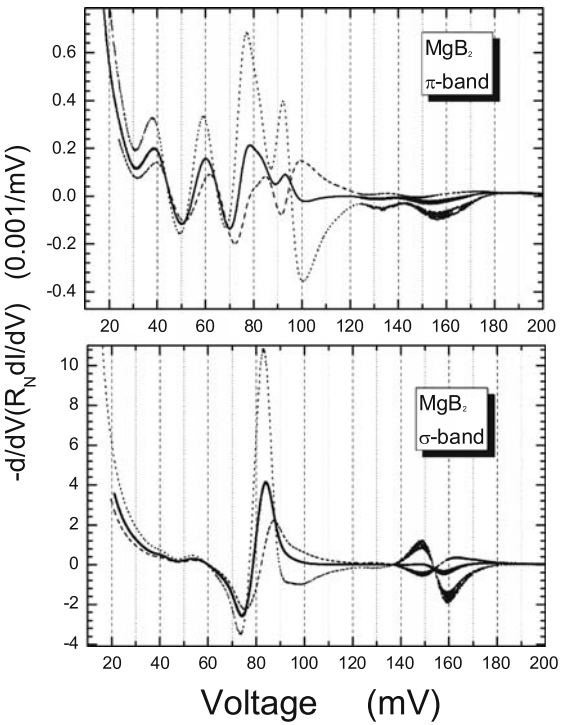

Figure 2. Calculated point-contact spectra for π- and σ-bands (upper and lower panels, respectively) of MgB_2 [12] for ballistic (dashed curve), diffusive (thick solid curve) and tunnel (dotted curve) regimes of current flow. Real and imaginary parts of $\Delta(\varepsilon)$ are taken from Fig. (1).

energy gap region and by observation of only the small gap $\Delta \approx 2.4$ meV characteristic of the π-band.

Special attention should be paid to the amplitude of the experimental curves, which roughly equals that predicted theoretically. In inelastic spectroscopy the amplitude of the EPI spectrum is an order of magnitude lower than expected one (see Fig. (1) in Ref.[14] and the discussion cited therein). This discrepancy may be explained either by the diffusive regime of current flow with and unknown mean free path l_i, or by the specific PC-transport character of the EPI function obtained from the inelastic backscattering spectrum.

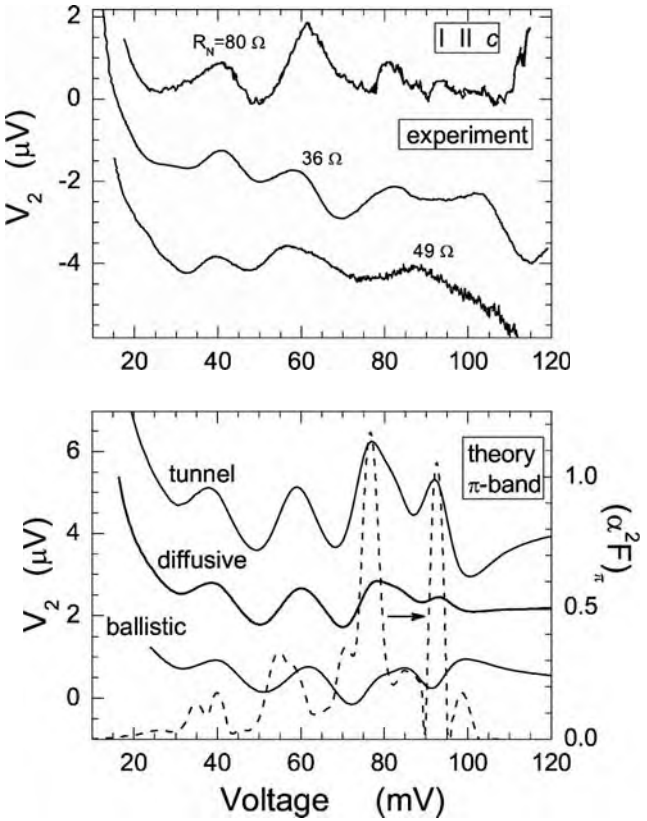

Figure 3. Comparison of experimental (upper panel) and calculated (lower panel) phonon structures in point-contact spectra of MgB_2. The contact axis is oriented along the c-axis. The normal state resistances are given for each curve. In the experimental panel the upper curve corresponds to the ordinate scale, and the other two are shifted down for clarity. $T = 4.2$ K. In the theoretical (lower) panel three transport regimes are illustrated on the same scale as in the experimental graph. Here, the lower curve corresponds to the ordinate scale, the other two are shifted up for clarity. The π-band EPI function (dashed curve) [15] is shifted to higher voltages by $\Delta_\pi = 2.4$ meV. The modulation voltage is taken equal to 3 mV.

Comparing theoretical and experimental spectra, one can infer that all the phonons are essential in the EPI function for the π-band. In the lower panel of Fig. (3) we plot the $(\alpha^2 F)_\pi$ function taken from Ref. [15]. As expected, the maxima in the EPI spectral function shifted by

$\Delta_\pi(0)$ to the right coincide approximately with the maxima in the second harmonic dependences $V_2(V)$.

4. Conclusion

The self-energy effect in the phonon feature of a superconducting point contact can be used, in principle, in the same way as the Rowell-McMillan program for determination of the EPI spectral function in tunneling spectroscopy of superconductors [16]. Two difficulties arise on this way. One is theoretical, since this program works well only for the one-band superconductor, and its application to the two-band case, like MgB_2, encounters difficulties [17]. The other is experimental, since all other sources of $I - V$ nonlinearities should be removed, and especially, the nonequilibrium effects in superconductor should be excluded.

The result obtained for superconductivity in MgB_2 is the first direct proof of validity of the calculated EPI function [15], at least in the π-band. Unfortunately, this method encounters difficulty, while applying it to the σ-band. In this case the very strong generation of nonequilibrium phonons cannot be efficiently excluded from the contact region and this destroys the superconductivity in the constriction.

The question may arise whether the self-energy effects are important in the normal state. These are known to be smaller than the inelastic backscattering nonlinearities in the ballistic regime [18]. If we decrease the contact size d or the elastic mean free path l_i in order to make the inelastic contribution negligible, the latter parameters become comparable to the Fermi wave length of charge carriers and the strong nonlinearities connected with localization occur, which masks the desired phonon structure [19].

5. Acknowledgements

The author is grateful to Yu.G. Naidyuk, S.I. Beloborod'ko, O.V. Dolgov and A.A. Golubov for collaboration. The work was carried out in part by the State Foundation of Fundamental Research under Grant Ф7/528-2001.

References

[1] I.O. Kulik, A.N. Omel'yanchuk and R.I. Shekhter, Sov. J. Low Temp. Phys. **3**, 840 (1977).

[2] I.K. Yanson, in book "*Quantum Mesoscopic Phenomena and Mesoscopic Devices in Microelectronics",* I.O. Kulik and R. Ellialtioğlu (eds.), p. 61, (2000) Kluwer Academic Publishers.

[3] I.O. Kulik and I.K. Yanson, Sov. J. Low Temp. Phys. **4**, 596 (1978).

[4] I.O. Kulik, R.I. Shekhter and A.G. Shkorbatov, Sov. Phys. JETP **54**, 1130 (1981).

[5] Yu. V. Sharvin, Sov. Phys. JETP **21**, 655 (1965).

[6] V.A. Khlus and A.N. Omel'yanchuk , Sov. J. Low Temp. Phys. **9**, 189 (1983).

[7] V.A. Khlus, Sov. J. Low Temp. Phys. **9**, 510 (1983).

[8] S.N. Artemenko, A.F. Volkov and A.V. Zaitsev, Solid State Commun. **30**, 771 (1979).

[9] G.E. Blonder, M. Tinkham and T.M. Klapwijk, Phys. Rev. B **25**, 4515 (1982).

[10] A.N. Omel'yanchuk, S.I. Beloborod'ko and V.A. Khlus, Sov. J. Low Temp. Phys. **14**, 630 (1988).

[11] S.I. Beloborod'ko and A.N. Omel'yanchuk, Sov. J. Low Temp. Phys. **14**, No.3, (1988).

[12] I.K. Yanson, S.I. Beloborod'ko. Yu.G. Naidyuk, O.V. Dolgov and A.A. Golubov, Phys. Rev. B (Rapid Communication), to be published (2004).

[13] I.I. Mazin and V.P. Antropov, Physica C **385**, 49 (2003).

[14] N.L. Bobrov, P.N. Chubov, Yu.G. Naidyuk, L.V. Tyutrina, I.K. Yanson, W.N. Kang, H.-J. Kim, E.-M. Choi, and S.-I. Lee, in book "*New Trends in Superconductivity",* J.F. Annett and S. Kruchinin (eds.), p. 225 (2002) Kluwer Academic Publishers.

[15] A.A. Golubov, J. Kortus, O.V. Dolgov, O. Jepsen, Y. Kong, O.K. Andersen, B. Gibson, K. Ahn, and R.K. Kremer, J. Phys.: Condens. Matter **14** 1353 (2002).

[16] E.L. Wolf, "*Principles of electron tunneling spectroscopy",* Oxford University Press, Inc. New York.

[17] O.V. Dolgov, R.S. Gonnelli, G.A. Ummarino, A.A. Golubov, S.V. Shulga, and J. Kortus, Phys. Rev. B **68**, 132503 (2003).

[18] A.G.M. Jansen, A.P. van Gelder and P. Wyder, J. Phys. C **13**, 6073 (1980).

[19] I.K. Yanson, O.I. Shklyarevskii and N.N. Gribov, J. Low Temp. Phys. **88**, 135 (1992).

A THEORETICAL APPROACH TO DESIGN UNCONVENTIONAL SUPERCONDUCTORS BY HETEROCYCLIC MOLECULES

C. Öğretir, T.Arslan, S.Yarligan
Chemistry Department, Faculty of Arts & Sciences, Osmangazi University, Eskisehir,Turkey

Abstract: Quantum chemical calculations at molecular mechanical level were carried out to search a possible correlation between the number of pyrrole units and the total energy, dipole moment and dihedral angles of the possible polymers of pyrrole molecule. The ideal superconductive polymer of that molecule could be formed by repeating asymmetric type of dimer up to 3 units.

Key words: superconductivity; quantum chemical; heterocyclic molecules; unconventional superconductors; dimer

1. INTRODUCTION

In last two decades molecular-based materials in intermediate or strong electron correlation regime have attracted much interest in relation to molecular magnetism, magnetic conductivity and superconductivity[1]. Films formed from the heterocyclic polymers have found to behave as good conductors and have been used in manufacture of chemically modified electrodes, sensors and solid batteries. Diverse composite materials such as synthetic electro-conductive nylon or polyester fibers covered with a thin layer of poly-pyrrole have been used as a coating for aeroplane fuselages to prevent the reflection of radar signals. The same textile has also been used to shield electronic equipment including computers and control systems[2]. Some recent reports on the theoretical aspects of molecule-based conductors exist in literature[3,4]. In the present work we are now reporting on the geometrical aspects of polymerization of pyrrole molecule which might well act as an unconventional conductor (i.e. molecular wire). The ultimate purpose study

J. Ashkenazi et al. (eds.), New Challenges in Superconductivity: Experimental Advances and Emerging Theories, 259-264.

is to find some kind of correlation between the computed physical parameters and the geometry of the polymer systems using simple level of theory.

2. METHOD OF CALCULATION

CS ChemOffice (R) version 4.5 packet program and MM2 method which is implemented in CS ChemOffice (R) version 4.5 were used [5].

3. RESULTS AND DISCUSSION

To enlighten some of the obscure parts of the possible experimental studies we have attempted to carry out some quantum chemical calculations on polymerization of pyrrole derivatives to drive predictive conclusion. The computed total energy values along with dipole moments and dihedral angles are depicted in Table 1. Among the other possible polymer forms A'A'A'A' and A'B'A'B' forms seems to require smaller energies and both dihedral angles (i.e α and β) have value of zero which suggest planar structures for those polymers and of course indicates the possibility of full conjugation and easiness of electron transfer from one end of the molecule to the other. The A'B'A'B form seems to have the smallest negative dipole moment also. All these data let us to speculate that if the planarity is essential for a molecule to be a conductor the ideal polymer of pyrrole will be obtained with repeating units of AA and A'B' forms up to X values of 10 (i.e s-form) and 6 (i.e. a-form) respectively as shown below.

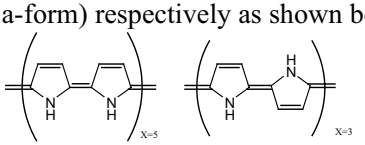

s a

symmetric dimer asymmetric dimer

Correlation graph of dihedral angles with number of pyrrole units (Figures 3-4) indicate that β angle keep the value of null steadely until n=5 in A'B' form whereas α angles has small fluctuations from null. The total energy values correlate well with number of pyrrole units up to n=11 for AB form whereas it degregates at n=9 for AA, n=8 for A'A' and n=5 for A'B' forms. On the other hand the dipole moments correlates well with number of pyrrole units for AB whereas deviation from linearity starts at n=6 for AA and A'A', n=5 for A'B' forms (Figures 1-2).

4. CONCLUSIONS

1. It seems that quantum chemical calculations can lead the experimental studies in predictive manner.

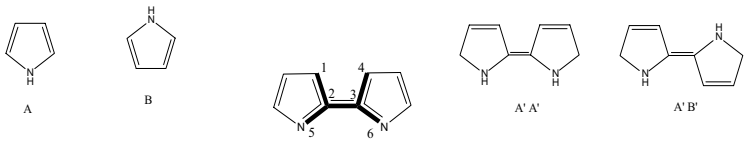

Table 1. MM2 calculated Total energy, E_T (kcalmol^{-1}), Dipol moment , μ(D), Dihedral angles for studied polypyrrole molecule.

	E_T (kcalmol^{-1})	μ(D)	α (1,2,3,4)	β(5,2,3,6)
AA	16.59	0.40	-1.343	-1.450
AB	16.83	0.15	-1.184	-1.142
A'A'	6.71	-0.56	0.000	0.000
A'B'	6.68	-0.98	0.000	0.000
AAA	22.57	0.82	-0.316	-0.547
ABA	23.03	0.31	0.000	0.000
A'A'A'	12.87	-0.11	-0.316	0.000
A'B'A'	13.07	-0.80	0.316	0.000
AAAA	28.58	1.23	-0.949	-1.002
ABAB	29.33	0.47	-2.147	-2.591
A'A'A'A'	19.09	0.36	-0.547	-0.706
A'B'A'B'	19.49	-0.62	0.000	0.000
AAAAA	34.57	1.65	0.316	0.000
ABABA	35.58	0.63	0.000	0.000
A'A'A'A'A'	25.26	0.85	0.000	-0.316
A'B'A'B'A'	25.96	-0.43	0.316	0.000
AAAAAA	40.81	2.07	0.000	0.000
ABABAB	41.64	0.79	0.316	0.000
A'A'A'A'A' A'	31.72	1.36	0.000	-0.448
A'B'A'B' A'B'	28.46	-0.39	-5.345	7.982
AAAAAAA	46.83	2.21	0.706	0.633
ABABABA	47.91	0.95	0.000	0.000
A'A'A'A'A'A'A'	36.56	1.51	0.000	0.000
AAAAAAAA	52.77	2.61	0.000	0.000
ABABABAB	54.04	1.11	0.000	0.000
A'A'A'A'A'A'A'A'	41.83	2.04	0.448	0.547
AAAAAAAAA	57.76	3.42	-2.193	-2.369
ABABABABA	60.28	1.28	0.000	0.000
A'A'A'A' A'A'A'A' A'	47.16	2.50	-2.553	-3.102
AAAAAAAAAA	61.40	4.13	1.614	2.238
ABABABABAB	66.36	1.43	0.000	0.000
A'A'A'A'A'A'A'A'A'A'	49.62	3.37	-2.123	-2.609
AAAAAAAAAAA	63.65	4.92	-0.949	-0.547
ABABABABABA	72.58	1.60	0.000	-0.316
AAAAAAAAAAA	70.23	4.88	0.000	-0.838

2. Better programs are needed (i.e. programs with no limitations) to be able to carry out more convincing and more reliable calculations which will produce closer data to the experimental results.

3. Nevertheless since the linearity of the polymer is important even the very rough calculations indicate that pyrrole molecule might be used as a versatile conductors providing that the appropriate polymerization reaction can be managed.

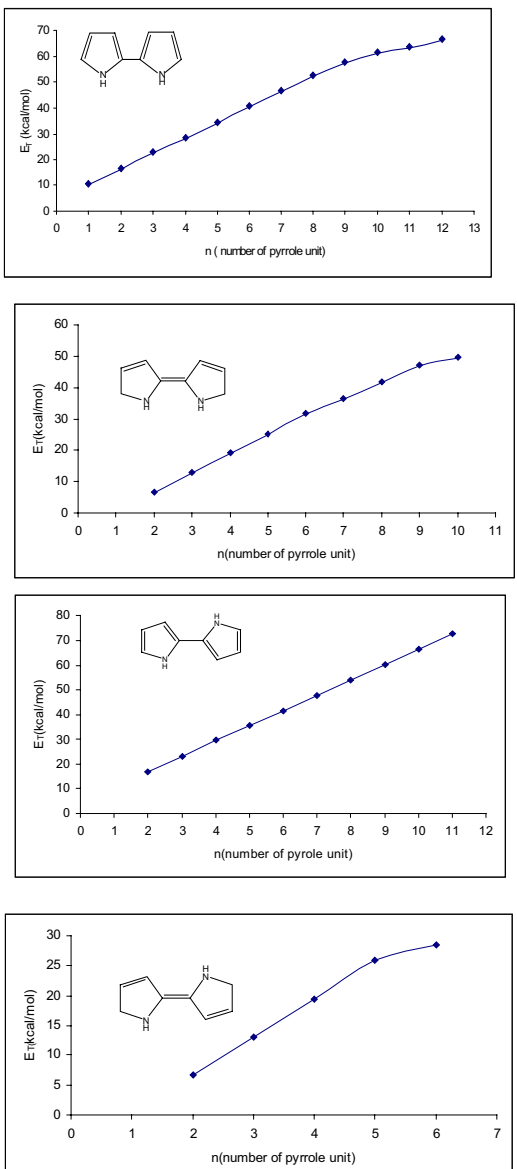

Figure 1. MM2 Total energy –number of pyrrole unit correlation diagrams for polymerization of pyrrole molecule.

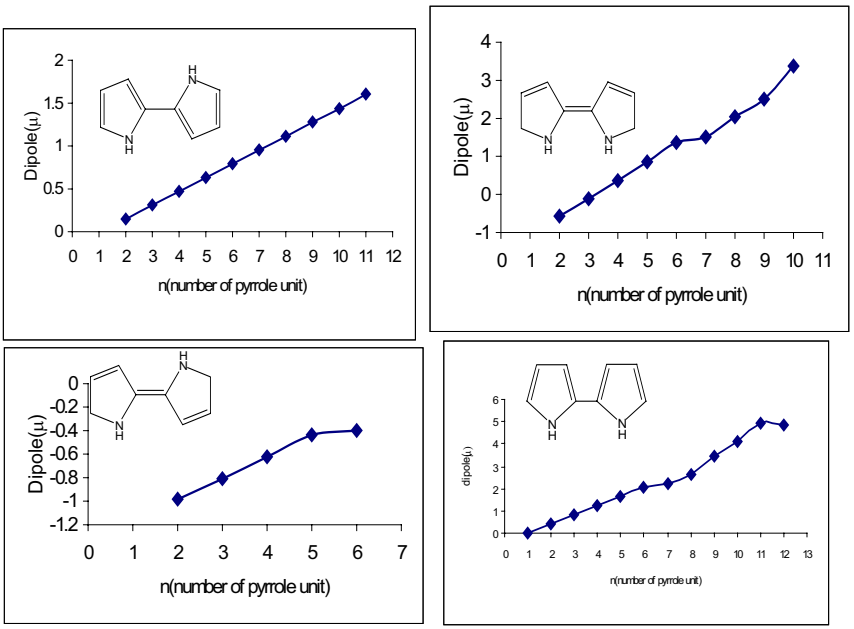

Figure 2. Dipole- number of pyrrole unit correlation diagrams for polymerization of pyrrole molecule.

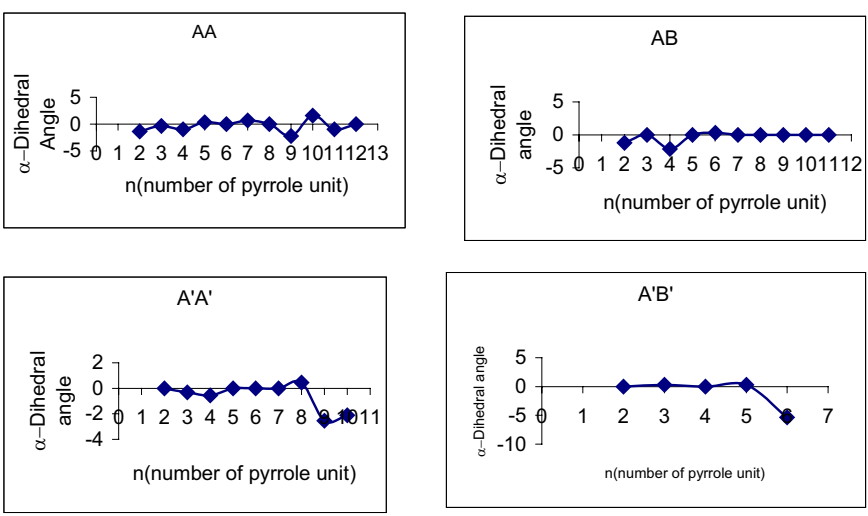

Figure 3. α dihedral angle- number of pyrrole unit correlation diagrams for polymerization of pyrrole molecule.

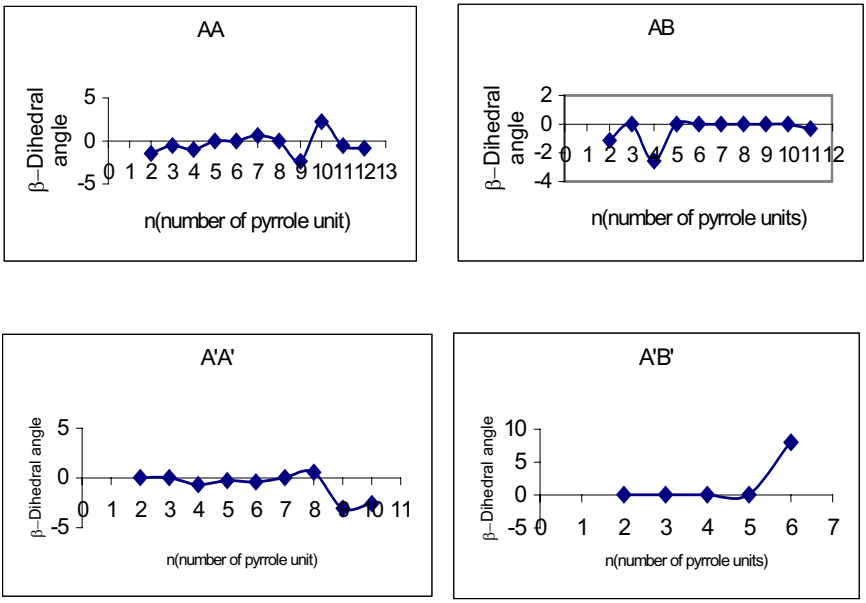

Figure 4. β dihedral angle- number of pyrrole unit correlation diagrams for polymerization of pyrrole molecule.

5. REFERENCES

1. J. G. Bednart; K. A. Miller, Z. Phys. **64** 189 (1986)
2. A.F. Pozharskii; A. T. Soldatenkov, A. R. Katritzky *Heterocycles in Life and Society* (John Wiley & Sons,1997)
3. K. Yamaguchi; T. Kawahami; T. Taniguchi; S. Nakano; Y. Kitagawa; H. Nagao; T. Ohsaku; R. Takeda, Polyhedron **22** 2077-2090 (2003)
4. Y. Yanase; T. Takanobu, T. Nomura; H. Ikeda; T. Hotta; K. Yamada,Physics Reports **387** 1-149 (2003)
5. A combination of PCMODEL 3.1 Serena Software and ChemOfficePro 4.5 Cambridge Soft.
6. F. Acar, S. S. Badesha, W. Frish, R. Gözoğul, O. □nel, S. □nel, R. A. Jones, C. Öğretir, D. C. Rustidge, Pyrrole Studies XXV.The Structure of Potentially Tautomeric *Chim.Acta Turc*. **9**(1) 225-237 (1981)

Subject Index